Volume 19, Number 2

August, 1965

SOVIET ATOMIC ENERGY

АТОМНАЯ ЭНЕРГИЯ
(ATOMNAYA ÉNERGIYA)

TRANSLATED FROM RUSSIAN

CONSULTANTS BUREAU

IMPORTANT NEW PHYSICS SERIES FROM CONSULTANTS BUREAU

Place your standing order today for books in these series. It will ensure the delivery of new volumes immediately upon publication; you will be billed later. This arrangement is solely for your convenience and may be cancelled by you at any time.

REVIEWS OF PLASMA PHYSICS

Acad. M. A. Leontovich, Series editor

A systematic, multi-volume review of the present status of plasma theory, serving both as an introduction for students and for researchers entering the field, and as a convenient, authoritative, up-to-date presentation of current knowledge for workers in plasma physics. This continuing series, translated from Russian, is prepared by internationally known Soviet experts. Each volume contains a number of integrated tutorial reviews, covering in depth and in breadth specific aspects of theory. In many cases, new material is presented.

Volume 1

A comprehensive introduction to "classical" plasma physics, containing authoritative papers on: Motion of Charged Particles in Electromagnetic Fields in the Drift Approximation, by D. V. Sivukhin; Particle Interactions in a Fully Ionized Plasma, by B. A. Trubnikov; Transport Processes in a Plasma, by S. I. Braginskii; and Thermodynamics of a Plasma, by A. A. Vedenov. Much of the material in the first two papers is presented here for the first time. Although the theoretical analyses are quite advanced, the experimental aspects of the subject are kept firmly in view throughout.

326 pages 1965 $12.50

Volume 4

Contains three papers: Hydrodynamic Description of a Collisionless Plasma, by T. F. Volkov; Cooperative Phenomena and Shock Waves in Collisionless Plasmas, by R. Z. Sagdeev; and Coulomb Collisions in a Fully Ionized Plasma, by D. V. Sivukhin.

241 pages 1966 $12.50

Further volumes in this series will be published during 1966.

LEBEDEV PHYSICS SERIES

Acad. D. V. Skobel'tsyn, Series editor

Complete English translations of the Proceedings ("Trudy") of the famed Lebedev Physics Institute of the USSR Academy of Sciences published as Special Research Reports translated from Russian.

OPTICAL METHODS OF INVESTIGATING SOLID BODIES

"Trudy" Volume 25

Includes a major paper by N. D. Zhevandrov on polarized luminescence of crystals. The second paper, by the late V. P. Cheremisinov, reports a study of the vibrational spectra and structure of oxides; a final paper by L. A. Vainshtein concerns the calculation of cross-sections for excitation of atoms and ions by electron impact.

194 pages 1965 $22.50

COSMIC RAYS

"Trudy" Volume 26

Contains an account of the experimental investigations into nuclear and electromagnetic interactions at high and ultra-high energies carried out in the last few years in the laboratories and research centers of the Lebedev Physics Institute.

254 pages 1965 $27.50

RESEARCH IN MOLECULAR SPECTROSCOPY

"Trudy" Volume 27

Devoted to spectroscopic investigations into matter in various states of aggregation by the methods of Raman scattering and infrared absorption. A special section is devoted to the methodological problem of correcting measured quantities for instrumental errors.

206 pages 1965 $22.50

Further volumes in this series will be published approximately 6 months after their appearance in the original Russian.

(c/b) **CONSULTANTS BUREAU** 227 West 17th Street, New York, New York 10011

SOVIET ATOMIC ENERGY

A translation of **ATOMNAYA ÉNERGIYA,**
a publication of the Academy of Sciences of the USSR

Volume 19, Number 2 August, 1965

CONTENTS

Annual Subscription: $95 **Single Issue: $30** **Single Article: $15**

CONTENTS (continued)

The Russian press date (podpisano k pechati) of this issue was 8/19/1965. Publication therefore did not occur prior to this date, but must be assumed to have taken place reasonably soon thereafter.

THE SEVENTIETH BIRTHDAY OF ALEKSANDR PAVLOVICH VINOGRADOV

Translated from Atomnaya Énergiya, Vol. 19, No. 2,
pp. 107-108, August, 1965

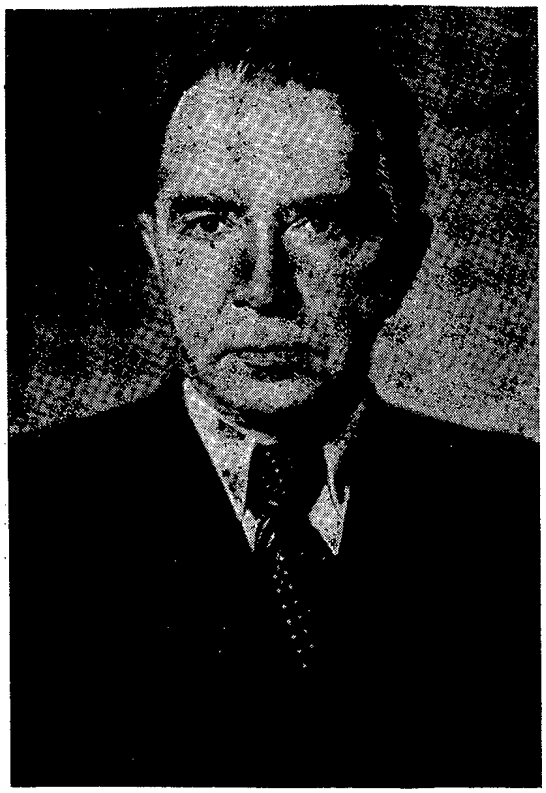

Academician Aleksandr Pavlovich Vinogradov was born August 21, 1895 in Petersburg. The years of the civil war, in which he participated as a volunteer, kept him from his youthful goal of devoting himself to science, but by 1923 he gave a report of his work on microelements in organisms before the student chemical society at Leningrad University, and he published his first scientific paper on organogenic elements in 1924. The military medicine academy which he finished in 1925 developed his interest in the broad problems of biology and the university supplied him with the methods of the exact sciences. That is why Academician V. I. Vernadskii, who was greatly excited that year by the creation of biogeochemistry and who reiterated that "nature becomes known through number and measurement," chose A. P. Vinogradov as his student.

The work of A. P. Vinogradov in the field of biogeochemistry—the monograph "Elementary Chemical Composition of Marine Organisms" published in many languages, the studies in biogeochemical fields and of the chemical composition of organisms as an indicator of type, and other work—gave him a world-wide reputation. It also led him to the problem of the role of isotopes in the phenomena of life; by 1932, he built the first equipment in the USSR for the concentration of heavy water by electrolysis, and he started on an ever expanding cycle of work on the isotopic composition of natural water (meteoritic, surface, and underground), on studies of the isotope exchange process and of the natural processes which change isotopic ratios. The isotopic ratios of hydrogen and oxygen proved to be the key which opened the way to most important problems for him and his school—the origin of atmospheric oxygen, temperature conditions of the geologic past, and the mechanism of photosynthesis in green plants.

Studying the natural ratios of pairs of elements with like properties (Br—Cl, Ni—Fe, etc.), he showed that the fewer the number of processes in which thse elements behaved differently, the more unambiguously one could judge as to the origin of natural objects on the basis of shifts in the ratios of these pairs of elements. Isotopes, being pairs closest in properties, became the chief object of his investigations which are expanding in this direction even now; these studies encompasss all the new areas of knowledge. The isotopic ratios of uranium, thorium, and lead, of strontium and rubidium, of argon and potassium, of carbon, which were investigated by him and his school in hundreds of natural objects, made it possible to create an absolute geochronology. The isotopic composition of sulfur in volcanic and sedimentary rocks, in sulfides and sulfates, now reveal the geochemistry of sulfur in a new fashion, particularly the role of organisms in the oxidation and reduction of its compounds. In the new, fruitfully developing branch of science—the geochemistry of isotopes—the Soviet school, created and headed by him, occupies a leading position.

The comparison of the isotopic compositions of terrestrial igneous rock and meteorites indicated an identical origin for objects in our solar system, and served as the starting point for his series of papers on cosmic chemistry: a study of nuclear-reaction tracks penetrating meteorite surfaces as the result of the action of cosmic rays, a comparison of the distribution of isotopes of the elements in the sun and in meteorites, etc.

The discovery of fission in the uranium nucleus found a lively response in him, and already in 1940 he, together with Academicians V. I. Vernadskii and D. I. Shcherbakov, presented to the government a plan for extensive work in investigating uranium ores in the Soviet Union.

The geochemical and biogeochemical studies of A. P. Vinogradov, which were mainly directed toward the study of the role of microelements, required the development of special, sensitive analytical methods; the school of analysts created by him acquired considerable experience which played a major role in checking the purity of reactor materials. The development and application of spectral, x-ray, electrochemical, radiochemical, and other instrumental techniques in the analysis of these materials by the Soviet atomic industry is in great measure to his credit. At the Geneva conferences, a large number of papers from his school were given on the physical-chemical methods for monitoring uranium production, on radiochemical studies of the products from nuclear transformations induced by bombardment with high-energy particles: the fission of uranium, thorium, and bismuth, spallation of bismuth, copper, and many other nuclei, and also many papers on the use of tracer atoms in analytic chemistry, on uranium geochemistry, etc.

In recent years, he has devoted a great deal of attention to the organization, compiling, and editing of a series of monographs on the analytic chemistry of the elements: some of the first monographs issued were on thorium, uranium, bismuth, beryllium, plutonium, zirconium, and boron.

A large number of papers on the accumulation of nuclear-explosion products (Sr^{90} and others) in plants and soils enabled him to justify the position of the Soviet delegation on the question of the prohibition of nuclear-weapon testing at several Pugwash conferences in which he invariably and actively participated.

His scientific and public activities received high appraisal: he was awarded the title of Hero of Socialist Labor, three times he was State prize laureate, and he was a Lenin prize laureate; he was decorated with the Orders of Lenin three times, with the Order of the Red Banner of Labor twice. Outside the country, his work also received recognition: in 1959, he was elected a member of the Serbian Academy of Science, and 1962, a member of the German Academy of Science at Halle. He is a member of many international scientific societies.

The editorial staff of "Atomnaya Énergiya," an active member of which he has been from the founding of the journal (1956), wishes him many more years of vigorous activity and joy in scientific creativity.

SYNTHESIS OF THE ISOTOPE OF ELEMENT 103 (LAWRENCIUM) WITH MASS NUMBER 256

(UDC 539.183.2)

E. D. Donets, V. A. Shchegolev, and V. A. Ermakov

Translated from Atomnaya Énergiya, Vol. 19, No. 2,
pp. 109-113, August, 1965
Original article submitted April 20, 1965

A new isotope of element 103 with mass number 256 was synthesized by means of the nuclear reaction $_{95}Am^{243}$ ($_{8}O^{18}$, 5n)$_{103}Lw^{256}$.

The detection and identification of $_{103}Lw^{256}$ was made through the isotope $_{100}Fm^{252}$, a product of electron capture in $_{101}Mv^{252}$ produced by α-decay of $_{103}Lw^{256}$. The half-life of $_{103}Lw^{256}$ is 45 sec.

The energy dependence of the $_{103}Lw^{256}$ production cross section in the $_{95}Am^{243} + {}_{8}O^{18}$ reaction was investigated. It was the shape of a curve with a maximum at an $_{8}O^{18}$ ion energy ≈96 MeV (lab system). The half-width of the curve is 9 MeV. At the maximum, the cross section is $6 \cdot 10^{-32}$ cm^2.

The work was carried out with the internal beam of the three-meter, multiply-charged ion cyclotron of the Laboratory for Nuclear Research, JINR.

The first and only paper dealing with the synthesis of element 103 was published in the spring of 1961 [1]. The authors reported they had synthesized an isotope of the new element 103 with mass number 257. In the experiments, an α-activity with E_α = 8.6 MeV and half-life $T_{1/2}$ = 8 sec was observed when targets containing various isotopes of californium were irradiated with accelerated B^{10} and B^{11} ions. Further, using the method of cross reactions, the authors concluded that the observed α activity belonged to the isotope 103^{257} which, for example, is produced in the reaction $_{98}Cf^{252}$ ($_{5}B^{10}$, 5n)103^{257}.

Because of the complex isotopic composition of the targets used in the experiments (50.8% $_{98}Cf^{252}$, 12.3% $_{98}Cf^{251}$, 32.8% $_{98}Cf^{250}$, 3.3% $_{98}Cf^{249}$), they were unsuccessful in demonstrating that the excitation function had the shape of an "evaporation" curve. Because of this, the mass number of the synthesized isotope, 257, was given as the most probable.

In honor of E. Lawrence, the authors proposed to give the name lawrencium to the 103-rd element of the periodic system discovered by them. This paper is concerned with further investigation of the properties of lawrencium, with particular reference to the isotope $_{103}Lw^{256}$. A study of the relationships in the formation of fermium and the transfermium elements [2] made us feel confident that the production cross section of $_{103}Lw^{256}$ in the nuclear reaction $_{95}Am^{243} + {}_{8}O^{18}$ would have a value of $(5\text{-}10) \cdot 10^{-32}$ cm^2. Such a cross section is completely accessible to investigation in the internal beam of the cyclotron.

EXPERIMENTAL

Experimental Method. The isotope $_{103}Lw^{256}$ was detected and identified by means of the technique used to investigate the isotope 102^{256} and described by us in detail previously [3].

It is proposed that $_{103}Lw^{256}$ undergoes radioactive decay either by the emission of α particles or by orbital electron capture: (See the structure at the top of the next page).

In this case, the apparatus (Fig. 1) which was used for the detection of $_{103}Lw^{256}$ through $_{100}Fm^{252}$, operated in the following manner: the products of the nuclear reaction ($_{95}Am^{243} + {}_{8}O^{18}$), among which was the nucleus $_{103}Lw^{256}$, were ejected from the target into an enclosed space because of the momentum of the emitted particles, were slowed down in the gas, and diffused to the walls which bounded the space. The nuclei which were adsorbed on the surface of the circular depression were transported from the irradiation region by rotation of the disc and into a region where recoil

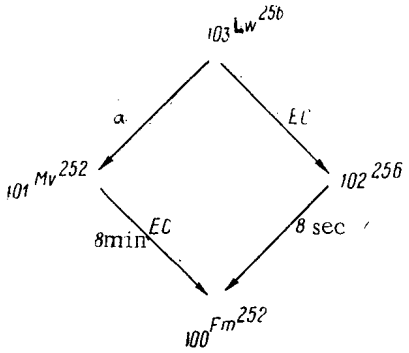

nuclei following α decay were collected. Here, α-decay products, ionized at the time of disintegration, were deposited on a collector by means of a negative voltage equalling −25 V.

Thus the detection of the nucleus $_{100}Fm^{252}$ on the collector was evidence of the synthesis, in the nuclear reaction, of $_{103}Lw^{256}$ which decayed according to the scheme shown. Naturally, other possibilities for the deposition of $_{100}Fm^{252}$ on the collector had to be eliminated.

From the distribution of $_{100}Fm^{252}$ activity on the collector and the rate of rotation of the disc, one can determine the half-life of $_{103}Lw^{256}$.

The fermium accumulated on the collector was chemically separated by ion-exhcange techniques. The α activity of the fermium fraction was measured on an α spectrometer. Surface-barrier Au−Si detectors were used in the α spectrometer. The spectrometers used had a rather good energy resolution of ~60 keV and extremely low background levels.

Experiments on the Synthesis of the Isotope $_{103}Lw^{256}$. The experiments for the synthesis of $_{103}Lw^{256}$ were lengthy (8-12 h) irradiations of an $_{95}Am^{243}$ target by a beam of accelerated $_{8}O^{18}$ ions with simultaneous accumulation of radioactive decay products on the collector. The total ion current, measured for octuply-charged $_{8}O^{18}$ ions, was 15-25 μA·h for each irradiation.

It was observed that varying amounts of $_{100}Fm^{252}$ atoms accumulated on the collector during irradiation depending on the intensity of the irradiation and the energy of the bombarding $_{8}O^{18}$ ions. In Fig. 2 is shown the α spectrum of the fermium fraction of the products accumulated on the collector during one of the irradiations at an $_{8}O^{18}$ ion energy of 97 MeV (lab system). It was established that the half-life of the α activity with E = 7.04 MeV was about 25 h (Fig. 3). The assignment of the accumulated products to the fermium fraction and the properties of the radiactive decay indicated that $_{100}Fm^{252}$ was actually being accumulated on the collector.

However, this fact is only a necessary condition which must be fulfilled if $_{103}Lw^{256}$ is synthesized, but it is by no means sufficient. Along with the necessary condition, another condition must also be fulfilled, namely: if $_{103}Lw^{256}$ is synthesized in the reaction $_{95}Am^{243}(_{8}O^{18}, 5n)_{103}Lw^{256}$, the dependence of its production cross section on the energy of the bombarding ions must have the shape of a curve with a maximum in the energy region 5-7 MeV higher than the Coulomb barrier and with a half-width of 8-10 MeV as in all well known cases of synthesis of transuranium elements [2]. Therefore, experiments were carried out to determine the shape of $_{100}Fm^{252}$ yield on the collector as a function of $_{8}O^{18}$ ion energy.

The results of the experiments are shown in Fig. 4. It appears that the curve has a typical "evaporation" shape with a half-width of ~9 MeV and a maximum at 96 MeV. This situation furnished the basis for supposing that $_{100}Fm^{252}$ actually appeared on the collector as a decay product of $_{103}Lw^{256}$. Its production cross section rises to $\sim 6 \cdot 10^{-32}$ cm^2 at the maximum which is in good agreement with the value which might be expected for this reaction from extrapolation of known data [2]. However, in order to reach unique conclusions about the synthesis of $_{103}Lw^{256}$, it is necessary to exclude all other possibilities.

Half-life Measurements and Control Experiments. 1. It is possible that $_{100}Fm^{252}$ reaches the collector as a product of α decay of 102^{256}, which is produced in the reaction $_{95}Am^{243}(_{8}O^{18}, p4n)102^{256}$. It is well known that reaction cross sections with evaporation of protons are very small in the region of the transfermium elements [4] and that their maxima are displaced into the region of high excitation energies. However, it seems to us that unambiguous experimental proof, which eliminates the indicated possibility, is required. The considerable difference in the half-lives of 102^{256} (8 sec) and $_{103}Lw^{256}$ offers such proof.

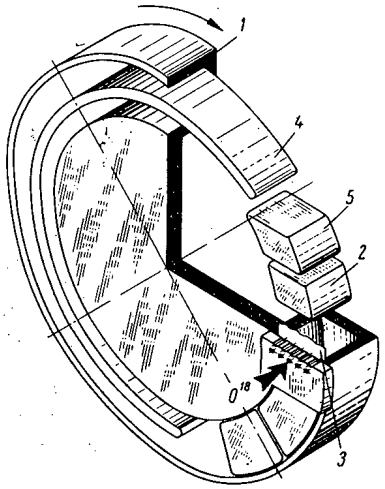

Fig. 1. Diagram of apparatus for synthesis of the isotope $_{103}Lw^{256}$ and the accumulation of its decay product $_{100}Fm^{252}$: 1) Copper disc with circular depression at its periphery; 2) mechanical plug bounding the space for collection of nuclear reaction products; 3) $_{95}Am^{243}$ target on aluminum foil backing; 4) decay product collector (voltage, −25 V); 5) "electrical plug" to protect the collector against deposition of nuclear reaction products (voltage, −25 V).

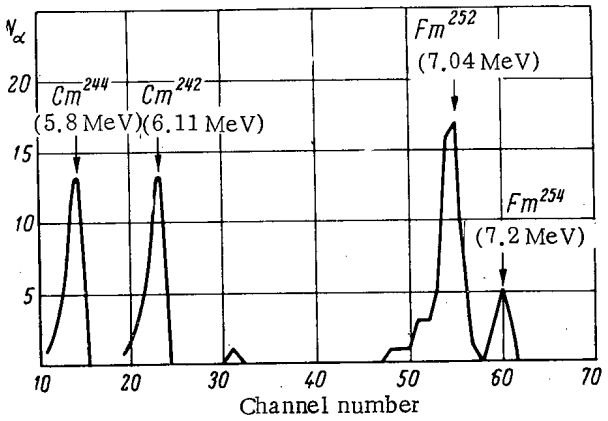

Fig. 2. Alpha spectrum of the fermium fraction of the products accumulated on the collector during $_{95}Am^{243}$ + $_{8}O^{18}$ irradiation for $E_{8}O^{18}$ = 97MeV (lab system). Besides the lines E_α = 7.04 MeV ($_{100}Fm^{252}$, a product of $_{103}Lw^{256}$ decay) and E_α = 7.2 MeV ($_{100}Fm^{254}$, a product of $_{101}Mv^{254}$ decay), the calibration lines of $_{96}Cm^{244}$ and $_{96}Cm^{242}$ are given.

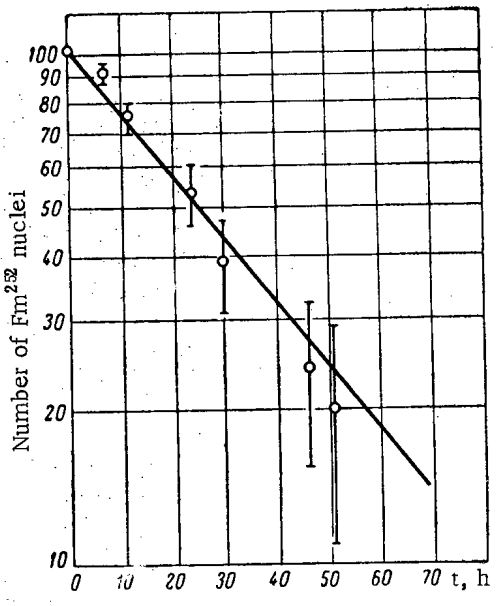

Fig. 3. Decay of the 7.04 MeV α activity contained in the fermium fraction.

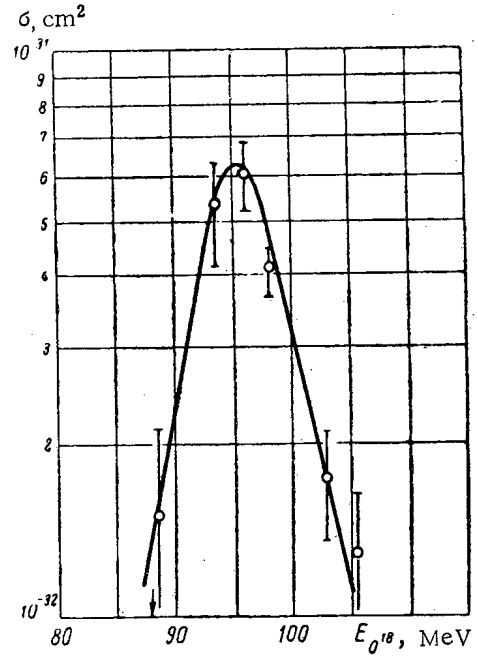

Fig. 4. Energy dependence of the $_{103}Lw^{256}$ production cross section in the $_{95}Am^{243}$ + $_{8}O^{18}$ reaction (obtained through the decay product, the isotope $_{100}Fm^{252}$).

The half-life was measured in the following manner. The rate of rotation of the disc was changed in each experiment. After irradiation, the collector was divided into two halves. The number of $_{100}Fm^{252}$ nuclei detected on the half closest to the target (in the direction of rotation of the disc) was taken as unity and as related to an initial time. The number of $_{100}Fm^{252}$ nuclei on the half farthest from the target was equal to a definite fraction of the assumed unit and was related to a time which depended on the rate of rotation.

The results of the experiments on the measurement of $_{103}Lw^{256}$ half-life are shown in Fig. 5. Its value proved to be close to 45 sec which differs considerably from the half-life of 102^{256} (8 sec).

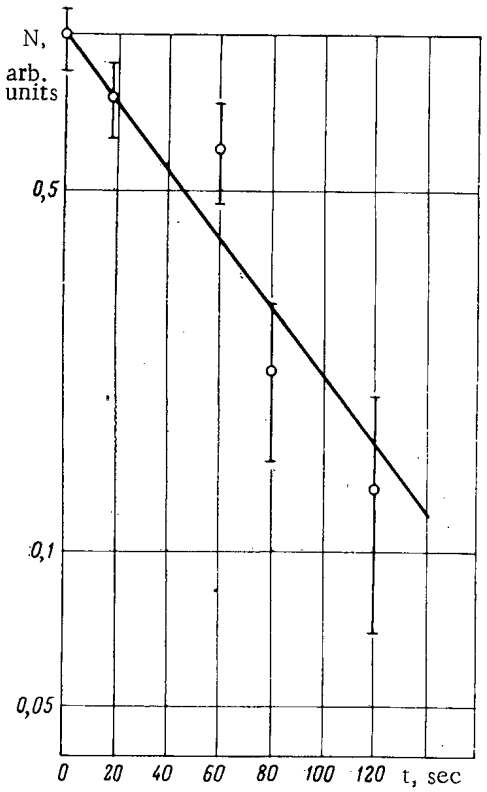

Fig. 5. Experimental results for the measurement of $_{103}Lw^{256}$ half-life ($T_{1/2}$ = 45 ± 10 sec).

2. It is possible that $_{100}Fm^{252}$ reached the collector as the result of the decay of $_{101}Mv^{252}$ which was produced in the $_{95}Am^{243}$ ($_8O^{18}$, α5n) $_{101}Mv^{252}$ reaction. However, it has been shown [2] that the isotope $_{101}Mv^{252}$ undergoes electron capture and is transformed into $_{100}Fm^{252}$ with a half-life for the process $T_{1/2}$ = 8 min. This value is markedly different from the 45 sec half-life of $_{103}Lw^{256}$. Furthermore, it should be noted that the excitation function for reactions of the type (I, α5n) is considerably different from the excitation function for the I, 5n) reaction; it is considerably broader and its maximum is shifted toward the high-energy region. It is well known [2] that electron capture products may be deposited on the collector, and, therefore, despite the noted differences in half-life and excitation function shape, the possibility indicated here was eliminated by another experiment. That experiment showed that the efficiency for the accumulation of $_{100}Fm^{252}$ on the collector as the result of decay following synthesis of $_{103}Lw^{256}$ was 100%. Such a collection efficiency is associated with α decay. At the same time, it was shown that $_{100}Fm^{252}$ accumulation following electron capture in $_{101}Mv^{252}$ did not exceed 15%. In this case, the $_{101}Mv^{252}$ was produced in the $_{92}U^{238}$ ($_9F^{19}$, 5n) $_{101}Mv^{252}$ reaction.

3. Finally, direct deposition on the collector of nuclear reaction products, among which might be $_{100}Fm^{252}$, was eliminated since the shielding system (see points 2, 5 in Fig. 1) reliably protected the target region from the region for daughter product collection. It was experimentally shown that less than 0.1% of all $_{100}Fm^{250}$ nuclei produced in the reaction $_{92}U^{238}$ ($_8O^{18}$, 6n) $_{100}Fm^{250}$ reached the collector. At the same time, the quantity of $_{100}Fm^{252}$ on the collector was ~20% of the entire amount of $_{100}Fm^{252}$ nuclei produced as the result of irradiation in experiments involving the synthesis of $_{103}Lw^{256}$. This value is a good indication that practically all the $_{100}Fm^{252}$ appearing upon irradiation of $_{95}Am^{243}$ with 97 MeV $_8O^{18}$ ions is the result of $_{103}Lw^{256}$ decay.

Therefore, it is possible to state unambiguously that $_{103}Lw^{256}$ with a half-life ~45 sec is synthesized in the reaction $_{95}Am^{243}$ ($_8O^{18}$, 5n) $_{103}Lw^{256}$. The production cross section of this isotope reaches $6 \cdot 10^{-32}$ cm^2 at the maximum. At the same time, data was obtained showing that $_{101}Mv^{254}$, which underwent electron capture with $T_{1/2}$ > 2 min, was produced in the $_{95}Am^{243}$($_8O^{18}$, α3n) $_{101}Mv^{254}$ reaction.

DISCUSSION OF RESULTS

Radioactive Properties of $_{103}Lw^{256}$. On the basis of the experimental data, it is impossible to state precisely what are the partial half-lives for α decay and electron capture in the isotope $_{103}Lw^{256}$ with an overall half-life of 45 sec. Theoretical estimates for electron capture give $T_{1/2}$ = 5 min and, for α decay, $T_{1/2}$ = 2 sec (without forbiddenness). Apparently, $_{103}Lw^{256}$ decays mainly by the emission of α particles, and undergoes electron capture in a few cases. In this situation, the forbiddenness factor for α decay is ~30.

In the future, we propose to set up experiments to measure the partial half-lives of the new isotope $_{103}Lw^{256}$.

Reaction cross section for $_{95}Am^{243}$($_8O^{18}$, 5n) $_{103}Lw^{256}$. A calculation of the energy characteristics of the reaction $_{95}Am^{243}$($_8O^{18}$, 5n) $_{103}Lw^{256}$ shows that the maximum probability for the evaporation of five neutrons from the compound nucleus is reached at energies which are 5-7 MeV higher than the Coulomb barrier of the $_{95}Am^{243}$ + $_8O^{18}$ system. This explains the location of the maximum in the $_{103}Lw^{256}$ production cross section on the energy axis (the value $E_{_8O^{18}}$ = 96 MeV agrees rather well with the calculated value).

The value $\sigma_{5n} = 6 \cdot 10^{-32}$ cm^2 gives the magnitude of the ratio, averaged over the evaporation cascade, of the probability for neutron evaporation to the probability for fission, $\overline{\Gamma_n}/\Gamma_f = 0.053$. This value agrees well with the extrapolated value of $\overline{\Gamma_n}/\Gamma_f$ for this reaction obtained in [2]. The agreement mentioned makes it possible to hope that now one will be able to predict the values of the maxima in the production cross sections for elements 104

($\sigma_{5n} = (1\text{-}2)\cdot10^{-32}$ cm^2) and 105 ($\sigma_{5n} = (2\text{-}5)\cdot10^{-33}$ cm^2) if the isotopes are produced by reactions involving the evaporation of five neutrons. It appears that these cross sections depend little on the choice of targets and particles available at the present time.

As before, the question of reaction cross sections for the evaporation of four neutrons remains less clear [2].

In conclusion, we consider it a pleasure to express our gratitude to G. N. Flerov for his interest in the work and for presenting the opportunity to carry it out. We thank A. N. Filipson and his group who provided reliable operation of the cyclotron while the experiment was being performed.

We are very grateful to L. Kumpf and A. M. Sukhov for developing the high-stability, background-free electronic equipment, to A. G. Pil'kov for construction and adjustment of the mechanical parts of the experimental equipment, and to É. Z. Ryndina and V. F. Kushniruk for development and preparation of the high-capacity semiconductor detectors.

We wish to express our appreciation to V. I. Kuznetsov and the staff of the Physical and Power Institute of the USSR State Committee for the Use of Atomic Energy, and to A. G. Kozlov and A. P. Smirnov-Averin whose work did much to facilitate the effective performance of the experiment.

LITERATURE CITED

1. A. G. Ghiorso, et. al., Phys. Rev. Letters, 6, 473 (1961).
2. E. D. Donets, V. A. Shchegolev, and V. A. Ermakov, JINR Preprint P-2114 [in Russian], Dubna (1965).
3. E. D. Donets, V. A. Shchegolev, and V. A. Ermakov, Atomnaya Énergiya, 16, 195 (1964).
4. V. A. Druin, JINR Preprint P-874 [in Russian] (1962).

NEUTRONS FROM THE FISSION OF EXCITED NUCLEI

(UDC 539.125.5 : 539.173.7)

V. P. Éismont

Translated from Atomnaya Énergiya, Vol. 19, No. 2,
pp. 113-116, August, 1965
Original article submitted July 28, 1964; in revised form, December 28, 1964

The time required for fragments to attain a given velocity was calculated and compared with the calculated lifetime of an excited nucleus with respect to neutron emission. On the basis of this, it is proposed that a certain fraction of neutrons (which increases with excitation) may be emitted before the time of complete acceleration of a fragment in the fission of nuclei excited to energies of 20 MeV and higher. Consideration of this situation makes it possible to eliminate some of the contradictions present in interpretations of experimental data. It is also pointed out that, because of this, the recently employed method for determining the dependence of neutron number on fragment masses by comparing the energies and velocities of the fragments may prove to be inapplicable in cases of high excitations.

It is customary to consider that neutrons are emitted by fragments after the latter have reached full velocity. Measurements of the prompt neutron spectrum at various angles to the direction of flight of a fragment in the case of spontaneous fission (Cf^{252}) and in thermal-neutron fission have verified this assumption [1, 2]. For fission at high excitation energies, such experimental data is lacking (with the exception of one paper [3] about which more will be said later). At the same time, one starts from the same assumption in the analysis of fission properties. In this paper, an evaluation is made of the validity of such an assumption, and the consequences deriving from the evaluation are discussed.

We shall calculate the time required for a fragment to attain a given velocity. The definite success of the statistical approach in the description of fission properties of heavy nuclei ($x \geqslant 0.7$) which depend on the later stages of the process (fragment masses, kinetic energies, excitation energy) permits one to conclude that thermodynamic equilibrium holds at the time of scission. Consequently, to the share of the translational motion of the fragment (one degree of freedom), there falls approximately $\frac{1}{2}T$ (where T is the temperature of the nucleus), i.e., about 0.5 MeV [4], which is much less than the average final velocity of the fragments equalling about 160 MeV. Therefore, one can assume that the initial velocity of the fragments is zero. Thus we shall consider that the fragments acquire energy solely by the action of the repulsive Coulomb force. In this situation, the solution of the equations of motion (hard sphere fragments) gives the following relations between the time t, the velocity v, and length of the path traversed s:

$$t = \frac{s_0}{v_k}\left\{\left[\frac{s}{s_0}\left(\frac{s}{s_0}-1\right)\right]^{1/2} + \frac{1}{2}\ln\frac{1+\left(1-\frac{s_0}{s}\right)^{1/2}}{1-\left(1-\frac{s_0}{s}\right)^{1/2}}\right\}; \quad (1)$$

$$v = v_k\left(1-\frac{s_0}{s}\right)^{1/2}; \quad (2)$$

$$t = \frac{s_0}{v_k}\left[\left(\frac{v_k}{v}-\frac{v}{v_k}\right)^{-1} + \frac{1}{2}\ln\frac{1+\frac{v}{v_k}}{1-\frac{v}{v_k}}\right]. \quad (3)$$

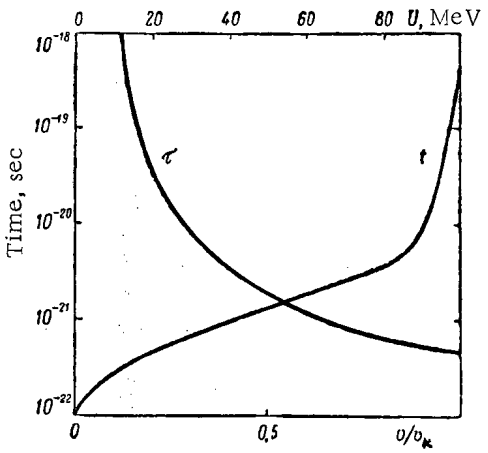

A comparison of the time for a fragment to attain the velocity v/v_k with the time for neutron emission by a fragment excited to an energy U.

Here, s_0 is the distance between fragment centers at the time of scission; v_k is the velocity of the fragments at infinity, equalling $\left[\frac{2(M-m)(Z-z)z}{mMs_0}\right]^{1/2}$, where M, Z, and m, z are the masses and charges of the fissioning nucleus and of the fragment, respectively. In a case typical of the thermal neutron fission of U^{235}, the light fragment has m = 100, $v_k = 1.4 \cdot 10^9$ cm/sec [5], and therefore s_0 = 17 fermi. The figure shows the calculated value of the time t required for acceleration of such a fragment to some velocity v (expressed as a fraction of v_k).*

We shall compare this time with the lifetime of the fragment. According to the statistical model (see, for example, reference [6]), the lifetime of the excited nucleus before neutron emission (neglecting even-even effects on nuclear level density) is

$$\tau = \frac{2A^{1/3}}{U - B_n} e^{B_n/T} \cdot 10^{-21} \text{ sec}, \qquad (4)$$

where A is the mass number of the nucleus; U is its excitation energy, MeV; B_n is the binding energy of a neutron in the nucleus, MeV; $T = \left[\frac{10(U-B_n)}{A}\right]^{1/2}$ is the temperature of the nucleus which emits a neutron. Formula (4) estimates the lifetime to an order of magnitude. It is considered that the values determined by this formula are close to the actual ones. Unfortunately, it is difficult to establish the reliability of the estimate because nuclear lifetimes are so small that they cannot be determined by the usual methods for the comparatively large excitations (several million electron volts above the neutron binding energy) where the statistical considerations leading to expression (4) are permissible. It is possible that the situation will be cleared up by experiments with well-monochromatized fast particles which will make it possible to observe the fluctuations in reaction cross sections and angular distributions of the products (as functions of particle energy) and to use them to determine τ [7].

Values of τ were calculated for fragments with A = 100 (B_n = 5 MeV) at various excitation energies (see figure). It is clear that the lifetime of the nucleus is $\sim 10^{-18}$ sec for an excitation energy of approximately 12 MeV, which corresponds roughly to the mean energy of the fragments in thermal-neutron fission of U^{235}.† In such a length of time, the fragments manage to attain practically full velocity (more than 0.99 v_k), which has been confirmed by experiment [1, 2]. For fission by 14 MeV neutrons, the excitation energy of a fragment is about 20 MeV. For such an excitation energy, the lifetime allows acceleration to approximately 0.95 v_k on the average. However, it is necessary to consider a number of circumstances. First, the fragments have a broad energy distribution and, consequently, a significant fraction of the nuclei have an excitation above the average (for a typical half width ~20 MeV, approximately 10% of the fragments have an excitation 10 MeV above the average). Second, higher excitation of the fragments corresponds to lower kinetic energies and, therefore, to longer times t (s_0 larger, v_k smaller). Third, with the exponential nature of the decay of excited states, about 10% of the nuclei live less than $1/10$ of the mean time. On this basis, one should conclude that even in the case mentioned above (when U ≈ 20 MeV) there may be a noticeable deviation from the usually assumed mechanism of evaporation from fully accelerated fragments. It is possible that the interesting observation described in [3, 8] is associated with exactly this sort of thing: the number of neutrons evaporated before fission, as determined from measurements of neutron spectra and the subsequent analysis of them on the assumption of neutron emission at $v = v_k$, is 1.2-1.4 times greater than the values which is obtained from known fission cross sections under the usual condition for heavy nuclei (that Γ_f/Γ_n is independent of excitation energy)[9, 10].

When U = 50 MeV, $\tau \approx 2 \cdot 10^{-21}$ sec and neutron emission occurs before the fragments attain half their final

* In order for the heavy fragment to reach the same velocity (with respect to its value for v_k), a time greater by the factor (M−N)/m is required.

† At the time of scission, a large fraction (for thermal fission) of the excitation energy of the fragments is concentrated in deformation energy. However, the latter rapidly (in comparison with acceleration time) changes into excitation energy.

velocity. Of course, the calculated values for τ, and those shown in the figure, refer to the emission of the first neutron. The time for the emission of succeeding neutrons must increase because of the increase in B_n and the reduction in T.

The considerable decrease in the translational velocity of the fragments which emit neutrons is reflected directly in E_n, the measured neutron energy. In the laboratory system, $\overline{E}_n = \overline{E}_{cm} + \overline{E}_f$, where $\overline{E}_{cm}$ is the average energy in the rest system of the fragments, $\overline{E}_f$ is the average energy of a fragment per nucleon at the time of neutron emission. For U^{235} thermal fission, $\overline{E}_{cm} = 1.21$ MeV and $\overline{E}_f = 0.74$ MeV [11], i.e., the translational-motion contribution is more than one third of the total neutron energy. At higher excitations, this contribution is significantly reduced because of the effect mentioned. The reduction in translational velocity has an even greater effect on the angular distribution of the neutrons (in the laboratory coordinate system). For neutrons with $\overline{E} = \overline{E}_{cm} = 1.21$ MeV, the velocity corresponding to $E_f = 0.74$ MeV leads to an anisotropy (ratio of the intensities at 0° and 90° to the direction of flight of the fragments) of 2.54; at half that velocity, the anisotropy is only 1.25. For neutrons of lower energies, which are the principal contributors to the anisotropy in the angular distribution of fission neutrons, the difference is even greater; thus, for E = 1 MeV, the corresponding values are 3.40 and 1.32.

Consideration of the facts mentioned makes it possible to eliminate some contradictions present in the physics of fission at medium and high energies. On the basis of experimental data for fission and (α, xn) reaction cross sections of nuclei heavier than thorium, one can conclude that the ratio of fission width to neutron width Γ_f/Γ_n, is independent of excitation energy (up to approximately 100 MeV) [9, 10]. Since $\Gamma_f \approx \Gamma_n$, it follows from the constancy of Γ_f/Γ_n that the majority of neutrons are emitted by the excited nucleus after fission.

However, the opposite conclusion was arrived at [12] from experiments on the angular distribution of neutrons in uranium fission by 147 MeV protons. In these experiments, it was found that the anisotropy of the neutron angular distribution was 1.27 ± 0.11. The authors explained such an insignificant anisotropy as a result of the fact that, of the 13 neutrons which accompany uranium fission by 147 MeV protons, only 1.5-3.5 neutrons (as is the case in thermal-neutron fission) were emitted from the moving fragments, the remainder being emitted before fission. This would mean that $\frac{\Gamma_f}{\Gamma_n} \to 0$ and does not remain constant at such excitations. It would appear that such an interpretation was also verified by the data on the energy spectrum of the neutrons; the average kinetic energy of the neutrons was found to be 2.4 ± 0.2 MeV [13]. From the estimates in this paper, it seems completely probable that in the fission of uranium nuclei excited to 100 MeV (which occurs for a proton bombarding energy of ~150 MeV [9, 14]), when fragments are produced with energies around 50 MeV (if Γ_f/Γ_n is large), the emission of neutrons from the fragments occurs in a very short time during which the fragments do not succeed in reaching high velocity. Although the neutrons are emitted from moving fragments, their average energy and anisotropy prove to be small. Thus one can explain the insignificant anisotropy at low kinetic energies of fission neutrons without assumptions about the reduction in Γ_f/Γ_n for large excitations of heavy nuclei.

The question of the relationship between fragment acceleration time and fragment lifetime is directly connected with the determination of the dependence of fission neutron number on fragment mass. The establishment of this dependence for spontaneous fission and thermal-neutron fission played an important role in explaining the effect of nuclear shells on the latter stages of the fission process [15, 16]. The determination of neutron number as a function of fragment mass in the medium-excitation-energy region will make it possible to check the validity of the hypothesis concerning two types of fission [17, 18]. An extremely efficient method for determining the number of neutrons from individual fragments is the method of mass-distribution comparison which is obtained as the result of measurements of fragment-pair energies, with the mass distribution obtained from velocity measurements [11]. This method appears to be particularly useful for investigating fission in excited nuclei. Recently, it was applied to the case of Th^{230} and U^{233} fission by α particles with energies of 25.7 and 29.5 MeV [18]. The method mentioned for the determination of the number of neutrons from individual fragments consists of the following: a measurement of the fragment velocities enables one to find their initial masses from the relations

$$A_L v_L = A_H v_H \quad A_L + A_H = A, \tag{5}$$

and a measurement of kinetic energies enables one to determine certain masses A'_L and A'_H:

$$\frac{A_{L'}}{A_{H'}} = \frac{E_L}{E_H} = \frac{A_L - \nu_L}{A_H - \nu_H}\left(\frac{A_H}{A_L}\right)^2, \tag{6}$$

where the subscripts "L" and "H" refer to the light and heavy fragments, respectively. From the preceding relations, it follows that [11]

$$\nu_L = A'_L - A_L + A_L \frac{\nu}{A}; \quad (7)$$

where $\nu = \nu_L + \nu_H$ and can be computed from the energy-balance equation. A similar expression can be written for the heavy fragment. It must be pointed out that the specified relations are valid only under the condition of neutron evaporation from fragments infinitely removed from one another and having full velocity. As has been demonstrated, this condition is well fulfilled for spontaneous and thermal fission. In this case, the data, obtained by the method discussed, is in good agreement with the results of direct measurements [18]. With large excitation, considerable deviations are possible. In particular, it follows from the present evaluation that the specified condition is apparently violated even for ~20 MeV excitation of the fissioning nucleus. The excitation energy of nuclei irradiated by α particles with energies of 25-30 MeV is of approximately such a magnitude. Therefore the use of relations (5)-(7) in that situation may not be completely justifiable. This may explain why the method discussed does not reveal the structure in the curve for the dependence of neutron number on fragment mass which is discovered by the method of comparing fragment-velocity data with radiochemical mass determinations [18, 19]. The observed [18] coincidence of mass distributions obtained from velocities and kinetic energies does not in itself indicate that the neutrons are distributed between the fragments in proportion to their masses as follows from relation (7) when $A_L - A'_L = 0$. In practice, the mass distributions will also coincide when all the neutrons are evaporated at the beginning of fragment acceleration.

LITERATURE CITED

1. H. Bowman, et. al., Phys. Rev., 129, 2133 (1963).
2. S. Kapoor, R. Ramanua, and R. Rama Rao, Phys. Rev., 131, 283 (1963).
3. Yu. A. Vasil'ev, et. al., ZhÉTF, 38, 671 (1960).
4. P. Fong, Phys. Rev., 102, 434 (1956).
5. J. Milton and J. Fraser, Canad. J. Phys., 40, 1626 (1962).
6. T. Ericson, Advances Phys., 9, 425 (1960).
7. T. Ericson, Phys. Rev. Letters, 5, 430 (1960).
8. Yu. A. Vasil'ev, et. al., Physics of Fission [in Russian], Gosatomizdat, Moscow (1962), p. 121.
9. N. A. Perfilov, Idem., p. 175.
10. I. Huizenga and R. Vandenboseh, Nucl. Reactions, II (1962).
11. J. Terrell, Phys. Rev., 127, 880 (1962).
12. G. Harding and F. Farley, Proc. Phys. Rev. Soc., 69, 853 (1956).
13. D. Skyrme and G. Harding, Nuovo Cimento, 9, 1082 (1958).
14. N. Metropolis, et. al., Phys. Rev., 110, 185 (1958).
15. M. V. Blinov and V. P. Éismont, ZhÉTF, 42, 180 (1962).
16. R. Vandenboseh, Nucl. Phys., 46, 129 (1963).
17. V. P. Éismont, ZhÉTF, 44, 744 (1963).
18. H. Britt and S. Whetstone, Phys. Rev., 133, B603 (1964).
19. S. Whetstone, Phys. Rev., 183, B163 (1964).

All abbreviations of periodicals in the above bibliography are letter-by-letter transliterations of the abbreviations as given in the original Russian journal. *Some or all of this periodical literature may well be available in English translation.* A complete list of the cover-to-cover English translations appears at the back of this issue.

PROMPT γ RAYS FROM FISSION

(UDC 539.173.4 : 539.166.2)

V. P. Zommer, A. E. Savel'ev, and A. I. Prokof'ev

Translated from Atomnaya Énergiya, Vol. 19, No. 2,
pp. 116-119, August, 1965
Original article submitted July 20, 1964; in revised form, January 16, 1965

The prompt γ-ray spectrum from the fragments of U^{235} thermal-neutron fission was calculated exactly within the framework of the basic assumptions of statistical theory for the emission of neutrons and γ rays from excited nuclei. The shape of the spectrum corresponded roughly to that obtained experimentally; however, the computed total energy carried away by the γ rays ($\lesssim 6.2$ MeV) was considerably below the experimental value (8-9 MeV). Conclusions are drawn as to the possibility of eliminating this disparity if the "thinness" of nuclear levels close to the ground state (0-2 MeV) in the fragments is taken into account in calculating residual excitation.

At the present time, calculations of fission γ-ray spectra are lacking in the literature. According to theoretical predictions of the total energy carried off by the prompt γ rays of fission [1-3], this energy should amount to 4-5 MeV. However, experimental data do not confirm these estimates. Experiments performed for the spontaneous fission of Cf^{252} [4-6] and for thermal-neutron fission of U^{235} [7-9] showed that the total energy of the prompt γ rays emitted per fission was 7-9 MeV, i.e., larger than the results of theoretical estimates by almost a factor of two.

One can hope that the agreement of theory with experiment might be improved if statistical theory is systematically used for the description of γ emission from fission fragments. If that does not happen, then, having the results of such calculations, it will be easier to discover the reason for the disparity.

To calculate γ-ray spectra, it is first necessary to know the excitation energy distribution of the fragments after the emission of each neutron. We determined these distributions on the basis of statistical theory of neutron evaporation.

Let the excitation energy distribution of the fragments after the emission of the $(\nu-1)$-th neutron be described by the function $R^0_{\nu-1}(E)$. Then the distribution after emission of the ν-th neutron is defined by the recursion relation:

$$R^0_\nu(E) = \int_{E+B_{n\nu-1}}^{E_0-\sum_{m=0}^{\nu-2} B_{nm}} R^0_{\nu-1}(E')\,\Phi_\nu(E, E')\,dE', \tag{1}$$

where $B_{n\nu}$ is the neutron binding energy in a nucleus which has emitted ν neutrons, E_0 is the maximum excitation energy of a fragment before evaporation of the first neutron, and the function $\Phi_\nu(E, E')$ represents the probability that a fragment having excitation energy E is in the state with energy E' after emission of the ν-th neutron. Using the statistical theory for neutron evaporation, we write for this probability

$$\Phi_\nu(E, E') = \varphi_\nu^{-1}(E)\,(E - E' - B_{n\nu-1})\,\varrho_\nu(E'), \tag{2}$$

where $\rho_\nu(E)$ is the level density in a nucleus which has emitted ν neutrons and which has excitation energy E and $\varphi_\nu(E)$ is a normalization factor.

The normalization condition takes the form

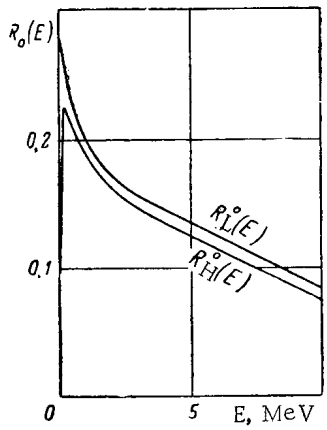

Fig. 1. Distribution of residual excitations for the two groups of fragments.

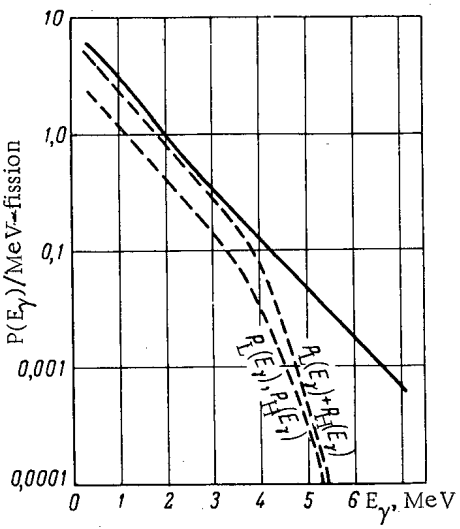

Fig. 2. Comparison of calculated and experimental γ -ray spectra.

$$\int_0^{E-B_{n\nu-1}} \Phi_\nu(E, E')\,dE' = \frac{\Gamma_{n\nu-1}(E)}{\Gamma_{n\nu-1}(E)+\Gamma_{\gamma\nu-1}(E)}, \qquad (3)$$

where $\Gamma_{n\nu}$ (E) and $\Gamma_{\gamma\nu}$, respectively, are the neutron and radiation widths for decay of a fragment which has emitted ν neutrons and which has excitation energy E.

The radiation width can be considered constant within the limits of the narrow energy region where the competition between neutron-and γ -ray emission is important. The dependence of neutron width on excitation energy, in the framework of the statistical theory, is determined by the principle of detailed balance [10]:

$$\Gamma_{n\nu-1}(E)=\frac{gM\sigma_c}{\pi^2\hbar^2}\cdot\frac{1}{\varrho_{\nu-1}(E)}\int_0^{E-B_{n\nu-1}}(E-B_{n\nu-1}-x)\,\varrho_\nu(x)\,dx, \qquad (4)$$

where g = 2 for a neutron, M is the reduced mass of the "neutron plus residual nucleus" system, and σ_C is the cross section for the process which is the inverse of the emission of a neutron from an excited nucleus.

If the excitation-energy distribution of the fragments before evaporation of the first neutron (the function R_0^0(E)) is known, the formulas given completely determine the distributions of interest.

A method of computing γ -ray spectra, which in principle applies to any nuclear reaction, has been described [11, 12]. In the case of fission, the γ -ray spectrum originating from a fragment with a certain mass number after the evaporation of ν neutrons from it is defined by the expression

$$P_\nu(E_\gamma)=\int_{E_\gamma}^{B_{n\nu}} R_\nu(E)\,w_\nu(E, E-E_\gamma)\,dE, \qquad (5)$$

where the function R_ν (E) is a solution of the integral equation

$$R_\nu(E)=R^0_\nu(E)+\int_E^{B_{n\nu}} R_\nu(E')\,w_\nu(E, E')\,dE', \qquad (6)$$

and the function w_ν (E, E') describes the probability of a radiative transition having energy E−E' in a fragment which has emitted ν neutrons.

If it is assumed that the γ -rays are emitted only as the result of electric dipole transitions and that the radial matrix elements for these transitions are identical for all states of the same nucleus, then

$$w_\nu(E, E')=f_\nu^{-1}(E)\,(E-E')^3\,\varrho_\nu(E'). \qquad (7)$$

Furthermore, if it is assumed that the γ rays are emitted only when the emission of neutrons becomes energetically impossible, the normalization condition for the probability of radiative transitions takes the form

$$\int_0^E w_\nu(E, E')\,dE'=1, \qquad (8)$$

which also defines the normalizing factor f_ν (E).

Since experimental data is lacking at the present time for spectra of γ rays which are emitted from fragments with definite mass numbers, all the expressions written down must be summed over all the energetically possible

values of ν and averaged over the mass distribution of the fragments in order to compare calculated and experimental data. To designate the result of such an operation, we omit the subscript in all expressions. Furthermore, it is convenient to divide the fragments into two groups: heavy and light.

The numerical computations were performed on an electronic computer for the case of U^{235} thermal-neutron fission. In computing both the residual excitation energies and the γ -ray spectra, we used the level density formula

$$\varrho(E) = \text{const} \exp \sqrt{4aE}, \tag{9}$$

where a is the level density parameter.

In Fig. 1 are shown the results of the numerical computations for the residual excitation functions of the light and heavy fragment groups, $R^0_L(E)$ and $R^0_H(E)$, respectively. The values for the binding energies were calculated from Cameron's formula [14], and the mass distribution of the fragments was taken from [13]. The dependence of the most probable fragment charge on mass number was determined in accordance with [15]. The function $R^0_0(E)$ was chosen in the form of a Gaussian with maximum at E = 17 MeV and a width of 8 MeV. The nuclear-level-density parameter was determined from the formula a = 0.05 A, where A is the mass number of the fragment. The value Γ_γ = 0.1 eV was chosen for the radiative width.

The averaged values for the neutron binding energy in a fragment were 6 and 6.5 MeV for the light and heavy fragments, respectively. The residual excitation functions determined in this manner were used for the computation of the γ -ray spectra.

Results of the calculation of γ -ray spectra for light and heavy fragments are shown in Fig. 2. The solid curve shows the experimental data [5]. It is clear that the calculated total γ -ray yield roughly corresponds to that experimentally observed. For a quantitative comparison, calculations were made of the total energy carried off by the fission γ rays:

$$\widetilde{E}_\gamma = \widetilde{E}_{\gamma L} + \widetilde{E}_{\gamma H}$$
$$= \int_0^{B_{nL}} E_\gamma P_L(E_\gamma)\, dE_\gamma + \int_0^{B_{nH}} E_\gamma P_H(E_\gamma)\, dE_\gamma.$$

In our case, the following results were obtained:

$$\widetilde{E}_{\gamma L} = 2.83 \text{ MeV}; \quad \widetilde{E}_{\gamma H} = 3.07 \text{ MeV},$$

i.e., the total energy per fission was 5.9 MeV which, as before, was below the experimental value. In addition, we derived an upper limit on the energy which was carried away by γ rays from fragments before the emission of neutrons became energetically impossible; its value was 0.3 MeV.

Thus even the strict application of statistical theory to the description of γ emission from fission fragments does not lead to good agreement with experiment. However, one can observe at least one of the reasons for the disparity from the shape of the functions $R^0_L(E)$ and $R^0_H(E)$ (see Fig. 1).

The curves in Fig. 1 indicate that a considerable portion of the fragments are left with small excitation energies (0-2 MeV) as the result of cascade evaporation of neutrons. However, such a result, exact in the framework of statistical theory, most likely does not correspond to reality since a large part of the fission fragments are nuclei in which levels close to the ground state are widely spaced. The actual excitation function must take into account this "thinness" of levels. By considering this situation, the number of fragments having excitation energies after neutron emission in the region close to the ground state will be less than results from our calculations. However, because the number of particles must be conserved, the number of fragments having higher excitation energies is increased. Further, it is obvious the total energy carried away by the γ rays will be greater. It is also possible that the experimentally observed large value for the total energy of fission γ radiation is to some extent due to the fact that fission fragments have high angular momenta [16].

LITERATURE CITED

1. R. Leachman and C. Kazek, Phys. Rev., 105, 1511 (1957).
2. R. Leachman, Phys. Rev., 101, 1005 (1956).
3. J. Terrel, Phys. Rev., 113, 527 (1959).
4. H. Bowman and S. Thompson, Proc. of the Second Intern. Conf. on the Peaceful Uses of Atomic Energy, Geneva, UNO, Vol. 15 (1958), p. 212.

5. A. Smith, et. al., Idem., p. 392.
6. J. Milton and J. Fraser, Phys. Rev., 111, 877 (1958).
7. V. V. Sklyarevskii, D. E. Fomenko, and E. P. Stepanov, ZhÉTF, 32, 256 (1957).
8. V. K. Voitovetskii, B. A. Levin, and E. V. Marchenko, Idem., p. 263.
9. F. Maienschein, et. al., Cf. [4], p. 366.
10. J. Francis and R. Gamble (in Report J. Fraser), Proc. of the Symposium on the Physics of Fission Held at Chalk River, Ontario (1956). Atomic Energy of Canada, Limited Report. CRP-642-A (1956), p. 239.
11. A. S. Davydov, Theory of the Atomic Nucleus [in Russian], Fizmatgiz, Moscow (1958).
12. V. M. Strutinskii, L. V. Groshev, and M. A. Akimova, ZhÉTF, 38, 598 (1960).
13. E. Troubetzkoy, Phys. Rev., 122, 212 (1961).
14. A. Cameron, Canad. J. Phys., 35, 1021 (1957).
15. R. B. Leachman, in Proceedings of the Second International Conference on the Peaceful Use of Atomic Energy, Geneva (1958), [in Russian Translation], Dokl. Inostr. Uchenykh, Vol. 2, Atomizdat, Moscow (1959), p. 342.
16. B. Pate, Canad. J. Chem., 36, 1717 (1958).

All abbreviations of periodicals in the above bibliography are letter-by-letter transliterations of the abbreviations as given in the original Russian journal. *Some or all of this periodical literature may well be available in English translation.* A complete list of the cover-to-cover English translations appears at the back of this issue.

ON THE CLASSICAL THERMAL CONDUCTIVITY IN A TOROIDAL PLASMA

(UDC 533.9)

V. D. Shafranov

Translated from Atomnaya Énergiya, Vol. 19, No. 2,
pp. 120-125, August, 1965
Original article submitted January 23, 1965

In toroidal equilibrium configurations the drift flow of heat causes a redistribution in plasma temperature along the magnetic surfaces. The resulting temperature gradient is equalized by an axial "nonmagnetic" heat flow, which leads to a certain effective flow of heat across the magnetic surfaces. This additional toroidal heat flow proves to be greater than the magnetic flow, which determines the heat loss from a plasma in a cylindrical geometry. The effective toroidal coefficient of thermal conductivity is calculated for "smooth" toroidal systems of Tokamak and stellarator types, the latter having a spatial figure-eight form. Expressions are also obtained for the distribution of the electric potential associated with the above-mentioned temperature redistribution.

It is well known that the idea of thermally insulating a plasma by means of a magnetic field depends on the fact that the coefficient of thermal conductivity depends strongly on magnetic field intensity. When charges collide in a magnetic field with straight lines of force they can be displaced across the lines of force only by a distance of the order of the mean Larmor radius $r_B = v_T \frac{eB}{Mc}$. It follows from this that the coefficient of thermal conductivity in a transverse direction is

$$\varkappa_\perp \sim \frac{nr_B^2}{\tau},$$

where τ is the average time between collisions of ions of given type. The manner in which the charges move in a toroidal geometry is complex. In addition to the main toroidal field, the additional magnetic field required to balance toroidal drift causes the charges to drift in the toroid cross section around circles whose center is shifted from the center of the cross section of the magnetic surface by an amount δ depending on the axial and transverse velocities. It was pointed out in [1] that when these drift trajectories for charges with different velocities are "mixed up", a further flow of heat must take place along the line of centers of the drift circles. The corresponding coefficient of thermal conductivity is

$$\varkappa_\perp \sim n\langle\delta^2\rangle/\tau.$$

If the drift in a toroidal (axial) magnetic field B_S is balanced by means of an axial current, producing an azimuthal field B_ω (Tokamak system), then according to [1]

$$\delta = \frac{2v_\parallel^2 + v_\perp^2}{2v_\parallel} \cdot \frac{Mc}{eB_\omega} \cdot \frac{\rho}{R} \approx \frac{\rho B_s}{RB_\omega} r_B,$$

where R is the toroid radius; ρ is the distance from the center of the magnetic surface cross section; $v_\parallel$ and $v_\perp$ are the axial and transverse components of charge velocity. It is clear from this that the thermal conductivity of a plasma in a toroidal geometry is about $1 + \frac{\rho^2 B_S^2}{R^2 B_\omega^2}$ times greater than in a cylinder, and is determined not by the main magnetic field but by the auxiliary B_ω (if it is not too strong).

The above formula for the coefficient of thermal conductivity was deduced without taking account of the electric fields ever present in a plasma, and consequently there is some doubt about its validity. Scant attention has been given in recent years to providing more accurate estimates for the coefficient of thermal conductivity, most work having been concerned with plasma instabilities. The lack of a satisfactory theoretical formula for the coefficient of heat conductivity has recently been pointed out once more by L. A. Artsimovich in connection with a comparison of theory based on the "classical" nonturbulent transfer equations with experimental data from Tokamaks. The question of thermal conductivity is clearly of prime importance when appraising the merits of toroidal systems for containing high-temperature plasmas.

In the present paper the conductivity in a toroidal geometry is worked out on the basis of a macroscopic description of the plasma utilizing the classical transfer equations. With the macroscopic approach the increased thermal conductivity is due to the drift and axial "nonmagnetic" flows of heat. The drift flow creates a certain mean temperature gradient in the direction of the binormal to the magnetic axis (in exactly the same manner as charge drift leads to the polarization of the plasma in the same direction). The surfaces T = const intersect the magnetic lines of force as shown in the figure. It can be seen from the figure that the axial temperature gradient of the nonmagnetic heat flow along the magnetic lines of force gives rise in effect to heat transfer in a direction across the isothermals. The expression for the heat flow obtained from the hydrodynamical transfer equations agrees with Budker's estimate based on a microscopic picture of charge motion.

In the present article the heat flow in a toroidal plasma is worked out both for Tokamak geometry and stellarator figure-eight geometry.

The appearance of a temperature gradient due to a drift flow of heat gives rise to a certain additional polarization of the plasma column; this is also taken into account in the present article.

Heat Transfer in Toroidal Geometry

The temperature gradient causes a heat flow which is carried by the charged particles of the plasma. The plasma is situated in a strong magnetic field, and the heat flow consists of a transverse magnetic flow $\mathbf{q}_\perp$, a drift flow q_Λ and a normal flow $q_\parallel$ [2]:

$$\mathbf{q} = \mathbf{q}_\perp + \mathbf{q}_\Lambda + \mathbf{q}_\parallel = -\varkappa_\perp \nabla_\perp T + \frac{5}{2} \cdot \frac{cnT}{zeB^2} [\mathbf{B}\nabla T] - \varkappa_\parallel \nabla_\parallel T, \tag{1}$$

where

$$\varkappa_\perp = \alpha_\perp \frac{nT}{M\omega^2\tau}; \quad \varkappa_\parallel = \alpha_\parallel \frac{nT\tau}{M}; \tag{2}$$

M and ze are the mass and charge of the particles under consideration (for electrons $z = -1$); n, T are their density and temperature; τ is the mean time between collisions; $\omega = zeB/Mc$, is the cyclotron frequency; $\alpha_\perp$ and $\alpha_\parallel$ are numerical coefficients which have the following values for a hydrogen-type plasma: for ions $\alpha_\perp = 2$, $\alpha_\parallel = 3.9$, for electrons $\alpha_\perp = 4.66$, $\alpha_\parallel = 3.16$.

For $\omega\tau \gg 1$ the above three flows differ greatly in magnitude

$$q_\parallel : q_\Lambda : q_\perp \approx 1 : \frac{1}{\omega\tau} : \frac{1}{\omega^2\tau^2}. \tag{3}$$

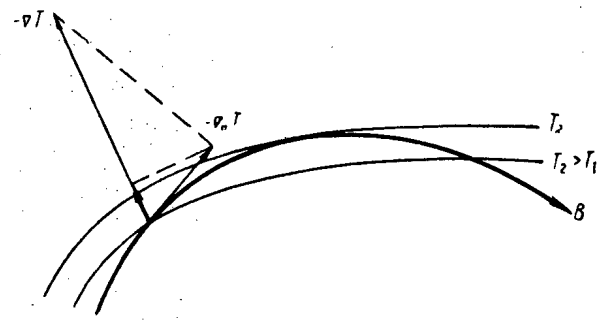

Heat transfer across isothermal by axial nonmagnetic flow.

However, from symmetry considerations, the axial flow in a cylinder is zero: $q_\parallel = 0$. The drift flow in a cylindrical plasma column is unequal to zero, although from the symmetry of the geometry its divergence must identically equal zero; heat transfer can thus only take place due to magnetic flow $q_\perp$.

To estimate the thermal conductivity in a toroidal geometry we expand the solution in terms of the small parameter $1/\omega\tau$.

1. In the zero-th approximation we drop all terms

in the heat transfer equation except that due to axial flow, so that the equation takes on the form

$$\operatorname{div} \mathbf{q}_{\parallel}^{0} = 0. \tag{4}$$

Since $\mathbf{q}_{\parallel}^{0} = h\mathbf{B}$, where $h = -\frac{\varkappa_{\parallel}(\mathbf{B}\Delta T^{\circ})}{B^2}$, this equation can be written in the following form, remembering that vector B is solenoidal

$$\mathbf{B}\nabla h = 0. \tag{5}$$

It follows from Eq. (5) that the function h is constant on the magnetic surface, whose equation we write in the form $\psi(r) = \text{const}$. Hence $h = h(\psi)$. Consequently,

$$\mathbf{B}\nabla T^{0} = \operatorname{div} \mathbf{B}T^{0} = -\frac{B^2}{\varkappa_{\parallel}} h(\psi). \tag{6}$$

On integrating this "magnetic differential equation" [3] with respect to the volume between two infinitely-close toroidal magnetic surfaces, we obtain

$$-h(\psi)\int \frac{B^2}{\varkappa_{\parallel}}\, dV = 0, \tag{7}$$

from which it follows that $h(\psi) = 0$, i.e., $\mathbf{B}\nabla T^{0} = 0$. In this manner, the temperature in the zero-th approximation is constant on the magnetic surface:

$$T^{0} = T^{0}(\psi) \tag{8}$$

and the heat flow $q_{\parallel}^{0} = 0$.

This result is valid for charges of any sort. In a magnetic field the equilibrium equation for the plasma has the form

$$\nabla p = \frac{1}{c}[\mathbf{jB}], \tag{9}$$

from which it follows that plasma pressure is also a "surface quantity" $p = p(\psi)$ [3], and so in the zero-th approximation the plasma density is constant on the magnetic surfaces:

$$n^{0} = n^{0}(\psi). \tag{10}$$

2. In the first approximation in an expansion in $1/\omega_{\tau}$ the heat transfer equation is the same as in the zero-th approximation

$$\operatorname{div} \mathbf{q} = 0. \tag{11}$$

The flow q now consists of a drift flow $\mathbf{q}_{\Lambda}^{0}$, in which we may take $T = T^{0}(\psi)$, and an axial flow $\mathbf{q}_{\parallel}^{(1)}$:

$$\mathbf{q} = \mathbf{q}_{\parallel}^{(1)} + \mathbf{q}_{\Lambda}^{0}. \tag{12}$$

In contrast to the case of cylindrical geometry, the divergence of the drift flow does not equal zero. Indeed, remembering (8) and (10), the expression for V_{0b} can be written in the form

$$\mathbf{q}_{\Lambda}^{0} = \frac{[\mathbf{B}\nabla F]}{B^2}, \tag{13}$$

where $F = F(\psi)$ is some surface quantity. This expression is completely analogous in form to the expression for the drift Larmor current

$$\mathbf{j}_{\perp} = c\frac{[\mathbf{B}\nabla p]}{B^2}. \tag{14}$$

It is known from the equilibrium theory of a plasma in a toroidal geometry that the Larmor current leads to charge separation, which is removed by an axial current $\mathbf{j}_{\parallel}$. The quantity $\mathbf{j}_{\parallel}$ is found from the condition that the total current $\mathbf{j} = \mathbf{j}_{\perp} + \mathbf{j}_{\parallel}$ is continuous:

$$\operatorname{div} \mathbf{j} = 0.$$

In exactly the same way condition (11) determines the value of the axial flow $\mathbf{q}_{||}$, by means of which the drift heat flow is closed. An equation for $\mathbf{q}_{||} = \frac{(\mathbf{qB})\,\mathbf{B}}{B^2}$ can conveniently be found by applying the div operator to the equality

$$\mathbf{q}B^2 = \mathbf{B}(\mathbf{qB}) + [\mathbf{B}\nabla F]. \tag{15}$$

In equilibrium configuration current flows over the magnetic surfaces [$\mathbf{j}\nabla\psi = 0$ from Eq. (9)] and so div [$\mathbf{B}\nabla$F] = rot $\mathbf{B}\nabla$F = 0, and from the condition div $\mathbf{q} = 0$ we obtain the equation

$$(\mathbf{B}\nabla)(\mathbf{qB}) = \mathbf{q}\nabla B^2. \tag{16}$$

Evidently, exactly the same sort of equation can be written for the current density as well. It follows that Eq. (16) is soluble in equilibrium configurations since the equation div $\mathbf{j} = 0$. Clearly $\mathbf{q}_{||}^{(1)}$ will be the same function of $\mathbf{q}_{\Lambda}^{0}$ as $\mathbf{j}_{||}$ is of $\mathbf{j}_{\perp}$.

3. Once we have found $\mathbf{q}_{||}$ from (16) we can find the component of the heat flow normal to the surface T = const

$$q_n = -\mathbf{q}\frac{\nabla T}{|\nabla T|} = \varkappa_{\perp}\frac{(\nabla_{\perp}T)^2}{|\nabla T|} + \varkappa_{||}\frac{(\nabla_{||}T)^2}{|\nabla T|} = \frac{q_{\perp}^2}{\varkappa_{\perp}|\nabla T|} + \frac{q_{||}^2}{\varkappa_{||}|\nabla T|}. \tag{17}$$

The first term of this expression is the normal magnetic heat flow written for uniformity in the same form as the second term, which represents the required additional heat flow due to the toroidal nature of the geometry. The projection of the vector $\mathbf{q}_{||} = -\frac{\varkappa_{||}\mathbf{B}(\mathbf{B}\nabla T)}{B^2}$ on the normal to the isothermal is a fraction $(\mathbf{B}\nabla T)/|\mathbf{B}||\nabla T|$, of the modulus $q_{||}$ that is a quantity of the first order of smallness, while the modulus itself is also a quantity of the first order of smallness. The additional heat flow will thus be a second order quantity, i.e., in the expansion in terms of $1/\omega\tau$ it is of the same order of magnitude as the magnetic heat flow.

Effective Coefficient of Thermal Conductivity in Tokamak and Figure-Eight Stellarator

To make the expression for the additional heat flow more concrete we consider "smooth" toroidal configurations with a circular cross section (Tokamak and figure-eight stellarator). We take the curvature of the system into account in the first approximation, when all toroidal corrections can be written the form [4]

$$f^{(1)} = Re\sum_{n=-\infty}^{\infty} f_n e^{i(\omega - \varkappa_n s)}, \tag{18}$$

where ω is the azimuthal angle reckoned from the toroid generator drawn perpendicular to the cross section; $\varkappa_n = \varkappa_0 - \frac{2\pi}{L}n$ (here $\varkappa_0$ is the mean angle through which the principal normal to the toroid axis is turned about the line ω = const; L is the length of the toroidal system; s is a coordinate reckoned along the toroid. Equation (16) for the Fourier components of the toroidal corrections gives

$$B_{\rho n}\frac{\partial}{\partial\varrho}(q_{\Lambda s}^0 B_s^0 + q_{\Lambda\omega}^0 B_{\omega}^0) + \frac{i}{\varrho}(B_{\omega}^0 - \varkappa_n\varrho B_s^0)(\mathbf{qB})^{(1)} = \frac{2i}{\varrho}(q_{\Lambda\omega}^0 - \varkappa_n\varrho q_{\Lambda s}^0)(B_s^0 B_{sn} + B_{\omega}^0 B_{\omega n}) + \frac{d(B_s^{02} + B_{\omega}^{02})}{d\varrho}q_{\rho n}. \tag{19}$$

The toroidal corrections to the magnetic field appearing here are expressed in terms of the displacement of the magnetic surfaces $\xi_n = -\frac{\psi_n}{(d\psi_0/d\varrho)}$:

$$B_{\rho n} = \frac{i}{\varrho}(B_{\omega}^0 - \varkappa_n\varrho B_s^0)\xi_n; \tag{20}$$

$$B_{\omega n} = -\frac{4\pi}{c}j_s^0\xi_n + \frac{1}{1+\varkappa_n^2\varrho^2}\times\left[\left(k_n\varrho + \frac{\xi_n}{\varrho}\right)(B_{\omega}^0 + \varkappa_n\varrho B_s^0) - (B_{\omega}^0 - \varkappa_n\varrho B_s^0)\frac{d\xi_n}{d\varrho}\right]; \tag{21}$$

$$B_{sn} = \frac{4\pi}{c}j_s^0\xi_n + \frac{1}{1+\varkappa_n^2\varrho^2}\times[k_n\varrho(B_s^0 - \varkappa_n\varrho B_{\omega}^0) - \varkappa_n\xi_n(B_{\omega}^0 + \varkappa_n\varrho B_s^0) + \varkappa_n\varrho(B_{\omega}^0 - \varkappa_n\varrho B_s^0)\frac{d\xi_n}{d\varrho}], \tag{22}$$

where k_n is the Fourier component of the relative curvature of the magnetic axis and is defined in [4]. Equation (20) is a direct consequence of the condition that the lines of force lie on the magnetic surface: $\mathbf{B}\nabla\psi = 0$. It is clear from (15) that, as $F = F(\psi)$, the flow $\mathbf{q}$ satisfies the same condition $\mathbf{q}\nabla\psi = 0$, and consequently its radial component appearing in (19) is expressed by analogy with (20) in the form

$$q_{\rho n} = \frac{i}{\varrho}(q_\omega^0 - \varkappa_n \varrho q_s^0)\,\xi_n. \tag{23}$$

On inserting expressions (20)-(23) into (19) and utilizing the zero-approximation equations

$$\frac{4\pi}{c} j_s^0 = \frac{1}{\varrho}\cdot\frac{d(\varrho B_\omega^0)}{d\varrho}\;;\quad \frac{4\pi}{c} j_\omega^0 = -\frac{dB_s^0}{d\varrho}, \tag{24}$$

the solution of Eq. (16) can be written in the form ($B_0^2 = B_\omega^{02} + B_s^{02}$):

$$(\mathbf{qB}) + \xi_n \frac{d}{d\varrho}(\mathbf{qB})^0 = \frac{2(q_\omega^0 - \varkappa_n \varrho q_s^0)}{(1+\varkappa_n^2\varrho^2)(B_\omega^0 - \varkappa_n \varrho B_s^0)} \times \left[(k_n - \xi_n \varkappa_n^2)\varrho B_0^2 \quad - (B_\omega^0 - \varkappa_n \varrho B_s^0)^2 \frac{d\xi_n}{d\varrho}\right]. \tag{25}$$

In the zero-th approximation the axial flow, as shown above, equals zero: $(\mathbf{qB})^0 = 0$. We simplify expression (25) in future by considering the practically important case $B_\omega^0 \ll B_s^0$, remembering that in order of magnitude $\xi_n \approx k_n\rho$ [4]. If the curvature and twist of the axial line of the toroidal system vary sufficiently smoothly along its length, we may consider that $\varkappa_n\rho \ll 1$ [4]. Under these conditions expression (25) takes on the form

$$(\mathbf{qB})_n = \frac{2k_n \varrho B_0^2}{B_\omega^0 - \varkappa_n \varrho B_s^0}\mathbf{q}_{\Lambda\omega}^0, \tag{26}$$

so that

$$(\mathbf{qB}) = \frac{5cnT^0}{ze}\frac{dT^0}{d\varrho} Re \times \sum_{n=-\infty}^{\infty} \frac{k_n \varrho B_s^0}{B_\omega^0 - \varkappa_n \varrho B_s^0} e^{i(\omega - \varkappa_n s)}. \tag{27}$$

On inserting the expression for the axial flow $\mathbf{qB}/|\mathbf{B}|$ into formula (17) giving the flow normal to the isothermals, we see that the additional "toroidal" heat flow is nonuniformly distributed along the surfaces $T = \text{const}$. For example, in an axially symmetric toroid (Tokamak), when $k_n = 0$ for $n \neq 0$, $\varkappa_0 = 0$, this heat flow is distributed according to a $\cos^2\omega$ law, i.e., it is concentrated mainly in the equatorial plane, in conformity with the microscopic picture. Along the magnetic surface the temperature is rapidly equalized by the large drift flow of heat, so that irregularity in the distribution of the toroidal flow will not substantially affect the temperature distribution on the magnetic surfaces. It is thus useful to average the expression for toroidal flow on each magnetic surface, after which the thermal conductivity in a toroid reduces to that in a cylinder with a certain effective coefficient of transerve thermal conductivity. Averaging is carried out according to the formula

$$\left\langle Re \sum_{n=-\infty}^{\infty} f_n e^{i(\omega - \varkappa_n s)} Re \sum_{n=-\infty}^{\infty} g_n e^{i(\omega - \varkappa_n s)} \right\rangle = \frac{1}{2} Re \sum_{n=-\infty}^{\infty} f_n g_n^*. \tag{28}$$

We obtain as a result

$$\langle q_\rho \rangle = -\varkappa_{\text{eff}} \frac{dT^0}{d\varrho}, \tag{29}$$

$$\varkappa_{\text{eff}} = \varkappa_\perp \left(1 + \frac{25}{2\alpha_\perp \alpha_\parallel} \sum_{n=-\infty}^{\infty} \frac{|k_n|^2 \varrho^2 B_s^{02}}{(B_\omega^0 - \varkappa_n \varrho B_s^0)^2}\right). \tag{30}$$

In the case of a hydrogen-type plasma in a Tokamak ($k_n = 0$ for $n \neq 0$, $k_0 = 1/R$), we find for the effective coefficient of ionic thermal conductivity

$$\varkappa_{\text{eff}} = \frac{2n_i T_i}{M\omega_i^2 \tau_i}\left(1 + 1.6\frac{\varrho^2 B_s^{02}}{R^2 B_\omega^{02}}\right). \tag{31}$$

Experiments show that the discharge is stable if $\rho^2 B_s^2 / R^2 B_\omega^{02} \gg 1$. In this case heat loss is determined only by the magnetic field of the current

$$\langle q_\rho \rangle = -\frac{3.2 M c^2 \varrho^2 n T_i}{c^2 B_\omega^{02} R^2 \tau_i} \cdot \frac{dT_i}{d\varrho} . \tag{32}$$

By equating this heat flow to the Joule heat dissipation $j^2/\sigma_{||}$, we can find a formula for the maximum attainable temperature in a plasma column with radii R and a for Joule heating:

$$\frac{8\pi p}{B_\omega^2(a)} \approx 2.2 \frac{R}{a} \left(\frac{2m}{M} \right)^{1/4} \approx 0.35 \frac{R}{a} \tag{33}$$

(m and M are the electron and ion masses).

For the stellarator the effective coefficient of ionic thermal conductivity is given by formula (30) for $B_\omega^0 = 0$:

$$\varkappa_{\text{eff}} = \varkappa_\perp \left(1 + 1.6 \sum_{n=-\infty}^{\infty} \left| \frac{k_n}{\varkappa_n} \right|^2 \right) . \tag{34}$$

For a figure-eight stellarator formed from arcs of circles [4] the ratio $k_n/\varkappa_n$ depends on the angle α_0 between the planes of the arcs, and decreases with α_0. For a figure-eight stellerator consisting of four semicircles and α_0 = 3/10, for example, it works out that $\sum_{n=-\infty}^{\infty} |k_n/\varkappa_n|^2 = 6.94$. The limiting value of this sum for $\alpha_0 \to 0$, identical for both the configurations considered in [4], equals

$$\sum_{n=-\infty}^{\infty} \left| \frac{k_n}{\varkappa_n} \right|^2 = \frac{2}{3} \pi^2 \approx 6.67. \tag{35}$$

Thus, in a stellarator with no axial current, the coefficient of thermal conductivity depends on the magnetic field in the same way as in a cylinder, although in the best case its numerical value is an order greater than for cylindrical geometry.

It is appropriate to recall here that in a toroidal geometry the flux of particles from an equilibrium configuration exceeds that from a cylindrical plasma column. The diffusion flux in a cylindrical plasma column contained by an axial magnetic field is related to the diamagnetic current dissipation [3, 5]:

$$(nv)_{\text{diff}} \sim \int \frac{j_\omega^{02}}{\sigma_\perp} dV. \tag{36}$$

The additional flux due to particle drift in a toroidal geometry is

$$(nv)_{\text{add}} \sim \int \frac{j_{||}^2}{\sigma_{||}} dV. \tag{37}$$

If we associate a diffusion factor $D_\perp$ with diffusion flow in a cylindrical geometry, then in a toroidal geometry we have an effective diffusion factor

$$D_{\text{eff}} = D_\perp \left[1 + \int (j_{||}^2/\sigma_{||})\, dV \Big/ \int (j_\perp^2/\sigma_\perp)\, dV \right] . \tag{38}$$

For a figure-eight stellarator the axial current density for $B_\omega^0 = 0$ is given by a formula similar to (26):

$$j_{||} = -\frac{2k_n}{\varkappa_n} j_\omega^0 = -\frac{2k_n}{\varkappa_n} j_\perp . \tag{39}$$

Consequently,

$$D_{\text{eff}} = D_\perp \left(1 + 2 \sum_{n=-\infty}^{\infty} \left| \frac{k_n}{\varkappa_n} \right|^2 \right) . \tag{40}$$

The effective diffusion factor in a toroidal geometry is at least $1 + 2 \times 6.67 \approx 14$ times greater than in a field with straight lines of force.

Plasma Polarization

The nonuniformity of the charged-particle temperature distribution on the magnetic surfaces leads to a nonuniform pressure distribution. The pressure gradient of charged particles of a given sort that appears on the magnetic surfaces can be supported only by an electrostatic field

$$\mathbf{E}^{(1)} = -\nabla\varphi^{(1)}. \tag{41}$$

The magnitude of this field can be found from the axial projection of the generalized Ohm's law; for a hydrogen-type plasma this has the form [5]

$$(\mathbf{jB}) = \varsigma_{||}\mathbf{B}\left(\mathbf{E} - \frac{1}{en}\nabla p_i + \frac{0.7}{e}\nabla T_e\right). \tag{42}$$

The variable part of the temperature on a magnetic surface $\delta T = T - T^0(\psi)$ can be expressed in terms of the axial flow found above $\mathbf{B}\nabla\delta T = -(\mathbf{Bq})/\varkappa_{||}$. For the "smooth" toroidal configurations already considered

$$\delta T_n = i\frac{\varrho}{B^0_\omega - \varkappa_n \varrho B^0_s}\cdot\frac{(\mathbf{qB})_n}{\varkappa_{||}} = \frac{2ik_n\varrho^2 B_0^2}{\varkappa_{||}(B^0_\omega - \varkappa_n\varrho B^0_s)^2}\, q^0_{\Lambda\omega}. \tag{43}$$

Since the coefficient of axial thermal conductivity is greater for electrons than for ions (by a factor of about $\sqrt{M/m}$), as far as electrons are concerned we may ignore the lack of constancy in the temperature along the magnetic surface. By utilizing δT_i to find the excess ion pressure on the magnetic surface, we can find from (42) the correction to the electrostatic potential $\varphi^{(1)}$. The correction to the axial current appearing in (42) is found in the same way as the correction to the heat flow (25).

For a stellarator with $B^0_\omega = 0$ the Fourier components of potential $\varphi^{(1)}$ turn out to be

$$\varphi^{(1)}_n = \varphi_{qn} + \varphi_{jn} = -2i\frac{k_n}{\varkappa_n^2}\left(\frac{T_e}{T_e + T_i}\cdot\frac{q^0_{\Lambda\omega}}{e\varkappa_{||}} - \frac{j^0_\omega}{\sigma_{||}}\right). \tag{44}$$

The second term in this expression φ_{jn} represents the potential maintaining the current that prevents the charges from separating due to the induced Larmor current (14). The potential φ_{qn} connected with the redistribution of temperature can readily be seen to be for $T_e \approx T_i\sqrt{M/N}$ times greater than potential φ_{jn}.

A similar result is found for the Tokamak. In the steady state, when the rotational electric field is distributed according to the law $E_s = \dfrac{E_{s0}}{\left(1 - \frac{\varrho}{R}\cos\omega\right)}$, we find that with the condition $B^0_s \gg B^0_\omega$ the potential turns out to be

$$\varphi^{(1)}(\varrho,\ \omega) = 2\frac{\varrho^2 B_s^{02}}{RB_\omega^{02}} \times \left[\frac{T_e}{T_e + T_i}\cdot\frac{q^0_{\Lambda\omega}}{e\varkappa_{||}} - \frac{j^0_\omega}{\sigma_{||}} + E_{s0}\frac{B_\omega}{B^0_s}\right]\sin\omega. \tag{45}$$

I should like to take this opportunity of thanking L. A. Artsimovich for suggesting the problem considered in this article.

LITERATURE CITED

1. G. I. Budker, Plasma Physics and Controlled Thermo-Nuclear Reactions [in Russian], Moscow Acad. Sci. USSR Press, Vol. 1 (1958), p. 66.
2. S. I. Braginskii, Problems of Plasma Theory [in Russian], Gosatomizdat, Moscow (1963), ed. 1, p. 183.
3. M. Kruskal and R. Kulsrud, Phys. Fluids, 1, 265 (1958).
4. V. D. Shafranov, Nuclear Synthesis, 4, 232 (1964).
5. V. D. Shafranov, Problems of Plasma Theory [in Russian], Gosatomizdat, Moscow (1963), ed. 2, p. 92.

INCOHERENT INSTABILITY OF BETATRON OSCILLATIONS IN ACCELERATORS AND STORAGE RINGS

(UDC 621.384.60)

V. I. Balbekov and A. A. Kolomenskii

Translated from Atomnaya Énergiya, Vol. 19, No. 2,
pp. 126-131, August, 1965
Original article submitted August 19, 1964

The problem of the transverse instability of a beam of charged particles circulating in a focusing system of the cyclical-accelerator or storage-ring type is considered. A dispersion equation for coherent vertical oscillations of the center of gravity of the beam is obtained and examined. It is shown that finite conductivity of the vacuum-chamber walls may lead to a dangerous instability. Conditions for the suppression of this are given and the maximum allowable number of particles circulating in the chamber is estimated.

Not long ago there appeared some experimental results which indicated the possibility of coherent vertical oscillations being excited in a charged-particle beam circulating in an accelerator [1]. Instability develops for a particular value of beam current, peculiar to the accelerator and accelerating conditions in question, and further increase of current thereupon becomes impossible, since the deviation of the beam from the center of the vacuum chamber leads to a loss of particles. This phenomenon is especially dangerous in storage rings and also in accelerators on injection. This paper is devoted to a theoretical study of the possible cause of the instability in question, the evaluation of its development time, and the conditions for its suppression.

Usually the radius of curvature of the vacuum chamber of an accelerator considerably exceeds its transverse dimensions, so that the chamber may be regarded as a cylinder with generator directed along the z axis. In this paper we suppose that the cross section of the chamber has the form of a rectangle with sides a and b. The coordinates of the chamber walls are $x = a/2$; $x = -a/2$, $y = 0$, and $y = b$, where x and y are the vertical and radial coordinates respectively.

Let a beam of particles move in the chamber, each particle having charge e and mass m. Apart from the space-charge field, the particles are acted on by an external force eG_{ext}. Usually the relative change in the focusing and guiding fields and in the energy of the particles takes place slowly, so that we may suppose that the external field does not depend on time and its longitudinal component (accelerating field) is zero.

In order to exclude radial betatron oscillations from consideration, we shall average over the corresponding coordinate and assume that the dependence of the charge density on radius (i.e., on y) remains unaltered.

Obtaining the Dispersion Equation

We shall start from the kinetic equation for the particle-distribution function $F(\mathbf{r}, \mathbf{p}, t)$:

$$\frac{\partial F}{\partial t} + \mathbf{v}\frac{\partial F}{\partial \mathbf{r}} + e\left(\mathbf{G}_{ext} + \mathfrak{E} + \frac{1}{c}[\mathbf{v}\mathcal{H}]\right)\frac{\partial F}{\partial \mathbf{p}} = 0, \tag{1}$$

where $\mathfrak{E}$ and $\mathcal{H}$ are the electric and magnetic fields created by the beam. In order to elucidate the question of the stability of the equilibrium solution F_0 we put

$$F = F_0 + f; \quad \mathfrak{E} = \mathbf{E}_0 + \mathbf{E}; \quad \mathcal{H} = \mathbf{H}_0 + \mathbf{H}, \tag{2}$$

where f, **E**, and **H** are small additions to the equilibrium solution, and we neglect second-order terms in (1). Then we obtain an equation for f:

$$\frac{\partial f}{\partial t}+\mathbf{v}\frac{\partial f}{\partial \mathbf{r}}+e\mathbf{G}_0\frac{\partial f}{\partial \mathbf{p}}+e\mathbf{G}\frac{\partial F_0}{\partial \mathbf{p}}=0, \tag{3}$$

where

$$\mathbf{G}_0=\mathbf{G}_{\text{ext}}+\mathbf{E}_0+\frac{1}{c}[\mathbf{vH}_0];\ \ \mathbf{G}=\mathbf{E}+\frac{1}{c}[\mathbf{vH}]. \tag{4}$$

In order to solve (3) we assume that as $t\to-\infty$ the nonequilibrium increment vanishes,* i.e., we confine ourselves to solutions not decreasing with increasing t, which corresponds to the character of the problem. Then from (3) we obtain

$$f(\xi,\ t)=-e\int_0^\infty \frac{\partial F_0}{\partial \mathbf{p}}\mathbf{G}\Big(\xi_0(\xi,\tau),\ t-\tau\Big)\,d\tau, \tag{5}$$

where $\xi = x, y, z, p_x, p_y, p_z$ are coordinates and momentum components of a particle having initial values ξ_0 and moving under the influence of a force $e\mathbf{G}_0$ created by the external field and the field of the equilibrium beam.

Let us assume that the equilibrium function F_0, and hence E_0 and H_0 are independent of z and t and transform in (5) to the Fourier image with respect to these variables:

$$f_{k\omega}(\xi)=-e\int_0^\infty e^{i(\omega-kv_z)\tau}\frac{\partial F_0}{\partial \mathbf{p}}\mathbf{G}_{k\omega}\Big(\xi_0(\xi,\tau)\Big)\,d\tau. \tag{6}$$

On the basis of the above remarks we may suppose that $\mathrm{Im}\omega > 0$. In order to simplify writing, the indices k and ω will subsequently be omitted.

The motion of the beam in a vertical direction has a complex nature (there may be oscillations of the beam as a whole and also of its dimensions, shape, etc.). In this paper we mainly consider oscillations of the center of gravity of the beam, i.e., the quantity

$$\bar{x}_{C.G.}=\frac{1}{b}\int f(\xi)\,x\,dx\,dy\,dp_x\,dp_y\,dp_z=\frac{\bar{d}}{e}, \tag{7}$$

where $\bar{d}$ is the x component of the dipole moment of the beam averaged over y. From expressions (6) and (7), transforming to integration over the variables x_0, y_0, p_{x0} and p_{y0}, we obtain

$$\bar{d}=-\frac{e^2}{b}\int_{-\infty}^{\infty}dp_z\int_0^\infty e^{i(\omega-kv_z)\tau}\,d\tau\times\int\frac{\partial F_0}{\partial \mathbf{p}_0}\mathbf{G}(\xi_0)\,x(\xi_0,\tau)\,dx_0\,dy_0\,dp_{x0}\,dp_{y0}. \tag{8}$$

We shall consider the betatron oscillations as linear:

$$x(\xi_0,\tau)=x_0\cos\omega_0\tau+\frac{v_{x_0}}{\omega_0}\sin\omega_0\tau, \tag{8'}$$

where $\omega_0(p_z)$ is the frequency of betatron oscillations, allowing for the effect of the field of the equilibrium beam. We note that the stationary function F_0 can only depend on the amplitude of the betatron oscillations and is hence an even function of x, p_x, p_y. Hence the terms containing v_{y0}, in the same way as $\partial F_0/\partial p_{y0}$, vanish on integrating over $dy_0\,dp_{y0}$. Moreover we assume that the amplitude of the betatron oscillations in the equilibrium beam $(x_0^2+\frac{v_{x0}^2}{\omega_0^2})^{1/2}$ is small in comparison with the dimensions of the chamber, so that we can neglect the term containing $\partial F_0/\partial p_z$. The term left in expression (8), proportional to $\partial F_0/\partial p_{x0}$, is now integrated with respect to dp_{x0}, using (8') and considering that $v_x, v_y \ll c$. Then we calculate the integral with respect to $d\tau$ and obtain

$$\bar{d}=-\frac{e^2N_1}{m\gamma b}\int_{-\infty}^{\infty}\frac{g(p_z)\,dp_z}{(\omega-kv_z)^2-\omega_0^2}\int f_0(x,\ y\times\Big(E_x-\frac{v_z}{c}H_y\Big)\,dx\,dy, \tag{9}$$

where N_1 is the number of particles coming into unit length of the chamber, γ is the relativistic factor, functions

* The so-called adiabatic inclusion of the field (see, for example, [2]).

$g(p_z)$ and $f_0(x, y)$, describing the particle distribution with respect to longitudinal momentum and cross section respectively, are normalized to unity, and f_0 is an even function of x.

In order to avoid cumbersome calculations, we suppose first that the radial distribution of charge has the form

$$f_0(x, y) = \frac{\pi}{2b} \varrho_0(x) \sin \frac{\pi y}{b}. \tag{10}$$

Substituting (10) into (9) and integrating with respect to dy, we find

$$d = -\frac{\pi^2 e^2 N_1}{8m\gamma b} \int_{-\infty}^{\infty} \frac{g(p_z)\, dp_z}{(\omega - kv_z)^2 - \omega_0^2} \times \int_{-\frac{a}{2}}^{\frac{a}{2}} \varrho_0(x) \left(E_x - \frac{v_z}{c} H_y \right) dx, \tag{11}$$

where d, E_x, H_y are the values of the respective variables for y = b/2.

The field components in (11) may be expressed in terms of the surface charge density and multipole moments. However, for a fine beam, all the moments beginning from the quadrupole are negligibly small. It is also not hard to see that the oscillations of the center of gravity of the beam in a vertical direction are independent of the surface charge density. In fact, for a beam position symmetrical with respect to the chamber walls, the field components of the charged plane E_x and H_y change sign on passing through the center of the beam and hence do not lead to its displacement. Hence it is enough to find just that part of the beam field which is determined by its dipole moment. If the average longitudinal particle velocity is $v_0 = \beta c$, the corresponding densities of charge and current will be

$$\varrho = -d\delta'(x);\ j_x = -i(\omega - kv_0)\, d\delta(x);\ j_y = 0;\ j_z = -v_0 d\delta'(x). \tag{12}$$

Actually j_y is essentially zero, but this does not matter, as on averaging over y, all the terms connected with j_y vanish.

At the chamber walls we must satisfy the following boundary conditions for the tangential components of field

$$\mathbf{E}_t|_\Sigma = \zeta [\mathbf{H}_t \mathbf{n}]|_\Sigma, \tag{13}$$

where ζ is the surface impedance of the wall, n the external normal to the surface of the chamber (see, for example, [3]). We shall suppose that the vertical walls of the chamber are ideally conducting; in this case expression (13) transforms into the ordinary condition that the tangential component of the electric field vanishes. For the horizontal walls (13) has the form

$$E_z\left(\pm\frac{a}{2}\right) = \mp \zeta H_y\left(\pm\frac{a}{2}\right);\ E_y\left(\pm\frac{a}{2}\right) = \pm \zeta H_z\left(\pm\frac{a}{2}\right). \tag{14}$$

Solving Maxwell's equations with current and charge density (12) and boundary conditions (14) and putting the result into (11), we obtain the dispersion equation for the vertical oscillations of the center of gravity of the fine beam:

$$1 = \frac{\pi^3 e^2 N_1}{4m\gamma b} \int_{-\infty}^{\infty} \frac{g(p_z)\, dp_z}{(\omega - kv_z)^2 - \omega_0^2} \left\{ \frac{2}{\gamma^2 x_0} + \varkappa \left(\frac{\pi\beta}{b\lambda}\right)^2 \times \frac{\frac{\omega}{c}\cos\frac{\varkappa a}{2} - i\varkappa\zeta \sin\frac{\varkappa a}{2}}{\frac{\omega}{c}\sin\frac{\varkappa a}{2} + i\varkappa\zeta\cos\frac{\varkappa a}{2}} + \frac{1}{\lambda^2}\left(\lambda^2 - \frac{\omega k\beta}{c}\right)^2 \right.$$

$$\left. \times \frac{\cos\frac{\varkappa a}{2} - \frac{i\omega\zeta}{\varkappa c}\sin\frac{\varkappa a}{2}}{\varkappa \sin\frac{\varkappa a}{2} + \frac{i\omega\zeta}{c}\cos\frac{\varkappa a}{2}} \right\}, \tag{15}$$

where $\varkappa^2 = \frac{\omega^2}{c^2} - k^2 - \frac{\pi^2}{b^2} = \frac{\omega^2}{c^2} - \lambda^2$; x_0 is the average amplitude of the betatron oscillations in the equilibrium beam.

In the same way we can obtain the dispersion equation of longitudinal oscillations for a finite conductivity of the chamber walls (this question was considered earlier [4]).

Study of the Dispersion Equation of the Vertical Oscillations

First let us consider equation (15) in a range of frequencies farily well-removed from the eigenfrequencies of the chamber, so that the denominator of the expression on the righthand side does not vanish. Considering that $|\varkappa x_0| \ll 1$ and for metals also $|\zeta| \ll 1$, and leaving in (15) only the largest real and imaginary terms, we obtain

$$1 = \frac{\pi^3 e^2}{2m\gamma} \int_{-\infty}^{\infty} \frac{g(p_z)\,dp_z}{(\omega - kv_z)^2 - \omega_0^2} \left\{ \frac{N_0}{\gamma^2} - \frac{icN_1\zeta}{2b\omega\lambda^2\varkappa^2 \sin^2 \frac{\varkappa a}{2}} \times \left[\frac{\omega^2}{c^2} \left(\lambda^2 - \frac{\omega k\beta}{c} \right)^2 + \left(\frac{\pi\varkappa^2\beta}{b} \right)^2 \right] \right\}, \tag{16}$$

where $N_0 = N_1/bx_0$ is the volume density of particles averaged over the beam cross section.

Let us take a distribution function with respect to longitudinal momentum

$$g(p_z) = \frac{\Delta}{\pi} \cdot \frac{1}{(p_z - p_0)^2 + \Delta^2}, \tag{17}$$

where p_0 is the momentum corresponding to velocity v_0 and Δ characterizes the energy spread in the beam. We shall suppose that $\mathrm{Im}\omega > 0$ and ω_0 is a slowly-varying function of p_z. After calculating the integral in (16) on these assumptions, we obtain

$$(\omega - kv_0 + i|k\Delta v|)^2 - \left(\omega_{00} - \frac{i}{k}|k\Delta v| \frac{d\omega_{00}}{dv} \right)^2$$

$$= \frac{\pi^3 e^2 N_0}{2m\gamma^3} - \frac{i\pi^3 e^2 N_1}{4m\gamma b} \cdot \frac{1}{\lambda^2\varkappa^2 \sin^2 \frac{\varkappa a}{2}} \times \frac{c\zeta}{\omega} \left[\frac{\omega^2}{c^2} \left(\lambda^2 - \frac{\omega k\beta}{c} \right)^2 + \left(\frac{\pi\varkappa^2\beta}{b} \right)^2 \right], \tag{18}$$

where Δv is the velocity spread corresponding to the energy spread Δ; $\omega_{00} = \omega_0(v_0)$; $\frac{d\omega_{00}}{dv} = \frac{d\omega_0}{dv}(v_0)$.

In practice the density of the particles is always fairly small, so that in equation (18) ω_{00}^2 greatly exceeds the righthand side. Moreover, if $\left|\frac{d\omega_{00}}{dv}\right| \ll \frac{\omega_{00}}{\Delta v}$, on the right-hand side we may put $\omega = \omega_1 = kv_0 \pm \omega_{00}$, $\varkappa^2 = \varkappa_1^2 = \frac{\omega_1^2}{c^2} - \lambda^2$, which gives

$$\omega = kv_0 \pm \omega_{00} \left(1 + \frac{\pi^3 e^2 N_0}{4m\gamma^3\omega_{00}^2} \right) - i \left| k\Delta v \left(1 \pm \frac{1}{k} \cdot \frac{d\omega_{00}}{dv} \right) \right|$$

$$\mp \frac{i\pi^3 e^2 c N_1}{8m\gamma b\omega_{00}} \cdot \frac{1}{\lambda^2\varkappa_1^2 \sin^2 \frac{\varkappa_1 a}{2}} \times \left[\frac{\omega_1^2}{c^2} \left(\lambda^2 - \frac{\omega_1 k\beta}{c} \right)^2 + \left(\frac{\pi\varkappa_1^2\beta}{b} \right)^2 \right] \frac{\zeta}{\omega_1}. \tag{19}$$

As we know, the quantity $\mathrm{Re}\zeta$ is always positive (see, for example, [3]). Remembering this, it is not difficult to see that the imaginary part of the frequency can only be positive (meaning an unstable beam) on satisfying the condition

$$|kv_0| > \omega_{00}. \tag{20}$$

These waves propagate in the direction of motion of the beam with a phase velocity smaller than v_0. Here $kv_0 > 0$ corresponds to the lower sign in (19) and $kv_0 < 0$ to the upper sign. Hence in the region of instability $|\omega| \approx |kv_0| - \omega_{00}$. It is thus clear that $\varkappa_1^2 < 0$, i.e., $\varkappa_1$ is an imaginary quantity. Hence in the denominator of the imaginary part of formula (18) we have a quantity $\mathrm{sh}^2 \frac{|\varkappa|a}{2}$ rising rapidly with increasing $|k|$. It is easy to see that for small values of k the imaginary correction to the frequency reaches a maximum, and therefore it is sufficient to consider the dispersion equation for waves the length of which substantially exceeds the transverse dimensions of the chamber $k \sim \frac{\omega}{c} b^{-1}$. Thus $\varkappa \approx i\lambda \approx i\frac{\pi}{c}$ and formula (19) simplifies considerably. Let us consider this case in more detail.

For metals the surface importance may be expressed in terms of the conductivity σ and magnetic permeability μ:

$$\zeta = (1 - i)\sqrt{\frac{|\omega|\mu}{8\pi\sigma}} \tag{21}$$

From (19) and (21) for long waves we obtain

$$|Re\omega| = |kv_0| - \omega_{00}\left(1 + \frac{\pi^3 e^2 N_0}{4m\gamma^3\omega_{00}^2}\right); \tag{22'}$$

$$Im\omega = -\left|k\Delta v\left(1 - \frac{1}{|k|}\cdot\frac{d\omega_{00}}{dv}\right)\right| + \left(\frac{\pi}{2}\right)^{\frac{9}{2}}\frac{\beta^2}{\gamma}\cdot\frac{e^2cN_1\,\mathrm{sh}^{-2}\frac{\pi a}{2b}\sqrt{\mu}}{m\omega_{00}b^3\sqrt{\sigma_0(|kv_0| - \omega_{00})}}. \tag{22''}$$

This solution relates to the region in which instability is possible, i.e., it is assumed that condition (20) is satisfied. The quantity $|\mathrm{Re}\omega|$ gives the frequency of perturbation. It follows from (22) that this quantity is determined mainly by the volume density of particles and depends little on the shape of the chamber. The imaginary part of the frequency characterizes the degree of instability of the beam, since the time for the instability to develop is $T_{instab} = (\mathrm{Im}\omega)^{-1}$. We see that $\mathrm{Im}\omega$ is determined only by the linear density of the particles and falls with increasing size of the chamber. In a chamber with idealy-conducting walls instability does not arise on the approximation considered.

As we should expect, the presence of energy spread favors the stabilization of the beam. Qualitatively this is explained by the fact that the resonance conditions $|\omega| = |\mathrm{kv}_0| - \omega_{00}$ cannot be satisfied for all the particles.

Expressions (22) with condition (20) are also true when ω_0 is proportional to v_z, as occurs in accelerators with similar orbits [5].

Let us now consider the general case in which the radial distribution of charge is given by the derivative of the normalized function h(y), vanishing for y = 0 and b. Expanding h(y) into a Fourier series, as before calculating the field of the system and putting the result into (9), we obtain the dispersion equation of the vertical oscillations, the solution of which, for long waves and energy distribution (17), takes the form

$$|Re\,\omega| = |kv_0| - \omega_{00}\left(1 + \frac{\pi e^2 b^2 N_0}{m\gamma^3\omega_{00}^2}\sum_{l=1}^{\infty}\alpha_l^2\right); \tag{23'}$$

$$Im\omega = -\left|k\Delta v\left(1 - \frac{1}{|k|}\cdot\frac{d\omega_{00}}{dv}\right)\right| + \left(\frac{\pi}{2}\right)^{\frac{5}{2}}\frac{\beta^2}{\gamma}\cdot\frac{e^2cN_1\sqrt{\mu}}{mb\omega_{00}\sqrt{\sigma(|kv_0| - \omega_{00})}}\sum_{l=1}^{\infty}\frac{l_2\alpha_l^2}{\mathrm{sh}^2\frac{\pi al}{2b}}, \tag{23''}$$

where a_l is the harmonic of function h(y). The condition of instability (20) is also satisfied in this case.

Let us apply the results obtained to a toroidal chamber with radius of the equilibrium orbit $R \gg b$. For this we put into (23) $|k| = n/R$ $(n = 0, 1, 2, \ldots)$; $v_0 = R\Omega$ where Ω is the angular velocity of the particle $\Delta v = R\Delta\Omega$; $\omega_{00} = v\Omega$,

$$\frac{d\omega_{00}}{dv} = \frac{v}{R} + \frac{\gamma^2}{R}\cdot\frac{dv}{d\ln p_0}.$$

Then we obtain

$$|Re\,\omega| = \Omega\left\{n - v\left(1 + \frac{\pi e^2 b^2 V_0}{m\gamma^3 v^2\Omega^2}\sum_{l=1}^{\infty}\alpha_l^2\right)\right\}; \tag{24'}$$

$$Im\,\omega = -\Delta\Omega\left|n - v - \gamma^2\frac{dv}{d\ln p_0}\right| + \left(\frac{\pi}{2}\right)^{\frac{5}{2}}\frac{e^2R\sqrt{\beta}N_1}{m\gamma bv}\sqrt{\frac{R\mu}{c\sigma(|n| - v)}}\sum_{l=1}^{\infty}\frac{l^2\alpha_l^2}{\mathrm{sh}^2\frac{\pi al}{2b}}, \tag{24''}$$

and instead of instability condition (20) we shall have the condition $|n| > v$.

As we see from (24'), the instability develops the more rapidly, the smaller $n - v > 0$, i.e., the smaller the perturbation frequency. It also follows from (24') that in the absence of an accelerating field $\mathrm{Im}\omega$ reaches a maximum for $\beta = 1/\sqrt{3}$, which corresponds to energy values of 210 MeV for protons and 115 keV for electrons. It should be noted that in a toroidal chamber the distribution of particles with respect to y (radius) is connected with the momentum distribution, since the radius of the equilibrium orbit is determined by the energy of the particle.

The quantity Imω depends linearly on the density of particles and becomes positive only for a fairly large N_1. Equating Imω to zero, we may estimate the maximum permissible (from the point of view of vertical stability) number of particles in the chamber:

$$N_{\max} = \Delta\Omega \left| n - \nu - \gamma^2 \frac{d\nu}{d \ln p_0} \right|^{3/2} \left(\frac{\pi}{2}\right)^{5/2} \times \frac{2\pi m b \nu}{e^2} \cdot \frac{\gamma}{\sqrt{\beta}} \sqrt{\frac{c\sigma}{R\mu}} \left(\sum_{l=1}^{\infty} \frac{l^2 \alpha_l^2}{\mathrm{sh}^2 \frac{\pi a l}{2b}} \right)^{-1}. \qquad (25)$$

In order to obtain as large as possible a value of N_{max} it is advantageous for the betatron frequency to exceed the nearest whole number (for example, $\nu = 7.25$ is better than $\nu = 7.75$). According to expression (25), for a whole-number value of ν, Imω formally passes to infinity. This means that the method used for solving the dispersion equation is unsuitable in this case, and hence we can only say that the development time of the instability becomes very small. In actual fact ν cannot equal a whole number, since this is inadmissible from the point of view of an approach to dangerous resonances, and we shall therefore not consider this case in any more detail.

The coefficients a_l depend on $\Delta\Omega$ as a result of the earlier-noted connection between the radial distribution and the energy. However, for a small radial spread of particles this dependence is weak, so that we may consider that N_{max} is measured approximately proportional to $\Delta\Omega$. In this case the sum of the series in formulas (23"), (24"), and (25) equals $0.85\ b/a^3$ with an accuracy adequate for the estimates.

In addition to this we considered the case in which the left-hand side of the dispersion equation (22) passed through zero, i.e., when the frequencies were close to the eigenfrequencies of the chamber. The investigation showed that for a finite value of σ the imaginary part of the frequency was negative (i.e., oscillations were attenuated) as a result of strong absorption of energy in the walls. For $\sigma = 0$ the amplitude of the oscillations did not depend on time.

The left-hand side of equation (22) can only vanish with small ζ in the case in which $\varkappa^2 = \frac{\omega^2}{c^2} - k^2 - \frac{\pi^2}{b^2} \geq 0$. The phase velocity of such waves exceeds the velocity of light. Thus only the emission of slow waves can lead to beam instability.

CONCLUSIONS

Our study has shown that, for a finite conductivity of the chamber walls in an accelerator or storage ring, growing vertical oscillations of the center of gravity of the beam may develop. Dangerous frequencies are $|\omega| = (n - \nu)\Omega$ (where $n = 1, 2, \ldots$); hence instability is only possible for $n > \nu$, the development time of the instability rising with increasing harmonic number. Harmonics with $n < \nu$ are stabilized as a result of the finite conductivity. Increasing the energy spread in the beam may suppress instability.

The MURA group in the USA has made experiments on instability in an electron ring phasotron with maximum energy 50 MeV at $\nu = 2.81$ [1]. Harmonics with n from -1 to $+6$ were studied. Spontaneous beam instability was found for n values of 3 and 4. Under the influence of an external sinusoidal-voltage pulse with corresponding frequency, the fifth harmonic was excited, which agrees with the results obtained above. The oscillations were coherent, the frequency values calculated from the formula $f = f_0(n - \nu)$ always exceeding the experimental results. The average value of this excess was 0.26 MeV, which agrees with (23') if we take the reasonable value of $\sim 10^{10}$ cm^{-3} for N_0.

On the basis of the results obtained we may estimate the maximum number of particles admissible for injection from the point of view of coherent vertical stability. Thus for the synchrophasotron of the Combined Institute of Nuclear Studies [6] we obtain the value $N_{max} \sim 10^{17}\delta$ where δ is the relative energy spread. For $\delta = 10^{-3}$ this gives $N_{max} \sim 10^{14}$. For the electron ring phasotron of the Physical Institute of the Academy of Sciences, USSR [7] we obtain $N_{max} \sim 10^{12}$, which corresponds to a circulating beam current around 3 A.

After this article had been sent to press, another article [8] was published; in this the coherent instability of betatron oscillations was examined by another method.

LITERATURE CITED

1. C. Curtis, et. al, In the Book "Transactions of the International Conference of Accelerators" [Russian Translation], Dubna (1963), Atomizdat, Moscow (1964), p. 620.

2. V. P. Silin and A. A. Rukhadze, Electromagnetic Properties of Plasma and Plasma-like Substances [in Russian], Atomizdat, Moscow (1961), p. 78.
3. L. D. Landau and E. M. Lifshits, Electrodynamics of Continuous Media § 67 [in Russian], Fizmatgiz, Moscow (1957).
4. A. A. Kolomenskii, Atomnaya Énergiya, 12, 7 (1964).
5. A. A. Kolomenskii, Atomnaya Énergiya, 3, 492 (1957).
6. A. A. Kolomenskii and A. N. Lebedev, Theory of Cyclical Accelerators [in Russian], Fizmatgiz, Moscow (1962), pp. 23, 295.
7. V. N. Kanunnikov, et. al., See [1], p. 653.
8. L. Laslett, V. Neil, and A. Sessler, Rev. Scient. Instrum., 36, 436 (1965).

All abbreviations of periodicals in the above bibliography are letter-by-letter transliterations of the abbreviations as given in the original Russian journal. *Some or all of this periodical literature may well be available in English translation.* A complete list of the cover-to-cover English translations appears at the back of this issue.

STUDY OF THE DYNAMIC CHARACTERISTICS OF THE FIRST UNIT OF THE I. V. KURCHATOV BELOYARSK ATOMIC-POWER STATION

(UDC 621.311.25)

I. Ya. Emel'yanov, P. A. Gavrilov, and B. N. Seliverstov

Translated from Atomnaya Énergiya, Vol. 19, No. 2,
pp. 131-137, August, 1965
Original article submitted September 18, 1964

Results of a study of nonstationary processes in the I. V. Kurchatov Beloyarsk Atomic-Power Station, using an electrical analog machine together with the actually-operating control apparatus, are presented. This enabled the dynamic characteristics of the power unit to be obtained and the optimum parameters for setting the main controls of the station to be selected.

The theoretical characteristics of the reactor were also compared with experimental results measured directly.

The I. V. Kurchatov Beloyarsk Atomic-Power Station (BAPS) is the first industrial atomic-power station in the world to use nuclear superheating of steam [1, 2]. The nominal and transitional operating conditions of the station constitute a complicated mass of neutron-physical and thermophysical processes in a complex technological scheme.

Under certain conditions, perturbation in the reactor and turbine may produce an abnormal deviation of the technological parameters and lead to emergencies, costly equipment being put out of action. Thus on increasing the power there may be a crisis of boiling in the evaporation channels, leading to their overheating. Surges of the level in the evaporators may be accompanied by spattering of nonseparated drops of water in the steam-superheating channels.

Experience gained in using present industrial plants did not indicate any dynamic laws for the system under consideration or determine the conditions for the accident-free operation of the BAPS system. Hence the problem was attacked by a mathematical modeling method. The physical principles of the mathematical model for the nonstationary thermal processes taking place in the technological system were verified experimentally on a thermal testing unit with the fundamental technological arrangements of the BAPS [3].

The investigations enabled us to substantiate the general assumptions made and to determine the limits within which theoretical results agreed closely with experimental. This enabled us to choose a reasonable mathematical model of the BAPS and study this over a relatively wide range of parameters.

The nonstationary thermophysical processes were described by a system of differential equations, which, on the assumptions generally made (as formulated in [3]), reflected the laws of the conservation of energy, mass, and momentum, and the heat-conduction equation. The neutron-physical processes were described by kinetic differential equations, using six groups of delayed neutrons, allowing for density and temperature changes in the heat carrier, uranium, and graphite.

The inhomogeneity of the distribution of heat carrier and thermal flux over the radius of the active zone in the reactor meant that, depending on the geometrical position, the heat-emitting elements had different dynamic characteristics. The inertia of the fuel elements rises from the center of the active zone to the periphery. This can easily be shown; in the first approximation (or more exactly for hollow cylindrical fuel elements with a ratio of internal to external diameter close to unity) the time constant of heat transfer from the wall of the fuel element to the heat carrier is determined by the equation

$$\tau^* = \frac{C_M M_M}{\alpha p} \text{ sec},$$

where C_M is the specific heat of the metal of the fuel element in kcal/kg·deg, M_M is the mass of metal in the fuel element per unit length in kg/m, α is the heat-transfer coefficient in kcal/m^2·h·deg, p the perimeter of the fuel element in contact with the heat carrier in m. The coefficient α is functionally connected with the mass flow of heat carrier G (kg/h) and the specific heat flux q (kcal/m^2·h); for single-phase sections $\alpha \sim G^{0.8}$, for two-phase $\alpha \sim q^{1.7}$.

If at some point of the active zone in the reactor there is a local change in the temperature of the fuel or moderator, then the density of thermal neutrons in the reactor also changes, this change depending on the geometrical position of the point in question. The effect of this perturbation on the critical condition of the reactor is determined to a first approximation by the distribution of neutron density over the reactor before the introduction of the perturbation.

For large homogeneous reactors the effect of a perturbation Δk a long way from the boundary of the active zone with a reflector is proporptional to the square of the unperturbed neutron density Φ_0 in the region of perturbation:

$$\frac{\Delta k}{k} \sim \frac{\int_{V_1} \Phi_0^2 \, dv}{\int_{V} \Phi_0^2 \, dv}.$$

Thus each group of channels situated on a circle of the i-th radius r_i will be characterized by its own time constant τ_{r_i} and gain factor C_{r_i}, which, characterizing the "value" of the neutron-density distribution, is determined by the relation

$$C_{r_i} \sim \frac{\Phi_{r_i}^2}{\bar{\Phi}_{a.z.}^2},$$

where Φ_{r_i} and $\bar{\Phi}_{a.z.}$ are the density of thermal neutrons at the point r_i and the average value of the neutron density over the whole active zone. Hence in the transitional process the temperature feedback may be represented by an infinite series of parallel inertia elements with their own time constants and gain factors. The greatest contribution, both with respect to rapidity of action and amplitude, in introduced by the central group of channels.

In order to realize this on the "Baikal" analog machine, the system of differential equations was linearized and, by using Laplace transformations, reduced to a system of parametric transcendental intermediary functions, and then approximated by a system of fractional-rational polynomials.

The automatic control system of the steam-producing equipment in the BAPS provides for maintaining the main technological parameters at a given level for operation in either the base or peak condition. Let us consider the automatic control systems for the reactor power and thermophysical parameters.

The reactor-power control system ensures automatic variation of the power and maintains it in conformity with the load on the power-station generator, also compensating changes in the reactivity caused by burn-up, poisoning, thermal effects, etc.

This system is also furnished with three independent automatic regulators operating in a range equal to 4 to 125% of the nominal power. Considering the large dimensions of the reactor and the inadmissibility of misalignments of heat evolution in the active zone, automatic control of the reactor power is effected by two rods disposed symmetrically with respect to the vertical axis of the system.

The automatic regulator is astatic, ensuring proportional control. Each automatic regulator receives a signal from an ionization chamber proportional to the actual average reactor power and a signal from a power controller. The error signal, proportional to the difference between the actual and assigned powers, is fed to the general automatic-control tract and then to two executive mechanisms. Each executive mechanism uses a two-phase asynchronous motor to move one of the rods. The maximum rod velocity for automatic control and a power deviation of 10% is 0.35 m/sec. The compensating factor of the rod belonging to one regulator equals $3.6 \cdot 10^{-3}$.

The automatic-control system for the thermophysical parameters of the station consists of primary measuring devices designed for operation with induction elements, thermocouples and resistance thermometers, electrical executive mechanisms, etc.

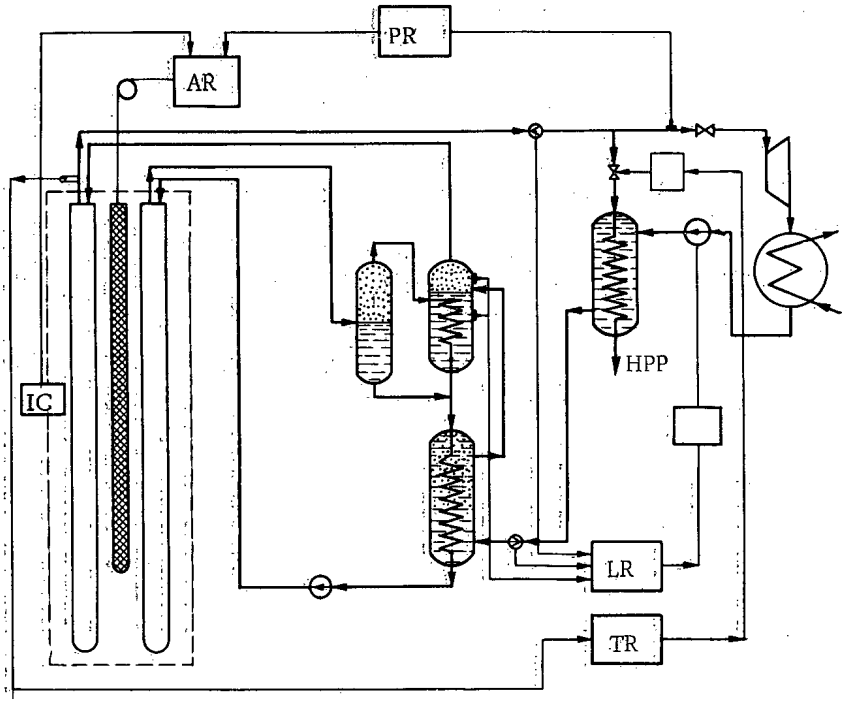

Fig. 1. Arrangement of steam-producing system. AR = automatic power control; IC = ionization chamber; PR = pressure regulator in front of the turbine; LR = evaporator-water level regulator; TR = superheated-steam temperature regulator.

In the peak condition the steam-pressure regulator in front of the turbine acts on the power controller of the reactor. On changing the load of the turbogenerator the steam pressure changes. A signal proportional to the pressure deviation falls on the load regulator, which restores agreement between the reactor power and turbogenerator load.

The superheated-steam-temperature regulator keeps the temperature at the assigned level from the moment when the steam appears in the steam main. The regulator receives an averaged signal from Chromel-Copel thermocouples situated on two parallel steam mains. Control is effected by changing the temperature of the water supply at the outlet from the high-pressure preheater (HPP); when the temperature of the superheated steam falls, that of the preheated water rises and vice versa.

In working conditions, the regulation of the second-circuit supply is reduced to maintaining the water level in the drum evaporators within assigned limits. The drum evaporators are connected by steam and water lines with low hydraulic resistances and form communicating vessels. This makes it possible to control the feeding of the second circuit by means of a single regulator acting simultaneously on the valves of both supply mains.

Six signals, indicating the level in the evaporators, the steam flow, and the flow of supply water for the left- and right-hand sides, fall on the regulator.

The main scheme of the steam-producing system used for the analog machine is shown in Fig. 1. In order to approximate the investigation to actual conditions, test automation systems were used, these being included in the over-all arrangement with the analog machine representing the dynamic model of the system being studied. A general view of the model with the actual operating control apparatus is shown in Fig. 2.

The functions of automatic power control in the station were fulfilled by an actual regulator with an electromagnetic power controller. For imitating the resistive torque, a pulley was placed on the shaft of the motor and a load hung on this. The resistive torque was thus 2.3 kg • m.

The functions of automatic regulators maintaining the pressure and temperature of the superheated steam in front of the turbine and also the level in the evaporators were fulfilled by electronic regulators of the ÉR-T-59 and ÉR-Sh-59 types. The regulators were linked to the model by means of special transfer mechanisms.

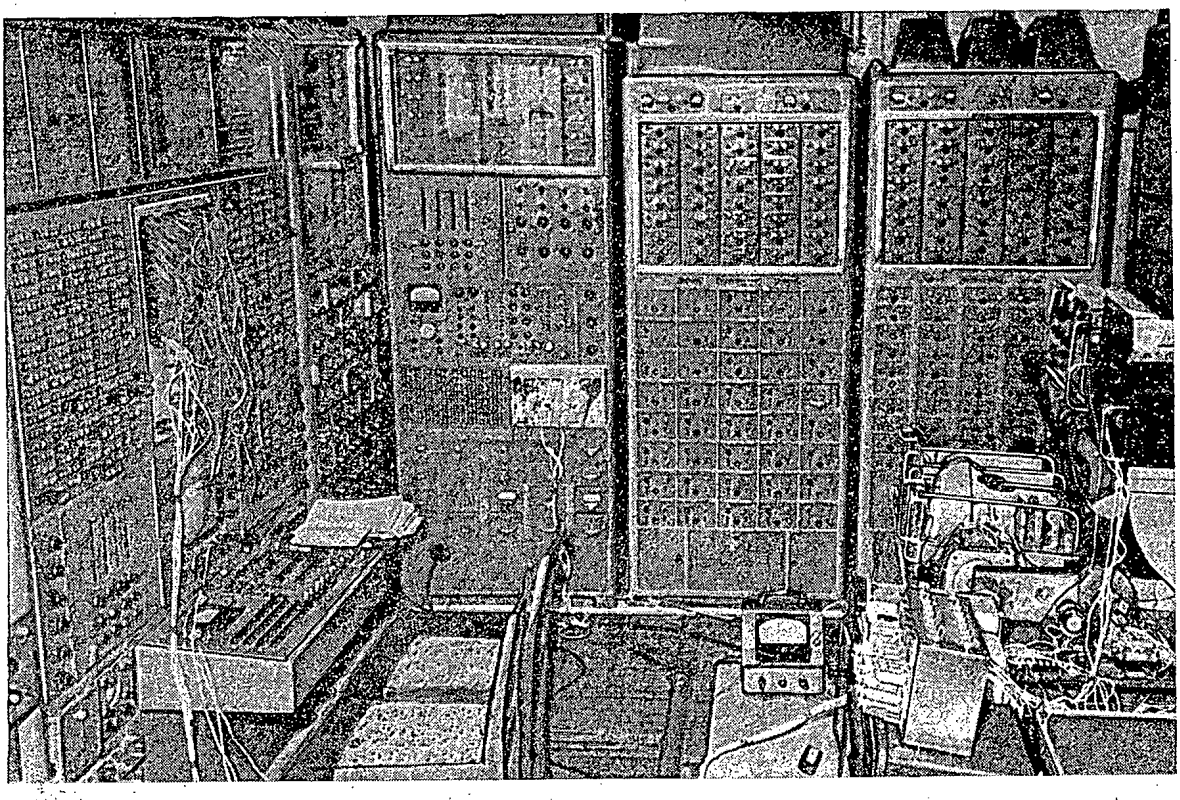

Fig. 2. General view of the mathematical model with the actually-operating control apparatus.

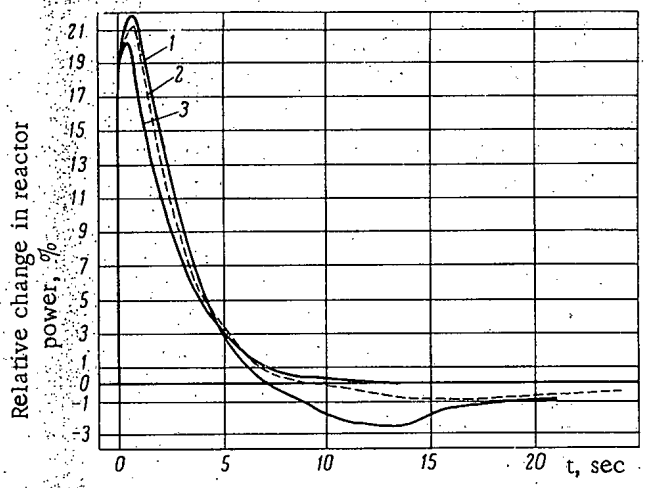

Fig. 3. Treatment of a reactivity jump of $\Delta\rho = 0.001$ by the actual AR regulator. 1) Without temperature feedback; 2) with computed temperature coefficients of reactivity; 3) with double the computed temperature coefficients of reactivity.

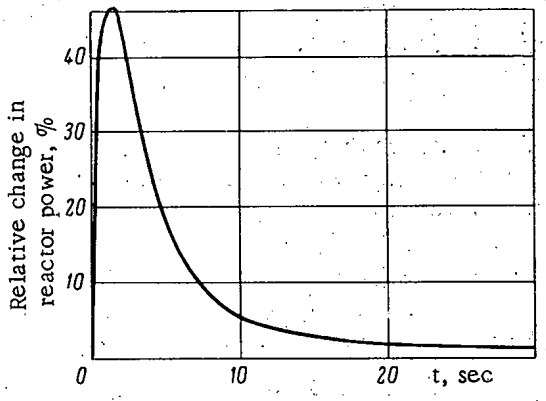

Fig. 4. Treatment of reactivity perturbation $\Delta\rho = 0.0018$ by an actual AR regulator.

The characteristics of the primary sensitive elements and executive organs corresponded to the planned characteristics of the automatic-control system of the first BAPS unit.

The efficiency of the automatic-control system when using the station in nominal conditions was studied for sudden perturbations in reactivity and turbine load.

Fig. 3 shows curves giving the change in power for a sudden perturbation in reactivity $\Delta\rho = 0.001$, for calculated and doubled temperature coefficients. The zone of insensitivity of the regulator was chosen equal to 0.5% of the power level controlled. As seen from the figure, increasing the temperature coefficients of reactivity leads to a fall in the power "throws" and to smoother control, although the regulation time is slightly increased.

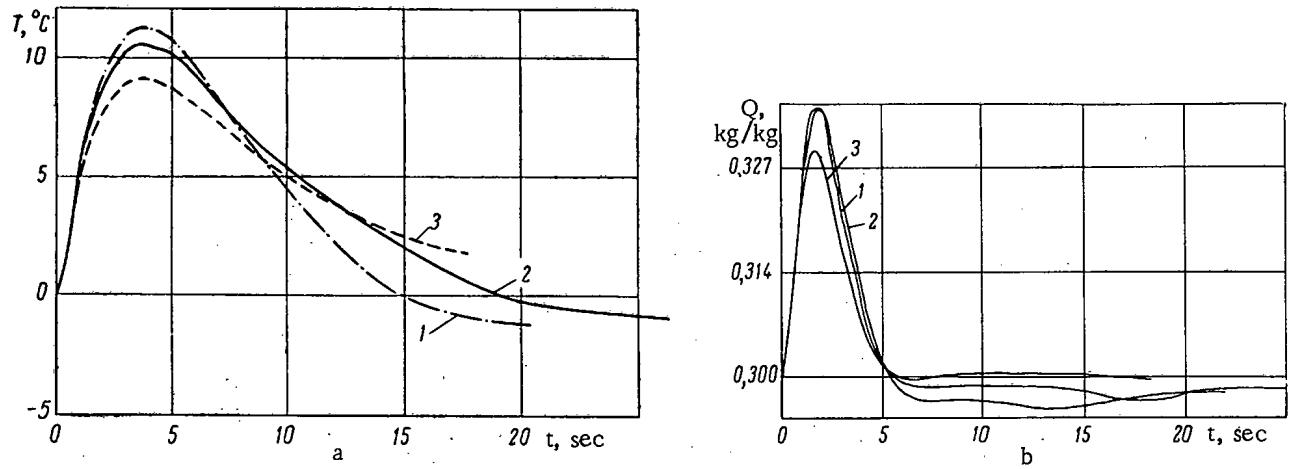

Fig. 5. Variation in the maximum temperature T of the uranium in the steam-producing channels (a) and the weight content of steam Q at the outlet from the evaporator channels (b) for a sudden perturbation of reactivity $\Delta\rho = 0.001$ (notation of curves as in Fig. 3).

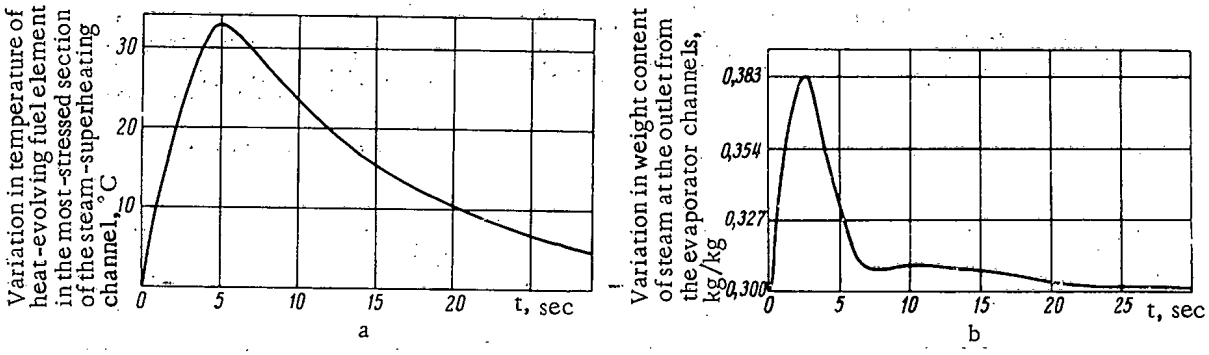

Fig. 6. Variation in the temperature of the fuel element in the stressed section of the steam-superheating channel (a) and weight content of steam at the outlet from the evaporator channels (b) for a sudden perturbation $\Delta\rho = 0.0018$. (Notation of curves as in Fig. 3).

Of no less interest is the treatment of a perturbation in reactivity equal to the full capacity of the automatic power control, when this is set in a central position relative to the height of the active zone (Fig. 4). The automatic regulator (AR) eliminates the perturbation ($\Delta\rho = 0.0018$) in 20 to 25 sec, the AR rods going out to the end positions.

In treating reactivity perturbations, features of special interest include an increase in the maximum temperature of the uranium in the most-stressed steam-producing channels, and also deviations in the weight content of steam in the evaporator channels, which may lead to a heat-transfer crisis.

We see from Figs. 5 and 6 that the increase in uranium temperature for $\Delta\rho$ equal to 0.001 and 0.0018 is 10.5 and 33°C respectively; the weight content of steam rises to 33.6 and 38% respectively. From these figures we see that even a comparatively large perturbation of the reactivity is eliminated by the regulator in 8 to 10 sec. Naturally for this short period of time the parameters of the station being regulated (temperature of superheated steam, steam pressure in front of the turbine, level in the evaporators, etc.) deviate by an amount comparable with the zone of insensitivity of their regulators. Hence these regulators must in general be adjusted with reference to the treatment of perturbations on the turbine side.

Since there are special demands made on the level in the evaporators (oscillations in level must not exceed ± 50 mm), the zone of insensitivity of the level regulator was chosen as 20 to 30 mm. For the adjustment of the regulator controlling the steam pressure in front of the turbine the zone of insensitivity was made equal to 1 abs. atm.

Fig. 7 shows the behavior of the main technological parameters of the station with the actually-operating regulation system for a sudden reduction of 5% in the turbine load. We see that an increase in the pressure-regulator

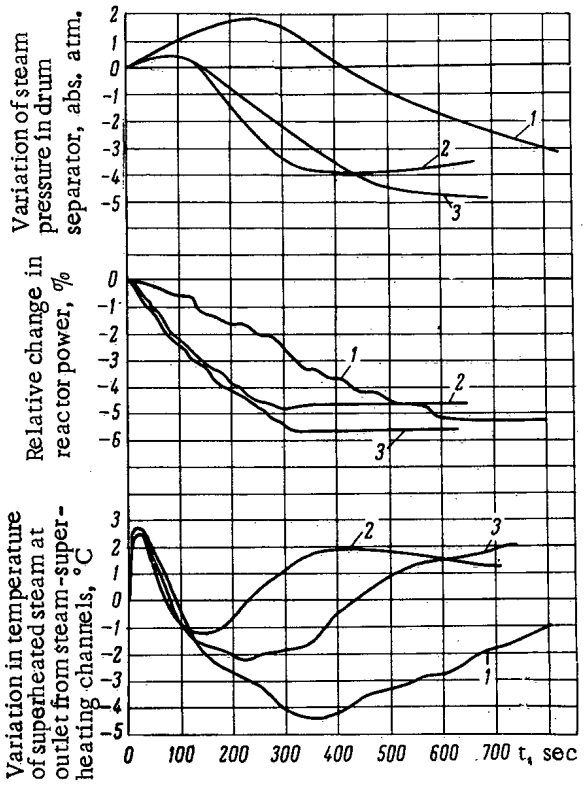

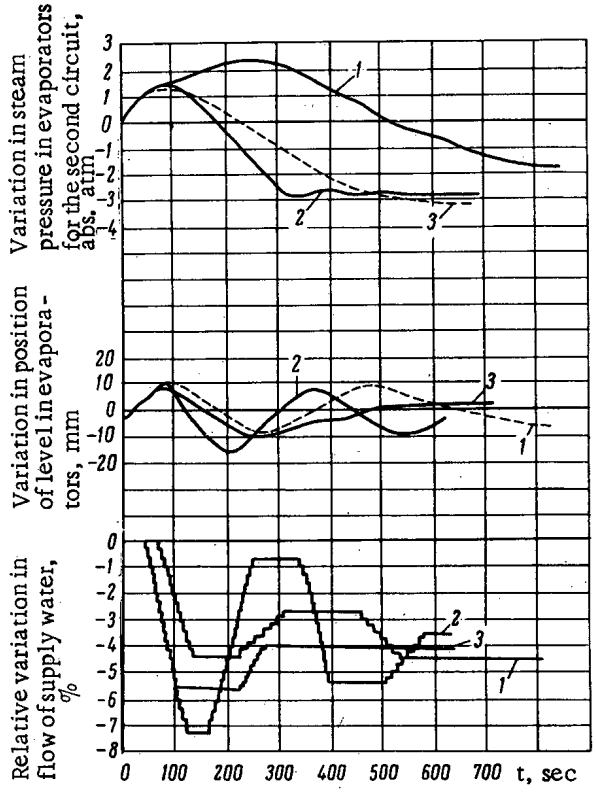

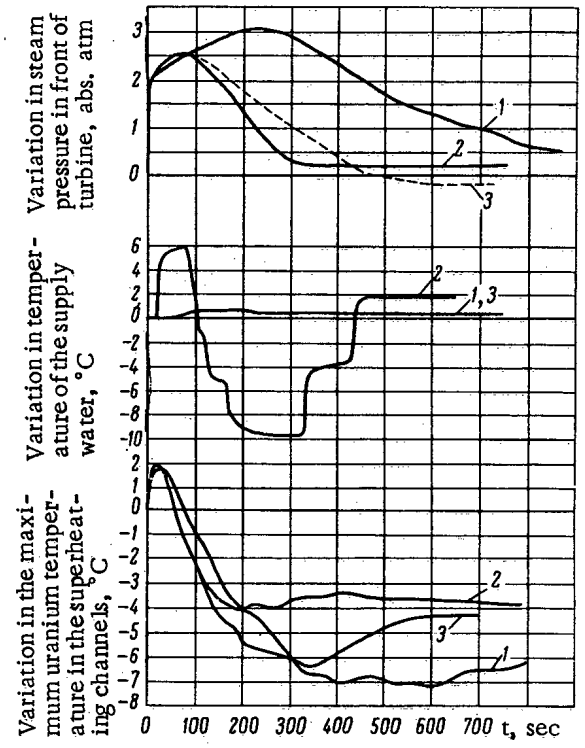

Fig. 7. Variation of the technological parameters of the station on reducing the turbine load by 5%: 1) Without steam-superheating regulator; isodrome time of pressure regulator T_{ip} = 100 sec; 2) with all regulators, T_{ip} = 15 sec; 3) without steam-superheating regulator, T_{ip} = 15 sec.

isodrome time T_i leads to delay in the transitional processes. Curve 2 corresponds to the optimum setting of the superheated-steam pressure and temperature regulators. It should be noted that for the selected setting of the parameters, but with the superheating regulator switched off, the quality of the transitional processes worsens.

Further reducing T_i to 3 or 5 sec produces oscillations in power, which leads to gain in the temperature of the superheated steam for any parameters of the temperature regulator. This is because the time constant of the steam temperature for changes in reactor power or turbine load is an order smaller than the time required for the control signal to pass through the superheating-temperature control network.

Since the whole system is a juxtaposition of a number of circuits both internal (feedback due to the temperature effect of reactivity) and external (reactor-power control, circuit for regulating steam pressure in front of the turbine, etc.), we cannot exclude the possibility that the oscillation of such parameters as reactivity, turbine load, etc., will lead to resonance phenomena. In view of this, we checked the operation of the control system with the selected regulator adjustments (see table) for stability.

Fig. 8 shows the amplitude/frequency characteristics of reactor power for reactivity perturbations following the law $\Delta\rho = 0.0001 \times \sin \omega t$ and turbine-load perturbations $0.08 n_0 \sin \omega t$ (n_0 = nominal turbine power). The resonance

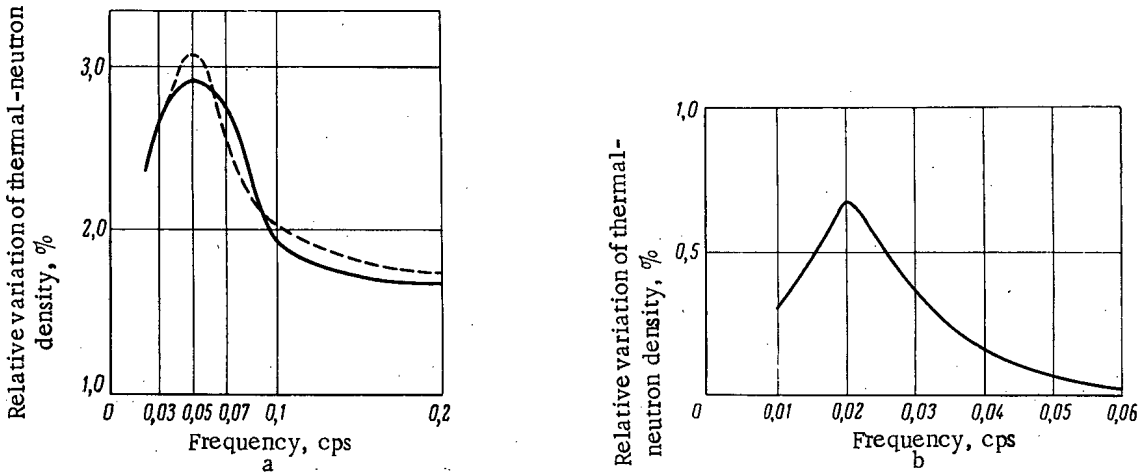

Fig. 8. Amplitude/frequency characteristics of reactor power for harmonic oscillations of reactivity (a) and turbine load (b): ---- calculation, ——— experiment.

Adjustment Parameters of Regulators

Adjustment parameters	Steam-superheating temperature regulator	Evaporator-level regulator	Pre-turbine steam-pressure regulator
Pulse length	4	2.2	—
Coupling velocity	6	0.5	1.6
Zone of insensitivity	1.5	2	5
Isodrome time T, sec	72	7.2	15
R, MΩ	2.4	0.24	0.5

Note. Pulse length, coupling velocity, and zone of insensitivity are given in fractions of the corresponding regulator scales.

peaks of the frequency characteristics lie within acceptable limits as seen from Fig. 8, the first experimental data obtained on the BAPS reactor during starting-up and adjusting operations qualitatively and quantitatively confirm the mathematical model of the reactor selected.

LITERATURE CITED

1. N. A. Dollezhal', et. al., In the book "Transactions of the Second International Conference on the Peaceful Uses of Atomic Energy", Contributions of Soviet Scientists [in Russian], Vol. 2, Atomizdat, Moscow (1958), p. 36.
2. P. I. Aleshchenkov, et. al., Atomnaya Énergiya, 16, 489 (1964).
3. P. A. Gavrilov and B. N. Seliverstov, Atomnaya Énergiya, 15, 115 (1963).

METHOD OF CALCULATING THE COST OF WATER AND ELECTRICAL POWER FOR NUCLEAR DESALINATION SYSTEM

(UDC 338.4 ;621.039.576)

Yu. I. Koryakin, A. A. Loginov, V. A. Chernyaev, and I. I. Zakharov

Translated from Atomnaya Énergiya, Vol. 19, No. 2, pp. 138-143, August, 1965
Original article submitted March 25, 1965

A method of determining the economic factors of double-purpose systems is set out; this provides separate and fairly strict determinations of the expenses involved in the production of electrical power and fresh water, and hence enables their net cost to be ascertained. The effect of the main parameters of the system on the net cost of fresh water is examined. The economic indices of double-purpose systems with reactors of various types are calculated for several values of their thermal power.

Preliminary technical-economical studies [1-4] have shown that the use of nuclear reactors for desalinizing salt water and producing electrical power is one of the most promising fields for the use of these systems.

From the technical point of view the possibility of using nuclear reactors as sources of heat for the simultaneous production of fresh water and electrical power raises no doubts. The economic aspects of using nuclear reactors for this purpose are considerably more complex, since the scale of their use will depend substantially on the economic competitiveness of such systems in relation to ordinary heat sources. Hence it is of particular present interest to study the economics of double-purpose nuclear reactors.

The degree of competitiveness of nuclear-power desalination systems is affected by the specific siting of the plant, the demands for fresh water and power, and also the question of optimizing the level of economy.

Clearly the most promising system for these purposes is a nuclear reactor characterized by a low value of the fuel component of the cost of power, and specific capital expenses which fall more sharply as the specific thermal power increases. Naturally for such reactors an increase in the power-utilization factor is especially important, since the fuel component is independent of this, while the capital component is inversely proportional to it. The possibility of storing the fresh water produced means that, in principle, there is a good possibility of exploiting a nuclear desalination plant with an extremely high power-utilization factor; this creates favorable conditions for the competitiveness of nuclear systems in relation to ordinary sources of heat.

Among the types of reactor most developed and adopted in the Soviet Union we must primarily mention the I. V. Kurchatov Beloyarsk Atomic-Power Station [5, 6], the Novo-Voronezh Atomic-Power Station [7], and to a smaller extent also the Shevchenkov Atomic-Power Station [8].

The only common factor for all desalination plants with such reactors is the principle of the combined development of electrical power and heat at a potential suitable for the heating steam used in desalinizing the water. This potential is determined by the operating conditions of the distillation plant.

An important index for power desalination systems is the quantitative relation between the two products, electrical power and fresh water. For a certain temperature level of the heating steam used in freshening the water, this ratio depends on the initial parameters of the cycle; the higher these are, the greater will be the relative yeild of electrical power. Hence systems with reactors of the Beloyarsk or Shevchenkov types will be characterized by a considerably higher proportion of usable electrical power than those with Novo-Voronezh-type reactors. This fact must be borne in mind when selecting the plant for a specific region, since the requirements for electrical power and fresh water may differ considerably for different regions as well as their cost.

An important question is also that of the specific power of the reactor. The problem of increasing this is most simply solved for reactors of the channel type.

Methodical Requirements for Determining the Cost of Fresh Water and Electrical Power

The existence of two forms of production in the double-purpose system creates a series of difficulties and arbitrary aspects in the calculation of its economic indices. In various countries, several methods of calculating the cost of electrical power and fresh water are used. For example, the most widely used is the method of naming (fixing) a value for the electrical power, considered as a side product of the desalination nuclear plant [2]. If the double-purpose plant is included in a power-supply system, the price for the electrical power produced is fixed by starting from the lowest price of electrical power from other sources in the supply system. This gives the lowest value of the arbitrary cost of the electrical power. If, however, the double-purpose nuclear plant is set up in a region where there is no electrical system or no power stations at all, then the price for the electrical power produced is fixed by considerations of economic conditions. This gives the highest arbitrary price of electrical power.

With this method of calculation, the cost of fresh water is determined by the yearly expenses of operating the double-purpose plant, less the sale of electrical power at the arbitrarily-fixed price.

For conditions in the USSR, from the popular-economy point of view, both forms of production from the double-purpose nuclear station are equally important, and another method of calculating the economic indices is required; this must enable the costs of electrical power and fresh water to be estimated individually and prices fixed in accordance with this. We have developed such a method and shall now indicate its principles.

In general, the annual cost of production for the nuclear double-purpose station is made up of the cost of production of fresh water ($S_{f.w.}$) and electrical power (S_{el}):

$$S = S_{f.w.} + S_{el} \quad \text{roubles/year.} \tag{1}$$

The cost of production of fresh water may be determined as the sum of the costs of the essentially evaporating part of the system ($S_{e.p.}$) and those of the heat used in the heating steam ($S_{h.s.}$):

$$S_{f.w.} = S_{h.s.} + S_{e.p.} \tag{2}$$

The value of $S_{e.p.}$ is determined by amortized deductions from the investment in the equipment of the evaporating part, expenses in repairs, wages, etc.

The problem is to determine the cost of production of the heating system.

For a fixed thermal power of the nuclear reactor (and its parameters) used in the double-purpose plant, the electrical power will always be lower than when this reactor operates in a condensation atomic-power station (APS). This is because the production of fresh water requires heating steam at a potential which could have been used in the condensation turbine. In other words the yield of heating steam is associated with a diminished yield of electrical power. Hence part of the costs of production of electrical power in a condensation APS (the part associated with the underproduction of the double-purpose station) must be treated as a cost of production for the heating steam.

Hence the annual costs of production for the heat in the heating steam may be determined as the difference between the costs of production of electrical power for the purely-condensation APS and those of the electrical power (at the same net cost) developed by the double-purpose station, i.e.,

$$S_{h.s.} = C_e(W_c - W_d). \tag{3}$$

Here C_e is the net cost of electrical power when using the given reactor in a condensation APS in kopecks/(kWh), W_c is the electrical-power yield in a condensation APS in kWh/year, W_d is the electrical-power yield using the same reactor in the double-purpose plant, also in kWh/year.

In determining the costs of production of fresh water, we must calculate the annual production costs (and hence net cost) of fresh water without counting the cost of the heat, and also the production costs of the heat in the heating steam associated with the underproduction of electrical power, regarding its net cost as the same both for the condensation APS and for the double-purpose plant. Strictly speaking, the latter is only valid if the transformation from the condensation APS to the double-purpose plant is not accompanied by the elimination of some equipment peculiar

to the condensation APS only. Hence, in calculating the net cost of the electrical power developed by the double-purpose plant, some correction must be made for the fall in production costs associated with the elimination of certain heat-engineering equipment (turbine condensers, regenerative preheaters, condenser-cooling systems, etc.). Estimates have shown that these corrections are small (3 to 5%).

Thus the annual production costs of the distillate and electrical power for the double-purpose nuclear station are made up of those relating to electrical power in a condensation-type APS with the same reactor ($S_{c\,APS}$) and the production costs of fresh water in a simple desalination plant with free heat:

$$S = S_{e.p.} + S_{h.s.} + C_e W_d = S_{e.p.} + S_{c\,APS}. \quad (4)$$

Cost of Fresh Water without Counting the Cost of the Heat in the Heating Steam

Of the many existing methods of desalinating salt water, for technical-economic analysis we chose that of distillation as the most industrially-adopted at the present time and the one most suited to the scale of the demand for fresh water.

In double-purpose nuclear plants it is desirable, both from the point of view of thermal operating conditions and that of increasing productivity, to use vertical distillation apparatus.

In this paper we analyze the effect of the main technical parameters of the desalination system on the cost of fresh water. In order to elucidate the general tendencies and conditions for obtaining a minimum net cost of fresh water, the range chosen for some of the parameters included values which at the present time would be difficult to achieve.

In general the specific net cost of fresh water, without counting the cost of the heat in the heating steam, is determined by the sum of the corresponding components

$$C^0_{f.w.} = \frac{S_{e.p.}}{M} = C_{a+r} + C_e + C_{s.w.} + C_w + C_{o.e.} \quad \text{kopecks/ton} \quad (5)$$

where M is the yearly production of fresh water in ton/year, C_{a+r} is the component of amortization and repair, C_e the component of expenses on electrical power required for operating the desalination system, $C_{s.w.}$ the component of expenses in preparing the salt water for desalination, C_w the component representing the wages of personnel, and $C_{o.e.}$ representing other expenses.

Clearly the specific net cost of fresh water depends on the accepted and admissible characteristics of the system, the temperature of the heating steam (T_{s0}), the temperature drop per stage (ΔT_{st}) and the number of stages of evaporation (n_{st}). Hence the calculation of $C^0_{f.w.}$ as a function of the variation of the main parameters influencing its value,

$$C^0_{f.w.} = f(T_{s0},\ \Delta T_{st},\ n_{st}),\ \text{kopecks/ton} \quad (6)$$

was made for a range of temperatures T_{s0} from 40 to 250°C, ΔT_{st} from 10 to 35°C, and n_{st} from 1 to 15, and on the assumption that the quantity C_{a+r} was directly proportional to the heat-exchange surface of the whole desalination system (evaporators, regenerators, condensers, etc.), and the remaining categories of expenditure, referred to 1 ton of fresh water produced, are constants for the desalination system with given fresh-water output.

Fig. 1 shows for illustration the dependence of the net cost of fresh water (without allowing for the cost of the heat) on T_{s0} for various values of the n_{st} of the desalination plant and ΔT_{st} per step.

It follows from the graphs that the values of $C^0_{f.w.}$ tend to saturation as n_{st} and ΔT_{st} increase.

Net Cost of the Heat of the Heating Steam

According to expression (3), the production costs of the heat of the heating steam were determined from the net cost of the electrical power for reactors of three types (Beloyarsk, Novo-Voronezh, and Shevchenkov APS) with a power-utilization factor of 0.8.

Using the data of [9], the net cost of electrical power [kopecks/(kWh)] for condensation APS in the electrical-power range 100 to 1000 MW may be approximated by the following expressions: for the Beloyarsk and Novo-Voronezh APS

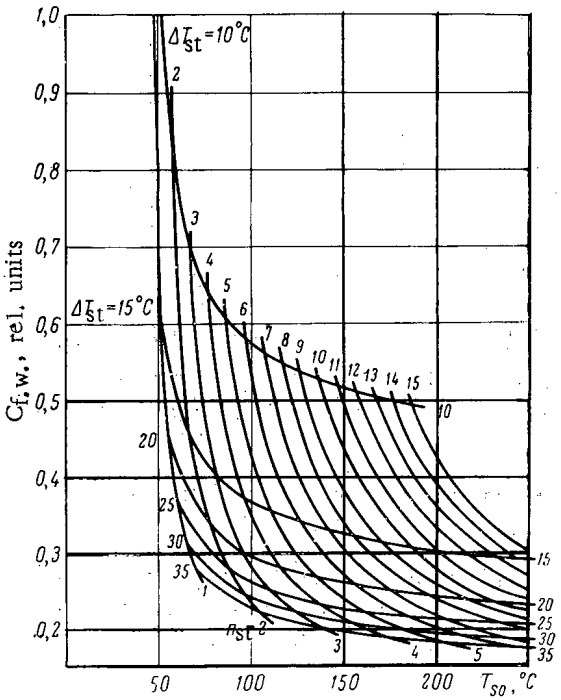

Fig. 1. Effect of the temperature of the heating steam on the net cost of fresh water, without counting the cost of the heat.

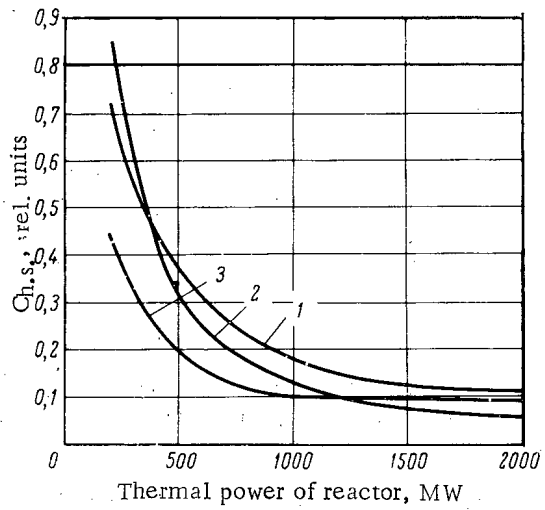

Fig. 2. Effect of the thermal power of the reactor on the net cost of released heat: 1) Reactor of the Novo-Voronezh APS type; 2) Shevchenkov APS type; 3) Beloyarsk APS type.

$$C_e = 0.457 + 3.8 \exp(-0.916 \cdot 10^{-2} N_e), \quad (7)$$

and for the Shevchenkov APS

$$C_e = 1073\, N_e^{-1.272}, \quad (8)$$

where N_e is the electrical power in MW.

The net cost of the heat of the heating steam

$$C_{h.s.} = \frac{S_{h.s.}}{Q_h}, \text{ roubles/g·cal} \quad (9)$$

where Q_h is the amount of heat expended in desalinating the water, was analyzed as a function of the thermal power of the reactor or of the type considered for various heating-steam saturation temperatures: for reactors of the Beloyarsk and Shevchenkov types this was from 80 to 200°C, for those of Novo-Voronezh type from 80 to 140°C. The initial parameters of the steam in the first case were 240 abs. atm, 535°C, and in the second 29 abs. atm, 230°C.

However, remembering that at the present time the admissible temperatures of desalinated water (from the point of view of salt deposition) equal approximately 110 to 120° C, in this paper we give the results of calculations for a heating-steam temperature of 130°C. For these conditions, Fig. 2 gives the variation of $C_{h.s.}$ with the thermal power of reactors of the types considered, used in double-purpose systems.

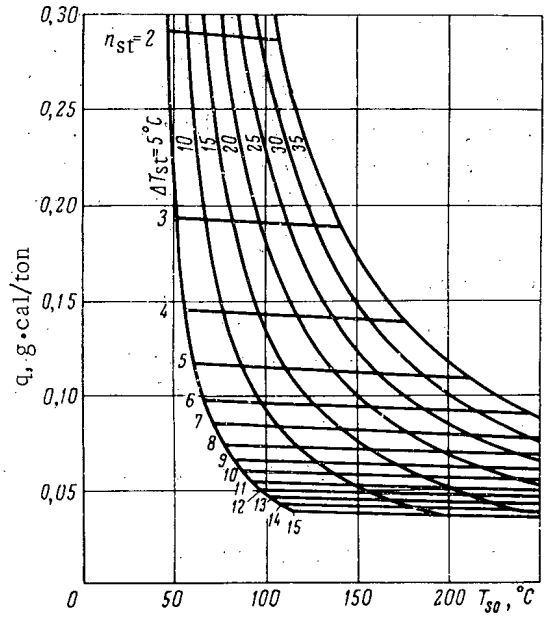

Fig. 3. Specific expenditure of heat on the production of fresh water, as a function of the temperature of the heating steam.

Total Net Cost of the Fresh Water

The total net cost of the fresh water produced by the double-purpose plant is determined by the expression

$$C_{f.w.} = C^0_{f.w.} + C_{h.s.} \cdot q, \text{ kopecks/ton} \quad (10)$$

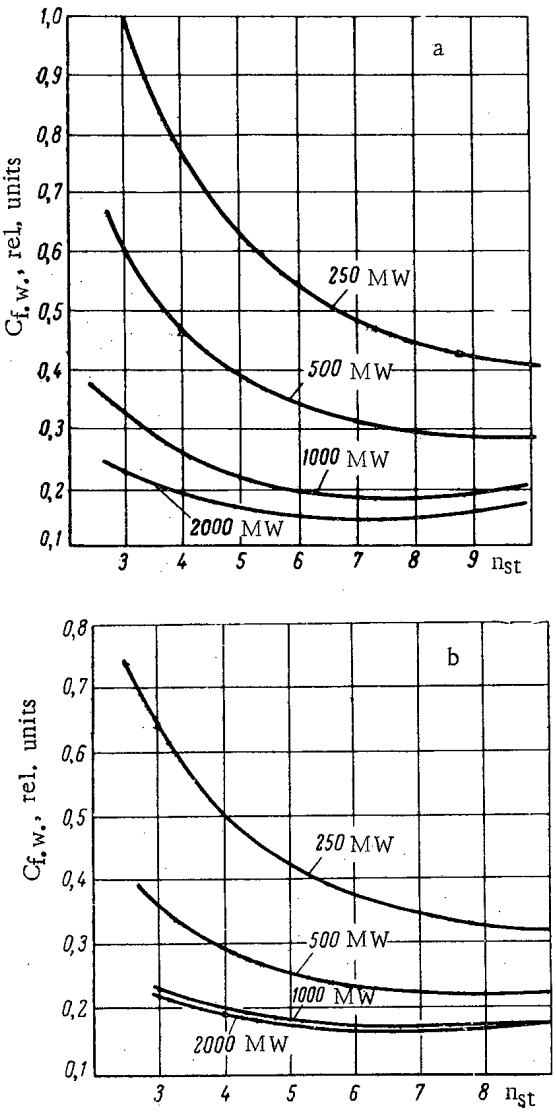

Fig. 4. Effects of the number of stages on the net cost of fresh water for various values of thermal power of the reactor; a) Novo-Voronezh type; b) Beloyarsk; c) Shevchenkov APS.

where q is the specific expenditure of heat on the production of 1 ton of fresh water. The dependence of q on T_{s0} for various values of n_{st} and ΔT_{st} appears in Fig. 3.

Thus, for the accepted conditions, we may construct relations between $C_{f.w.}$ and n_{st} for the types of reactor considered for various values of the specific thermal power of the reactor Q_r. These relations appear in Fig. 4a, b, c.

It follows from the graphs that, for constant thermal power of the reactor, the net cost of fresh water expressed as a function of the number of stages has a minimum; for larger values of thermal power this corresponds to smaller numbers of stages. This is because in expression (10), for a fixed thermal power of the reactor, an increase in the number of stages leads to a rise in $C^0_{f.w.}$ and a fall in q. On the descending part of the curve (Q_p = const) the relative fall in q precedes the increase in $C^0_{f.w.}$, and on the ascending part vice versa. To each value of n_{st} corresponds a definite value of $T\Delta_{st}$ (see Fig. 3).

Technical Economic Indices of the System

Using the method set out in this paper, we calculated the technical-economical indices of double-purpose systems with the types of reactor in question for different thermal powers. The results are shown in the table. It should be remembered that these data are valid within the limits of the initial conditions taken and on the assumptions here made.

A considerable influence on the technical-economical indices of nuclear power/desalination systems is exerted by the net cost of the electrical power of the condensation APS. The data on the net cost of electrical power for the reactors considered here were given in [9] and taken as basis for the calculation of the production costs of the double-purpose system; they reflect the level of reactor technology reached in 1964 and the efficiency of the use of nuclear fuel in existing APS projects. Clearly when APS equipment is manufactured on a production-line basis, the technology of reactor construction is improved, the depth of nuclear-fuel combustion increased, and various progressive methods undertaken, we can expect an improvement in the economic indices of both condensation APS and double-purpose systems. Hence the economic indices given in the table must be considered as conservative, but at the same time giving a first-approximation idea of the technical-economic indices of the double-purpose plant.

Technical-Economic Indices of Nuclear Double-Purpose Plants with Various Kinds of Reactors

Type of reactor	Thermal power of reactor, MW	Electrical power, MW	Production of fresh water, tons/day	Cost of electrical power, kopecks/kWh	Net cost of fresh water, kopecks/ton
Beloyarsk APS	250	75	55,000	1.64	29.6
	500	150	100,000	0.92	19.8
	1000	300	175,000	0.51	14.4
	2000	600	352,000	0.45	14.1
Novo-Voronezh APS	250	40	67,500	2.5	42.2
	500	80	135,000	1.49	28.9
	1000	160	212,000	0.74	18.7
	2000	320	425,000	0.48	15.4
Shevchenkov APS	250	75	55,600	2.1	47.0
	500	150	111,000	1.09	26.4
	1000	300	175,000	0.45	16.4
	2000	600	302,000	0.30	11.0

It is well-known that data on the net cost of electrical power and fresh water for systems with different types of reactor will not yet enable us to judge the popular-economical efficiency of these systems and their relative economy. A criterion for this comparison, using the Soviet-accepted method [10], is a composite index involving computed expenses which, for double-purpose nuclear plants, may be written in the following form:

$$Z = S_{f.w.} + S_{ed} + (K_A + K_{e.p.})P, \text{ roubles/year,} \quad (11)$$

where K_A in the investment in the atomic plant producing the electrical power and heat for desalinating the water, $K_{e.p.}$ is the investment in the peculiarly evaporating part of the system, and P is the "normal" investment-efficiency coefficient (P = 0.125).

Moreover, included in the investment are not only the net cost of the basic project (in the present case the double-purpose nuclear plant) but also the investment in allied production (for example, in fuel-cycle plants, which constitute essential requirements of nuclear power). Of course, in order to determine the popular-economical efficiency of double-purpose nuclear plants by the method of computed expenses we must compare such systems with other ordinary heat and electrical-power sources, so as to find the required minimum level of economy in the nuclear systems. Such an investigation demands complex consideration of scaling and the conditions of the power and fresh-water requirements of the particular district, these questions being bound up with the planning and development prospects of the popular economy in the district in question.

LITERATURE CITED

1. Desalination of Water Using Conventional and Nuclear Energy. Technical Reports Series, No. 24, IAEA, Vienna (1964).
2. J. Ramey, et. al., Paper No. 220 Presented by the United States to the Third International Conference on the Peaceful Uses of Atomic Energy[Russian Translation], Geneva (1964).
3. J. Gaussens, N. Moulle, and F. Duthell, Ibid., Paper No. 46, Presented by France.
4. A. S. Gorshkov, Yu. I. Koryakin, A. A. Loginov, and E. Ya. Sokolov, Ibid., Paper No. 319,Presented by USSR.
5. N. A. Dollezhal', et. al., Ibid., Paper No. 309, Presented by the USSR.
6. A. N. Grigor'yants, et. al., Ibid., Paper No. 308,Presented by the USSR.
7. G. L. Lunin, et. al., Ibid., Paper No. 305, Presented by the USSR.
8. A. I. Leipunskii, et. al., Ibid., Paper No. 311 ,Presented by the USSR.
9. N. M. Sinev, B. B. Baturov, and V. M. Shmelev, See [2-8], Paper No. 294, Presented by the USSR.
10. Fundamental Methodical Concepts of Technical-Economical Calculation in Power Engineering [in Russian], Gostekhizdat, Moscow (1959).

AGING OF BERYLLIUM

(UDC 546.45)

I. I. Papirov

Translated from Atomnaya Énergiya, Vol. 19, No. 2,
pp. 144-153, August, 1965
Original article submitted August 25, 1964

A survey of studies devoted to the possibility of increasing the plasticity of technical-purity beryllium within the temperature region 400-600°C is given. It is shown that the heat treatment of beryllium at 600-800°C leads to the deposition of the superfluous phases from the supersaturated solution. This is accompanied by a substantial change in the properties of the metal, in particular, the plastic and strength characteristics, hardness, creep, and electric resistance. The results of metallographic, electron microscopic, electron diffraction, x-ray diffraction, and other investigations of the microstructure of beryllium in various states are cited. The mechanism of the aging of beryllium is described on the basis of the available data, and practical conclusions are drawn on the possibilities of increasing the plasticity of beryllium at high temperatures.

The plasticity of beryllium is increased by heating to only 350-400°C, but then begins to drop, and reaches a minimum at 600°C (Fig. 1). This phenomenon is sometimes called high-temperature brittleness, in distinction from low-temperature brittleness, characteristic of the technical-purity metal at room temperature. High-temperature brittleness substantially limits the possibilities of technological processing (extrusion, rolling) of beryllium and has an unfavorable effect upon the properties of objects designed for use within the temperature region 400-600°C, which is of the greatest practical interest.

In 1954 Beaver and Wikle [2] showed that the annealing of hot-pressed extruded beryllium at a temperature of 750°C substantially increases its plasticity close to the minimum, and hypothesized that the cause of this is aging. Later Mach [7] confirmed the hypothesis of aging, showing that a substantial change in the properties of beryllium can be achieved by thermal or thermal mechanical treatment of it. Detailed investigations of the properties of aged beryllium and the mechanism of the process of aging were begun in 1960 after the studies of Martin [1] and Gelles and associates [8] appeared.

Technical-purity beryllium is essentially a weakly alloyed alloy. Heating it to a temperature above 850°C leads to the dissolving of a number of the basic impurities in the matrix, i.e., to homogenization. Rapid cooling results in the formation of a metastable supersaturated solid solution, capable of dispersion hardening and aging. Since the solubility of various impurities in beryllium differs and ends at different temperatures, the arbitrary integral process of solution is regarded as homogenization.

Dispersion hardening, or the formation of dispersed interlayers enriched in impurities, hinders plastic deformation and reduces plasticity. This process frequently has time to occur during cooling after homogenization, if the latter is not accompanied by quenching, but it occurs chiefly under the action of stresses during deformation in the temperature region 400-600°C. We shall regard the aging of beryllium as the completed process of deposition of phases from a supersaturated matrix upon heating at a temperature region 600-800°C, accompanied by an increase in the depositions and an increase in the plasticity. Thus, beryllium may exist in three states: homogenized, aged, and intermediate. The latter is also sometimes called initial and is characteristic of the technical metal, slowly cooled from the region of homogenization; the properties of the initial and homogenized beryllium essentially differ little.

In this work it was shown that the high-temperature brittleness of beryllium is due both to dispersion hardening and to the formation of liquid phases on the grain boundaries.

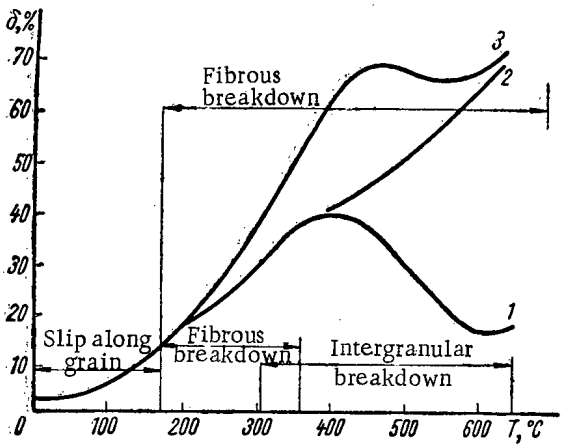

Fig. 1. Temperature dependence of the relative elongation of beryllium: 1) Homogenized metal; 2-3) aged metal (function 2 is observed in [1], function 3 in [2-6]).

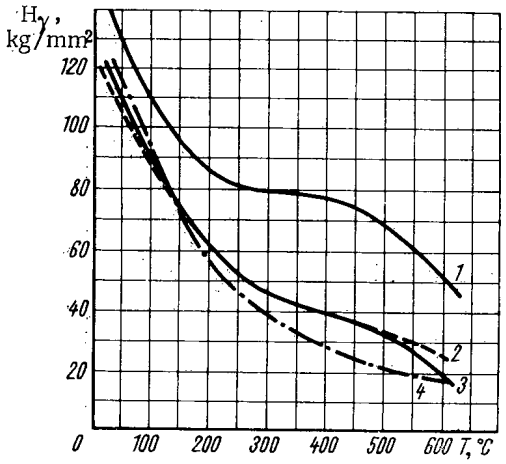

Fig. 2. Temperature dependence of the hardness of beryllium [12]: 1) Initial magnesium-thermal beryllium; 2) the same after aging at 800°C and 72 h (cooling for 120 h); 3) initial electrolytic beryllium; 4) the same after aging at 800°C and 72 h (cooling for 120 h).

Change in Properties during Aging of Beryllium

Plasticity. The values of the relative elongations δ or constriction ψ of the samples during tensile testing are usually used as the characteristics of plasticity of a material. As has already been noted, aging promotes a substantial improvement of the plasticity within the temperature region 400-600°C; the plasticity minimum in the region of 600°C either disappears upon aging [1] or is substantially smoothed out [4-6] (see Fig. 1). In particular, according to the data of [1], the relative elongation of extruded magnesium-thermal low-purity beryllium, measured at 600°C after annealing at 780°C for 120 h, followed by slow cooling, increases from 12 to 70%. In this case, the intercrystalline breakdown in the region of 400-600°C, characteristic of the initial beryllium, is not observed, and a fibrous fracture appears, typical of the plastic state. The influence of heat treatment on the plasticity is smaller the higher the purity of the metal. However, as the purity increases, the plasticity minimum already is smoothed out in the initial state, and in 99.6% pure beryllium, the relative elongation at 600°C exceeds 40% [9].

The plasticity characteristics depend to a definite degree upon the temperature of aging and the rate of deformation but do not depend on the rate of cooling after aging. The general trend is such that the value of $\delta_{600°C}$ increases with decreasing temperature of aging, although at lower temperatures the duration of heat treatment must be sharply increased. Decreasing the rate of deformation (from 2.75 to 0.2%/min) of samples aged at 800°C for 2 h leads to a decrease in δ and the appearance of intergranular breakdown in place of the fibrous fracture [11]. More prolonged annealing smoothed out the indicated difference.

A pronounced region of plastic deformation appears on the curves of deformation of the samples after aging. It is interesting that the activation energy of plastic flow is equal to 48 kcal/mole, which is in good agreement with the value of the activation energy of the diffusion of iron in beryllium [4].

The Hardness of beryllium at room temperature is weakly dependent upon the state of the sample. However, in measurement of the hot hardness, it was found [12] that the hardness of the matrix in homogenized contaminated beryllium is substantially higher than in aged beryllium (Fig. 2). In purer electrolytic beryllium, this effect is far more weakly expressed. The measured values of the hardness are reversible upon aging of the homogenized and homogenization of the aged metal.

Strength. Data on the strength characteristics (σ_B and σ_T) of beryllium in various states are contradictory. In certain studies [1, 6, 11], a decrease in the strength of aged samples and a disappearance of the plateau on the curve of the temperature dependence of the strength in the region of 350-500°C was observed. In [8], a certain increase in the breaking strength in aged samples was observed. Statistical treatment of the results of [13] shows that the breaking strength in aged and homogenized samples is practically the same. The differences in the results are explained either by the fact that the tests were conducted only once and by the dispersion of the data, or by the dependence of the strength on the nature of the impurities present, in particular, on the ratio of the amounts of aluminum and iron.

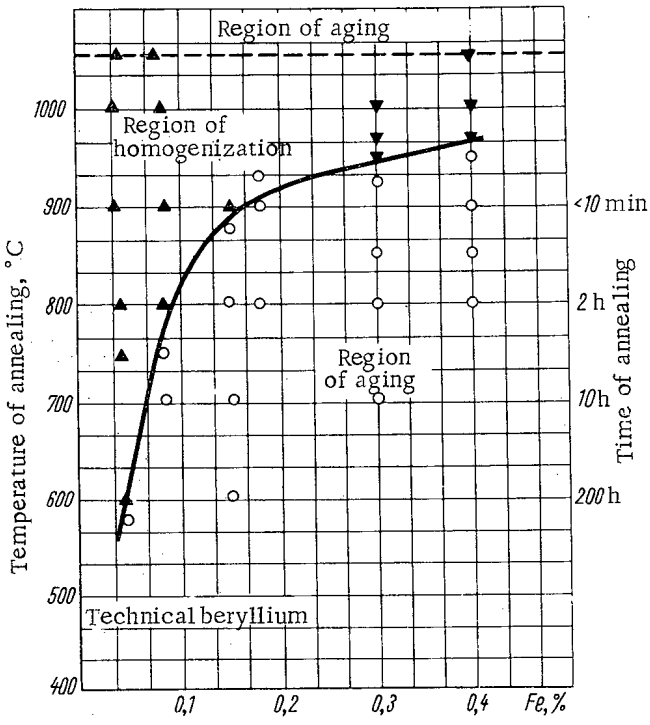

Fig. 3. Curve of solubility of iron in beryllium, constructed according to data of mechanical testing of heat-treated samples [10]: ▽) Sliding surface; ▲) intergranular breakdown; ○) fibrous breakdown.

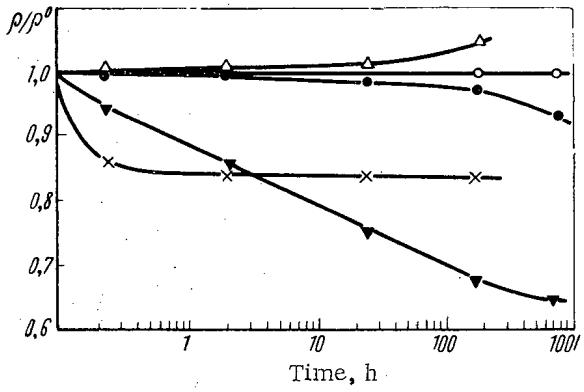

Fig. 4. Variation of the electric resistance of beryllium during heat treatment [8]. Temperature, °C: △) 1000; ○) 200; ●) 400; ▽) 600; ×) 800.

Let us mention that the yield point is characterized by the greatest sensitivity to aging [6, 8]. The yield plateau on the deformation curves arises even after aging at 300°C and for more than 20 h, at 350°C and duration more than 1 h, and at 400°C and duration about 15 min [6].

In homogenized samples, repeated slip related to impurities is observed. It is the result of alternating processes of stripping of dislocations from Cottrell clouds, followed by their surrounding by new impurities. In the aged samples, there is no repeated slip.

Creep [6, 13]. As was noted above, the plasticity of beryllium depends on the rate of deformation. This dependence is manifested especially distinctly in tests for creep. The maximum resistance to plastic deformation during creep is exhibited by homogenized samples, less by the initial samples, and minimum by the aged samples. The plasticity reserve during creep is low, independent of the state of the samples; breakdown is always intercrystalline in character; the relative elongation comprises 1-4% and decreases with decreasing rate of creep. The lower plasticity of beryllium during creep is explained by the development of micropores on account of diffusion of vacancies. The micropores evidently develop when creep is retarded at boundary inclusions. Hence, in the aged metal, deposits promote the formation of micropores, causing a decrease in the strength.

Aging of Alloys. An appreciable influence of aging on the properties of more contaminated beryllium led to the idea of the possibility of increasing its properties within the region 400-600°C by alloying with special additives. Alloys of beryllium with iron have been investigated in the greatest detail from this standpoint [10, 14].

The solubility curve for Be–Fe alloys has been constructed according to the data of mechanical testing of the samples (at 600°C) after heat treatment in the temperature region 575-1000°C (Fig. 3). Homogenized samples with low plasticity during breaking showed an intercrystalline fracture and high yield point (points above the solubility curve in Fig. 3). After aging, the characteristics were improved: the corresponding points lay below the solubility curve. In addition to the temperature scale, the time scale corresponding to the system of annealing is plotted on Fig. 3. The minimum time required for obtaining maximum plasticity is an exponential function of the temperature. It is interesting that treatment of the corresponding data makes it possible to obtain a value of the activation energy of the aging process (47 kcal/mole) close to the value of the activation energy of diffusion of an iron impurity considered earlier (~48 kcal/mole). From Fig. 3 it follows that the temperature of aging is higher, the greater the iron content in the beryllium.

The plasticity of the samples depends on the temperature of homogenization. If it is 50°C greater than the temperature of complete solubility, then the process may be accompanied by growth of the grains, which will lead to a decrease in the plasticity during subsequent aging. Moreover, the alloys Be–0.4% Fe, superheated by 20°C (to temperatures above 990°C) generally is insensitive to subsequent aging. Only the influence of deformation (3%

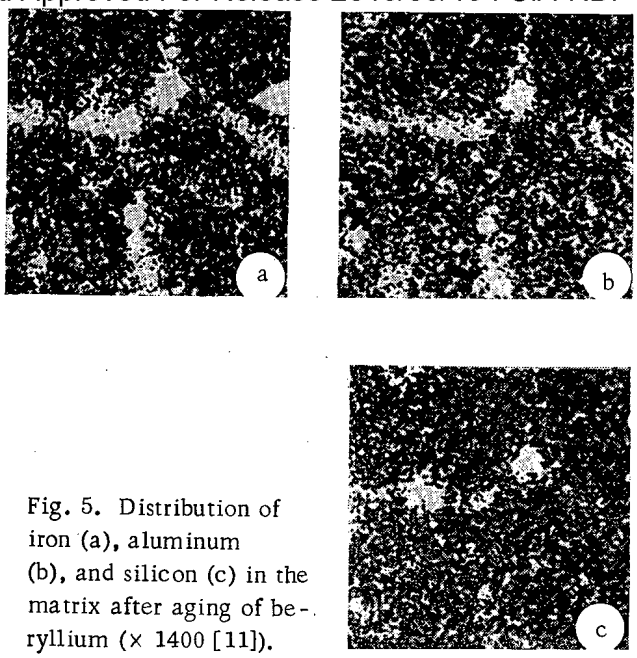

Fig. 5. Distribution of iron (a), aluminum (b), and silicon (c) in the matrix after aging of beryllium (× 1400 [11]).

stretching at 850°C) makes it possible to increase the platicity after aging. Increasing the grain size in the alloy of Be–0.3% Fe from 80 μ (homogenization at 950°C, 10 min) to 250 μ (homogenization at 1000°C, 2 h) decreases δ of aged alloys from 37 to 10%.

Electric Resistance. A change in the resistance of aged beryllium was first observed in [4, 8]. Fig. 4 presents the dependence of the relative resistance on the time of exposure and temperature for samples of beryllium ~99% pure, preliminarily homogenized at 1100°C for 1 h. At 200°C, the electric resistance method does not permit detection of any change in the structure of the samples. At 600°C, the kinetics of aging is characterized by a monotonic decrease in the resistance of the samples, all the way to 100 h of exposure. At 800°C, the process of deposition is completed in 1 h, while around 1000°C there is some solution of the deposits (Fig. 4). It is noteworthy that the integral change in the intensity of the impurity peak, probably Be_5(Fe, Al), measured with an x-ray diffractometer, obeys exactly the same temperature dependence as the electric resistance [4]. The identical kinetics of the drop in the resistance and increase in the intensity of the impurity peak indicates that the two methods record the same process–deposition of impurities from the matrix.

Subsequently the method of electric resistance for studying aging was developed in [5]; it was proposed that the relative residual resistance $\delta_R = R_{4.2°K}/R_{room\ t.}$ be used to increase the sensitivity of the method. On the basis of the method developed for determining the optimum systems of aging, it was demonstrated that even the maximum-purity metal (~99.96% Be) has a tendency for aging, and the temperature of heat treatment increases with increasing content of impurity.

Change in Structure during Aging

The Metallographic Data of most researchers show that the deformation of aged samples, in contrast to the deformation of homogenized samples, is accompanied by intensive slip along the planes (001) and (100); the grains are elongated in the direction of the deformation; the fracture becomes fibrous and passes along the grain. Only in [13] was breakdown along the grain boundaries observed in all the broken samples. The deposition of phases during aging and their dissolving after homogenization was observed metallographically in [4, 13].

Electron Diffraction and X-Ray Spectral Point Microanalyses using microbeams permit the determination of individual impurities in regions of several microns. Such a resolution makes the method extremely promising for investigating the distribution of impurities in various treatments. The aging of beryllium was studied by this method in [4, 11, 14, 15]. In samples of beryllium homogenized at temperatures above 1000°C, iron is uniformly distributed

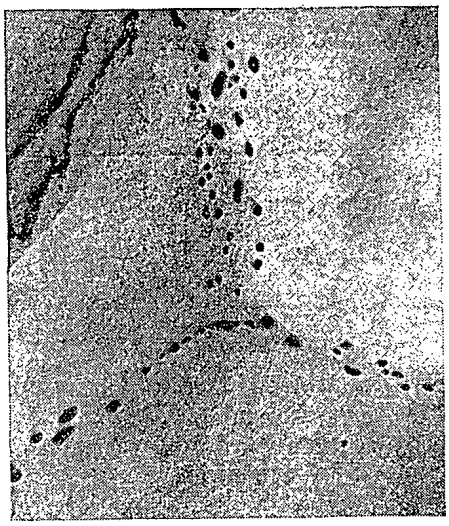

Fig. 6. Photomicrograph of alloy of Be–0.15% Fe after annealing at 800°C for 8 h (× 10,000 [11]).

in the matrix. Aging within the temperature region 700-800°C leads to enrichment of the grain boundaries in iron (Fig. 5); moreover, the degree of enrichment increases with time, which indicates diffusion of iron toward the boundaries. As a rule, places with an increased iron concentration are also enriched in aluminum and silicon; this is evidently due to the formation of complex compounds during the aging process. Although the deposition of iron along the boundaries is accompanied by impoverishment of the matrix, according to the data of [14, 15], in a later investigation [11] it was shown that the average iron concentration in the matrix is practically unchanged after aging. This means that the deposits are also formed in the grain itself; moreover, the pathway of migration of atoms to such deposits is short. It is interesting that some impoverishment in iron of the regions situated around the deposit was observed in [4]. In beryllium containing an average of 0.15% iron, after heat treatment (800°C, 120 h), the iron concentration in the deposits on the boundaries reaches 7% [11]. In alloys with increased iron content (1-5%), aging is accompanied by diffusion of iron to the boundaries, defects, and pores, where inclusions of $Be_{13}Fe$, containing 31% iron (equilibrium content 32.4% iron) are formed. Fine deposits of intermetallic compounds are frequently formed parallel to the planes {001} of the beryllium lattice.

Point microanalysis of the initial samples, existing in an intermediate state, did not reveal any deposits of iron on the grain boundaries. A distinguishing feature of the initial samples in comparison with homogenized samples is the presence in the matrix of inclusions with a somewhat increased iron concentration (0.3% at an average content of 0.18%). Evidently these accumulations correspond to an early stage of deposition of the impurity. The material in the initial state is characterized by low mechanical properties [11].

In aged alloys of beryllium with manganese (0.18%) and chromium (0.2%), enrichment of the grain boundaries in impurities is not very noticeable. Manganese and chromium are deposited in the form of large inclusions, containing up to 30% of the alloying element, and usually enriched in iron, aluminum, and silicon. The chromium content in the matrix decreases to 0.02% after aging.

Inclusions of aluminum and silicon on the grain boundaries are observed in all three states of the material, which is evidence of their low solubility in beryllium. Heat treatment has little effect both upon the distribution of these impurities and upon properties of the corresponding alloys, containing 0.4% aluminum or silicon. It is only accompanied by diffusion of iron, present in the form of an impurity, toward the inclusions of aluminum and silicon.

Electron Microscopy [6, 11, 14] gives evidence of the presence of deposits ~0.1-0.5 μ in size, formed within the grain, in aged (800°C, 2 h) samples. The deposits are laminar and evidently are arranged parallel to the planes {001}. Their density reaches $\sim 10^{14}/cm^3$.

In the intermediate state, characterized by intergranular breakdown, the inclusions are concentrated in a zone ~2 μ wide, adjoining the boundaries [14]. Aging leads to purification of this zone and the deposition of phases on the boundaries and in smaller amounts in the matrix; the zone near the boundary is free of deposits (Fig. 6). In spite of a certain growth of the deposits during prolonged exposures, aging is characterized by the formation more likely of fine inclusions than of large equilibrium phases. The structure of the homogenized samples is characterized by the absence of deposits in the matrix and on the boundaries [11]. No evidence of breakdown of the supersaturated solid solution is detected in annealing all the way up to 450°C.

Phase Analysis of the samples at different states was conducted by chemical [16], x-ray diffraction [4, 13, 14, 17, 18], and electron-diffraction [13] methods. In the latter case, the precipitate formed after solution of the sample was analyzed. BeO, Be_2C, free silicon, and several other phases were found in technical beryllium. In particular, Moore [14] observed two cubic phases with lattice K12, a = 4.04 A and K6, a = 4.33 A. The first of them was also detected by Rooksby [17] and most likely belongs to inclusions of aluminum. Coarse inclusions (~30 μ) of a cubic intermetallic compound with parameter a = 10.4 A, close in composition to $MgBe_{13}$ [13], have also been observed [13].

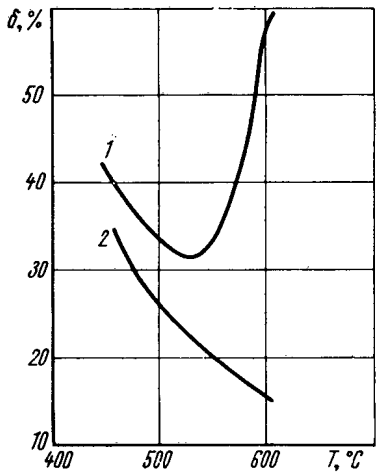

Fig. 7. Dependence of the relative elongation on the temperature for beryllium with various iron and aluminum contents [19].

After aging of the samples, a compound isostructural with the cubic phase of Be_5Fe (a = 5.88 A), but with parameter a = 6.05-6.10 A [4, 13, 14, 16-18] is deposited. It may be identified as Be_5 (Fe, Al); however, the ratio of iron and aluminum in this phase has not been established [17].* A double beryllide is present both in homogenized and in aged alloys of beryllium with iron and aluminum (1% each). In the aging of beryllium under definite conditions, instead of Be_5(Fe, Al), a hexagonal phase $Be_{11}Fe$ (in [18] it is identified as $Be_{12}X$) is formed.

After homogenization of the samples at 900°C for 6 h, Be_5(Fe, Al) is converted to a solid solution and is not detected by x-ray diffraction study. Aging is accompanied by the deposition of a double beryllide with regular orientation with respect to the matrix: {111} and {110} $Be_5(Fe,Al) \parallel$ {001} and {100} Be [4, 17, 18]. Deposition is also promoted by a stressed state of the sample, created before or during aging [13].

If homogenization is conducted at higher temperatures (1000° C, 6 h) or with more prolonged exposure (950°C, 50 h), then instead of $Be_5(Fe,Al)$, during subsequent aging $Be_{11}Fe$ is formed, also with regular orientation with respect to the matrix: {001} and {110} $Be_{11}Fe \parallel$ {001} and {100} Be. The cause of the change in the type of deposits depending on the system of homogenization has not been definitively established. According to the data of [13], $Be_5(Fe,Al)$ is formed in the association of $Be_{11}Fe$ with aluminum. During homogenization, iron is deposited from $Be_5(Fe,Al)$ and is discharged into the solution, while aluminum practically does not dissolve. Hence, it may be that at higher temperatures or increased duration of homogenization, iron dissolves more uniformly, which hinders its subsequent interaction with aluminum.

Formation of Liquid Phases at the grain boundaries in technical-purity beryllium has been observed in a series of studies [3, 15, 19, 20], the authors of which explain the reduced plasticity of beryllium within the temperature region 400-600°C by weakening of the boundaries. The improvement of the properties of beryllium after aging in this case is explained by two factors: diffusion of iron to the grain boundaries, which leads to plasticizing of the matrix, and its interaction on the boundaries with aluminum, forming more refractory phases and strengthening the boundaries. Such phases are evidently $Be_5(Fe,Al)$ with parameter a = 6.07 A (in [15] it is interpreted as a Be—Fe—Al—Si phase) or $FeAl_3$, which is formed only at high contents of aluminum and iron in beryllium.

Experimentally, the liquid phase enriched in aluminum and silicon is detected on the grain boundaries of technical beryllium by x-ray diffraction and thermal analyses and by a direct electron-microscopic method.

The melting point of the triple eutectic Be—Al—Si, formed in the technical metal with an increased aluminum and silicon content, according to the data of [3], is equal to 440°C, which corresponds to the temperature of the beginning of the drop in plasticity and the beginning of intergranular breakdown. In this same work it was shown that the effect of heat treatment of beryllium depends on the ratio of aluminum and iron impurities. If the amounts of these impurities are comparable, then aging (650°C, 90 h) leads to an increase in the plasticity of beryllium (Fig. 7, curve 1) on account of the interaction of iron with aluminum, disappearance of the liquid phase, and elimination of intergranular breakdown. The predominance of the aluminum impurity over iron is undesirable, since the reaction does not go to completion, and therefore the liquid eutectic is partially preserved and intergranular breakdown is not eliminated after aging (see Fig. 7, curve 2). The critical ratio of contents of aluminum and iron impurities in beryllium is ~0.8 [19]; moreover, when it is further increased, the effect of heat treatment decreases.

The Influence of Heat Treatment (650°C, 110 h) on the Mechanism of the Plastic Deformation of technical beryllium during stretching of the samples in the temperature region 20-900°C was investigated in detail in [19]. To determine the role of the liquid phase, the authors of this work selected two grades of beryllium: grade A, containing 0.1% Al, 0.028% Fe, and 0.02% Si, with a ratio Al/Fe = 3.5, and grade B, containing 0.012% Al, 0.018% Fe,

*In [21], a triple compound of beryllium, the stoichiometric composition of which corresponds to the formula $AlMBe_4$ (here M represents Fe, Mn, or Ni), was produced artificially by fusion of the components. The coincidence of the structures and parameters of $AlMBe_4$ and the phase detected in beryllium gives a basis for concluding that these phases are identical.

0.0028% Si, with a ratio Al/Fe = 0.67. In metal A, there is a liquid phase on the grain boundaries at 500°C. Deformation of this metal at the indicated temperature is accomplished on account of shear along the boundaries and ends in intergranular breakdown; at 600°C, moreover, the formation of deposits is observed in the grains. Aging of metal A does not eliminate the liquid phase on the grain boundaries.

In beryllium B, the liquid phase is not observed. Deformation of the metal in the initial state at 150-300°C is characterized by the appearance of lines of slip along the planes (001) and (100) and faults within the grains. The authors note that bending of the planes during the formation of faults increases with increasing temperature. Above 350°C, the faults mutually intersect. If the texture of the sample promotes slip along (001), then at 500°C the faults possess greater amplitude and form complexes; the slip bands in this case are broad and break up the grain into blocks. At the temperatures 650-750°C, the faults precede other types of deformations and are extremely mobile.

Aged beryllium, grade B, differs from the initial beryllium in two features: 1) within the temperature region 500-600°C, not only slip packets, but also very thin, uniformly distributed slip lines are observed; 2) the mobility of the faults increases, and at 500°C they behave just as in the initial metal at 650°C. The authors explain this increase in the mobility by refinement of the grain on account of the migration of iron to the aluminum accumulations at the boundaries.

The influence of heat treatment on the plastic deformation of single crystals of beryllium was investigated in [22], in which a difference of the mechanisms of aging at temperatures above and below 575°C was detected. If the yield point of the single crystals is substantially lowered after aging at 575°C, then heat treatment at lower temperatures is accompanied by the reverse effect. The activation energy of plastic flow in this case changes substantially, from 48 kcal/mole above 575°C to 16 kcal/mole in the region of 300-550°C.

The absence of a positive effect of aging at low temperatures and exposures sufficient for diffusion is explained by the authors of [22] by two factors. In the first place, the conditions of interaction of substitutional impurities with aluminum, which crystallizes at low temperatures, while at high temperatures it exists in the form of a liquid phase, are changed. The change in the activation energy may be explained by a second factor—by a predominant contribution of interstitial atoms to diffusion, for example, of carbon. Both of the indicated principles will need an experimental verification.

Mechanism of Aging

The experimental data on the aging of beryllium permit a sufficiently full representation of the picture of this process. Although not all details have been confirmed experimentally, the general mechanism of the process is rather clear.

From the microscopic standpoint, the following observations are the most important for characterizing aging: the removal of certain impurities (for example, chromium) from the matrix after aging, segregation of a number of elements (for example, iron) to the boundaries and other active points in the matrix, refinement of the matrix from impurities in the zone close to the boundaries, intensive development of slip and faults in the aged metal, the absence of multiple slips, a harmful influence on the plasticity of the liquid phases.

Obviously aging represents a rather complex process, leading to a substantial change in the properties both of the matrix and of the grain boundaries. It is inadvisable to distinguish these two factors, as is done in a number of studies.

In the homogenized (or intermediate) state of the metal, its matrix represents a supersaturated solid solution. It is rather improbable that this solution is homogeneous; evidently even in the case of high rates of cooling, small zones enriched in impurities have time to form in the matrix, while in the case of low rates of cooling, even dispersed deposits, which do not yet possess phase boundaries, can be formed. As a result of the smallness of these regions and the absence of boundaries, it is most difficult to study the metal in the homogenized state; at the present time there are practically no direct data on the structure of beryllium existing in the state of predeposition. Nonetheless, diffuse dispersed regions with an increased concentration of impurities do exist, which is evidenced by the absence of any appreciable difference of the lattice parameters in homogenized and aged beryllium.

In the case of deformation above 350-400°C, thermal activation and a stressed state, facilitating diffusion, promote a further occurrence of the deposition process: dispersed deposits, coherently bounded to the matrix, are formed along the shearing planes and at the boundaries. Thus, dispersion strengthening is one of the causes of the

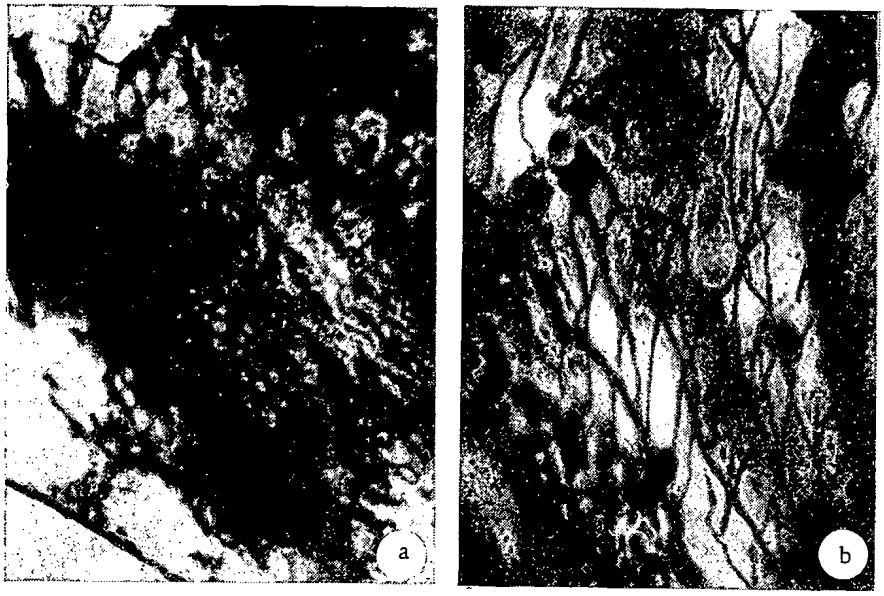

Fig. 8. Dislocation structure of homogenized beryllium [a(× 80,000)] and beryllium aged at 800° C for 120 h [b(× 100,000)] [11].

decrease in the plasticity in the region of 400-600°C. From dislocation concepts it follows that when dispersed phases are present in the matrix, relatively nonmobile accumulations of dislocations are formed. The presence of such accumulations and networks of dislocations in the homogenized state has been confirmed experimentally (Fig. 8, a) [11]. For comparison, Fig. 8, b shows the dislocation picture of aged beryllium, characterized by the presence of long and sharply intersecting lines of dislocations, which lie in the base plane. Since the shearing of dislocations in the homogenized matrix is hindered and is manifested only in the case of great stresses in the form of multiple slip, the deformation of the samples is accomplished chiefly through shearing on the boundaries. Relaxation stresses in the boundary regions, where dispersed deposits are very numerous, is impossible; hence, deformation along the boundaries leads to premature breakdown.

Aging produces growth of the deposits and a change in the state of the boundary regions and of the boundaries themselves. However, the process of deposition with the formation of phase boundaries is not so simple as was believed in earlier works. Although aging leads to an almost complete deposition of chromium from the matrix and a reduction of its hardness in beryllium-chromium alloys, in beryllium-iron alloys the iron content in the matrix changes little. It would be incorrect to think that the deposits of new phases are formed exclusively at the grain boundaries. They also grow within the matrix itself, but after the appearance of phase boundaries they cease to exert a strengthening effect upon it. It is extremely important that the process of growth of the deposits proceeds on account of a refinement of the matrix in close-lying portions. Since the grain boundaries are evidently the deepest potential wells in comparison with all other defects, they are responsible for the most powerful drainoff of impurities; hence, the impurity-free zone is broadest close to the boundaries. Thus, the refinement of the matrix, eliminating (or weakening) the interaction of dislocations with the impurities, on the one hand, and the formation close to the boundaries of zones free of impurities and capable of relaxing the stress of the boundaries, on the other—these are the basic conditions for improving the plasticity of beryllium after aging, related to the properties of the matrix.

The change in the state of the boundaries after aging is determined by two mechanisms: by the possible removal of the liquid phase in beryllium enriched in aluminum and silicon, on account of the formation of $Be_5(Fe, Al)$ or other compounds, and by strengthening of the boundaries by the particles of the deposits. In connection with the latter mechanism, let us mention that it is scarcely expedient to introduce the concept of the "wedging" effect of deposits on the boundaries, as is done in a number of studies. If, on the other hand, we speak of the micromechanism of the processes related to the boundaries, then the best model for aging is the removal of the thin brittle interlayer of dispersed deposits present near the boundaries, and the formation of coarse deposits, which are observed experimentally [11]. Moreover, plastic flow is obtained in the regions adjoining the boundaries. Thus, the elimination of reduction of shearing along the grain boundaries through a facilitation of plastic deformation of the matrix and of the regions around the boundaries is another condition for improving the plastic properties of aged samples, related to the properties of the grain boundaries.

It is somewhat more difficult to interpret the influence of aging on the strength properties of beryllium. Since the process is accompanied by softening of the matrix, on the one hand, and by an increase in the strength of the boundaries, on the other, then the summary effect may depend on the grade of the metal, the type and amount of impurities. Depending on which of the indicated mechanisms predominates, both a general decrease and a certain increase in the strength of the samples are possible. In practice, most often the strength changes little after aging.

It will be difficult to expect any significant effect of aging upon the plastic properties of beryllium at room temperature. If, after the completion of aging, the solid solution may be considered as at equilibrium in the temperature region ~600°C, then at room temperature, when the solubility of the impurities is appreciably reduced, the matrix is supersaturated by the impurities and is in a strengthened state.

As can be seen from the above, the mechanism of aging cited is not confirmed experimentally in all respects and contains a number of hypotheses. It does not consider the extremely probable influence of oxide, carbide, and other light phases upon the aging process. Aging may not be a single process, responsible for the change in the properties of beryllium after heat treatment. Hence, it should be considered as a first approximation to the true picture.

CONCLUSIONS

1. The plasticity of beryllium objects within the temperature region 400-600°C can be substantially increased by aging.

2. The system of aging depends on the type and content of impurities. Usually when their content increases, the temperature of aging increases.

3. The duration of annealing may be reduced through the use of a preliminarily-stressed material or by deformation aging.

4. The aging of beryllium containing large quantities of aluminum and silicon promotes a slight increase in the plasticity. Supplementary alloying of such metal with iron may increase the effectiveness of heat treatment.

5. The aging of objects subject to creep deformation leads to an improvement of their properties. The best preliminary treatment for such material is homogenization.

LITERATURE CITED

1. A. Brown, F. Morrow, and A. Martin, Nature, 187, 494 (1960); J. Less-Common Metals, 3, 62 (1961).
2. W. Beaver and K. Wikle, Trans. AIMME, 200, 559 (1954). Translation in the Col.: Beryllium [Russian Translation], No. 4, Izd. Inostr. Lit., Moscow (1956), p. 65.
3. M. Weisz, J. Mallen, and J. Baron, J. Nucl. Materials, 10, 56 (1963).
4. A. Wolff, S. Gelles, and L. Aronin, In the Metallurgy of Beryllium, Chapman and Hall, London-New York (1963), p. 150.
5. I. G. D'yakov, I. I. Papirov, and G. F. Tikhinskii, Fiz. Metallov i Metallovedenie, 19, 788 (1965).
6. G. Old, et. al., In the Metallurgy of Beryllium, Chapman and Hall, London-New York (1963).
7. D. Mach, Trans. AIMME, 203, 1235 (1955).
8. S. Gelles, I. Pickett, and A. Wolff, J. Metals, 10, 789 (1960).
9. V. M. Amonenko, et. al., Atomnaya Énergiya, 16, 426 (1964).
10. F. Morrow and A. Moore, Report AWRE-013/63 (1963).
11. G. Ranzetta and V. Scott, J. Nucl. Materials, 10, 113 (1963).
12. R. Thompson, B. Begley, and A. Martin, J. Less-Common Metals, 3, 170 (1961).
13. A. Jones and R. Weiner, J. Less-Common Metals, 6, 266 (1964).
14. A. Moore, J. Nucl. Materials, 3, 113 (1961).
15. Y. Adda, et. al., C. r. Acad. Sci., 254, 1052 (1962).
16. H. Rooksby and I. Green, Analyst, 87, 539 (1962).
17. H. Rooksby, J. Nucl. Materials, 7, 205 (1962).
18. P. Pointy, et. al., C. r. Acad. Sci., 250, 2365 (1960); 256, 4419 (1953).
19. P. Bastien and P. Pointu, J. Nucl. Materials, 10, 63 (1963).
20. G. Donze, et. al., J. Nucl. Materials, 6, 137 (1962).
21. I. Carrabine, J. Nucl. Materials, 8, 278 (1963).
22. D. Beasley, Paper No. 16, Conference internationale sur la Metallurgie du beryllium. Grenoble, 17-20 Mai (1965).

CORROSION OF STAINLESS STEEL APPARATUS IN CONCENTRATION OF RADIOACTIVE SOLUTIONS BY EVAPORATION

(UDC 620.193.4)

M. M. Kurtepov

Translated from Atomnaya Énergiya, Vol. 19, No. 2,
pp. 153-157, August, 1965
Original article submitted August 20, 1964

The peculiarities of the corrosion of austenite stainless steel of the 18-8 type, used as construction materials for apparatus for concentrating nitric acid solutions of radioactive wastes by evaporation, are discussed. The influence of the concentration and temperature of the HNO_3 solutions, as well as of of the corrosion products on the corrosion of stainless steel apparatus is demonstrated.

Possible methods of controlling apparatus corrosion are discussed.

During the chemical reprocessing of nuclear fuel, large quantities of liquid nitric acid solutions with medium and high radioactivity are accumulated. The storage of such solutions involves serious difficulties, which gives rise to the need for concentrating these solutions to small volumes. The most widely used and effective method of concentrating liquid wastes is their evaporation in apparatuses of chromium-nickel austenite steels of the 18-8 type [1]. In this case, concentrated solutions of nitric acid with a substantial content of nitrates of the alkali metals and uranium, possessing high oxidation-reduction potentials, are obtained. This communication is devoted to a consideration of the corrosion of austenite stainless steels in such nitric acid media.

It is known that chromium-nickel austenite steels possess high corrosion resistance in many aggressive media as a result of the ease of the formation of phase, oxide, or adsorption films upon their surfaces. The corrosion of apparatus of austenite stainless steels in the passive state is minor and is determined chiefly by the rate of solution of the protective film on the surface. All conditions guaranteeing a preservation of the protective film on the stainless steel surface will promote maintenance of the passive state and a reduction of the corrosion rate.

Recently many researchers have established the existence of a definite relationship between the rate of corrosion of metals and alloys and their potentials in various media. Chromium-nickel austenite steels possess high corrosion resistance only within a quite definite region of potentials. Characteristic regions, in each of which the solution of steel possesses its own peculiarities, may be distinguished on a graph of the dependence of the rate of corrosion of steel on the potential (Fig. 1) [2]. The region of potentials in which steel is passive is bounded on the side of negative values by the activation potentials ε_A, and on the side of positive values by the potential of the beginning of overpassivation ($\varepsilon_{b.\,over}$). A displacement of the potential of steel from ε_{st} to $\varepsilon_{b.\,over}$ is not accompanied by any appreciable increase in the corrosion rate. Corrosion of steels in dilute HNO_3 solutions at low temperatures corresponds to this case. In the region of high positive potentials (above $\varepsilon_{b.\,over}$), a great increase in the rate of corrosion of steels from the state of overpassivation is observed. Such a case is realized in concentrated HNO_3 solutions at the boiling point. The disturbance of the passive state of stainless steels at high positive potentials is due to oxidation of the protective film on the surface of the steel to readily soluble higher oxides or compounds.

In our studies, it has repeatedly been shown that the corrosion of stainless steels of the 18-8 type in solutions of HNO_3 up to a concentration of 16 M at temperatures up to 100°C proceeds from the passive state at low rates, which do not exceed 0.2 g/m^2/h. However, at the boiling point the corrosive aggressiveness of HNO_3 solutions is substantially increased, and at a concentration above 8 M, the rate of corrosion of steels rises sharply (Fig. 2). Under these conditions, the oxidation-reduction potential of the solution exceeds the potential of breakdown of the passive state of the steel (for example, in 14 M acid, the stationary potential of the steel is equal to 1.4 V), and the corrosion of steel from the state of overpassivation becomes thermodynamically possible. The corrosion of stainless steels

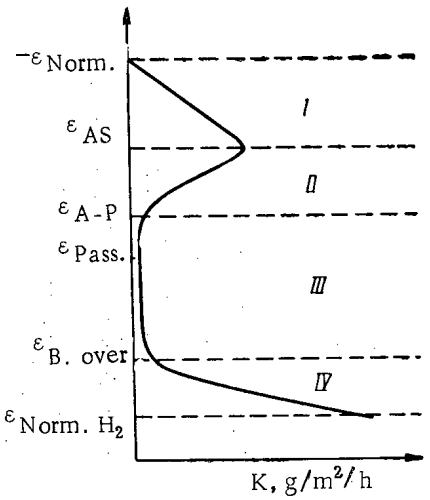

Fig. 1. Dependence of the rate of corrosion (K) of stainless steel on the potential ε in various regions: I) active state; II) active-passive state; III) stable passive state; IV) state of overpassivation.

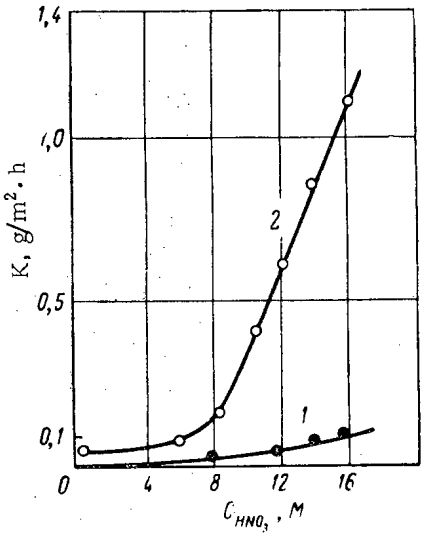

Fig. 2. Dependence of K of 18-8 steel with titanium on the HNO_3 concentration C_{HNO_3} and the temperature: 1) 60°C; 2) boiling point.

in boiling concentrated HNO_3 solutions proceeds with predominant cathodic control on account of the inhibition of the processes of reduction of HNO_3. We should mention that at low temperatures the cathodic processes of reduction of HNO_3 to HNO_2 and N_2O_4 occur on the passivated surface, while in boiling concentrated solutions they occur on the surface of stainless steel in a state of overpassivation.

The observed increase in the rate of corrosion of stainless steels of the 18-8 type in boiling solutions of concentrated HNO_3 is due not only to an increase in the oxidative properties of the solutions, but also to the accumulation of corrosion products in solution in the form of ions of metals of high valence, for example, Fe^{+3}, Cr^{+6}, Mn^{+7} [3]. The formation of such ions is possible both as a result of the oxidation of ions of metals of lower valence in the volume of the solution and in the oxidation of protective (oxide) films on the surface of the steel as a result of the high oxidizing properties of the solution. Of course, metal ions of higher valence will be reduced in the corrosion process, and the reduction products will participate in the corrosion process. Thus, extremely complex corrosion processes may take place in boiling solutions of concentrated HNO_3. The presence of Fe^{+3}, Cr^{+3}, Cr^{+6}, Mn^{+2}, Mn^{+4}, and Mn^{+7} ions in boiling solutions of concentrated HNO_3 leads to a substantial intensification of the corrosion of type 18-8 stainless steels. The corrosion rate of the steels increases with increasing HNO_3 concentration and with the content of ions of metals of variable valence in the solution.

The corrosion of steel is appreciably increased when the solution contains Fe^{+3} ions (Fig. 3). We should mention that in the same solutions at lower temperatures (up to 80°C), no increase in the corrosion of steel by the Fe^{+3} ion is observed, and the steel is dissolved from the passive state. The corrosion of stainless steel is also intensified in boiling dilute (for example, 2.5 N) HNO_3 solutions, in the presence of a high content of ferric nitrate. The observed increase in the corrosion of steel by the Fe^{+3} ion is accompanied by a shift of the potential of steel in the region of high positive values and by a facilitation of the cathode processes. One of the conditions of facilitation of cathode processes on the surface of corroding steel is evidently the formation of HNO_2, which is catalyzed by the Fe^{+3} ion. An extremely strong effect upon the corrosion of stainless steel in boiling solutions of HNO_3 is exerted by Cr^{+6} ions. The rate of corrosion of steels under these conditions is greatly increased even when the solution contains small amounts of Cr^{+6} ions (for example, in dilute solutions of HNO_3 at 100°C) (Fig. 4). Since nitric acid solutions with the Cr^{+6} ion possess a high oxidation-reduction potential, under these conditions the passive state of the stainless steels is easily disturbed, and their corrosion proceeds at great rates from the state of overpassivation.

The rate of corrosion of steels in boiling solutions of concentrated HNO_3 is also increased by the Cr^{+3} ion (Fig. 5). In this case, the intensification of the corrosion of steel is due to an increase in the depolarizing properties of the solution on account of the formation of chromium compounds of higher valence.

The corrosion of stainless steels in boiling concentrated solutions of HNO_3 is intensified by manganese ions of any valence, which are easily oxidized under these conditions to ions and compounds of higher valence (Fig. 6). At low temperatures, such an effect is observed only in the presence of Mn^{+7} ions in solution. The effect of manganese ions in boiling solutions of concentrated HNO_3 is analogous to the action of Cr^{+6} ions. The corrosion of steels occurs at high positive potentials from the state of overpassivation. In the presence of a large content of nitrates of metals (of constant of variable valence), intensification of the corrosion of stainless steel in boiling concentrated solutions of HNO_3 is possible on account of the facilitation of cathode processes.

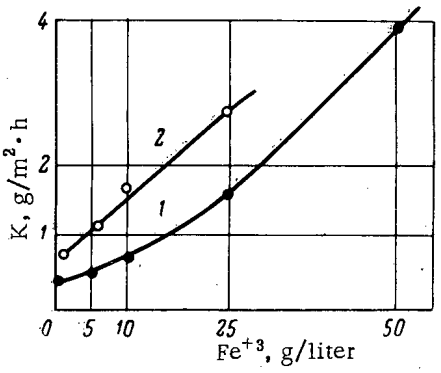

Fig. 3. Influence of Fe^{+3} on K of 18-8 steel with titanium in boiling solutions of HNO_3: 1) 12 N; 2) 14 N.

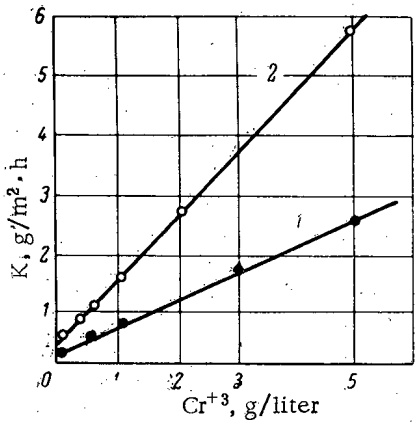

Fig. 5. Influence of Cr^{+3} on K of 18-8 steel with titanium at various concentrations in boiling HNO_3 solutions: 1) 12 N; 2) 14 N.

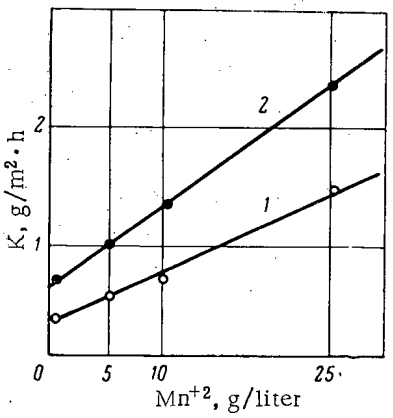

Fig. 6. Influence of Mn^{+2} on K of 18-8 steel with titanium at various concentration of boiling HNO_3 solutions: 1) 12 N; 2) 14 N.

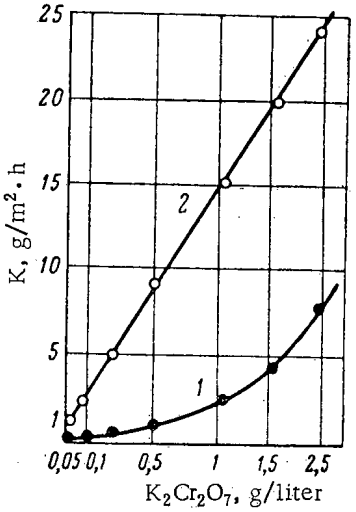

Fig. 4. Influence of Cr^{+6} on K of 18-8 steel with titanium at 100°C and various HNO_3 concentrations: 1) 1 N; 2) 2.5 N.

The introduction of a small amount of Cl^-, SO_4^{-2}, or PO_4^{+3} anions into a solution with high oxidation-reduction potential does not increase the corrosion of stainless austenite steels. As for the effect of radioactive radiation of the solutions, in this case even an increase in the corrosion resistance of stainless steel apparatus may be observed as a result of the decrease in the agressiveness of the solutions on account of the reduction of metal ions of high valence, serving as stimulators of corrosion.

The corrosion of austenite stainless steels from the passive state depends little upon their composition. However, it should be mentioned that steels with molybdenum and titanium undergo stronger corrosion in the state of overpassivation.

Moreover, it is important to emphasize that stainless steels of the 18-8 type undergo strong intercrystallized corrosion in solutions with high oxidation-reduction potential. Our study of the conditions of appearance and development of intercrystallite corrosion on 18-8 stainless steels have shown that all steels are subject to such corrosion breakdown, independent of their composition, stabilization, (with titanium, niobium), and heat treatment. The development of intercrystallite corrosion under these conditions is due to the predominant solution of phases rich in chromium (carbides, sigma-phase) along the boundaries of the crystallites.

The guarantee of high corrosion resistance of welded joints is of great importance for reliable and prolonged operation of austenite-stainless-steel apparatus. As is well known, welded joints are zones with reduced corrosion resistance in comparison with the basic metal, as a result of their structural inhomogeneity. Moreover, intercrystallite corrosion may develop at the sites of the defects. A great effect upon the corrosion resistance of welded joints is exerted by heat treatment [4, 5]. In boiling concentrated HNO_3 solutions, high corrosion resistance is observed in welded joints quenched and not heat treated. Brief tempering under any systems of heat treatment, independent of the composition of the steel and alloying of the seam (with titanium, niobium),

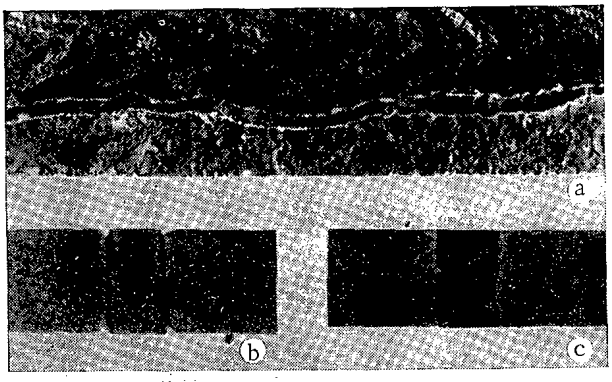

Fig. 7. Knife corrosion of a welded joint of austenite stainless steel of the 18-8 type in acid oxidizing solutions (a, b, c—various stages of corrosion of an industrial part).

increases the corrosion of the welded joint. A useful heat treatment, followed by brief tempering of the welded joint in the zone of dangerous temperatures, is stabilizing annealing, which increases the stability to intercrystalline corrosion. Stabilization of the seam metal with titanium increases the general corrosion of the welded joint, and, moreover, after brief repeated heating, the unstabilized and titanium-stabilized seam metal undergoes intercrystalline corrosion [4]. Hence, when type 18-8 steel with titanium is used for evaporating apparatus, anticorrosion protection is essential.

Recently it has been established in a number of studies that welded joints even of stabilized (with titanium, niobium) steels of the 18-8 type are subject to a new type of intercrystalline corrosion breakdown in boiling solutions of concentrated HNO_3—the so-called concentrated, or knife corrosion along the line of fusion of seam-base metal (Fig. 7) [6-8]. Concentrated (knife) corrosion damages chiefly the portions of the welded joint that are first heated to high (>1370°C) temperatures, at which the carbides of the stabilizing elements dissolve, and then subjected to brief repeated heating within the interval of dangerous temperatures, which creates conditions for breakdown of austenite along the grain boundaries and the deposition of chromium carbides. As a result, the steel acquires a tendency toward intercrystalline corrosion. The intercrystalline corrosion of austenite stainless steels and their welded joints is a local breakdown of the passive state. Such corrosion damage of apparatus during the concentration of liquid radioactive wastes requires thorough deactivation during repairs.

Various methods may be used to control corrosion of austenite stainless steel apparatus in the concentration of radioactive nitric acid solutions by evaporation: reduction of the oxidation-reduction potential of the solutions by lowering the temperature during evaporation; removal of ions of metals with variable valence from the solution during evaporation; introduction of corrosion inhibitors into the solutions; use of stainless steels with increased corrosion resistance; cathodic protection from the external current source.

An analysis of the experimental data on the corrosive aggressiveness of HNO_3 solutions with respect to austenite stainless steels permits us to draw the following brief conclusions:

1. The corrosion of steels in boiling (8-16 M) HNO_3 solutions proceeds with a breakdown of the passive state according to the mechanism of overpassivation.
2. The accumulation of corrosion products in HNO_3 solutions in the form of ions of metals of variable valence increases the corrosion rate.
3. In concentrated boiling solutions of HNO_3, stainless steels of the 18-8 type undergo intercrystalline corrosion, while their welded joints undergo concentrated (knife) corrosion along the line of fusion seam-basic metal.

LITERATURE CITED

1. Waste Products of Atomic Industry. Collection of Articles Edited by Glueckhauf [Russian Translation], Gosatomizdat, Moscow (1963).
2. M. M. Kurtepov and E. N. Mirolyubov, Atomnaya Énergiya, 15, 37 (1963).
3. M. M. Kurtepov and A. S. Gryaznova, Dokl. AN SSSR, 135, 899 (1960).
4. M. M. Kurtepov and A. S. Gryaznova, Metallovedenie i Termich. Obrabotka Metallov, 4, 41 (1959).
5. B. I. Medovar, Welding of Chromium-Nickel Austenite Steels [in Russian], Mashgiz, Moscow (1958).
6. B. I. Medovar, N. A. Langer, and M. M. Kurtepov, Intercrystalline Corrosion and Corrosion of Metals in the Stressed State [in Russian], Mashgiz, Moscow (1960).
7. M. M. Kurtepov, Dokl. AN SSSR, XCIX, 2, 305 (1964).
8. Yu. I. Kazenov, Avtomat. Svarka., 9, 91 (1955).

CONTINUOUS, CENTRALIZED MONITORING OF INDIVIDUAL RADIATION DOSES*

(UDC 614.8 : 539.12.08)

V. S. Zhernov, N. V. Ryzhov, V. M. Skatkin, and V. S. Starovoitov

Translated from Atomnaya Énergiya, Vol. 19, No. 2, pp. 157-161, August, 1965
Original article submitted February 25, 1965

Possible methods are discussed for constructing a continuous, centralized monitoring system for individual personnel radiation doses based on the capabilities of modern nuclear electronics, radio technology, and computing techniques.

Versions of a monitoring system using dosimeters supplied with transmitters and one using fixed detectors of ionizing radiation are compared. An analysis is made of the problems involved in suitably representing and storing information concerning the magnitude of individual radiation doses after various time intervals when using individual dosimeters and also continuous, centralized monitoring.

One of the coming methods for the improvement of individual dosimetric monitoring is the introduction of continuous, centralized monitoring. This supposes a type of monitoring which assured, at every point in time, the remote acquisition at a single central console of information about the radiation dose rates of all workers and the appropriate treatment of this information to determine and store individual doses after various periods of time.

The remote, centralized measurement of individual radiation doses permits maximum automation of the monitoring process, elimination of a large number of manual operations, and avoidance of the need for evaluation of the radiation situation by the workers themselves. A qualified specialist, the health physicist on duty, who is located at a central console, makes such an evaluation and transmits the necessary instructions to the people who are in a hazardous radiation area. A single central installation to measure individual radiation doses, in which the number of units of electronic equipment is limited to a lesser degree than in individual dosimeters, permits considerable expansion of the monitoring function. In particular, it is easy to record not only the total doses, but also the nature of the variation of individual radiation doses with time, the need for which has been indicated [1].

Automation of Individual Dose Monitoring

We consider the possible methods for automating the storage and summation of individual dose values when ordinary, individual dosimeters are being used, which is a practical thing to do because automatic equipment is involved in a system of continuous, centralized monitoring.

Storage of Individual Doses. At the present time, it is recommended [2] that data obtained from individual dosimeters be written in a book in a form which is a three-dimensional record: worker number, data, and magnitude of dose (see table). One can achieve this kind of a record by means of the digital printers which are used for the output of information from digital computers and multichannel analyzers [3]. To cover the entire dose range of interest from 10 mR to 1000 R, it is sufficient to use four symbols, including the decimal point, for each individual. The use of a bicolored ribbon makes it possible to distinguish the values of doses which exceed permissible levels. The total dose after a required period of time is set apart by additional intervals between the rows. With this kind of a record, the number of controlled workers is limited by the carriage width of the digital printer (no more than

* This paper is an abbreviated version of a report given at the conference of SÉV member-countries on the dosimetry of ionizing radiation (Budapest, September-October, 1964).

Various Types of Records for Individual Radiation Doses

No.	Name \ Date	1	2	...	31	Total
1	Ivanov, I. I.	0,02	0,01		0,05	0,8
2	Sokolov, V. M.	0,03	0,01		0,01	0,7

a

Date \ Worker No.	Dose 1	2	...	31
1	0,01	0,04		0,03
2	0,02	0,03		0,01
...	0,05	0,1		0,04
31	0,05	0,1		0,01
Total	0,8	0,7		1,2

b

Date	Worker No.	Date	Date	Worker No.	Date
1	1	0,02	...	1	0,04
	2	0,05		2	0,06
	...			...	
		0,01			0,02
2	1	0,01	31	1	0,01
	2	0,03		2	0,07
	...			...	
		0,02			0,04

c

30 individuals per standard carriage width). There is also possible a two-dimensional type of record (see table, part c), less suitable from the point of view of using the results in the record, which allows one to control a practically unlimited number of workers.

Summation and Storage of Individual Dose Values. As can be seen in the table (part a), the recommended form of record for individual dose values includes the integral value for an extended period of time. With a large number of controlled workers, the operation of computing integral doses is rather laborious. If information on the dose magnitude is coded by a number of pulses, the dose-summation process can be automated with the help of multichannel pulse counters [4], "assigning" one of the channels for each controlled worker. This counter is a modification of the ferrite core memories used in computers and multichannel analyzers. It contains input shapers, ferrite matrix, adders, generators for readout and writing currents, and operates in the single-pulse recording mode. Information about the integral dose value for each controlled worker is stored in the corresponding row of the ferrite matrix, and can be output on auxiliary equipment by means of the adders.

By this means, one can set up the following system which assures the automatic recording and summation of doses measured with individual dosimeters (Fig. 1). An individual dose, of one kind or another, recorded by the individual dosimeter, is changed by the measuring apparatus into a current (or voltage) of proportionate magnitude which is then transformed by a converter into a number of pulses. The pulses are sent to the first multichannel counter. The required input of the multichannel counter is selected by pushing the appropriate button on the panel. Multichannel counter 1 accomplishes summation and storage of the number of pulses until the time when information is output to the printer, and permits the output of information to the printer channel by channel in the required sequence. A timer which triggers the distributor produces the command (once an hour or once a day) for output of information from multichannel counter 1. In this way, information from a row of the ferrite matrix is copied into the adders whence it is output to the printer, and then it is copied into multichannel counter 2, with erasure of the information in counter 1, by means of a pulse train generator. Simultaneously, the distributor controls the operation of multichannel counter 2. Thus the number from counter 1 is added, in the adder of counter 2, to the number which is stored in the corresponding row of counter 2. In this way, the numbers which correspond to the integral radiation doses of each controlled worker are stored in the ferrite matrix of counter 2. The integral dose values are output from counter 2 to the printer on call at arbitrary time. To accomplish this, the distributor is triggered, and it, in turn, outputs numbers from multichannel counter 2 with or without erasure of information. By means of call buttons on the digital readout, one can output information about the dose value in any channel of the counters (without erasing the information). The portion of the diagram bounded by the dashed lines in Fig. 1 accomplishes automation of the counting process for individual doses in those cases where the value of the dose is characterized by a series of pulses.

Centralized Monitoring of Individual Doses

Use of Fixed Sensors. If the radiation levels in working areas are constant in space, individual monitoring can be accomplished by means of sensors in remotely-controlled, fixed dosimetric instruments (Fig. 2). The residence

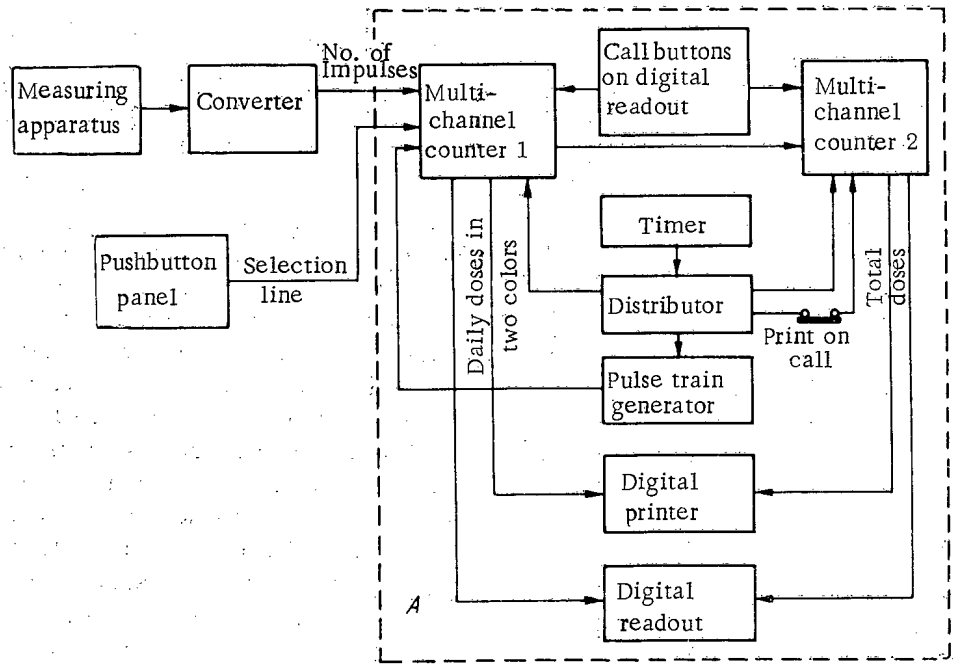

Fig. 1. Block diagram of arrangement for automatic recording and summation of doses measured by individual dosimeters.

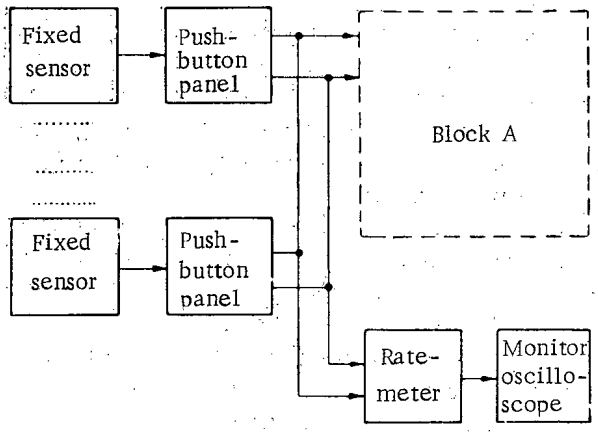

Fig. 2. Block diagram of an arrangement for individual monitoring by means of sensors in fixed dosimetric instruments.

time of workers in an area controlled by one of the sensors can be recorded on a central console by one means or another. This can be done, for example, by means of pushbutton panels distributed about the area of continuous operation. Activation of a pushbutton on the panel provides transmission of pulses from the sensor to the central console over the associated connecting line. The number of pulses which is transmitted over each connecting line characterizes the individual radiation dose for a particular person. The pulses are transmitted to an automatic individual dose counter arrangement of the kind shown in block A (see Fig. 1) where all the operations described are carried out. In contrast to the operation of the equipment for sequential reading of individual dosimeters, the pulses in the situation under discussion, which are transmitted simultaneously over many channels, are statistically distributed in time. Multichannel counter 1 can provide recording of these pulses. To do this, it is provided with input blocking during the handling of an individual pulse. During this time, the pulses which are being transmitted over other inputs are not counted, leading to an error in dose determination. The magnitude of this relative error is estimated by the expression

$$\delta = \frac{\tau \sum_{i=1}^{M} n_i}{1 + \tau \sum_{i=1}^{M} n_i},$$

where τ is the blocking time; M is the number of channels in the multichannel counter; n_i is the average rate of pulse transmission over the i-th input. In order that the error be small, it is necessary to decrease the blocking time and to reduce the average counting rate at the sensor output as far as possible.

Centralization of individual dosimetric monitoring makes it possible to follow continuously and remotely the radiation dose rates for each person. To accomplish this, the pulses from the sensors, which are transmitted over the

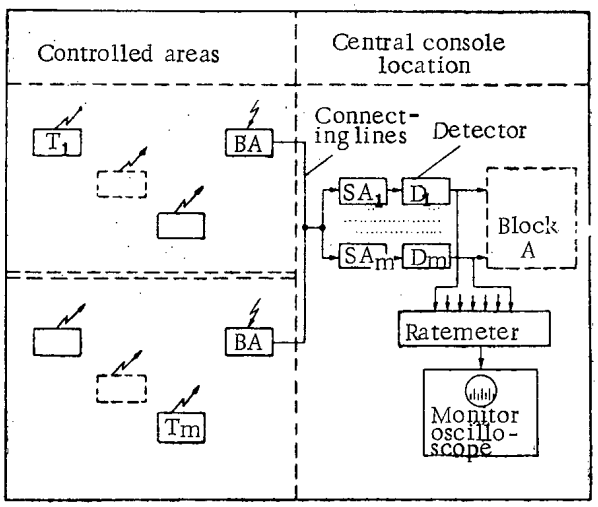

Fig. 3. Block diagram of an arrangement for telemetric measurement of individual doses.

connecting lines, are fed into a ratemeter which has an output voltage proportional to dose rate. Observation of dose rates is realized by means of a monitoring oscilloscope [5]. On its screen, vertical luminous lines are presented whose lengths are proportional to the voltages at the ratemeter.

Telemetric Measurement of Individual Doses. Generally, a radiation field changes not only in time but also in space. For that reason, it is expedient to consider a telemetric method of measuring individual doses based on radio transmission [1] of information from a pocket dosimeter (which measures dose rates). The achievements of modern electronics make it possible to produce fairly compact and simple dosimeters with transmitters which can be supplied to maintenance personnel and which will not interfere with their work. One of the possible ways of constructing a system for measuring individual doses by such a method is shown in Fig. 3. In this case, the fixed sensors in the arrangement shown in Fig. 2 are replaced by pocket dosimeters with a receiving-transmitting section.

A dosimeter with transmitter T which radiates a signal of fixed wavelength is attached to each of the M controlled workers. Antennas are located in each of the controlled areas and, where necessary, an input broadband amplifier BA to increase the strength of the signal which is transmitted along connecting lines to a central console. The signals from the connecting lines are fed into the inputs of the selective amplifiers SA, each of which is tuned to the wave length of the corresponding transmitter.

By means of these amplifiers, separation of signals of the required wave length and the required filtration of signals from other transmitters is accomplished. The pulses obtained after detection, which characterize the radiation dose rates of the workers, are sent to an arrangement similar to that shown in Fig. 1 (block A).

Such a method of monitoring individual radiation doses acquires the advantages of individual dosimeters in regard to the recording of radiation doses in radiation fields which are changing in time and space, and at the same time, it allows one to monitor dose rates continuously and remotely and to record dose magnitudes after an arbitrary period of time just as in monitoring with fixed sensors.

In conclusion, it should be noted that practically all the units in the scheme for monitoring individual radiation doses that has been discussed can be realized on the basis of well known and widely used methods in modern nuclear electronics and computing technology.

LITERATURE CITED

1. R. Sievert, A Method for Recording Individual Doses and Dose Rates while Working with Radioactive Sources, Euratom Symposium on Radiation Dosimetry, Euratom, Madrid (1963).
2. Handbook of Radiochemical and Dosimetric Techniques [in Russian], edited by N. G. Gusev, et. al., Medgiz, Moscow (1959).
3. Proceedings of the Fifth Scientific Technical Conference on Nuclear Electronics, Vol. IV, Automation of Measurements and of Data Analysis [in Russian], edited by V. N. Moiseev, Gosatomizdat, Moscow (1963).
4. N. V. Ryzhov and V. M. Skatkin, Nuclear Instrument Construction [in Russian], Gosatomizdat, Moscow (1964).
5. De Kimpe and Greif, An Automatic System for Analysis of Telemetry Data. Remote Control and Measurement [Russian Translation], Vol. II, Izd-vo Inostr. Lit., Moscow (1959).

THE PROVISION OF RADIATION SAFETY OF PERSONNEL IN THE EXTRACTION OF URANIUM ORES

(UDC 621.039.58 : 622.349.5)

A. V. Bykhovskii, N. I. Chesnokov, and I. L. Shalaev

Translated from Atomnaya Énergiya, Vol. 19, No. 2,
pp. 161-168, August, 1965
Original article submitted November 20, 1964

The radiation hazard to the respiratory organs of miners in uranium mines is assessed and a set of measures is worked out for ensuring radiation safety in the prospecting and extraction of uranium ores. Measures are described and justified which, as a result of achieving them, enable a standard to be set for a mining atmosphere and also to prevent external radiation overexposure and radioactive contamination of the integumenta of people working in the uranium mines.

In the problem of ensuring radiation safety in the peaceful uses of atomic energy, problems concerned with the uranium-extraction industry occupy an important position.

The principal factors of the effects of radiation in this branch of industry are radon and its decay products; radioactive isotopes of the uranium family which enter into the composition of mine dust; external β-γ radiation in the mine workings; radioactive contamination of working clothes and of the integumenta of the workers. In addition, a number of factors may have an effect on the human organism, inherent in the mining industry: pneumoconiosis hazard from dust, explosive gases, noise, vibration, etc.

In the course of hygenic and dosimetric investigations, commenced almost simultaneously with the development of uranium deposits, it was shown that of all the specific factors, the decisive effect is that of radon and its short-lived daughter products [1, 2]. A timely estimate of the hazard from overexposure to radiation of the respiratory organs under mining conditions led to the development of a set of counter-radiation and anti-dust measures in the exploration of deposits and the extraction of uranium ores in conjunction with dosimetric control for the observance of the maximum permissible levels and maximum permissible concentrations laid down in the USSR:

I. Measures of a technological nature, directed at the reduction of dust formation and the release of radon and dust in the mining atmosphere include:

1) A field method of preparing deposits for working;
2) the replacement in a number of cases of prospecting by deep blasting and bore holes;
3) concentration of purification processes;
4) reverse procedure for working the mining field;
5) organization of an inspection management.

II. Measures for the dilution and removal of the released radon and the dust which is formed include standard mining ventilation, specifying compulsory artificical ventilation of all mines by the continuous operation of standard mining ventilators. Standard mining ventilators are to be remotely controlled and in the mines automatic ventillation doors are to be installed.

In planning the ventilation of uranium mines, the following stipulations are made:

1) A pressure method of general mine ventilation is used;
2) the calculation of the required quantity of air is carried out according to the radon and its daughter products;
3) the construction of a barrier in the operative workings is specified; this is to prevent the inflow of radon.

In order to control the dust, the necessary quantity of air is calculated according to the dust factors.

In addition to standard mine ventilation, the following measures are to be adopted for ensuring the efficient ventilation of the working forces:

1) Compulsory local ventilation of all dead-end workings;
2) forced-ventilation method with air supply directly to the working locality through flexible nozzles or tubes;
3) continuous ventilation cycle with the use of a relay for the automatic repeated startup in the case of cutting-out of the ventilator;
4) the use of filtration equipment for purifying the air fed to the mining face from the daughter products of radon and from dust;
5) ensuring the maximum shortness of the air in the mining faces (for monitoring radon and its daughter products).

III. Special measures for controlling harmful contaminations.

Measures for controlling radon and its daughter products:

1) Isolation of nonoperative workings by hermetically-sealed doors;
2) anti-radon covering of air-feeding excavations;
3) catchment of active mine eaters.

Measures to control dust:

1) Suppression of dust at the sources of its formation (drilling with flushing solutions of dust-wetting additives);
2) the use of drilling bits with intermittent knife edges;
3) sprinklers for explosive operations;
4) sprinkling of the mine spoil removed for burial-dumping operations and transportation;
5) removal of dust from ventilating currents and preventing its rising;
6) installation of water screens in the movement channels of the ventilating jets;
7) sprinkling of excavations with irrigation machines.

Anti-radon Measures

The radiation hazard of radon is associated in particular with the deposition of its daughter products in the human respiratory organs. Certain of these products (mainly free atoms of RaA) are deposited selectively in the upper respiratory tracts and the remaining atoms, associated mainly with condensation nuclei, more or less uniformly irradiate the pulmonary tissue. Since the development of radiation pneumosclerosis and the cancerous effect of very high radon concentrations is possible [3-5], it was assumed that for radiation control and the organization of improved sanitary precautions it is advisable to take account of the concentration of radon in the mine air as well as the content of its daughter products.

Investigations into the radon abundancy in uranium mines formed the basis of the project for the establishment of safety precautions. During the course of the investigations, the values of the radon discharge from different excavations, sections and mines as a whole were determined. These investigations enabled a quantitative estimate to be made of the principal source of accumulation of radon in the galleries—its continuous release (emanation) from the outcrop faces of the ore rocks, and also to define the specific role of supplementary radon sources. Of the latter, the most important are inflows of air enriched in radon from idle workings and fissure zones into operative galleries. The inflows of radon into the workings, which occur mainly in the warm period of the year, increase in certain cases the radon discharge from the mine by a factor of 1.5-2. In certain individual galleries the increases in radon concentration are associated with the mine waters, but on the whole the specific role of this source very rarely exceeds 5-10% in the total radon discharge throughout the mine. Intensification of radon release as a result of blasting operations is of a sporadic nature and is timed to the period when there are no people in the mine workings.

The regular nature of the main source of radon release in uranium mines has enabled methods of prediction to be worked out, which are based on two indexes: S'—the equivalent emanating surface (EES) and E—the specific equivalent radon release (SER). The EES is an arbitrary expression for the surface area of rock outcrops (m^2) and their radium content (%). We take $1 m^2$ of ore outcrop with a uranium content of 1% (3.4 to 10^{-7}% radium) as the unit for the EES. The equilibrium shift is taken into account by the introduction of the appropriate coefficient.

The specific equivalent radon release is an experimentally-established index of the relative radon abundance, defining the radon release per unit of the equivalent emanating surface. The values of the SER (curie/sec·m^2·%) are found by dividing the radon discharge rate (curie/sec) by the area of the equivalent emanating surface of the exploring drift,section or mine (m^2·%). Radon surveys, carried out systematically in tens of mines, have shown that for similar geological-geophysical characteristics of the mines, the values of the SER are similar in magnitude. The maximum values of the SER (of order 10^{-8} curie/sec·m^2·%) are characteristic for deposits of sedimentary origin. In hydrothermal deposits the SER is usually of order 10^{-9} curie/sec·m^2·%. An attempt to plan uranium mines confirms the feasibility of predicting the radon release based on the planned values of the EES.

Knowing the values of SER for a given ore field (in isolated cases for different sections of the ore field or for several ore fields), the planner selects a system of opening, excavation and ventilation for which the relationship $s\nu = 10^7 s'E$ between the cross section of the air-feeding galleries and the value of the EES of the ventilated sections is supported, where s is the cross section of the air-feeding galleries, m^2; ν is the permissible speed of movement of the air through the gallery, m/sec (usually 12 or 16 m/sec); s' is the magnitude of the EES of the section, m^2·%; E is the magnitude of the SER, curie/sec·m^2; 10^7 is a factor which takes into account the quantity of air necessary for diluting the radon.

A reduction of the EES is achieved by undertaking work in the minimum number of levels, by concentrating the work in the minimum number of blocks, by using a field system of preparing the deposit and by substituting the cutting of certain exploratory drifts by boreholes. The use of the reverse order of working the levels (from the edges of the mine field to the shaft) also plays an important role.

The basis of the anti-radon precautions is total ventilation of the mining field, calculated on the basis of the actual or predicted radon discharge, with the assumption of the attainment of the MPC of radon in the emergent stream. The calculation is carried out by the formula

$$Q = \frac{D}{\mathrm{MPC}_{\mathrm{Rn}}} = 10^7 \cdot D,$$

where Q is the quantity of air required, m^3/sec; D is the actual or probable radon discharge, curie/sec.

In addition, on the basis of [6], the number of air exchanges which will ensure a concentration of radon daughter products in the emergent stream not exceeding the equilibrium concentration at $5 \cdot 10^{-11}$ curie/liter is determined.

The artificial total-field ventilation of uranium mines is carried out continuously by the use of remote servo-control with the main ventilators. Of the specific requirements for total-field ventilation, the use of a forced-circulation method is particularly important which, as shown experimentally, reduces or eliminates radon inflows in the operative excavations. In the case of the emergency use of a suction method for total-field ventilation, the influxes of air can be prevented to a considerable extent by creating a local pressure head with specially-installed ventilators in the region of the working level.

Local ventilation of idle workings under radon-release conditions is carried out by a forced circulation method as a result of continuous operation of the ventilators. In order to bring the supply of fresh air to the face of the ore piles, flexible pipelines or flexible spurs—nozzles on metal conduits are used. The quantity of air supplied is calculated according to the magnitude of the radon discharge from the workings.

In order to purify the air supplied to the ore face by the local ventilators, filtration devices are used in a number of cases; these are equipped with fabric filters or other high-efficiency filtering materials, in particular glass wool. For example, the use of units employing LAIK filters [7] allow the total concentration of daughter products in the air supply to be reduced by 96%.

An important role in reducing the level of radon contamination of the inflowing air is played by special precautions for reducing the radon releasing volume, such as radon-impermeable protective coverings for the walls of intensely-emanating workings [8], capping of active mine waters and isolation of idle workings, usually constituting in operative mines a considerable fraction of the total volume of the drifts. The bulkheads, by which isolation is accomplished, are hermetically sealed by a layer of a bitumen-petroleum jelly mixture, bitumen-latex emulsion or polymerized materials; the installation of hermetically-sealed bulkheads in idle workings which are in communication with the surface is of particular importance.

Some results of the precautions taken to standardize the atmosphere of mines are illustrated by the example of a number of mines. A test shows that in intensively ventilated mines, even with high specific equivalent radon re-

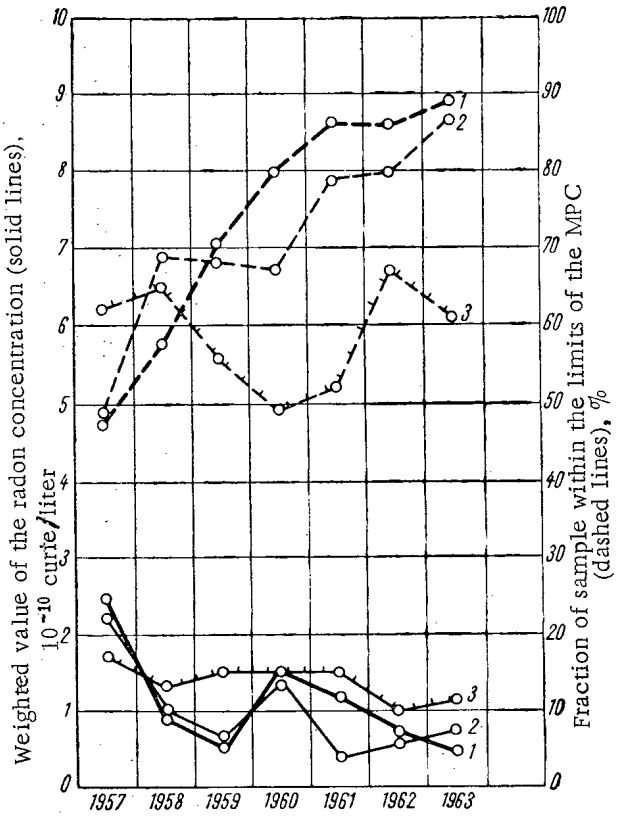

Fig. 1. Concentration of radon in the mining atmosphere of uranium mines, designed by taking into consideration the necessity for intensifying ventilation: 1) Mine No. 5; 2) Mine No. 6; 3) Mine No. 9.

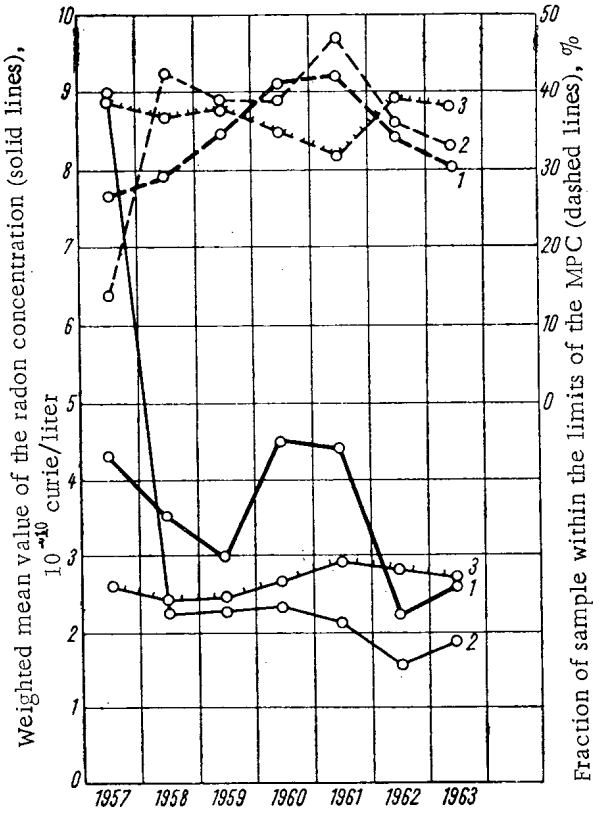

Fig. 2. Concentration of radon in the mine atmosphere of uranium mines, planned without taking radon into account: 1) Mine No. 7; 2) Mine No. 8; 3) Mine No. 11.

lease (of order 10^{-8} curie/sec·m^2·%), the radon concentration is close to the maximum permissible concentration (MPC). It can be seen from Fig. 1 that the weighted mean value of the radon concentration at the working faces of three of these mines over a period of six years amounted to not more than $1.5 \cdot 10^{-10}$ curie/liter and the greater part was less than $1 \cdot 10^{-10}$ curie/liter.

In mines where the ventilation was planned without taking the radon into account, but only for the removal of explosive gases and dust, high radon concentrations were observed which were reduced later to a level of $2\text{-}3 \cdot 10^{-10}$ curie/liter (Fig. 2). Ventilation of these mines is planned according to the results of radon surveys. The data given in Fig. 1 concerning the content of radon in the mine air of uranium mines is less than in many foreign and USSR nonuranium mines [9, 10].

Anti-Dust Precautions

In order to prevent or reduce dust formations, technological types of precautions are employed, in particular processing systems which have the minimum capacity for dust-forming operations, and the appropriate drilling rig are used. Measures for dust suppression, by combining or collecting it directly at the sources of formation are widely used: standardized boring with flushing by dust-wetting solutions, hydro-dust removal in explosions, burial-dumping operations and transportation of mine spoil, etc.

Methods are used for precipitating dust from the mine atmosphere and preventing its repeated entry into the air: water screens, and machines for spraying the excavations. The comprehensive and standardized application of these methods is associated with efficient dust-removing ventilation [11].

As an example, Fig. 3 shows the dynamics of the weighted-mean dustiness factor at the working faces of certain mines. It can be seen from the graphs that the concentration of dust in the mine air of these units during five years has remained steady at a level of 1-1.5 mg/m^3, i.e., it is below the MPC accepted in the USSR for mine dust with a

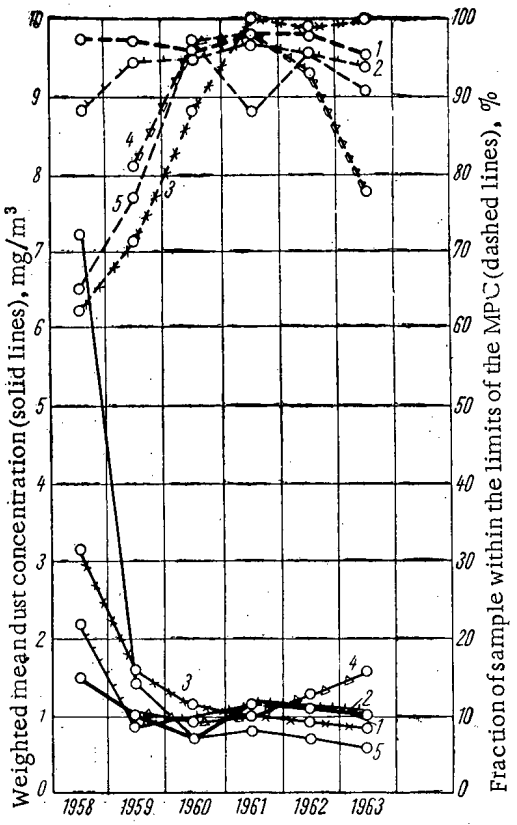

Fig. 3. Dustiness of the mine atmosphere of uranium mines (1-5 are mines No. 1-5 respectively).

free silica content of 10-70% (2 mg/m^3); the fraction of samples having a dustiness which lies within the limits of the MPC is, as a rule, more than 90%.

Independent Shielding of the Respiratory Organs

A complex of anti-radon and anti-dust precautions is supplemented by the use of independent shielding of the respiratory organs: ShB-1 ("Lepestok") and "Astra-2" respirators, and LIZ-3 pressurized masks [12]. The "Lepestok" valveless respirator is obtaining particular popularity; this has a low resistance (3 to 4 mm water), a high filtration factor (99.9% for mineral dust) and a small weight (10 g). These methods enable overexposure to radiation of the respiratory organs to be prevented when undertaking emergency and overhaul operations, as a result of visiting idle workings and intermittent periods of the duty personnel (staff) in emergent streams and also at isolated mines in the period when standardization of the mine atmosphere has not yet been achieved.

Shielding from External Radiation

The upper limit of the dose intensity of γ-radiation from uranium or thorium ore is the dose intensity P_γ inside an infinitely long ("saturated" with respect to γ-radiation) layer of ore. We calculate it by means of the following formula, obtained in [13, 14]:

$$P_\gamma = 16.4C_U + 8.9C_{Th} + 0.035C_K, \text{ mrad/h},$$

where C_U, C_{Th} and C_K are the percentage contents of uranium, thorium and potassium in the ore. Values of the dose intensity calculated by this formula agree well with the results of similar calculations carried out by other methods [15, 16]. "Thick" layers of γ-emitting ore are seams with a thickness of 30-50 cm (70-80 g/cm^2). In these cases, about 80% of the equilibrium radiation intensity is produced by a layer with a thickness of 15-20 cm.

The MPL for γ-radiation (0.1 rad/week) is exceeded only at concentrations of 0.16% uranium and 0.33% thorium in the ore. Under actual conditions a persistent excess over the MPL external radiation is noted at higher concentrations of radioactive substances.

A significant external β-irradiation is observed only at close distances from the emitting surface of uranium or thorium ore. Thus, at distances not exceeding a few centimeters, the dose intensity in air from an infinitely "thick" β-emitting ore seam with a thickness of 1.6 g/cm^2 can be determined by the formula

$$P_\beta = 6C_U + 1.2C_{Th}, \text{ mrad/h}.$$

The intensity of the absorbed dose of β-radiation falls rapidly according to the distance from the ore surface and at distances of 1-2 m the dose concentration of the β-radiation is reduced to a value which comprises 10-30% of the γ-radiation dose intensity.

Shielding from external radiation is ensured by the interchange of the operating personnel in the cleaning and drift faces. Manual operations with high-grade uranium and thorium ores are not permitted.

Dosimetric Monitoring

In order to ensure radiation safety in uranium mines, the careful monitoring of mine-air contamination, radioactive contamination of protective clothing and the integumenta of the workers, etc., play an important role. The periodicity of monitoring of radiation safety factors is established as a function of the stability of the recorded levels of effect and their values relative to the MPL and the MPC.

Accuracy of Measuring the γ-Radiation Dose Intensity of a Thick Ore Seam with Instruments Calibrated with Radium or Cobalt Standards, %

Detector	Uranium ore		Thorium ore	
	calibrated by Ra^{226} standard	calibrated by Co^{60} standard	calibrated by Ra^{226} standard	calibrated by Co^{60} standard
Gas-discharge counter of the STS type, in an aluminum case (wall thickness 2 mm)	Indicated value greater than the true value 20-25%		Indicated value greater than the true value 30-35%	
Scintillation counter with NaI(Tl) crystal, dimensions 3 × 2 mm in an aluminum case (wall thickness 3 mm)	By a factor of 4.8	By a factor of 11	By a factor of 4.6	By a factor of 10
Personal film-badge (X-ray film XX with filter, 0.75 mm thickness of lead)	Readings less than true value by 2-3%			
Pocket ionization chamber, Type DK-02	Readings greater than true values by 3-4%			

Concentrations of radon are measured by ionization and scintillation methods. Methods for controlling the short-lived daughter products of radon, based on the use of special fine-fibered filters [7, 17], differ in the sampling time, the method of recording the filter activity, the duration and number of measurements. These methods can be divided into three groups according to the final results obtained:

1) The total concentration of short-lived daughter products from emanation is determined. For this, the value of the effective half-life T_{eff} = 35 min is used for the daughter products of radon and T_{eff} = 10 h for the decay products of thorium, or the activity of the filter is measured at the time of taking the sample after the establishment in it of dynamic "equilibrium" between the rate of deposition of the daughter products and their rate of decay [18].

2) The separate concentrations of RaA, RaB and RaC are determined. In this case measurements are used of the accumulation of decay of the activity on the filter at different instants of time [17, 19].

3) The "latent energy", released as a result of the total decay of the products of emanation which are found in the air being investigated, is determined [20, 21]. In this case, the concentration of RaA can also be measured separately [18].

It should be pointed out that the shift of equilibrium between the emanations and their daughter products to the side of reduction of the total content of the latter is not a basis for increasing the permissible concentrations of radon and thorium in comparison with the established MPC's.

The Commercial-type, portable instrument—the RVR-1 [22]—has been specially constructed for monitoring the radon hazard in the extraction of uranium ores. In order to measure low concentrations, methods are also used which are based on the absorption of radon by activated carbon (charcoal) or by radiometry of a filter installed at the exit from the chamber where preliminary purification from aerosols of the air being investigated is carried out. Instruments measuring directly the emanation concentrations are based on the latter principle.

Monitoring of the content in the air of radioactive aerosols is accomplished by an aspiration method using special fine-fibered aerosol filters. Even for ultramicroscopic particles sizes, the "creep-through" factor for these filters does not exceed 1-5%.

Ejector pumps and mobile aspirators, fed from accumulators or the mains supply, are used for pumping the air through the filter.

The content of radioactive aerosols is determined in the same samples which are intended for estimating the total dust content. Normally, uranium and radium are determined in the dust, but in the case of necessity, analyses can be undertaken on any of the daughter products of uranium, in particular on polonium, ionium, etc.

In order to monitor the level of γ-radiation, battery-operated portable radiometers are used, in which gas-discharge low-voltage halogen counters with a thin steel cathode are used as detectors (type STS).

The energy spectrum of the γ-radiation occupies the region from a few hundreds of eV to 2.45 MeV for uranium and to 2.62 MeV for thorium ore. In this case, the multiple scatterings of γ-radiation with quanta energies below 0.3 MeV produces approximately 70% of the total flux of quanta and 25-30% of the total dose intensity (the total dose contribution of the scattered radiation amounts to 55-60%). Fig. 4 shows the relative contribution of dif-

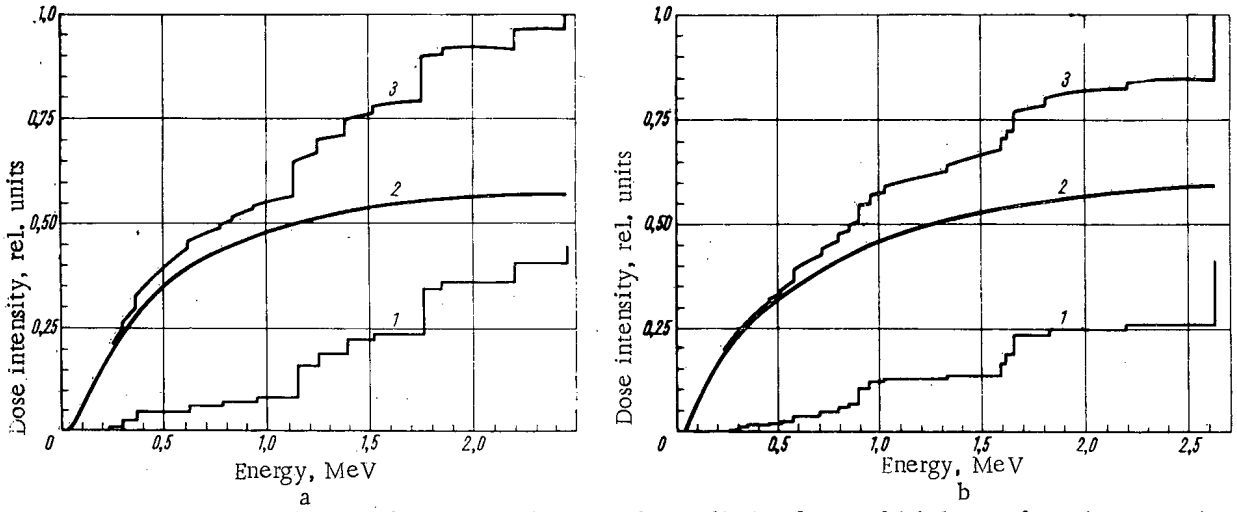

Fig. 4. Relative dose contribution of primary and scattered γ radiation from a thick layer of uranium ore (a) and thorium ore (b): 1) Primary radiation; 2) scattered radiation; 3) total curve.

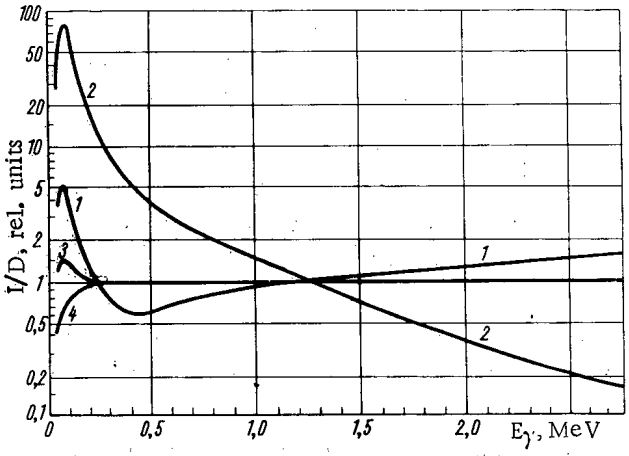

Fig. 5. "Behavior with hardness" of certain γ -radiation detectors: 1) Gas-discharge counter with steel cathode, type STS in aluminum case with thickness 2 mm; 2) crystal of NaI(Tl), size 3 × 2 mm, in aluminum case, thickness 3 mm; 3) pocket ionization chamber type DK-02; 4) personal film-badge (x-ray XX film under a filter).

ferent parts of the spectrum in the total dose, due to γ -radiation of extended thick seams of radioactive ores. The table, for specified conditions, shows the approximate estimation of the accuracy in measuring the dose intensity with different instruments calibrated by the γ -radiation from standard preparations of Ra^{226} and Co^{60}. The errors are obtained by a numerical method, by taking account of the "behavior with hardness" of different types of detectors (Fig. 5).

A considerable fraction of the soft γ radiation under mine conditions makes the monitoring of external β radiation directly in units of dose intensity extremely complex, and therefore β-particle fluxes are usually measured by instruments with thin-walled gas-discharge counters or thin organic scintillators of the stilbene type.

In order to determine personal doses of γ radiation, pocket ionization chambers are used as well as personal film-badges with filters. Systematic monitoring of personal doses of external radiation is introduced with a uranium content in the ore in excess of 0.5%.

Radiometric monitoring of the contamination of protective clothing and of the integumenta is accomplished with portable and fixed scintillation radiometers with a sensitive area of up to 150 cm^2.

Other Prophylactic Measures

In a system for ensuring the radiation safety in uranium mine workings, the monitoring of possible contamination of air, water, soil, vegetation and other biological items by radioactive substances, occupies an important place.

In the construction of workmens' settlements serious consideration is given to the choice of structural materials which do not contain excessive concentrations of natural radioactive isotopes (less than 0.002% of uranium). The observance is fulfilled of adequate health-protection zones, separating the settlements from the mines (1000 m) and the air-intake plants from the sites of release of dust and gas (100 m) etc.

In the prophylaxis of sickness, the selection of mining staff on the basis of preliminary medical inspections of all entrants and periodic (once or twice per year) medical inspections of all who have contact with radioactive materials play an important role. An important characteristic of the prophylactic procedure undertaken is its complex nature and the extensive scale of introduction of the measures used.

LITERATURE CITED

1. V. I. Baranov and L. V. Gorbushina, Problems of Safety in Uranium Mines [in Russian], Atomizdat, Moscow (1962).
2. A. V. Bykhovskii, Hygiene Problems as a Result of Underground Processing of Uranium Ores [in Russian], Medgiz, Moscow (1963).
3. V. S. Kushneva, Data on the Toxicology of Radioactive Substances. Edited by A. A. Letavet and É. B. Kurlyandska [in Russian], Medgiz, Moscow (1957), p. 130.
4. V. S. Kushneva, The Hygiene of Labor and Occupational Illnesses [in Russian], No. 1, 22 (1960).
5. F. L. Leites and L. S. Ruzer, Arkhiv Patologiya, 21, 20 (1959).
6. Yu. P. Bulashevich and N. P. Kartashov, Atomnaya Énergiya, 6, 584 (1959).
7. B. L. Ogorodnikov, et. al., Atomnaya Énergiya, 15, 230 (1963).
8. A. V. Bykhovskii and D. G. Faustova, Protective Coverings in Nuclear Technology, Gosatomizdat, Moscow (1963), p. 137.
9. P. Jacoee, Arch. Industr. Hyg., 8, 118 (1953).
10. S. S. Dinkelis, Proceedings of the Avitsen Tadzhik Medical University [in Russian], 51, 33 (1964).
11. D. T. Desyatnikov and N. I. Chesnokov, et. al., Reduction of the Dust Content of a Mine Atmosphere [in Russian], Gosgortekhizdat, Moscow (1962).
12. S. M. Gorodinskii, et. al., Radiation Hygiene [in Russian], Medgiz, Moscow (1962), p. 87.
13. G. M. Voskoboinikov and N. P. Kartashev, Atomnaya Énergiya, 6, 42 (1959).
14. R. M. Kogan and I. D. Fridman, Izv. AN SSSR. Ser. Geofiz., No. 4, 530 (1960).
15. B. Hultqvist, Kgl. Svenska Vetenskapsakad. Handle., B6, No. 3 (1956).
16. E. G. Gusev, Collection of Radiochemical and Dosimetric Methods [in Russian], Medgiz, Moscow (1959), p. 390.
17. I. L. Gusarov and V. K. Lyapidevskii, Hygiene and Sanitation [in Russian], No. 1, 56 (1964).
18. K. P. Markov, N. V. Ryabov, and K. N. Stas', Atomnaya Énergiya, 12, 315 (1962).
19. Yu. T. Kapitanov, A. S. Serdyukova, and I. N. Korenkov, Izv. Vyssh. Uchebn. Zavedenii. Geologiya i Razvedka, No. 11, 106 (1961).
20. H. Kuznetz, Amer. Industr. Hug. Assoc. Quart., 17, 85 (1956).
21. I. L. Shalaev, Med. Radiologiya, No. 10, 56 (1960).
22. K. P. Markov, et. al., Collection of Papers concerning Some Problems of Dosimetry and Radiometry of Ionizing Radiations. Issue II. Editor, Yu. V. Sivintseva [in Russian], Atomizdat, Moscow (1961).

All abbreviations of periodicals in the above bibliography are letter-by-letter transliterations of the abbreviations as given in the original Russian journal. *Some or all of this periodical literature may well be available in English translation.* A complete list of the cover-to-cover English translations appears at the back of this issue.

CONCERNING THE PROBLEM OF USING THE ISOTOPIC RATIO U^{234}/U^{238} FOR INTERPRETING URANIUM ANOMALIES IN FRIABLE FORMATIONS

(UDC 622.036 : 553.495)

N. G. Syromyatnikov

Translated from Atomnaya Énergiya, Vol. 19, No. 2,
pp. 169-174, August, 1965
Original article submitted August 13, 1964

The results are presented of the determination of the U^{234}/U^{238} ratio in sections of two exogeneous uranium deposits from an arid zone, for the purpose of establishing their genetic origin.

For a uranium anomaly, confined to the contact of granites with amphibolites, on the basis of the U^{234}/U^{238} determination in the secondary uranium mineralization zone of oxidation and of the regenerating zone, in the waters of the region and of the granite massif, and also in extracts of soils, the source of the uranium (granites) is established and a mechanism is proposed for the accumulation of uranium in the surface friable formations and in the cementation zone. The time of formation of the sooty uranites is estimated (~3 million years). For a uranium anomaly confined to the "gypsumized" section of the tertiary clays, on the basis of the U^{234}/U^{238} determination in the extracts of clay the conclusion is drawn that the most probable mechanism of uranium accumulation is the mobilization of the syngenetically-scattered uranium of the clays themselves and its concentration in the sections with the most rapid evaporation.

An isotopic-uranium criterion for the non-metalliferous origin of uranium anomalies is proposed.

In a paper published earlier [1], mention was made of the relationships between the relative migration U^{234}/U^{238} and the possibilities of using the ratio $U^{234}/U^{238} = \varepsilon$ for interpreting radiohydrochemical anomalies. In [2], the prospects of the isotopic method are confirmed for uranium-ore prospecting by the hydrochemical dispersion ratio.

Recently, the author of this paper has studied the possibility of using the isotopic method for explaining the origins of uranium deposits in friable formations (a lithochemical version of this method has been worked out). It was suggested that if the isotopic composition of the reasonable uranium component of the friable formation is analyzed, then, just as with the analysis of water, a metalliferous or nonmetalliferous origin can be established for uranium anomalies.

The results are given in this present paper of a study of the isotopic ratio U^{234}/U^{238} in sections of two exogenic uranium accumulations. Both sections are located in arid climatic conditions (semidesert landscape): one of them is located in an area of development of granites and the other in an area of diffusion of tertiary clays. Although the concentration of uranium in the sections is quite high in places, on the whole both uranium deposits are of no practical value and can be considered as nonmetalliferous anomalies.

Uranium Anomalies in the Plane of Development of Granites

The section of the anomaly is timed to the contact of the granite massif with amphibolites. In the granites, all varieties of greisen and quartz formations are observed, migrating towards a tectonic fissure and a high-temperature quartz vein. Within the limits of the uranium ore manifestation, quartz formation is traced at a depth of 300 m and is accompanied by insignificant sulphide mineralization. A thick core of weathering (average thickness 8-10 m, maximum up to 30 m) has been developed, distinguished by the close relationship with the zone of fissuring. The intensity of weathering varies over wide limits. In places, the crystalline rocks are changed only superficially by weathering; nevertheless, their complete conversion to kaolin clays is sometimes observed. The whole of the mass

TABLE 1. Values of ε in Different Formations of a Section of the Anomaly and of the Region

Sample characteristics	No. of samples	ε	Mean value of ε
Waters from granite massif	8	2.7-3.5	3.0 ± 0.2
Waters from ore manifestation (from a bore)	21	1.8-3.8	3.1 ± 0.5
Schroekingerite	11	1.9-3.7	2.9 ± 0.4
Johannite	2	2.7-2.9	2.8 ± 0.2
Free extract from soil formations within the limits of the salt halo (underlying rocks—clay core from weathering of granites and amphibolites)	21	1.8-3.1	2.6 ± 0.4
Free extract from soil formations beyond the limits of the salt halo (base rocks —granites)	12	1.8-3.6	2.8 ± 0.6
Extract of active samples from the zone of cementation (sooty uranites)	11	1.2-2.8	1.9 ± 0.3

of fractured granite has been subjected to intense gypsum formation. In the soil layer of tertiary pebble clays and also in the core of weathered granites and ultrabasic rocks, abundant secondary uranium mineralization is observed, represented in the primary schroekingerite. The mineralization has gravitated towards the limonite-and gypsum-formation zones. In the surface zone, finely dispersed mineralization besides visible mineralization has also been developed, which emits a characteristic radiation in ultraviolet light. The total area of the uranium halo is about 2.5 km^2. The anomalous γ -activity and the enhanced molybdenum concentration was recorded at the surface.

The combination of geological-mineralogical and radiochemical data described served at one time as the basis for undertaking detailed prospecting operations in the section. As a result of this, sooty uranites were observed in almost all the boreholes, beginning at a depth of 30-40 m. The maximum concentration in "blacks" has gravitated towards the contact of amphibolites with the granites, throughout which zones of fractionation and fissuring of different scales were noted. However, the total quantity of sooty uranites is small, in consequence of which the mineralization has no practical importance. A suggestion was made concerning the infiltration origin of the uranium mineralization which has been confirmed by the following factors: 1) within the limits of the section, the water table is located close to the surface, through which their partial discharge takes place; deep down, the interstitial waters are of a pressurized nature (some bores gushed); 2) the distribution of the black and schroekingerite mineralization is regulated mainly by intensely fissured and porous uraniums; 3) the zone most concentrated in schroekingerite is observed in the zone of intensive evaporation of ascending solutions (0.5-0.8 m from the surface); 4) the sooty uranites gravitate towards an intermediate product of weathering (association with chlorites, nontronite and siderite) and towards dense screens in the path of movement of the water.

The factors mentioned cannot give an unambiguous answer to the problem of the infiltration origin of uranium mineralization. In view of this, a radiochemical study of the region of the anomaly and the granite massif was undertaken (I. P. Koshelev, T. M. Vechkutova and N. G. Syromyatnikov). As a result of these tasks it was established that the waters from the region of the anomaly and the uranium minerals of the zone of oxidation have a nonequilibrium isotopic uranium ratio, equal in magnitude to this ratio in the waters of the granite massif (ε varies around 3). The sooty uranites are characterized on the average by a smaller value of ε (~1.9) which, however, also differs significantly from the equilibrium value (ε = 1). This confirms the regenerative origin of the glyptics, since other sooty uranites do not contain excess U^{234}.

Analyses were recently carried out repeatedly by the author of certain water samples in secondary uranium minerals of this ore manifestation. In addition, soil formations, selected along one of the prospected profiles were studied. Table 1 shows data on the isotopic ratio of U^{234}/U^{238} in different formations of the section and of the region.

On the basis of Table 1, a conclusion can be drawn concerning the relationship between the uranium from the oxidation zone of the anomaly and the uranium in the water from the granite massif. This relationship exists also under present-day conditions. The lower value of ε in the glyptics is explained, obviously, by the fact that a considerable quantity of uranium recorded in the concentration zone is excluded from intensive exchange, and in this

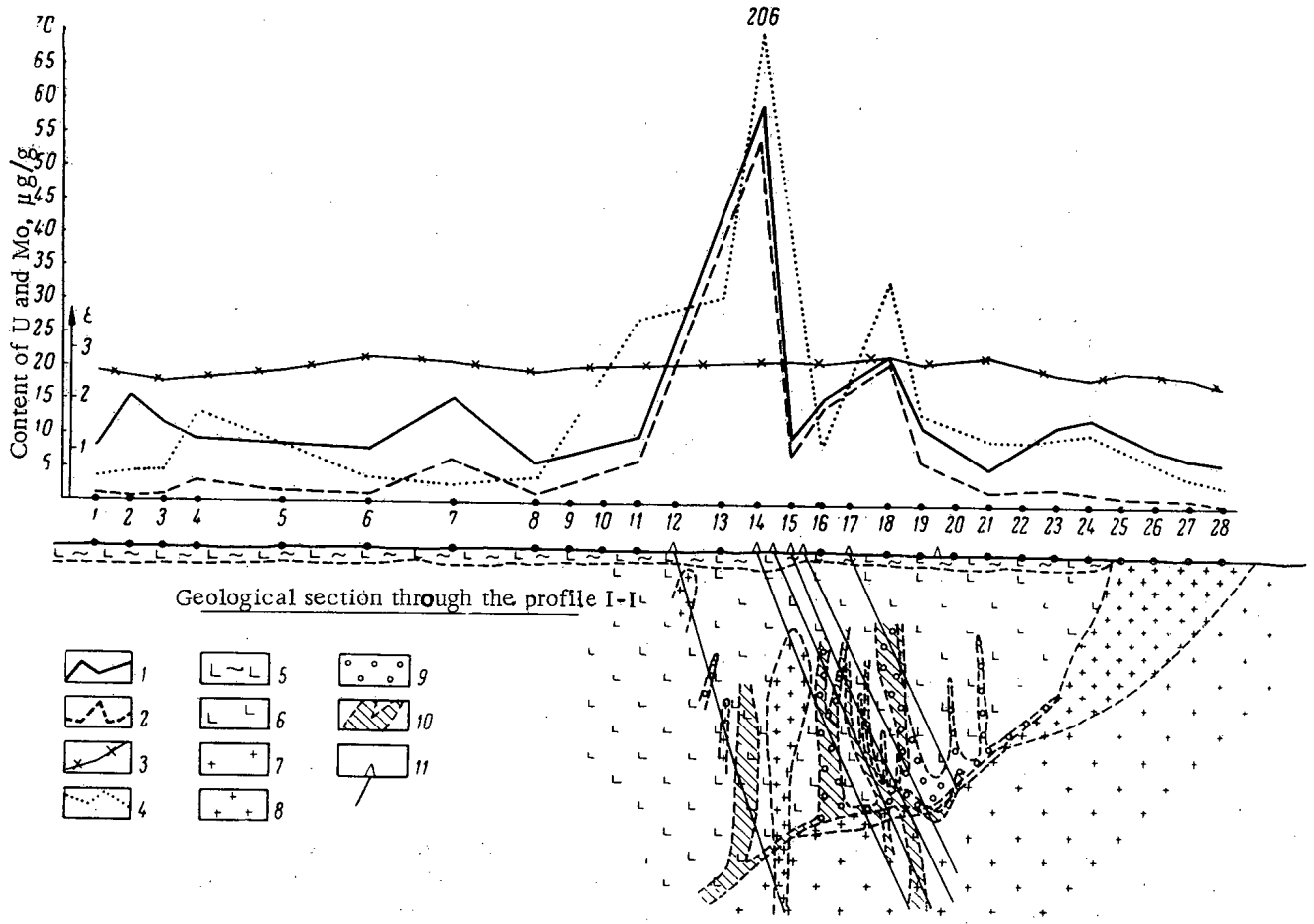

Fig. 1. Uranium anomaly in a contact of granites with amphibolites. 1) Uranium; 2) removable uranium; 3) U^{234}/U^{238} ratio of removable uranium; 4) molybdenum; 5) weathered clay core; 6) amphibolites; 7) coarse-grained granites; 8) fine-grained granites; 9) microgranites; 10) zones of black mineralized uranium; 11) bores.

TABLE 2. Results of Radiochemical Analysis of Soils within the Limits of the Uranium Salt Halo

Sample No.	Sample characteristics	pH value of suspension	Content of radioelements in units of U^{238}, γ/g				Th, γ/g	Value of ε	
			U^{238}	U^{234}	Io	Ra		in the sample	in the extract
3a	Loamy soil	6.0	37	89	97	96	31	2.4	3.2
3c	Clay core from granite weathering	6.3	60	166	63	110	40	2.6	2.8
6a	Sandy soil	5.4	48	158	99	56	30	3.3	3.5
6c	Clay core from weathering of amphibolites	6.6	34	82	97	108	32	2.4	3.0
7a	Sandy soil	6.5	40	104	68	60	25	2.5	2.6

section the decay of surplus U^{234} commences. It can be seen from comparison of the data in Table 1 that the sooty uranites of the cementation zone cannot be the main source of the uranium in the zone of oxidation, since according to its isotopic composition it is undoubtedly the younger. Obviously, the uranium from the zone of oxidation is also partially excluded from the exchange with the uranium in the water, since the latter is characterized by a somewhat higher value of ε.

Fig. 1. shows the results of a study of soil formation samples, selected along a prospected profile. Soils within the limits of the district are represented mainly by loams, salinized to some degree or other. The samples were selected from depths of 10-20 cm. It can be seen from the figure that in soils above the ore body a distinct anomaly is recorded according to the uranium and molybdenum content and a straight-line correlation is noted between their

contents. A large part of the uranium of the anomalous samples is found to be in easily-extractable form, whilst in the soil samples taken beyond the limits of the anomaly, the fraction of removable uranium is decreased sharply. Independently of the uranium content, its isotopic ratio in the extracts from the soils remains almost constant throughout the whole profile ($\varepsilon \approx 2.5$-3.0).

Data are presented in Table 2 of a more detailed radiochemical study of certain soil samples and samples selected in the subsoil layer of the weathered core. It can be seen from the table that equilibrium between U^{238} and Ra is shifted significantly to the side of excess radium (by a factor of 1.20-3); at the same time, the quantity of radium is found to be approximately in equilibrium with the Io content. Taking into account the weak migration capability of Io into the zone of hypergenesis, a conclusion could have been drawn concerning the loss of uranium for some time past from soils in the weathered core. However, it is necessary to take into account that Io and Ra are accumulated from U^{234}, which is approximately 3 times greater than U^{238}. The quantity of U^{234} in the samples is close to or exceeds the quantity of Io and Ra. The close values for the quantity ε in the samples and in the extracts confirm the fact that almost the whole of the uranium in the samples is introduced in the process of recent salt accumulation. By taking these data into account, completely substantiated reasons can be stated for the mechanism of accumulation of uranium in the surface formations and in the depths.

The waters from the granite massif and the region of the anomaly are almost indistinguishable in chemical composition (sodium-hydrocarbonate-sulphates, pH = 7 – 8, amount of HCO_3 varies within the limits 2-3.5 mg-equ/liter). In the waters from the territory, the uranium content is $n \cdot 10^{-4}$ g/liter. It was established experimentally by us that the uranium in the waters is probably in the form of a negatively-charged carbonate complex $UO_2(HCO_3)_4^{2-}$. The experiments which we carried out indicated that the pH of suspensions of soils and clays varies within the limits 5.4-6.5. Therefore, it can be assumed that as a result of interaction with acid saltierra (or, "solonchak") clays the pH of the solution is reduced and the uranium is collected by the clay formations in the form of products of uranyl hydrolysis.

After saturation of the sorption capacity of the clays the uranium, having been concentrated because of evaporation processes, is precipitated together with the carbonates and gypsum in the form of aqueous uranyl carbonate-sulphate (schroekingerite) and frequently in the form of other salts [3]. In periods of reduced evaporation and increased humidity, partial dissolution of the uranium salts is possible in the rain water and they penetrate into the zone of infiltration, where the uranium is almost irreversibly fixed in the form of sooty uranites. Penetration of the uranium solutions into the reducing zone takes place according to the mechanics in the relaxed zones. In the area being considered, this zone is the contact of granites with amphibolites towards which the main bulk of the glyptics gravitates also in the depths. The uranium reducing agent is probably the ferrous oxide of the amphibolites. In periods of drought, replenishment of the uranium takes place in the zone of oxidation because of evaporation of the ground waters inflowing from the granite massif. Thus, continuous renewal of a considerable part of the uranium in the zone of oxidation and its accumulation in the zone of cementation occurs.

This mechanism agrees well with the data given above by determining the isotopic ratio U^{234}/U^{238} in the waters ε_{aq}, with the uranium from the zone of oxidation $\varepsilon_{z.o.}$ and from the sooty $\varepsilon_{s.u.}$ ($\varepsilon_{aq} \gtrsim \varepsilon_{z.o.} \gtrsim \varepsilon_{s.u.}$) and it enables us to estimate the time of formation of the glyptics by the difference between ε_{aq} and $\varepsilon_{s.u.}$. If we take for the value of ε_{aq} the most characteristic maximum value for the waters from the granite massif (3.2) and for $\varepsilon_{s.u.}$ the most characteristic minimum for the glyptics (1.6), then a straightforward calculation shows that in the case of uniform inflow of uranium to the zone of cementaion, the formation of the glyptics was started approximately 1.3 million years ago, i.e., in the quaternary period and it has probably extended to the present time.

Uranium Anomaly in Regions of Propagation of Tertiary Clays

The anomaly is located in the plain-locality of a semiarid landscape. The region is closed by deluvial sediments from fragments of extrusifs. At the surface, the anomaly is defined by the increase of γ activity (up to 20 μr/h) in the form of a patch with a size of 10 × 20 m. The total area of the anomaly in the isogam amounts to about 130 × 70 m. The radon concentration in the ground air is equal to 175 eman. A cross-section of pits was studied down to the level of the water table (Fig. 2). The pits exposed under the soil crust the tertiary clays with fragments of foundation rocks (extrusifs) and gypsum-formation zones, towards which activity of up to 750 μr/h has migrated. It was established that the activity decreases with depth to 150 μr/h. At the gypsum-formation sites, a secondary uranium mineralization is detected, in the form of schroekingerite. Part of the uranium is bound directly with the clays in a sorption form. The experiments which we conducted showed that these clays are distinguished by

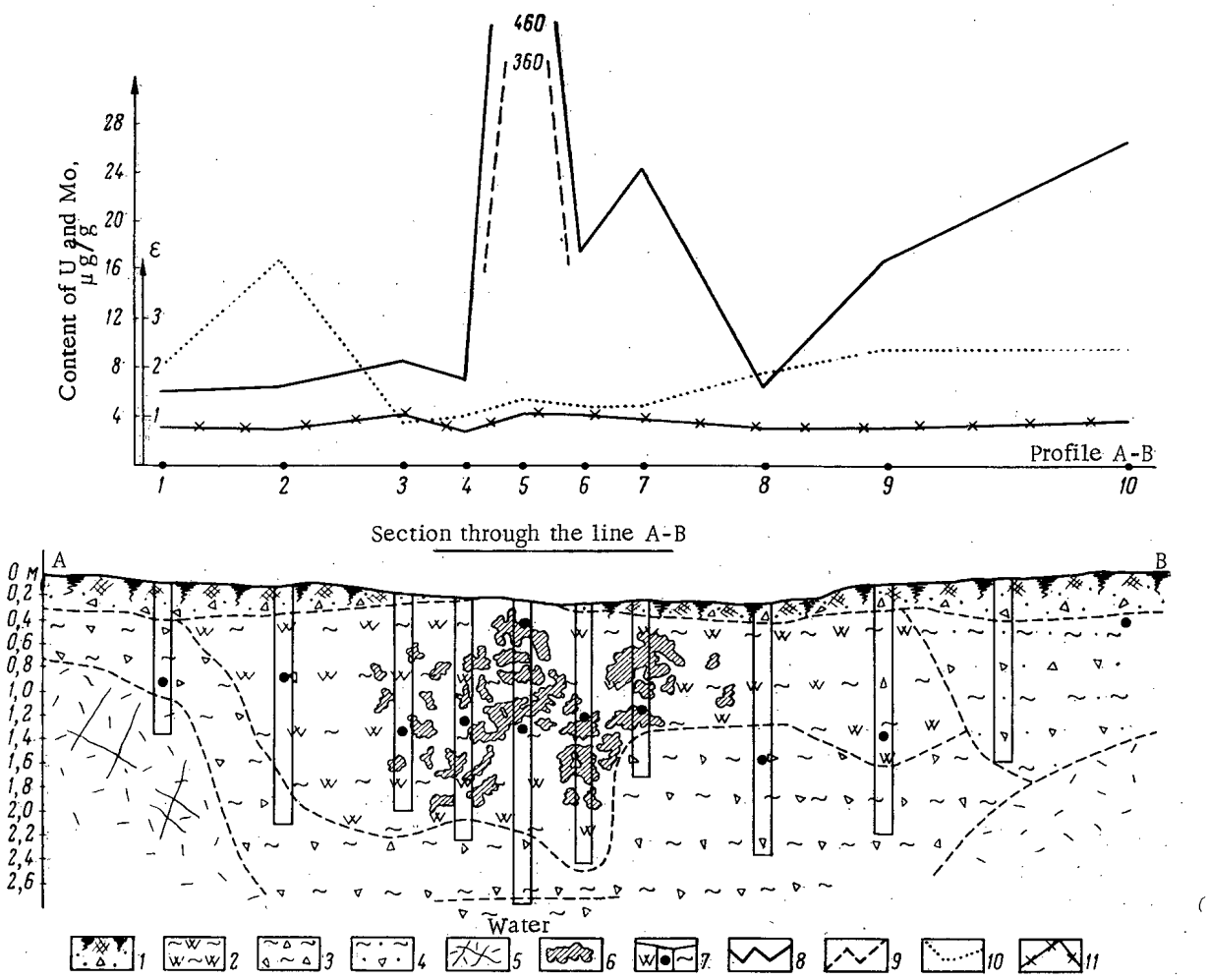

Fig. 2. Uranium anomaly in tertiary clays. 1) Soil-vegetation layer; 2) viscous, uniformly-"gypsumified" clays; 3) clays with fragments of feldspathic porphyry; 4) rock-debris clays; 5) strongly-fissured feldspathic porphyry; 6) gypsum exhudation; 7) site of taking samples; 8) uranium; 9) removable uranium; 10) molybdenum; 11) ratio U^{234}/U^{238} of removable uranium.

their high viscosity and that they swell strongly in water; they have a pH within the limits 7.5-8.5 and EH is equal to +150 mV.

A. I. Perel'man [3] suggests that similar accumulations of uranium in territories with an arid climate are related to the relicts of the superaqueous stage of formation of the solonchak soils, formed either in a geochemical conjugate with the indigeneous rocks or during the eluvial weathering of the clays. The uranium anomaly being considered, as we shall show below, most likely belongs to the second type.

Fig. 2 shows the results of analyses of samples of "gypsumified" clays, collected from the bores. The absence of excessive molybdenum contents is characteristic of the anomaly. About 80% of the uranium contained in the anomalous samples is found to be in an easily-dissolvable form. The value of ε of the removable uranium varies within the limits 0.8-1.1, i.e., it is very close to the equilibrium value. This fact confirms that the addition of uranium from the indigenous rocks, even if it did occur in the quaternary period, was very trivial. In the contrary case we should have noticed a marked shift of equilibrium to the side of excess U^{234}. In the given case, at the flanks of the anomaly a certain deficiency of U^{234} is observed in samples with low uranium contents ($\varepsilon \approx 0.8$), but in samples with higher concentrations of uranium there is equilibrium ($\varepsilon = 1$) or a small surplus of U^{234} ($\varepsilon \approx 1.1$). These facts agree well with the assumption that the specified uranium accumulation has been formed because of the mobilization of syngenetically-dispersed uranium from tertiary clays.

The mechanism of this process consists, probably, in the following. The underground waters leach out the dispersed uranium from the clays, and some concentration of the solution in the U^{234} isotope occurs, as it is more

removable in comparison with U^{238}. In dry and sultry periods the solutions, because of capillary forces, gravitate towards the surface and first of all towards the regions with the most rapid evaporation. In the process of evaporative concentration, the uranium is precipitated together with calcium sulphate. It can be seen from Fig. 2 that the maximum gypsum seperation gravitates towards the region of the surface, stripped of the soil covering, where, in fact, it can be assumed that there is a higher rate of evaporation of the soil moisture.

CONCLUSIONS

By the example of two explored uranium anomalies in friable (or, unconsolidated) formations of a semiarid landscape, it is shown that the determination of the U^{234}/U^{238} ratio enables us to establish the nature of the uranium accumulations and to estimate the time of its buildup.

The present-day infiltration origin of the uranium anomaly is established, which is confined to the contact of a granite massif with amphibolites. The mechanism is suggested and the time of formation of sooty uranites is estimated in the reduction zone (~1.3 million years).

It is established for the uranium anomaly in "gypsumized" tertiary clays, that the most probable mechanism for its formation is evaporative concentration of syngenetically-dispersed uranium from these clays (eluvial weathering).

The criterion for the non-metalliferous origin of uranium anomalies in surface formations is the absence of significant changes of the U^{234}/U^{238} value with transition from the background concentrations of uranium to the anomaly.

LITERATURE CITED

1. N. G. Syromyatnikov, Migration of the Isotopes of Uranium, Radium and Thorium and the Interpretation of Radioactive Anomalies [in Russian], Alma-Ata, Izd.-vo AN KazSSR (1961).
2. K. E. Ivanov and R. G. Kudryashova, Col.: Problems of Applied Radiogeology [in Russian], Edited by D. Ya. Surazhskii, Gosatomizdat, Moscow (1963), p. 244.
3. L. S. Evseeva and A. I. Perel'man, Geochemistry of Uranium in the Zone of Hypergenesis [in Russian], Atomizdat, Moscow (1962).

All abbreviations of periodicals in the above bibliography are letter-by-letter transliterations of the abbreviations as given in the original Russian journal. *Some or all of this periodical literature may well be available in English translation.* A complete list of the cover-to-cover English translations appears at the back of this issue.

NOTES ON ARTICLES RECEIVED

THE PRESSURE BALANCE IN A TOROIDAL PLASMA PINCH

(UDC 533.9)

V. D. Shafranov

Translated from Atomnaya Énergiya, Vol. 19, No. 2,
p. 175, August, 1965
Original article submitted January 23, 1965; note received May 17, 1965, No. 25/3197

One method for determining the pressure in a high-temperature plasma in a magnetic field is to use the equation of pressure balance for the plasma and field. This equation is well-known in cylindrical geometry. To use it for toroidal geometry, we must consider the problem of errors in pressure measurement which arise if we do not make toroidal corrections. To solve this problem we derive the pressure balance equation, taking account of the corrections, which are quadration in the curvature of the toroidal plasma pinch. This equation has the form

$$\langle p\rangle \equiv \frac{1}{V}\int p\,dV = \frac{B_a^2}{8\pi} - \frac{B_0}{4\pi}\cdot\frac{\delta\Phi}{\pi a^2} - \frac{1}{V}\int\frac{(\delta B)^2}{8\pi}\,dV + \frac{B_a^2}{8\pi}\cdot\frac{a^2}{R^2}\left(\Lambda_1 + \frac{1}{2}\Lambda_1^2\right)$$
$$-\frac{1}{a^2R}\int_0^a\left\{\Delta(\varrho)\left[\frac{dp_0}{d\varrho} + \frac{1}{8\pi\varrho}\cdot\frac{d}{d\varrho}(\varrho B_{\omega 0}^2)\right] + \frac{B_{\omega 0}^2(\varrho)}{8\pi}\cdot\frac{\varrho}{R}\Lambda_1(\varrho) + \frac{\varrho}{R}\cdot\frac{B_{\varphi 0}^2 - B_0^2}{8\pi}\right\}\varrho^2\,d\varrho, \tag{1}$$

where

$$\Lambda_1 \equiv \Lambda_1(a);$$

$$\Lambda_1(\varrho) = \frac{16\pi[\langle p\rangle_\rho - p_0(\varrho)] + \langle B_{\omega 0}^2\rangle_\rho - B_{\omega 0}^2(\varrho)}{B_{\omega 0}^2(\varrho)}; \tag{2}$$

$$\Delta(\varrho) = \int_a^\rho \frac{\varrho'}{R}[\Lambda_1(\varrho') + 1]\,d\varrho'. \tag{3}$$

Here $B_a = 2J/ca$; J = longitudinal current in plasma pinch; a, R = smaller and greater radii of toroidal plasma pinch; $B_{\omega 0}(\rho)$ = azimuthal magnetic field, neglecting curvature; the pointed brackets with index ρ indicate averaging over the cross section of radius ρ: $\langle p\rangle$ is the pressure, averaged over the whole volume V of the toroidal plasma pinch. The longitudinal toroidal field has the form

$$B_\varphi = \frac{B_0}{1 + \frac{\varrho}{R}\cos\omega} + \delta B(\varrho, \omega), \tag{4}$$

where ρ is the polar radius reckoned from the center of the cross section of the pinch; ω = azimuthal angle; $\delta\Phi$ = excess current of longitudinal field B_ϕ in the plasma pinch, measured directly during the experiment; and δB = excess longitudinal field. Let us introduce the symbols $\eta = 8\pi\langle p\rangle_a/B_a^2$, $\varepsilon = c^2B_0\delta\Phi/2\pi J^2$. With uniform current and parabolic pressure distribution, we get from (1)

$$\eta = 1 - \varepsilon + \frac{a^2}{R^2}\left(\frac{17}{96} + \frac{25}{12}\eta - \frac{19}{6}\eta^2\right) - \frac{\langle\delta B\rangle^2}{B_a^2}.$$

Hence, even for comparatively tight toroids, R/a ≈ 4, the toroidal correction in the pressure balance equation is significant only for very small plasma pressures, $\eta \lesssim 5\%$. Thus, for practically any "Tokamak" installations, where $\langle\delta B\rangle^2 \ll B_a^2$, we can determine the pressure by means of the formula

$$\frac{8\pi\langle p\rangle_a}{B_a^2} = 1 - \frac{c^2B_0\delta\Phi}{2\pi J^2}.$$

It is only necessary to remember that B_0 is the value of the external longitudinal field on the line $\omega = \pm\pi/2$, going through the center of the plasma-pinch cross section.

SOME CHARACTERISTICS OF ACCELERATOR TUBES WITH OBLIQUE FIELDS

(UDC 621.384.6)

V. A. Romanov and A. N. Serbinov

Translated from Atomnaya Énergiya, Vol. 19, No. 2,
p. 176, August, 1965
Original article submitted May 10, 1965; No. 30/3296

The main drawback of accelerator tubes in electrostatic accelerators with voltage >3 MV is that the admissible potential gradient along the tube decreases as the tube length increases: this is called the total voltage effect. It is a consequence of the electronic loading of the tube, which is accompanied by powerful x-ray radiation which weakens the gas insulation of the electrostatic generator. Various methods have been used to strengthen accelerator tubes, but it is only by using tubes with oblique fields that the total voltage effect is practically eliminated. The idea of using oblique fields in accelerator tubes was suggested and adopted by Van de Graaf, Rose and Wittkower [1].

After theoretical [2] and experimental work and technological development, an oblique-field tube for the ÉG-1 accelerator was built at the beginning of 1964 and brought into use in May, 1964. Allowing for the constructional features of the ÉG-1, which was built in 1955, the rated gradient was taken as 1.8 MV/m. The accelerator tube has three units. In the upper and middle units, gradients of 1.7 MV/m were attained, and in the lower unit, despite the replacement of some defective insulators, the remaining low-quality insulation limited the gradient to 1.26 MV/m, which thus determined the working gradient of the whole tube. Allowing for the characteristics of tubes with oblique fields, a high-frequency ion source was installed with automatic focusing [3] (which was necessary in practice).

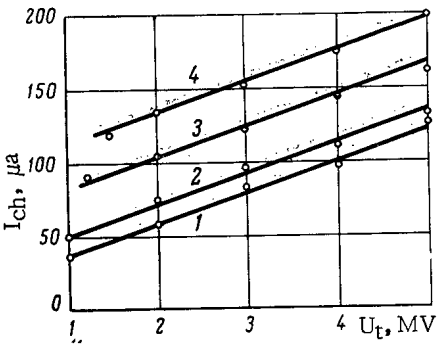

Graph of I_{ch} versus U_t for various beam currents: 1) 0; 2) 14; 3) 50; 4) 85 μa.

Using the tube with oblique fields, the ÉG-1 attained a voltage of 5 MV at beam current 85 μa. The tube characteristics stated were measured during preparation and use. The working life of the tube in nuclear physics research was over 2000 h.

The graph shows the belt charging current I_{ch} versus the tube voltage U_t for various beam currents, and with zero ion current in the tube. It is seen that electron loading is practically absent, as shown by the fact that the x-ray dose rate was more than two orders of magnitude less than with a conventional diaphragm tube. The maximum energy of the radiation spectrum was determined by the section of the tube without oblique field. Disturbance of the potential distribution along the tube leads to displacement of the beam on the target. The time required to age the tube is less than for conventional tubes.

LITERATURE CITED

1. R. Van de Graaff, P. Rose, and A. Wittkower, Nature, No. 4848, 1292 (1962).
2. V. A. Romanov and A. N. Serbinov, Pribory i Tekhnika Éksperimenta, No. 6 (1965).
3. V. A. Romanov and A. N. Serbinov, Pribory i Tekhnika Éksperimenta, No. 5 (1965).

INDIUM-GALLIUM RADIATION CIRCUIT FOR SWIMMING-POOL REACTORS

(UDC 621.039.573)

G. I. Kiknadze, V. G. Gambaryan, B. I. Litvinov,
R. B. Lyudvigov, Z. G. Razmadze, L. I. Fel'dman,
and V. M. Chanturiya

Translated from Atomnaya Énergiya, Vol. 19, No. 2,
pp. 176-177, August, 1965
Original article submitted April 14, 1965; No. 31/3276

This article describes the construction and technical data of an indium-gallium radiation circuit put into service on the IRT-2000 reactor of the Institute of Physics of the Georgian Academy of Sciences. The circuit could be constructed in practically any reactor of the swimming-pool type, either during operation or in the course of construction; it does not require special biological shielding, and in an emergency can be comparatively rapidly removed from the reactor tank. The circuit is fitted with a monitoring and control system and a semi-automatic operating and shielding system, the readings from which are displayed on the control of panel of the IRT-2000 reactor. The circuit is maintained by the reactor staff.

Radiation circuit before installation in tank of IRT reactor.

The portable underframe enables the circuit to be moved about so that the activity generator can be placed level with various neutron fluxes. Thus, without altering the reactor power, the gamma-ray dose rate in the irradiating unit of the circuit can be varied over a wide range.

The article describes a plant for preparing the indium-gallium alloy, and also the technology of preparing it and pouring it into the circuit's main tube without coming into contact with the atmospheric air.

The operation of the circuit does not in practice require the available power of the reactor; radioactive In^{116} nuclei are generated by leakage neutrons.

The construction of similar units in active swimming-pool reactors will enable research on present problems of radiation chemistry, radiobiology and radiation agriculture to be considerably extended at little cost.

With reactor power of 1000 kw the irradiating unit gives radioactivity equivalent to 16,000 g radium, which gives gamma dose rate of $\sim 0.85 \cdot 10^6$ r/h in a volume of 10.5 liter.

The authors' experiments have shown that, using an IRT type reactor of power 5000 kw, a gamma-ray source equivalent to $1 \cdot 10^6$-$1.5 \cdot 10^6$ g radium can be obtained. It thus becomes possible to irradiate objects placed next to the reactor core, behind the layer of indium-gallium alloy, with fluxes of gamma rays and fast neutrons (with energies above 1.44 eV).

By fitting an IRT type reactor with a radiation unit of the circulation type, this comparatively-cheap reactor can be used for experiments on a semi-industrial scale.

Titanium and its welded joints are stable in circulating indium-gallium alloy at least up to 300°C. Hence VTI-1 titanium has marked advantages over stainless steel 1Kh18N9T as constructional material for a radiation circuit. It is thus desirable to use VTI-1 titanium as the main constructional material for indium-gallium radiation apparatus.

DETERMINING THE DURABILITIES OF STAINLESS STEEL 1Kh18N9T AND TITANIUM VTI-1 IN CONTACT WITH AN INDIUM-GALLIUM ALLOY

(UDC 669.018 : 669.87 : 621.039.573)

G. I. Kiknadze, D. M. Zakharov, and L. V. Mel'nikova

Translated from Atomnaya Énergiya, Vol. 19, No. 2,
pp. 177-178, August, 1965
Original article submitted April 22, 1965; No. 33/3286

Work on an RK-II indium-gallium radiation circuit at the Physics Institute of the Georgian Academy of Sciences made it necessary to test the stability of stainless steel 1Kh18N9T and titanium VTI-1 in contact with a liquid eutectic indium-gallium alloy (20.5 wt. % indium, 79.5 wt. % gallium).

In investigating the interaction of these constructional materials with the alloy, we used x-ray structural analysis and metallographic methods, and also chemical analysis of the alloy after isothermal immersion of the specimens, and studies of weight changes in steel specimens in relation to the temperature and time of immersion in the alloy.

It was found that in static immersion conditions the stainless steel does not react with the alloy up to 250°C. However, at 320°C the steel is already reacting rapidly with the alloy components, so that two layers of intermetallic compounds are formed on the specimens' surfaces: the outer layer is of the very brittle $FeGa_4$ (body-centered cubic lattice, a = 8.36 kX) and the inner layer is of FeIn (body-centered cubic lattice, a = 9.14 kX) which adheres relatively tightly to the specimen substrate.

We studied the most probable mechanism for the reaction of steel with the alloy components: this is based on the diffusion of indium atoms through the previously formed $FeGa_4$. Approximate calculations showed that the experimentally measured quantity of FeIn phase formed on the specimens' surface agrees with the quantity which would appear according to our proposed mechanism for the steel-alloy reaction.

It was found that welded joints in steel 1Kh18N9T are less resistant than the metal itself: most of them react with the alloy at temperatures as low as 220-250°C.

In static immersion conditions, titanium is stable up to 350°C; welded joints in this metal are also highly stable.

At 400°C, titanium reacts noticeably with the alloy; on the surface of the specimens there forms a titanium-indium compound (γ phase), which gives lines on x-ray diffraction photographs characteristic of a simple cubic lattice with spacing 4.22 A. Reaction of the γ phase with gallium also forms a small amount of the intermetallic compound Ti_3Ga (hexagonal lattice, a = 5.75, c = 4.64 kX).

The presence on the titanium surface of an oxide film with the rutile structure, or of a hydride film, markedly improves its stability when in contact with an indium-gallium alloy.

To determine the effect of alloy circulation on the stability of constructional materials, some experiments were conducted in a model circulation apparatus, or with specimens rotated in the alloy at ~10 cm/sec linear vel.

It was found that the moving alloy does not cause erosion of the materials, but that it does cause chemical reaction between the alloy and the steel at lower temperatures than those for static conditions. In consequence, welded joints in steel in contact with the circulating alloy are insufficiently reliable: lower-grade joints begin to react below 100°C, and this might on occasion cause leaks.

INDIUM-GALLIUM ALLOY AS A GAMMA-CARRIER FOR RADIATION CIRCUITS

(UDC 669.018 : 668.87 : 621.039.573)

G. I. Kiknadze, A. I. Desipri, D. M. Zakharov, and L. V. Mel'nikova

Translated from Atomnaya Énergiya, Vol. 19, No. 2, p. 178, August, 1965
Original article submitted April 22, 1965; No. 32/3287

One of the main problems arising in the construction of radiation circuits is the choice of a reliable and convenient gamma carrier. For this purpose it is convenient to use a liquid eutectic alloy of indium and gallium. In the first model of the radiation circuit put into service with the IRT-2000 reactor of the Physics Institute of the Georgian Academy of Science, we tested an indium-gallium alloy containing 24.5 wt. % indium.* This alloy was circulated via the circuit lines for 1000 h without irradiation by neutrons.

After dismantling the apparatus, it was found that the indium content of the alloy had decreased by 2 wt. %, while an indium-based solid had collected in the joints of the circuit. Thus it was established that an alloy of gallium with 24.5 wt. % indium is unstable and contains excess indium over the eutectic composition. Owing to the smallness of the thermal effect of the transition, an investigation of gallium-indium alloys by differential thermal analysis failed to determine exactly the eutectic composition, but it showed that it must contain 20-22.5 wt. % indium and melt at 15.8 ± 0.1°C.

In parallel experiments, we observed the composition changes occurring in alloys of gallium with 24.8 wt. % indium when these were left to stand in glass tubes at 16°C. The excess indium gradually separated out so that after 80 days the amount of indium was stabilized at 22.5 wt. %. On testing the indium-gallium alloy with 22.5 wt. % indium in a model radiation circuit, we found that this alloy cannot act as a gamma-carrier. After 10,000 h's circulation the indium content decreased to 20.5 wt. %, while an indium-based solid accumulated in the joints of the apparatus. It was clear that the experiments had not lasted long enough, and the eutectic concentration had not been reached. In addition, the experimental results showed that the rate of separation of excess indium is a function of the ratio of the total alloy volume to the surface area of the vessel containing it; as this ratio decreases, the excess separates out more rapidly. By contact melting of the metals as a method of finding the eutectic alloy composition, we found that in this system the eutectic contains 20.5 wt. % indium. Being capable of very stable supercooling, this alloy can be used as a gamma-carrier in radiation circuits, beginning at ~13°C. At room temperature its viscosity is $2.5 \cdot 10^{-2}$ poise, and its density is 6.3 g/cm^3.

These experiments not only enabled us to find a working substance for radiation circuits, but also to improve our knowledge of the phase diagram of the indium-gallium alloy system with 0-25.5 wt. % indium.

At the present time, an indium-gallium alloy containing 20.5 wt. % indium is the only thoroughly-studied, tested and reliable gamma-carrier.

LITERATURE CITED

1. M. Hansen, Structure of Binary Alloys [Russian translation], Metallurgizdat, Moscow (1958).

* According to the results of Hansen [1], this alloy is eutectic and melts at 15.8°C.

ANGULAR AND ENERGY DISTRIBUTIONS OF GAMMA RADIATION AT SURFACE OF VOLUME SOURCE

(UDC 539.122 : 539.121.73 : 539.121.64)

B. F. Gromov, S. M. Ermakov, E. E. Kazarnikova, and M. A. Solodyankin

Translated from Atomnaya Énergiya, Vol. 19, No. 2, pp. 179-180, August, 1965
Original article submitted March 20, 1965; note received June 5, 1965; No. 28/3255

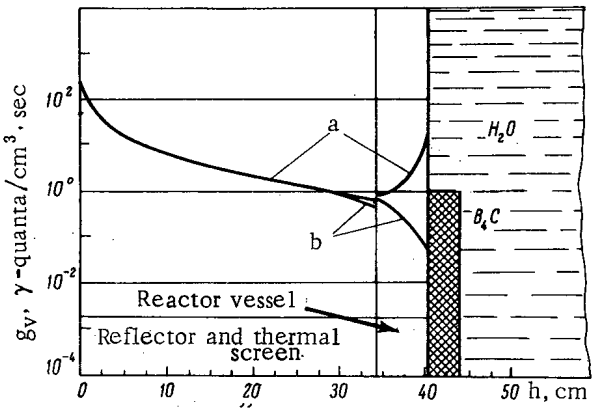

Fig. 1. Density of sources of capture gamma radiation in steel. a) q_V without boron screen; b) q_V with boron screen.

As a rule, nuclear power reactors have, outside their cores, a thick layer of steel (reflector, "thermal screen" and reactor vessel), which forms a powerful volume gamma source with a complex graph of gamma-generation density across its thickness.

In making mathematical analyses of biological shielding from sources of this type, it is convenient to convert the complex volume source to a surface with known angular and energy gamma-radiation distribution.

In this paper we study the angular and energy distributions of gamma radiation on the outer surface of the reactor vessel, taking the two cases when (1) the reactor vessel is in water and is not shielded by a boron screen, and (2) the reactor vessel is in water and shielded by a boron screen (Fig. 1).

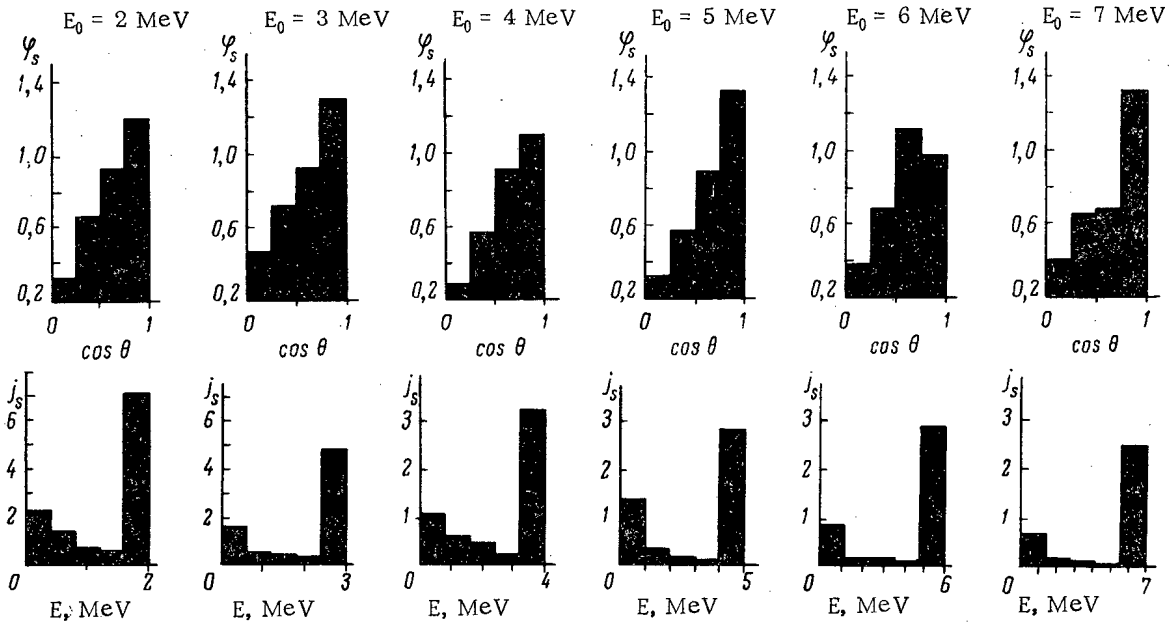

Fig. 2. Angular [$\varphi_s(\Theta)$, γ-quanta/(cm²·sec·steradian)] and energy [$j_s(E)$, γ-quanta/(cm²·sec·Mev)] distributions of gamma radiation at surface of source a (see Fig. 1).

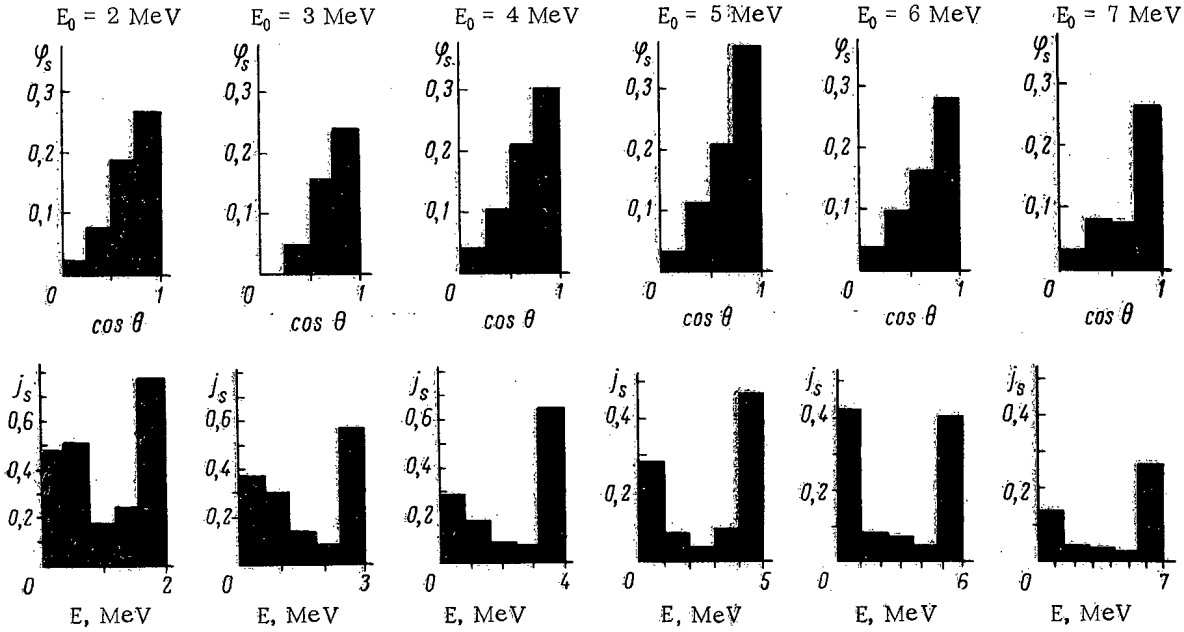

Fig. 3. Angular [$\varphi_s(\Theta)$, γ-quanta/(cm^2·sec·steradian)] and energy [$j_s(E)$, γ-quanta/(cm^2·sec·Mev)] distributions of gamma radiation at surface of source b (see Fig. 1).

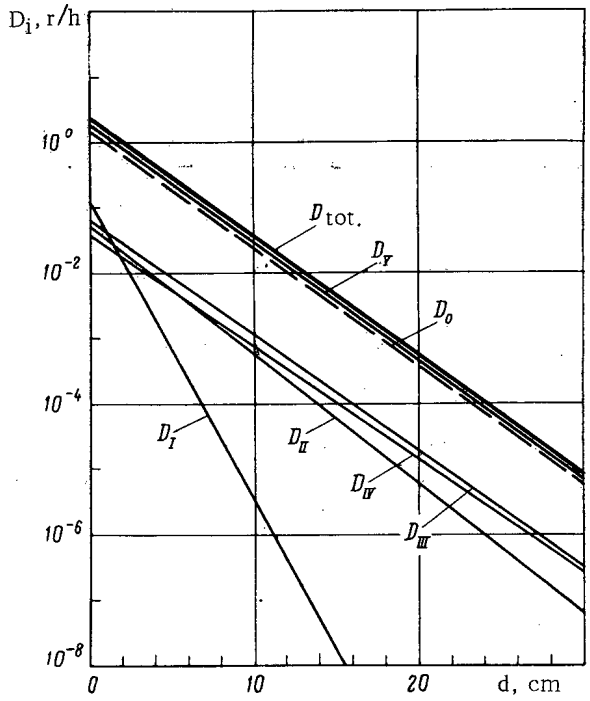

Fig. 4. Attenuation of dose rate D_i for gamma radiation in lead:

The spectrum and angular distribution of gamma radiation at the source's surface were determined by the Monte Carlo method with an M-20 computer.

The calculation was performed by direct simulation of the source, assuming that gamma rays are generated with initial energies E_0 equal to 2, 3, 4, 5, 6, and 7 MeV.

After 12,000 trials the maximum statistical error was below 25% for the angular distribution and 20% for the energy distribution.

Fig. 2 and Fig. 3 give the total spectra and angular distributions of gamma radiation in the form of histograms. The angular distribution and intensity of non-scattered gamma radiation were determined analytically. From the results we calculated the accumulation dose factors at the surface of the source.

We also analysed the attenuated full-spectrum gamma radiation from source a (see Fig. 1), which generates gamma radiation with E_0 = 7 MeV, in lead shielding.

Fig. 4 gives the results of the analysis. From the results we can calculate the contribution to the dose outside the shielding made by gamma rays undergoing multiple scattering in the source, and also the contribution to the heat emission inside the biological shielding.

Group number	Energy range, MeV
I	0—1,4
II	1,4—2,8
III	2,8—4,2
IV	4,2—5,6
V	5,6—7,0
0	Unscattered gamma-radiation; E_0 = 7 MeV

LETTERS TO THE EDITOR

INTERNATIONAL COMPARISON OF NEUTRON SOURCES

(UDC 539.16.08 : 539.125.5)

O. L. Andreev, Yu. S. Silin, G. M. Stukov, V. I. Fominykh,
V. T. Shchebolev, and I. A. Yaritsyna

Translated from Atomnaya Énergiya, Vol. 19, No. 2,
pp. 181-183, August, 1965
Original article submitted October 13, 1964

At the present time, fairly accurate absolute measurments of a number of neutron sources are being made in all the leading metrological laboratories of the world. The errors of these measurements are 1-3%.

As a rule, the most accurate yield determinations can be made on Ra$-\alpha-$Be or Ra$-\gamma-$Be sources. To verify the validity of any absolute method of measurement, and also to reveal unknown systematic errors, measurements must be made by several absolute methods.

The best method for testing the measurements made in different countries (and hence the validity of the corresponding units) is to make international comparisons. Measurements are made of different national standard neutron sources in a single laboratory, and also of the same neutron source in different laboratories of the world, enabling us to derive a mean international value for the yield of a given neutron source.

The first attempt at making an international comparison of neutron sources was made in the 'fifties, the results being published in 1954 by Hughes [1]. In 1951 and 1954, comparisons were made in which six countries took part: the same neutron source was measured in various laboratories. The discrepancy of the 1951 measurements was 20%, that of the 1954 measurements only 10%.

In 1958 Larsson published the results of his international comparisons. In these, six countries took part. Here the Soviet Union was participating in international comparisons for the first time: the Soviet N-22 and N-26 neutron sources were directly compared with a Swedish source. The results of these international comparisons are shown in in Fig. 1.

In order to obtain unity of measurement in different countries, in January 1961 the first conference of the Working Group on Neutron Measurements at the International Bureau of Weights and Measures at Paris decided that it was advisable to make cyclic comparisons of neutron sources, i.e., to measure the same source in different countries. At this time the Canadian neutron source No. 200-1 was measured in Britain, Sweden, the USA, the Federal German Republic and Belgium. The results are given in [3]. This source was measured by Geiger (Canada) by two absolute methods, manganese activation [4] and comparison in a manganese tank with the yield of a polonium fluoride source of which the yield was determined absolutely [5].

The No. 200-1 source was constructed in 1948: it contains 183 mg radium mixed with 2000 mg beryllium. To ensure physical stability, the active mass was pressed into a tablet and enclosed in a cylindrical capsule of Monel metal of thickness 2 mm; the capsule height and diameter are 19 mm. In 1961 the 200-1 was transferred to the International Bureau of Weights and Measures for international comparison. In recent years this source has been measured in Holland, Israel, the USSR, France, Japan and the International Bureau of Weights and Measures.

Except for Canada, Britain and the USSR, all the countries listed above made only relative measurements of the source by various methods. We considered it more effective to make absolute rather than relative measurements. As well as some loss of accuracy due to the comparison, and to measurement in open geometry (e.g., with a long counter), there is asymmetry in the neutron radiation from the source. Even if this only reaches 2-3%, it can significantly affect the result.

We measured the asymmetry in the distribution of neutrons from the Canadian source in open geometry with a long counter from the All-Union Metrology Research Institute (VNIIM). This counter had a special fitting enabling

Results of International Comparison of Canadian Neutron Source

Country and laboratory	Year of comparison	Error	Yield of Canadian source No. 200-1 on January 1, 1963, $\cdot 10^6$, neutrons/sec
International Bureau of Weights and Measures (Sevres)	1962	2%	3.20
England (National Physical Laboratory)	1959	1.5%	3.18
Belgium (laboratory of mining company)	1959	2%	3.28
Holland (Institute of Nuclear Physics)	1962	3%	3.16
Israel (Research Institute)	1963	1.7%	3.22
Canada (National Research Council)	1958	1.5%	3.26
USSR (All-Union Research Institute of Metrology)	1963	1%	3.26
USA (National Bureau of Standards)	1959	2%	3.27
France (Saclet)	1962	1.5%	3.27
Federal German Republic (Federated Physico-Technical Institute)	1959	2%	3.27
Sweden (Atomic-Energy Company)	1959	2%	3.23
Japan (Electrical Engineering Laboratory)	1962	3.1%	3.33

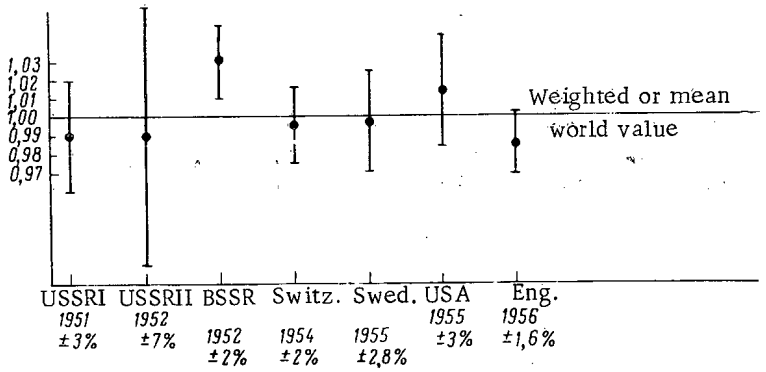

Fig. 1. Results of international comparison of neutron sources, published by Larsson in 1958 [2].

the measured source to be turned through any required angle. With the source disposed so that its axis of rotation coincided with that of the cylinder, we found an asymmetry of 1%; on turning the source on its side surface, the asymmetry was 1.5%. We then measured the yield of the Canadian neutron source with a long counter by comparing it with the VNIIM 2ÉN-100 Ra$-\alpha-\beta$ source, of which the yield was measured by an absolute method. According to the relative measurements, the yield of the Canadian neutron source is $3.25 \cdot 10^6$ neutrons/sec (uncertainty 1.3%). In these measurements, as in the measurements of the asymmetry of neutron distribution from the Canadian source, the source was placed 1 m from the front surface of the long counter.

We then made absolute measurements of the yield from the Canadian neutron source. To eliminate possible systematic errors, we measured the yield in three different independent ways: the method of accompanying particles, the method of manganese activation, and the method of gold-foil activation. The yield, as measured by the method of accompanying particles [6], was $3.27 \cdot 10^6$ neutrons/sec (1.4%) in December 1962. The yield as determined by manganese activation [7] was $3.26 \cdot 10^6$ neutron/sec in January 1963.

In January 1963 the yield of this source was determined by the activation of gold foils [8]; it was $3.22 \cdot 10^6$ neutrons/sec (2.2%). From these three absolute measurements, the weighted mean yield from the Canadian neutron source No. 200-1 was $3.26 \cdot 10^6$ neutrons/sec in January 1963 (uncertainty 1%).

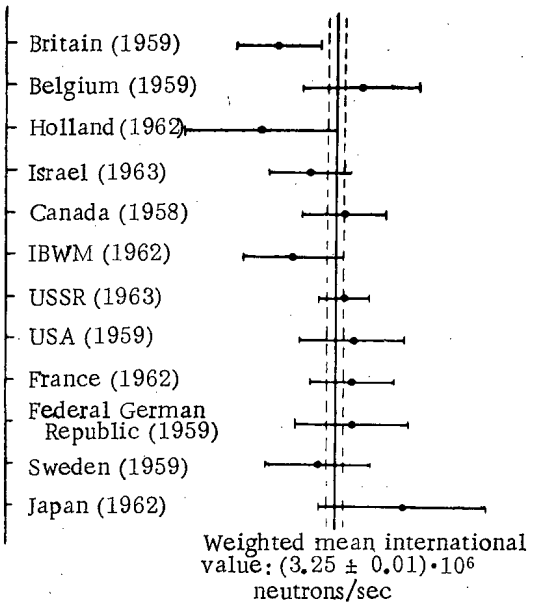

Fig. 2. Results of international comparison of Canadian neutron source No. 200-1.

Fig. 2 gives the results of international comparisons of the Canadian neutron source at all the points at which it was measured. The weighted mean international value of the neutron yield of the 200-1 Ra–α–Be source in January 1963 was $3.23 \cdot 10^6$ neutrons/sec. The error of the weighted mean was 0.3%. Our value for the yield agrees satisfactorily with the data of the other laboratories [3, 9].

LITERATURE CITED

1. D. Hughes, Nucleonics, No. 12, 26 (1954).
2. K. Larsson, J. Nucl. Energy, 6, 322 (1958).
3. K. Geiger, Canad. J. Phys., 38, 569 (1960).
4. K. Geiger and G. Whyte, Canad. J. Phys., 37, 256 (1959).
5. K. Geiger, Canad. J. Phys., 37, 550 (1959).
6. A. S. Karamyan, et. al., Atomnaya Énergiya, 16, 251 (1964).
7. A. A. Konstantinov, V. I. Fominykh, and I. A. Yaritsyna, Ibid., p. 253.
8. O. L. Andreev, et. al., Ibid., p. 255.

All abbreviations of periodicals in the above bibliography are letter-by-letter transliterations of the abbreviations as given in the original Russian journal. *Some or all of this periodical literature may well be available in English translation.* A complete list of the cover-to-cover English translations appears at the back of this issue.

RESONANCE INTERACTION OF NEUTRONS WITH MOLECULES

(UDC 539.172.4)

G. K. Ivanov and Yu. S. Sayasov

Translated from Atomnaya Énergiya, Vol. 19, No. 2,
pp. 183-184, August, 1965
Original article submitted October 26, 1964

The total resonance-absorption cross section for neutrons in atomic gases depends on the Döppler effect which is due to thermal motion of the atoms [1]. Resonance absorption of neutrons by nuclei in crystals is, according to Lamb's formula [1], determined by the pulse spread of the nuclei which is due to their vibratory motion.

Resonance scattering of neutrons by nuclei chemically combined into molecules must differ from both these cases, because the pulse spread of a nucleus in a molecule (and hence the resultant spread in the Döppler effect) is complex, depending simultaneously on the rotational and vibrational motions of the nuclei and the translational motion of the molecule.

In this note we describe the results of a calculation of the neutron-resonance scattering and absorption cross sections of nuclei forming part of molecules (which are regarded as free). Strictly speaking, the formulae below are valid only for molecular gases. However, they can be applied to molecular liquids and crystals as well, provided that the interactions of the molecules can be typified by damped rotation frequencies which are small by comparison with the molecular vibration frequencies. This is usually true for heavy molecules.

Let us suppose that the width of the resonance level Γ and the recoil energy of the nucleus $R_\nu \approx \frac{m}{M_\nu} E_n$ (where m and M_ν are the masses of the neutron and scattering nucleus of the molecule, E_n the energy of the incident neutron) are much greater than the mean difference between the vibration levels of the molecule, ω, i.e.,

$$\Gamma \gg \omega, \quad R_\nu \gg \omega. \tag{1}$$

These assumptions are true for heavy enough nuclei. By the general formula (11) of reference [2], which was derived in the momentum approximation (for $\Gamma \gg \omega$) and the simplifying assumption that there is a large energy transfer ε ($\varepsilon, R_\nu \gg \omega$), the neutron scattering is represented by fairly simple and physically-intelligible formulae. In this case, the second-differential cross section of elastic scattering is given by the formula

$$\frac{d^2\sigma_\nu}{d\varepsilon\, do} = \frac{1}{4\pi} \cdot \frac{k'}{k} \left\langle \sigma_{\nu 0}\left(\frac{M_\nu}{M_\nu + m} E_n - \frac{\mathbf{kp}_\nu}{M_\nu} \right) \times \delta\left(\varepsilon - \frac{\varkappa^2}{2M_\nu} - \frac{\boldsymbol{\varkappa}\mathbf{p}_\nu}{M_\nu} \right) \right\rangle . \tag{2}$$

Hence the total scattering cross section is

$$\sigma_\nu = \left\langle \sigma_{\nu 0}\left(\frac{M_\nu}{M_\nu + m} E_n - \frac{\mathbf{kp}_\nu}{M_\nu} \right) \right\rangle . \tag{3}$$

Here $\mathbf{k}$ is the momentum of the neutron before scattering, $\mathbf{k}' = \mathbf{k} - \boldsymbol{\varkappa}$ is the momentum of the neutron after scattering, o is the solid angle of scattering of the neutrons, p_ν is the momentum of the bound nucleus; $\sigma_{\nu 0}(E)$ is the paired-scattering cross section of free atoms, and in the case of resonance takes the following form:*

$$\sigma_{\nu 0}(E) = \frac{\pi}{k_1^2} \cdot \frac{\Gamma_e^2}{(E - E_0) + \frac{\Gamma^2}{4}}, \quad k_1 = \sqrt{2 \frac{m M_\nu}{m + M_\nu} E},$$

where Γ_e is the elastic width of neutron-nucleus resonance, E_0 the resonance energy.

Formulae (2) and (3) give the cross section of paired scattering by free atoms, averaged over their quantum-mechanical internal motion. The total cross section differs from that in (3) only in that Γ_e^2 is replaced by $\Gamma_e(\Gamma - \Gamma_e)$.

* In what follows we use a system of units in which the Planck and Boltzmann constants are equal to unity.

The spectra of scattered neutrons, given by (2), are typified by having two-peaked maxima in the angular distribution. The first of these, obtained from the condition $\varepsilon = R_\nu$ ($R_\nu = \frac{\varkappa^2}{2M_\nu}$), is associated with the properties of the momentum distribution of the atoms in the molecule, which has a maximum at $p_\nu = 0$. The second maximum is observed at $\frac{M_\nu}{M_\nu + m} E_n - E_0 - \frac{1}{2}(\varepsilon - R_\nu) = 0$ and is caused by the appearance of a shift of $\frac{1}{2}(\varepsilon - R_\nu) \approx \frac{\varkappa p_\nu}{M_\nu}$ in the energy dependence of the Breit-Wigner cross section. For scattering of neutrons into the reverse hemisphere, when the vectors $\mathbf{k}$ and $\varkappa$ are almost parallel, (2) takes the following specially simple form:

$$\frac{d^2\sigma_\nu}{d\varepsilon\, do} = \frac{1}{4\pi} \cdot \frac{k'}{k} \sigma_{\nu 0} \left[\frac{M_\nu}{M_\nu + m} E_n - \frac{1}{2}(\varepsilon - R_\nu) \right] \times \left\langle W\left(\frac{(\varepsilon - R_\nu) M_\nu}{\varkappa} \right) \right\rangle_\Omega ,$$

where $\langle W(p_\nu \varkappa) \rangle_\Omega$ is the distribution of the momentum components of the atom in any arbitrary direction for a given orientation of the molecule, averaged over the molecular orientations.

By (3), the formula for the total scattering or absorption cross section is

$$\sigma_\nu = \frac{4\pi}{k_1^2} \cdot \frac{\Gamma_e^2}{\Gamma^2} \int \psi(\xi, x) \frac{d\Omega}{4\pi} . \tag{4}$$

Here

$$\psi(\xi, x) = \frac{\xi}{2\sqrt{\pi}} \int_{-\infty}^{\infty} \exp\left[-\frac{\xi (x-t)^2}{4} \right] \frac{dt}{1+t^2} ,$$

where $\xi = \frac{\Gamma}{\Delta}$; $x = \frac{\frac{M_\nu}{M_\nu + m} E_n - E_0}{\Gamma/2}$; $\Delta = \sqrt{2 \frac{m}{M_\nu} E_n \omega}$ is the Döppler width. ω depends on the angular orientation of the molecule, and is given by the formula

$$\omega = \sum_{i=1}^{s} (\mathbf{n} c_\nu^i)^2 \omega_i \operatorname{cth} \frac{\omega_i}{2T} + 2T \mathbf{n} \hat{m}_\nu^{-1} \mathbf{n} \quad (\omega \to 2T \text{ as } T \to \infty), \tag{5}$$

where $\mathbf{n}$ is an arbitrary unit vector characterizing the orientation of the molecule, c_ν^i is the amplitude vector characterizing the vibration of an atom of type i, $\hat{m}_\nu$ is the tensor of the atomic masses in the molecule [3], T is the temperature of the molecular medium, and s is the number of vibratory degrees of freedom of the molecule.

Let us choose a system of coordinates with its origin in the ν-th atom, such that in it ω (ω being the quadratic projection function of the unit vector $\mathbf{n}$) has the canonical form

$$\omega = \omega^{(1)} \cos^2\theta + \omega^{(2)} \sin^2\theta \cos^2\varphi + \omega^{(3)} \sin^2\theta \sin^2\psi,$$

where $\omega^{(1)}$, $\omega^{(2)}$, $\omega^{(3)}$ are complex functions of the components of the amplitude vectors and mass tensor. Then integration of (4) over the solid angle $d\Omega = \sin\Theta\, d\Theta\, d\varphi$ gives the energy dependence of the cross section: it differs markedly from the Lamb function, and depends on the detailed structure of the molecule, i.e., on c_ν^i and ω_i. For example, in the most interesting case, $\xi_1 = \frac{\Gamma}{\Delta_1} \ll 1$ $\left(\Delta_1 = \sqrt{2 \frac{m}{M_\nu} E_n \omega^{(1)}} \right)$ in the region $\xi_1^2 x \ll 1$, (4) leads to

$$\sigma_\nu = \frac{\pi}{k_1^2} \cdot \frac{\Gamma_e^2}{\Gamma^2} \pi^{1/2} \xi_1 f(\varrho^2); \quad \varrho^2 = \frac{1}{4} \xi_1^2 x^2; \tag{6}$$

the function $f(\rho^2)$ is evaluated in [4].

In the particular case when $\omega^{(2)} = \omega^{(3)} < \omega^{(1)}$, $f(\rho^2)$ takes the form

$$f(\varrho^2) = \frac{\beta}{2\sqrt{\beta - 1}} \int_1^\beta \frac{e^{-\rho^2 t}}{t\sqrt{\beta - t}} dt; \quad \beta = \frac{\omega^{(1)}}{\omega^{(2)}} > 1. \tag{7}$$

Provided that the condition $\xi \ll 1$ is obeyed, (4) and (6) are applicable to any linear molecules, and also for some

molecules with a high degree of symmetry (e.g., CCl_4). However, calculations by (4), (6) and (7) are very complicated; it is therefore convenient to investigate the possibility of using, instead of (4), the simple formula

$$\sigma_v = \frac{4\pi}{k_1^2} \cdot \frac{\Gamma_e^2}{\Gamma^2} \psi(\bar{\xi}, x) \tag{8}$$

$\left(\xi = \Gamma/\bar{\Delta};\ \bar{\Delta} = \sqrt{2\frac{m}{M_v} E_n \bar{\omega}}\right)$, which is obtained from (4) by introducing the quantity $\bar{\omega}$, averaged over all the molecular orientations,

$$\bar{\omega} = \int \omega \frac{d\Omega}{4\pi} = \frac{\omega^{(1)} + \omega^{(2)} + \omega^{(3)}}{3}. \tag{9}$$

This approximation is analogous to the introduction of the mean mass in the theory of Krieger and Nelkin [3]. For the CCl_4 molecule (at T = 300°K) we obtained the following values: $\omega^{(1)} = 0.078$ eV, $\omega^{(2)} = \omega^{(3)} = 0.058$ eV—i.e., in this case $\omega^{(1)}/\omega^{(2)} = 1.42$. (The frequencies and force constants required for this calculation were taken from [5]). Using (7) and (8), we calculated the energy dependence of the total cross section for the chlorine nucleus with resonance parameters $\Gamma = 0.8$ eV and $E_0 = 4300$ eV [6], corresponding to $\xi_1 = 0.18$. The agreement was quite satisfactory.

On the other hand, for the Cl_2O molecule, for example, for which $\omega^{(1)}/\omega^{(2)}$ and $\omega^{(1)}/\omega^{(3)}$ are greater than two The discrepancy between (6) and (8) is appreciable. For a criterion of the applicability of (8) we can therefore use the inequalities $\frac{\omega^{(1)}}{\omega^{(2)}}, \frac{\omega^{(1)}}{\omega^{(3)}} < 2$

LITERATURE CITED

1. A. I. Akhiezer and I. Ya. Pomeranchuk, Some Problems in the Theory of the Nucleus [in Russian], Gostekhteorizdat, Moscow (1950).
2. G. K. Ivanov and Yu. S. Sayasov, ZhÉTF, 45, 1456 (1963).
3. T. J. Krieger and M. S. Nelkin, Phys. Rev., 106, 290 (1957).
4. G. K. Ivanov, ZhÉTF, 44, 573 (1963).
5. M. V. Vol'kenshtein, M. A. El'yashevich, and B. M. Stepanov, Molecular Vibrations [in Russian], Fizmatgiz, Moscow (1959).
6. Yu. P. Popov and F. L. Shapiro, ZhÉTF, 40, 1610 (1961).

RELATIVE YIELDS OF GROUPS OF DELAYED NEUTRONS IN THE PHOTO-FISSION OF U^{238}

(UDC 539.173.3)

O. P. Nikotin and K. A. Petrzhak

Translated from Atomnaya Énergiya, Vol. 19, No. 2,
pp. 185-186, August, 1965
Original article submitted October 5, 1964

We studied the relative yields of groups of delayed neutrons in the fission of U^{238} by bremsstrahlung radiation with maximum quantum energy 10-15 MeV. The target was a plate of uranium metal of size 15 × 10 × 3 mm. It was irradiated, in a special device built inside the chamber of a betatron, either until the delayed neutron activity reached saturation, or for 10 sec. The short-duration irradiation enabled us to determine the contribution made by short-lived groups to the total decay curve for delayed neutron activity.

0.1 sec after the completion of irradiation, the target was transferred pneumatically into the counting apparatus. A special system measured the flight time of the target in each experiment, simultaneously switched off the control circuit of the betatron, and, at the moment at which the target was locked into the counter unit, switched on the neutron-recording device. To record delayed neutrons, we used a system of proportional slow-neutron counters in a paraffin moderator, an amplifier with a discriminator, and a 55-channel pulse time analyser. The efficiency of the counter unit for neutrons with energies 0.1-1.0 MeV was determined by means of photoneutron sources; the yields of neutrons from these sources were compared by means of a manganese bath. The channel width of the pulse time analyser increased with increasing channel number from 0.05 to 8.0 sec. The total time of recording delayed neutrons was 280 sec.

The time distribution of delayed neutron activity, measured in 20-50 experiments, was summed, and the sum curves were analyzed graphically to separate the groups of delayed neutrons. We give the results of more than 700 irradiations. For U^{238} we observed six groups of delayed neutrons with half-lives of 55.0 ± 2.0; 21.0 ± 0.6; 5.4 ± 0.3; 2.2 ± 0.2; 0.7 ± 0.2 and 0.18 ± 0.03 sec. The relative yields of these groups at maximum energy of bremsstrahlung radiation 14.0 MeV were 0.020 ± 0.001; 0.158 ± 0.008; 0.142 ± 0.012; 0.340 ± 0.014; 0.180 ± 0.010 and 0.160 ± 0.020 respectively.

The relative yields for the various groups of delayed neutrons were corrected for the varying efficiency of the counter unit for neutrons of different energies (Fig. 1). The mean energies for the first, second, third and fourth groups of delayed neutrons were taken from [2], and were 250, 460, 405 and 450 keV respectively. The mean energies for the fifth and sixth groups were taken as equal and were 450 keV. The errors quoted for the relative yields are standard scatters of a series of repeated measurements.

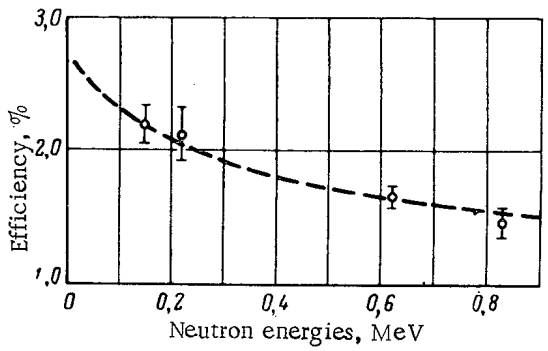

Fig. 1. Detector efficiency versus neutron energies. ---) Efficiency of similar detector described in [1]; o) experimental points.

When the maximum bremsstrahlung energy was varied from 10 to 15 MeV, the relative yields of the first, second, fourth, fifth and sixth groups did not vary by more than the experimental error. For the third group, there was an appreciable rise in the relative yield with increasing energy of fission excitation (Fig. 2).

It is interesting to note that the sixth group of delayed neutrons had a much greater relative yield than that displayed by the same group when U^{238} fission is caused by neutrons of the fission spectrum [3]. Perhaps this is indirect evidence that the mean energy of the sixth group is appreciably dis-

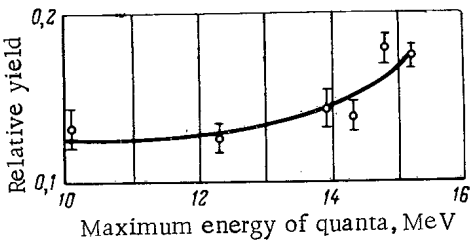

Fig. 2. Variation of relative yield of third group of delayed neutrons with maximum energy of bremsstrahlung radiation.

placed towards lower values. This conclusion is prompted by the following observation: our counting equipment's efficiency for neutrons increases somewhat with decreasing neutron energy; however, the relative yields of the first five groups of delayed neutrons in our experiments differ from the corresponding yields of these groups in the fission of U^{238} by fast neutrons [3, 4] somewhat less than the yield of the sixth group.

LITERATURE CITED

1. C. Johnson, A. Galonsky, and J. Ulrich, Phys. Rev., 109, 1243 (1958).
2. R. Batchebor and H. Mc. Hyder, J. Nucl. Energy, 3, 7 (1956).
3. G. Keerin, T. Wimett, and R. Zeigler, J. Nucl. Energy, 6, 1 (1957).
4. B. P. Maksyutenko, ZhÉTF, 35, 815 (1958).

DELAYED GAMMA RAYS FROM U^{235} FISSION

(UDC 539.173)

L. A. Popeko, G. V. Val'skii, D. M. Kaminker,
and G. A. Petrov

Translated from Atomnaya Énergiya, Vol. 19, No. 2,
pp. 186-188, August, 1965
Original article submitted November 17, 1964

Most of the gamma quanta from U^{235} fission emerge in less than $5 \cdot 10^{-11}$ sec [1]. However, some of them are known to emerge after much greater delay times [2].

With the apparatus shown in Fig. 1, we measured the delayed gamma radiation from the fission fragments in the time range 10-70 nsec and the energy range 30-500 keV. About 200 μg of U^{235} was deposited on an Al_2O_3 substrate of density ~20 $\mu g/cm^2$ in the form of an 8 mm diam. spot. The target was set up in a vacuum chamber through which was passed a beam of neutrons from a VVR-M reactor.* The fission fragments were registered by a silicon detector of diam. 32 mm, located 58 mm above the target. The fragments complementary to those registered, after travelling ~100 mm, fell on the thin aluminum wall of the chamber, immediately behind which was the NaI(Tl) crystal, of size 35 × 40 mm, of a scintillation gamma spectrometer. The energy resolution of the spectrometer for the Cs^{137} line was 10%. Fragments approaching the gamma detector could be absorbed by an aluminum shutter of thickness 4 mg/cm^2, placed 15 mm from the target. The mean solid angle over which the gamma rays from these fragments could be recorded, after they had been stopped, was 15 times greater with the shutter open than with it closed. Thus measurements with open shutter effectively recorded the delayed gamma rays from the fragment, while those with the shutter closed measured the background count.

The electronics were a "fast-slow" coincidence system with a (delay time)-(pulse amplitude) converter. The time resolution of the fast section was 6-8 nsec; its output pulse was used to control the amplitude of an AI-100 analyser, the input of which was fed with pulses either from the gamma detector, from the fragment detector, or from the amplitude-time converter. A discriminator in the fragment-detector channel enabled us to distinguish roughly between pulses from heavy and light fragments.

Fig. 1 shows the experimental arrangement and the time distributions of the coincidence pulses obtained with the shutter open and closed. The difference between these curves, normalized to a constant number of detected fissions, gives the decrease in time of the gamma-ray intensity of a fragment: this was found to be practically a pure exponential curve. The mean lifetime in this delay-time range was $\tau_T = 28 \pm 3$ nsec for the heavy-fragment group, and $\tau_L = 35 \pm 4$ nsec for the light-fragment group.

In determining the lifetime, attention was paid only to the points corresponding to times between 10 and 70 nsec after the fission, when practically all the fragments had already been stopped. In the measurements of the amplitude spectra, the corresponding time interval was isolated by means of a discriminator in the amplitude-time converter channel.

In Fig. 2, curve 1 is the pulse-amplitude distribution for fragments without coincidences, curve 2 is the pulse-amplitude distribution for fragments corresponding to delayed gamma radiation. Although it will be seen that the energy resolution of the fragments is poor (mainly owing to the thickness of the target), nevertheless a comparison of curves 1 and 2 makes it clear that most of the gamma radiation in this time range is emitted by light fragments.

Fig. 3 gives the spectra of the delayed gamma radiation. Curve 1 was measured without discriminating between the fragment pulses. Curve 2 corresponds to delayed gamma rays from the heavy-fragment group; curve 3 is the difference between curves 1 and 2 and corresponds to delayed radiation from light fragments. The points 4,

* Water-moderated water-cooled power reactor—Publisher's note.

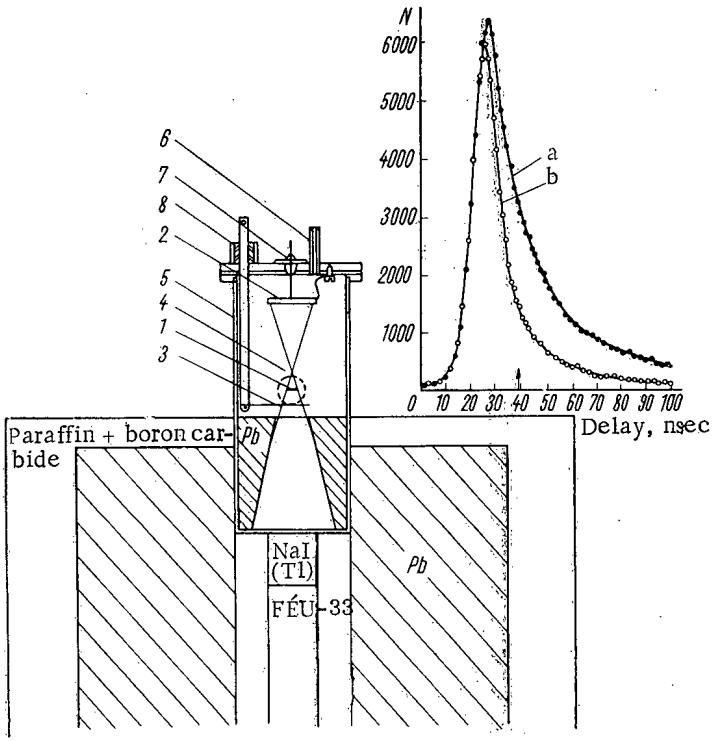

Fig. 1. Experimental arrangement and time distribution of coincidence pulses with shutter open (a) or closed (b). Experimental arrangement: 1) Target; 2) fragment detector; 3) shutter; 4) (dashed line) boundary of neutron beam; 5) casing of vacuum chamber; 6) pipe for evacuation; 7) vacuum lead; 8) Wilson gland.

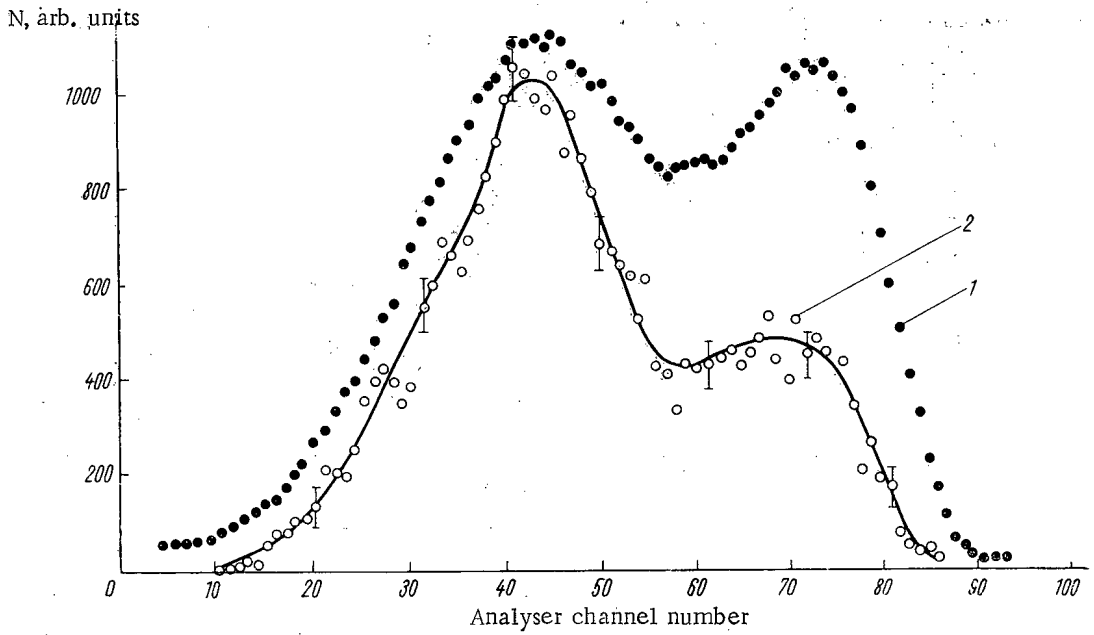

Fig. 2. Pulse amplitude distribution for fragments without coincidence.

represented by white circles, were obtained with the discriminator differentially separating pulses from a heavy fragment, i.e., they must also correspond to radiation from a light fragment. It is seen that they lie fairly closely on curve 3. The instrumental spectra (curves 2 and 3) could be separated into a relatively small number of lines, of which the energies and yields are given in the table. In calculating the yields we made corrections for the gamma-detector efficiency, for absorption in the aluminum and for decay (with the measured lifetimes, τ).

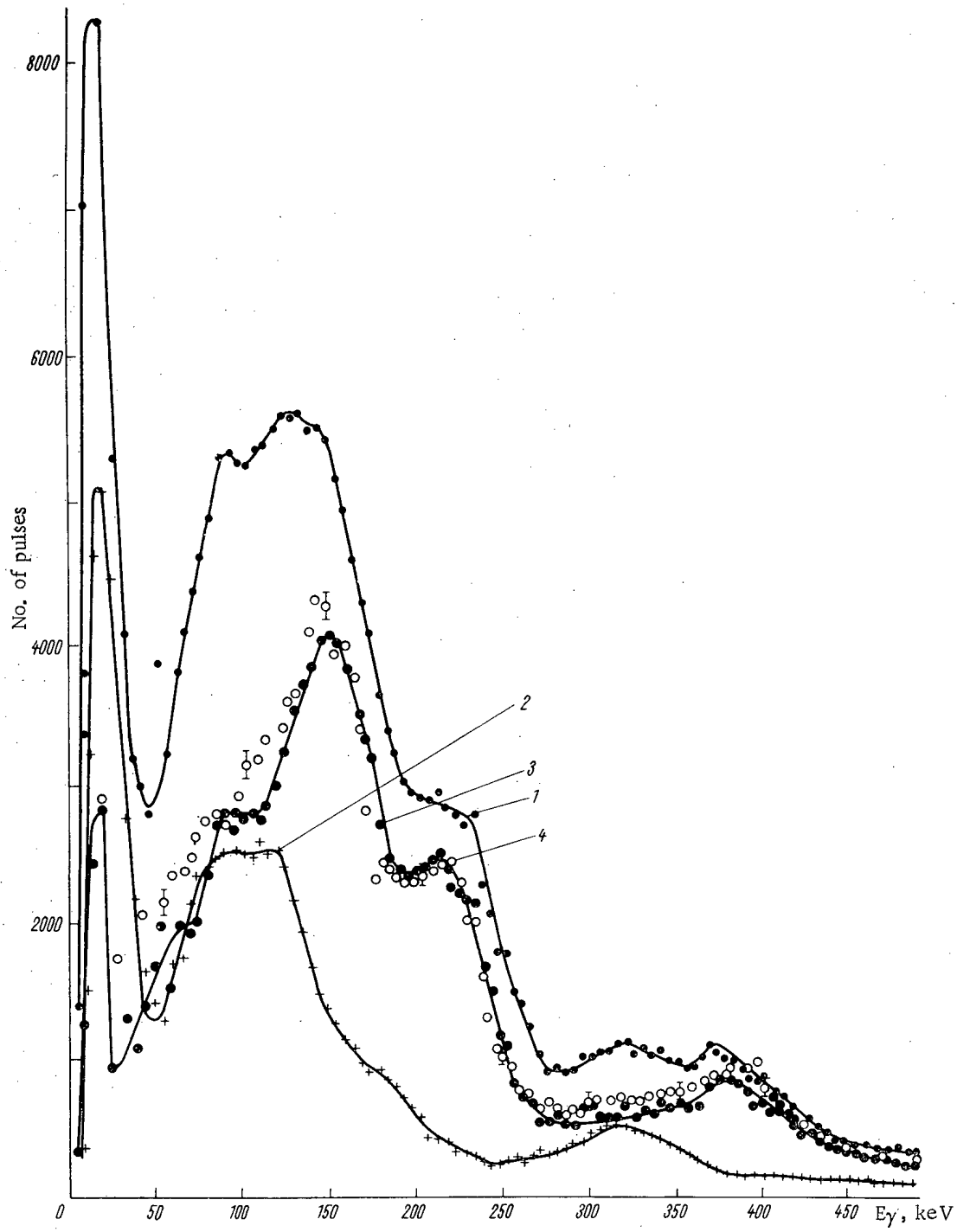

Fig. 3. Spectra of delayed gamma radiation.

Those lines in the gamma spectra of the light-and heavy-fragment groups which are of nearly equal energies may possibly be the same lines, possibly as a consequence of inadequate resolution of these fragment groups. The 30 keV line is evidently a mixture of the x-ray K-lines of the heavy-group fragments. The intensity of this line ray have been reduced in our experiments by instrumental cut-off.

The small number of lines in the delayed gamma-ray spectra can be explained either by the very similar decay schemes of the lower levels of the fragment nuclei, or by supposing that the delayed radiation mainly belongs to a small group of nuclei distributed near the most probable masses. No explanation has yet been found for the practically identical lifetimes of the light and heavy groups of fragments.

Energies and Yields of Delayed Gamma Quanta

Heavy fragments		Light fragments	
$E\gamma$, keV	no. of quanta per 100 fissions	$E\gamma$, keV	no. of quanta per 100 fissions
30 ± 5	$>1,7$	—	—
80 ± 5	$1,0\pm0,4$	85 ± 5	$0,7\pm0,4$
110 ± 5	$1,1\pm0,4$	115 ± 10	$0,5\pm0,5$
140 ± 5	$0,7\pm0,4$	140 ± 5	$1,8\pm0,8$
175 ± 10	$0,4\pm0,2$	165 ± 10	$1,0\pm0,5$
		210 ± 8	$2,3\pm0,4$
310 ± 10	$1,4\pm0,2$	320 ± 10	$0,5\pm0,2$
		365 ± 10	$2,3\pm0,2$
Total yield less 30 keV	$4,6\pm0,5$	—	$9,1\pm1$

The delayed-radiation spectrum (curve 1, Fig. 3) is very similar to the instantaneous-radiation spectrum [2-4], though the gamma-quantum yields are quite different and cannot be reconciled with the lifetime given in [3]. We can suppose that, in the 0-450 keV range, the instantaneous gamma radiation corresponds to transitions between lower levels of essentially the same fragment nuclei as for the delayed radiation, but in the case of delayed radiation only one or a few isomeric levels, lying somewhat higher, disintegrate. On this assumption the result is specially interesting if we pay attention to the possibility of the formation of fragment nuclei with large momenta.

The authors take this opportunity of thanking A. I. Egorov for making the target, V. F. Afanas'ev for making the semiconductor detector, and V. D. Yurchenko and É. B. Rodzevich for help in the measurements.

LITERATURE CITED

1. G. V. Val'skii, et. al., Atomnaya Énergiya, 18, 223 (1965).
2. Maienshain, et. al., In: "Proceedings of Second International Conference on the Peaceful Uses of Atomic Energy," Report of Non-Soviet Scientists, Atomizdat, T. 2. Moscow (1959), p. 297.
3. V. V. Sklyarevskii, D. E. Fomenko, and E. P. Stepanov, ZhÉTF, 32, 256 (1957).
4. V. K. Voitovetskii, B. A. Levin, and E. V. Marchenko, ZhÉTF, 32, 263 (1957).

All abbreviations of periodicals in the above bibliography are letter-by-letter transliterations of the abbreviations as given in the original Russian journal. *Some or all of this periodical literature may well be available in English translation.* A complete list of the cover-to-cover English translations appears at the back of this issue.

REACTOR BURN-UP CROSS-SECTION OF Pm^{149} AND POISONING BY SAMARIUM

(UDC 621.039.516.23)

I. A. Kondurov, L. M. Gracheva, A. I. Egorov,
D. M. Kaminker, A. M. Nikitin, and Yu. V. Petrov

Translated from Atomnaya Énergiya, Vol. 19, No. 2,
pp. 188-190, August, 1965
Original article submitted July 20, 1964

An important problem arising in the construction of reactors with large fluxes of thermal neutrons is that of "samarium pits". Sm^{149}, which has a large capture cross section for thermal neutrons (~75,000 barn [1]), is not formed directly by nuclear fission, but by the decay of Pm^{149} (τ = 77.5 h [2]). After the reactor is shut down the accumulated promethium begins to be converted to samarium, which may reach such quantities that it becomes impossible to start the reactor again. In contrast to the case of "xenon pits", it is no good waiting for the samarium pits to disappear, as Sm^{149} is stable. The degree of samarium poisoning depends on the promethium content when the reactor is shut down: this in turn depends on the burn-up cross section of Pm^{149}.

We measured this cross section by means of the amount of Pm^{150} formed from Pm^{149} when the latter is irradiated by thermal neutrons. The radioactive Pm^{149} was in turn obtained from Nd^{148} by the reaction

$$Nd^{148}(n, \gamma)Nd^{149} \xrightarrow[\beta]{1.84\ h} Pm^{149}.$$

The oxide of Nd^{148} was irradiated for three days in a flux of $5 \cdot 10^{13}$ neutrons/cm^2·sec. After leaving it to stand for 10 h, we separated the promethium fraction by ion exchange, using a column of diameter 1.2 × 20 cm with KU-2 resin. Elutriation was carried out at room temperature with 0.5% nitrilotriacetic acid at pH 3.2 and 0.3-0.5 ml/min. Preliminary studies showed that this acidity gives the best separation of promethium from both samarium and neodymium. Fig. 1 gives a curve illustrating the purification standard. The quantity of neodymium in the specimen was reduced to 10^{-3} of that in the original composition.

The Pm^{149} thus obtained was again irradiated by a flux of 10^{14} neutrons/cm^2·sec in the water space of the VVR-M reactor. The specimen was then again subjected to ion-exchange purification in a column of diameter 1.2 × 20 mm. The main radioactive contamination (Na^{24} and Mn^{56}) was removed by washing with 0.5 M nitric acid, after which the promethium was washed with a solution of nitrilotriacetic acid with pH 4. The radioactive residue was transferred to an aluminum foil which was placed in a scintillation gamma spectrometer with a 60 × 40 mm NaI(Tl) crystal. The measurements were carried out over three days. Fig. 2 shows the soft-gamma-ray spectrum thus obtained. It is seen that, as well as the activity peak at 285 keV due to Pm^{149} [2], the spectrum also contains peaks, at 340 and 410 keV, for which the intensity falls off more rapidly than that of Pm^{149}. Measurements of the half-life of these lines (2.7 h) enables us to identify the short-lived activity with Pm^{150} [3]. The 103 keV line belongs to Sm^{153}, the appearance of which in the promethium fraction is due to the method of choice of the sample for the first separation: for the second irradiation we used only the left side of the promethium peak, with minimum Nd^{149} contamination. The presence of Sm^{153} does not interfere with the measurements, as the gamma spectrum of this isotope does not contain lines with energy above 103 keV.

To determine the capture cross section of Pm^{149} for thermal neutrons, we must know the ratio of the Pm^{150} and Pm^{149} activities and the value of the neutron flux in which activation was carried out. To measure the flux in the Pm^{149} container, weighed control specimens of cobalt foil were placed in it. At the same time we measured the cadmium ratio of promethium, which was found to be above 15.

The neutron-capture cross section of Pm^{149} was calculated from the formula

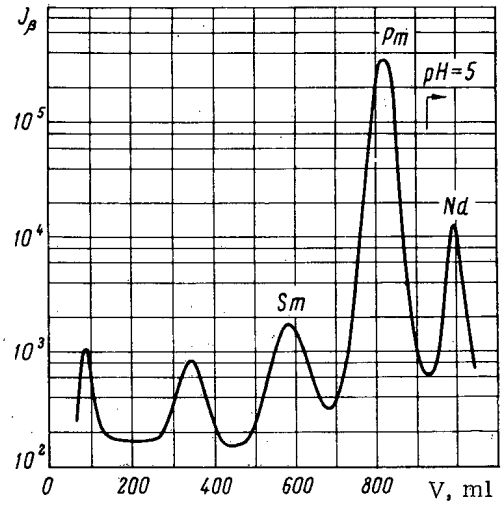

Fig. 1. Curve for separation of rare earths.

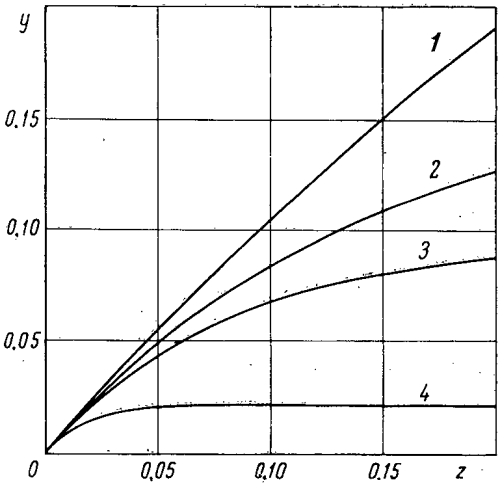

Fig. 3. y versus z (U^{235}) for various fluxes of thermal neutrons, Φ neutrons/cm²·sec: 1) 10^{16}; 2) 10^{15}; 3) $5\cdot10^{14}$; 4) 10^{14}.

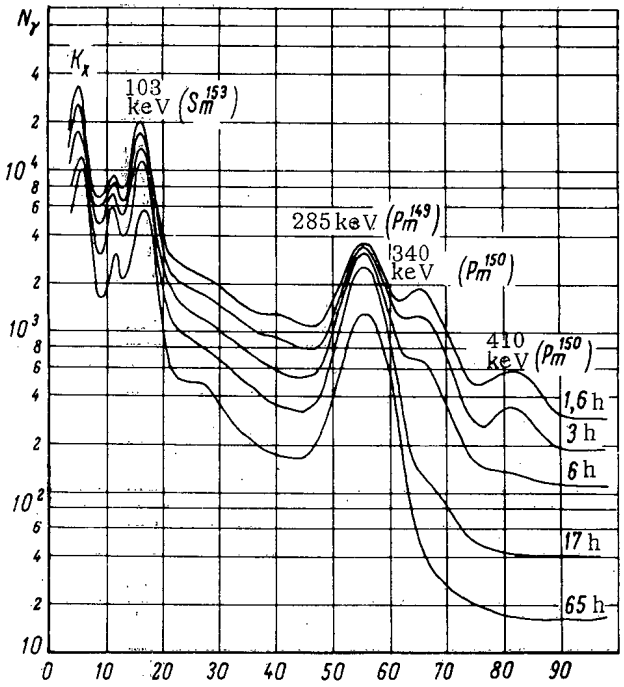

Fig. 2. Soft-gamma-ray spectrum of Pm^{149} irradiated in the water space of a VVR-M reactor. Figures on right-hand side are times after irradiation; N_γ count is in analyser channel.

$$\sigma_{Pm}=\sigma_{Co}\frac{A(\varepsilon,\ t)}{J_{Co}}\cdot\frac{J_{340}}{J_{285}}\cdot\frac{\alpha_{285}}{\alpha_{340}}, \qquad (1)$$

where σ_{Pm} and σ_{Co} are the cross sections for promethium and cobalt, J_{340}/J_{285} is the ratio of the intensities of gamma transitions with energies 340 keV (Pm^{150}) and 285 keV (Pm^{149}), α_{340} and α_{285} are the yields of gamma quanta for beta decay of Pm^{150} and Pm^{149}, J_{Co} is the activity of the cobalt control specimen, and $A(\varepsilon, t)$ is a coefficient governed by the experimental conditions.

The high cadmium ratio of Pm^{149} gives grounds to suppose that the cross section of Pm^{149}, like that of cobalt, obeys a $1/v$ law in the thermal-energy region. Consequently, if in (1) we substitute the tabular value $\sigma_{Co} = 37 \pm 1.5$ barn [4], measured for neutrons with $v = 2200$ m/sec, we get σ_{Pm} for neutrons of the same energy. The activities of the cobalt specimens were measured by comparing them with a standard Co^{60} source. The effect of cobalt activation by resonance neutrons was taken into account by calculating the activity due to hyper-cadmium neutrons.

The J_{340}/J_{285} ratio was measured from the 340 and 285 keV peaks with a correction for the ratio of the detector efficiencies for these quanta. As the gamma line energies were close together, this correction had a negligible error.

The greatest error in the measured cross section is introduced by the $\alpha_{285}/\alpha_{340}$ ratio; it is therefore convenient, after substituting the experimental values in (1), to write this ratio out separately:

$$\sigma_{Pm}=(39\pm5)\cdot10^3\frac{\alpha_{285}}{\alpha_{340}}\ \text{barn}. \qquad (2)$$

Measurements by several authors of the yield of γ quanta with energy 285 keV in the decay of Pm^{149} gave the following results: 1.5 ± 0.5% [2]; 8 ± 3% [5]; 1.6 ± 0.3% [6]; 2.6 ± 0.4% [7]. In view of the marked discrepancies between these results, we measured the intensity of the transition with energy 285 keV, by means of a 4π β-counter and a calibrated scintillation spectrometer. The value of α_{285} thus obtained was 3.2 ± 0.3%.

Reference [8] studies the beta decay of Pm^{150}: analysis of the results enables us to estimate the yield of gamma quanta with energies 340 keV ($\alpha_{340} = 71 \pm 4\%$). On substituting these values of α_{340} and α_{285} in (2), we get $\sigma_{Pm} = 1700 \pm 300$ barn (for neutrons with $v = 2200$ m/sec).

Knowing the burn-up cross section of promethium, we calculate the additional Sm^{149} poisoning arising after prolonged standstill of a reactor. It is

$$y \equiv \frac{\langle \sigma_a^{Sm} \Phi \rangle N_{Pm}}{\langle \sigma_a^F \Phi \rangle N_F}, \tag{3}$$

where N_{Pm} and N_F are the numbers of promethium and fuel nuclei per unit volume at the moment of shutdown. The capture cross sections of fuel and samarium, σ_a^F and σ_a^{Sm}, are the means over the energy spectrum of the reactor in a small volume. Since σ_a^{Pm} is not much greater than σ_a^F, we must always take account of the burn-up of fuel when we calculate the burn-up of promethium. The amount of fuel decreases exponentially with time constant $\langle \sigma_a^F \Phi \rangle^{-1}$. Using the results in [1], let us introduce the quantity z, characterizing the burn-up of fuel in a reactor working continuously for time T:

$$z \equiv \langle \sigma_a^F \Phi \rangle T. \tag{4}$$

Ignoring the transition time of Nd^{149} and Pm^{149}, we get, for poisoning of a reactor in which promethium was absent before shutdown, the following formula

$$y = C_0 \frac{\langle \sigma_f^F \Phi \rangle}{\langle \sigma_a^F \Phi \rangle} \frac{\langle \sigma_a^{Sm} \Phi \rangle}{\langle \sigma_a^F \Phi \rangle} z \frac{1 - e^{-u}}{u}, \tag{5}$$

where

$$u \equiv \left[\frac{\langle \sigma_a^{Pm} \Phi \rangle}{\langle \sigma_a^F \Phi \rangle} + \frac{1}{\langle \sigma_a^F \Phi \rangle \tau} - 1 \right] z.$$

Here C_0 is the proportional yield of promethium during fission, σ_f^F is the fission cross section of the fuel, τ is the decay constant of Pm^{149}.

For a reactor with U^{235} fuel, working with thermal neutrons, (neglecting the deviation of capture and fission cross sections from the $1/v$ law) by substituting numerical values ($\sigma_a^{Sm} = 74500$ barn, $\sigma_a^F = 694$ barn, $\sigma_f^F = 582$ barn, $C_0 = 1.3\%$ [4]) we can write (5) as

$$y = 1.2z \frac{1 - e^{-u}}{u}, \quad u = \left[1.4 + \frac{1}{\langle \sigma_F \Phi \rangle \tau} \right] z.$$

Fig. 3 plots samarium poisoning y against the fuel burn-up z for various fluxes Φ.

The value of y would have to be averaged over the whole volume of the reactor, for which it is necessary to know the distribution of Φ throughout the reactor; this, however, does not alter the qualitative character of the results. From Fig. 3 it follows that, for large enough Φ and z, the poisoning will be harmful, in the sense that it will be impossible to re-start the reactor because the margin of reactivity will be too small. Even with a brief shutdown, the reactor will fall into an iodine pit, and after emerging from it will be poisoned with samarium.

What has been said applies to a reactor working mainly with thermal neutrons. In the cases of reactors with fast and intermediate neutrons, a small multiplier $\beta \equiv \frac{\langle \sigma_a^F \Phi_{th} \rangle}{\langle \sigma_a^F \Phi \rangle}$; must be introduced into (5):

$$\frac{\langle \sigma_a^{Sm} \Phi \rangle}{\langle \sigma_a^F \Phi \rangle} \approx \beta \frac{\langle \sigma_a^{Sm} \Phi_{th} \rangle}{\langle \sigma_a^F \Phi_{th} \rangle},$$

where Φ_{th} is the flux of thermal neutrons only. In principle, for such reactors, when the proportion β of fission by thermal neutrons can be made small enough, samarium poisoning becomes negligible.

LITERATURE CITED

1. A. D. Galanin, Theory of Nuclear Reactors Using Thermal Neutrons [in Russian], Atomizdat, Moscow (1959).

2. L. Bunney, J. Abriam, and E. Scodden, J. Inorg. Chem., 12, 228 (1960).
3. V. Fisher, Phys. Rev., 96, 1549 (1954).
4. Handbook of Nuclear Physics [in Russian], Fizmatgiz, M. (1960).
5. L. Schmid and S. Burson, Phys. Rev. Letters, 5, 124 (1960).
6. C. Chapman, et. al., Proc. Roy. Soc., 259, 377 (1960).
7. A. Artna and M. Law, Canad. J. Phys., 38, 1577 (1960).
8. N. Gove and G. O'Kelley, Bull. Amer. Phys. Soc., 7, 352 (1962).

HEAT TRANSFER IN BOILING ALKALI METALS

(UDC 621.039.553.3)

V. M. Borishanskii, K. A. Zhokhov, A. A. Andreevskii,
M. A. Putilin, A. P. Kozyrev, and L. L. Shneiderman

Translated from Atomnaya Énergiya, Vol. 19, No. 2,
pp. 191-193, August, 1965
Original article submitted November 3, 1964

The published experimental data [1-5] on heat transfer in boiling alkali-metal heat-transfer agents do not as yet enable us to give recommendations on the calculation of heat exchange. It is thus of current interest to get new experimental data on heat transfer in boiling alkali metals.

Since 1956 the authors have been studying heat transfer in sodium and potassium boiling in large spaces. We have constructed a number of experimental assemblies, each comprising a boiler with working section and condenser, heating and cooling systems, a gas-vacuum system, and systems of control and measuring devices. The working section was a tube of steel 1Kh18N9T containing a heating element (a Silit or graphite rod). The external diameter of the working section was in the range 20-40 mm, and its length 160-200 mm.

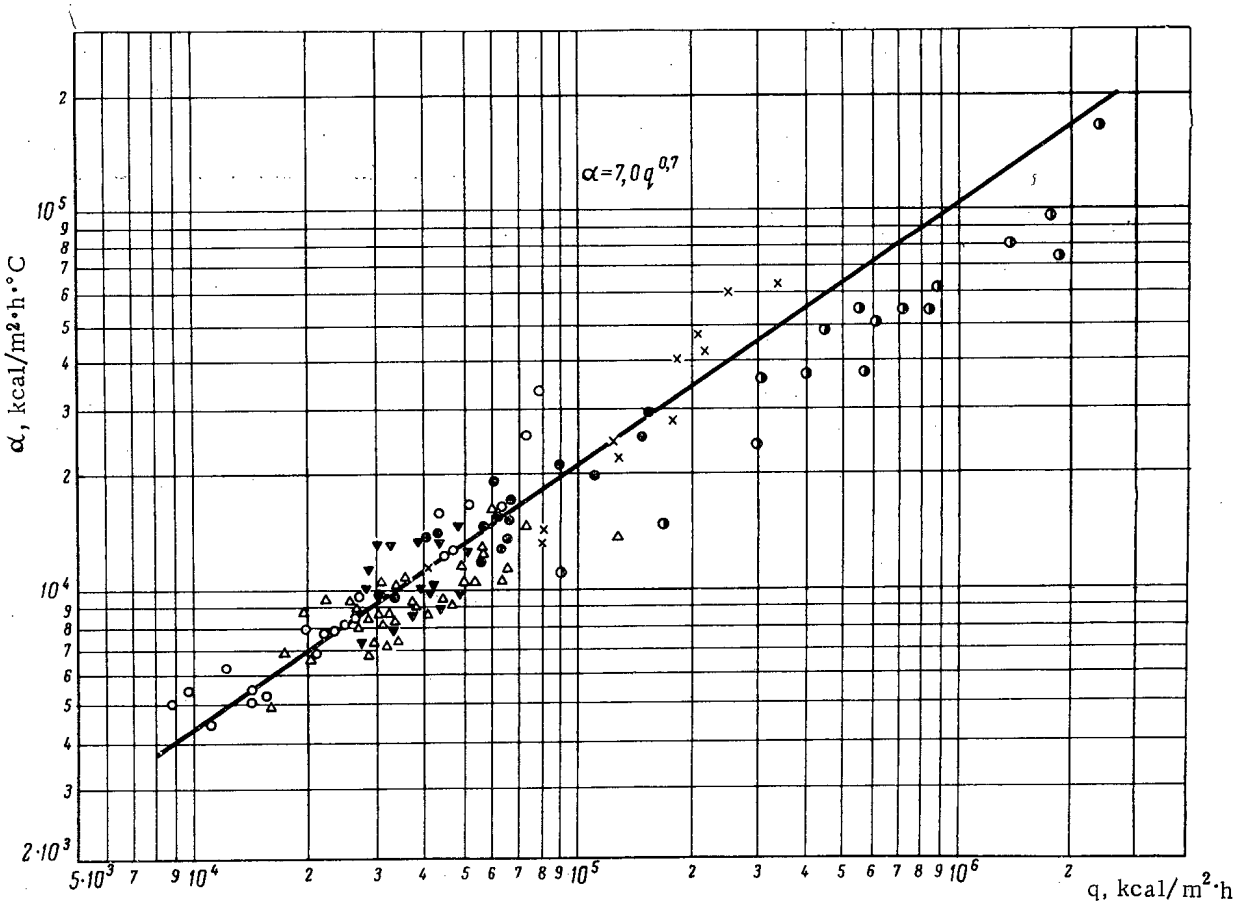

Fig. 1. Heat transfer in boiling sodium in large volumes and in annular gaps. △) Large volume, horizontal section (authors' data); ▼) large volume, vertical section (authors' data); o) vertical gap, δ = 4 mm (authors' data); ●) vertical gap, δ = 2 mm (authors' data); ×) large volume ([2]); ◑) large volume ([3]).

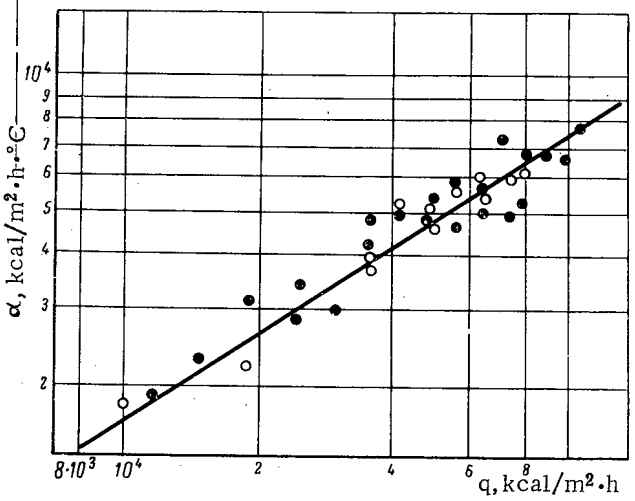

Fig. 2. Heat transfer for potassium boiling in large volume. ●) Side generatrices; o) top generatrix.

One of the assemblies was fitted with an external jacket so as to form a ring-shaped gap in the vertical working section.

The experiments on boiling sodium in large volumes were performed in a range of thermal loadings, (14-125)·10³ kcal/m²·h, approx. The saturation pressure and temperature were varied over the ranges 0.15-1.25 atm and 697-905°C.

Fig. 1 gives experimental results for nuclear boiling of sodium on horizontal and vertical heat-exchanging surfaces. There is good agreement between the experimental points for various positions in space of the working section. Thus the effect of the working section's position on heat transfer is within the scatter (± 30%) of the experimental data. This figure also plots experimental data on heat transfer when sodium is boiled in the upper part of a vertical ring gap, with clearance δ of 2 or 4 mm, in

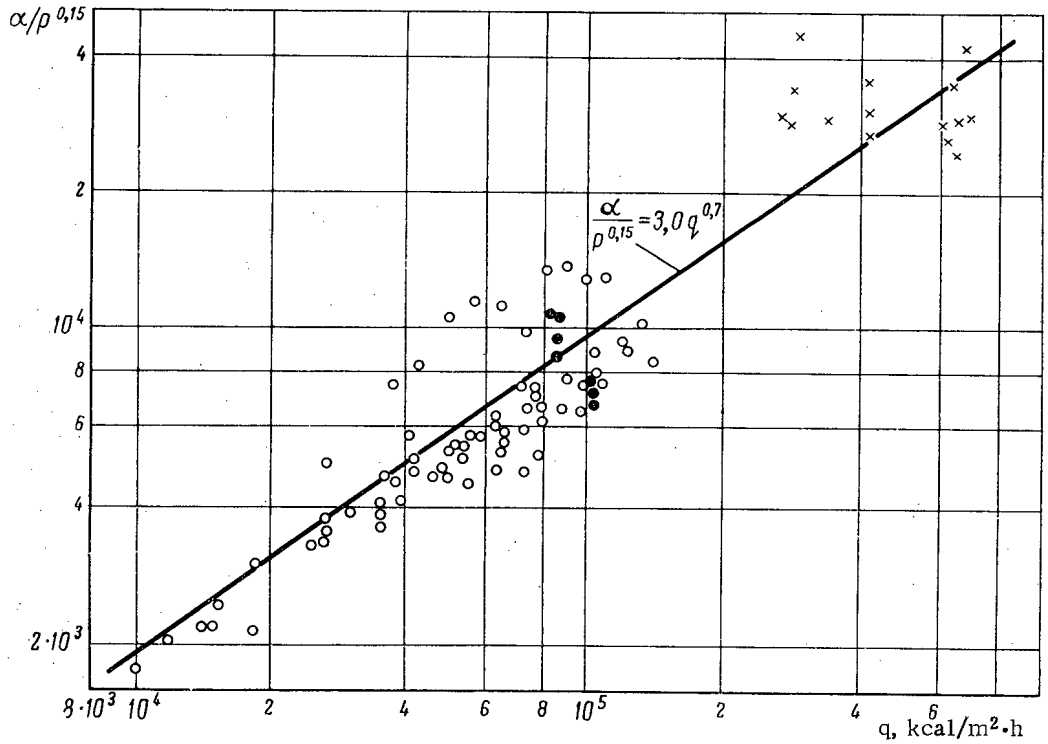

Fig. 3. Heat transfer for potassium boiling in large volume and in tubes. o) Large volume (authors' data); ●) tube of 22 mm diam. ([4]); ×) tube of 8.3 mm diam. ([4]).

natural convection conditions (p = 0.1-0.2 atm approx, q = 10,000-160,000 kcal/m²·h approx.). The graph shows that the graph of heat transfer versus thermal load in a ring gap with heating from one side only has the same general appearance as that for boiling in a large space. The absolute heat-transfer coefficients agree perfectly.

The effect of pressure on heat transfer was not studied in detail in the experiments with sodium, and most of the results on sodium boiled in a large volume were obtained with saturation pressures close to atmospheric. However, there does seem to be a tendency for the heat transfer to increase with rising pressure. Starting from the general laws derived from the theory of thermodynamic similarity, we can calculate the influence of the liquid's physical properties on heat transfer in a two-phase current [6]: it is found that the heat-transfer coefficient for boiling liquid metals is proportional to the pressure raised to the power n ≅ 0.1-0.2. Fig. 1 also plots data from [2, 3] on

heat transfer in boiling sodium in a large volume at pressures close to atmospheric. A single averaged line can be drawn for all the experimental points, and is represented by

$$\alpha = 7 \cdot q^{0.7}, \text{ kcal/m}^2 \cdot \text{h} \cdot ^\circ\text{C}. \quad (1)$$

Experiments on heat transfer in potassium boiling on vertical and horizontal tubular heat-exchange surfaces were performed at absolute pressures of 0.04, 0.4, 0.75 and 1.15 atm with thermal loads in the range 150,000-140,000 kcal/m^2·h.

Fig. 2 plots results on heat transfer with the working section horizontal. It is seen that the points obtained for the side and top generatrices agree with each other. A single averaged line can be drawn for all the experimental points, and corresponds to an exponent of about 0.7 for the specific thermal load.

Comparison of the experimental data for the same thermal loads at different saturation pressures showed that the heat-transfer coefficient increases to some extent with rising pressure. To a first approximation, we can draw an averaged line through the experimental points for different pressures; it corresponds to an equation with an exponent of n = 0.15 for the pressure—in agreement with the theory given in [6].

Fig. 3 gives the authors' data on heat transfer in potassium boiling in a large volume on vertical and horizontal heating surfaces, compared with data from [4] on potassium boiling in tubes. The experimental points all agree and can be described by a single equation,

$$\alpha = 3.0 p^{0.15} q^{0.7}, \text{ kcal/m}^2 \cdot \text{h} \cdot ^\circ\text{C}. \quad (2)$$

From what has been said we can draw the following conclusions.

1. For sodium and potassium boiling in a large volume in conditions of natural convection, the heat-transfer coefficient depends on the thermal load to the power 0.7. The absolute pressure is found to have a slight effect on heat transfer.

2. For nuclear boiling of potassium and sodium in a large volume, to calculate the heat transfer to a first approximation we can recommend the empirical equation

$$\alpha = A p^{0.15} q^{0.7}, \text{ kcal/m}^2 \cdot \text{h} \cdot ^\circ\text{C},$$

where for sodium A = 7.0, for potassium A = 3.0. The same formula can be used to calculate heat transfer for developed nuclear boiling of potassium and sodium in tubes and ring gaps, in the absence of effects from vapor content.

LITERATURE CITED

1. S. S. Kutateladze, V. M. Borishanskii, I. I. Novikov, and O. S. Fedynskii, Liquid Metal Heat Transfer Agents [in Russian], Atomizdat, Moscow (1958).
2. R. Lyon, et. al., Chem. Engng Progr. Symposium, 51, 41 (1955).
3. R. Noyes, Trans. ASME, Ser. C, 85, 59 (1963).
4. A. Fraaz, Atomnaya Tekhnika za Rubezhom, No. 6, 12 (1964).
5. M. I. Korneev, Teploénergetika, No. 4, 44 (1955); No. 7, 25 (1955).
6. V. M. Borishanskii and K. A. Zhokhov, Atomnaya Énergiya, 18, 294 (1965).

A METHOD FOR CALCULATING THE GAMMA-RADIATION EFFICIENCY OF IRRADIATION APPARATUS WITH PLANE RADIATORS

(UDC 539.106)

F. A. Makhlis and A. Kh. Breger

Translated from Atomnaya Énergiya, Vol. 19, No. 2,
pp. 193-196, August, 1965
Original article submitted July 28, 1964; revised February 1, 1965

As distinct from calculations of the efficiencies of radiation-chemical apparatus of various geometries [1, 2], or from methods of calculating the dose fields created by sources arranged in one plane [3-7], the present letter suggests a method for calculating the efficiency* of radiation apparatus with various ratios between the dimensions of the plane of irradiators and the irradiated object; this complements the data of [8]. We use the gamma method, which was used in [9] to solve the shielding-physics problem and in [10] for calculations on radiation-chemical apparatus. To get an additional estimate, we used the Monte Carlo method to calculate the distribution of absorbed energy from a point Co^{60} source in water. In addition, ferrous sulfate dosimetry was used to measure the absorbed dose rate within rectangular vessels filled with water, and also in aluminum and iron blocks. By comparing the results of these methods, it was found that the use of the gamma method to calculate the absorbed doses in materials made up of light elements gives errors below ±10% (allowing for 12-13% self-absorption in the sources [1]).

Let us consider a mono-energetic point source of gamma quanta, arranged so that its projection coincides with one of the vertices of a rectangular irradiated object (Fig. 1). In this case, the integral absorbed dose rate $W_{a.p}$ in the object will be given by

$$W_{a.p} = 47{,}2qiE_0\Phi, \text{ rad} \cdot \text{cm}^3/\text{sec}, \tag{1}$$

where

$$\Phi = \gamma \int_0^a \int_0^b \int_{h-d}^{h} \frac{e^{-\gamma \frac{d}{h} \sqrt{x^2+y^2+z^2}}}{x^2+y^2+z^2}\, dx\, dy\, dz;$$

E_0 = initial energy of gamma quanta, γ = coefficient of electronic conversion, q = source activity, i = number of gamma quanta per disintegration. In this case, efficiency = $\Phi/4\pi$. Values of $\Phi(a/h, b/h, \gamma d)$, calculated by numerical integration, are given in Table 1.

If the projection of the point at which the gamma-ray source is located does not coincide with a vertex of the rectangular object, it becomes necessary to use the additivity rule.

Let us consider a linear source, placed so that we can always find two points, whose projections coincide with two vertices of the rectangular irradiated object, on it or on its prolongation (cf. Fig. 1). Numerical integration of $W_{a.p}$ along the length l of the source, with uniform distribution of activity q along its length, led to the following expressions for the integral absorbed dose rate in the object, W_{al} and the efficiency:

$$W_{al} = W_{aA}K_1\left(\frac{a}{2h}, \frac{l}{a}\right) = 94{,}4qiE_0\Phi \times \left(\frac{a}{2h}, \frac{b}{h}, \gamma d\right) K_1\left(\frac{a}{2h}, \frac{l}{a}\right); \tag{2}$$

$$\text{Efficiency} = \frac{\left(\frac{a}{2h}, \frac{b}{h}, \gamma d\right) K_1\left(\frac{a}{2h}, \frac{l}{d}\right)}{2\pi}. \tag{3}$$

* The term "gamma-radiation efficiency of an irradiation apparatus" means the ratio of the quantity of energy absorbed by the irradiated object to the energy generated in the same time by the radiation source [11].

TABLE 1. Values of $\Phi(a/h, b/h, \gamma d)\cdot 10^3$, Required for Calculating Absorbed Energy and Efficiency of System of Point Sources and Rectangular Irradiated Object

b/h	a/h	γd 0,1	0,2	0,5	0,75	1,0	1,5	2,0	3,0
0.1	0,1	0,94	1,80	3,88	5,20	6,23	7,67	8,55	9,38
	0,2	1,86	3,57	7,70	10,2	12,3	15,2	17,0	18,6
	0,5	4,34	8,26	18,2	24,1	29,0	35,1	38,8	42,0
	1,0	7,30	14,0	29,3	39,5	46,6	57,0	63,0	66,5
	2,0	10,4	19,7	40,8	53,5	62,6	74,7	82,0	87,3
	5,0	12,5	23,0	47,0	61,0	70,0	83,0	91,0	96,0
	10,0	13,0	24,0	48,0	62,0	71,0	84,0	92,0	97,0
	20,0	14,0	25,0	49,0	63,0	72,0	85,0	93,0	98,0
0.2	0,2	3,70	7,07	15,2	20,2	24,3	30,0	33,6	36,5
	0,5	8,60	16,4	35,7	47,8	57,1	69,6	77,0	83,1
	1,0	14,6	27,8	59,2	78,2	92,4	112,0	124,0	131,0
	2,0	20,8	39,0	81,2	106,0	124,0	148,0	162,0	173,0
	5,0	25,0	46,0	94,0	121,0	140,0	165,0	180,0	190,0
	10,0	26,0	48,0	96,0	123,0	142,0	167,0	182,0	192,0
	20,0	27,0	49,0	97,0	124,0	143,0	168,0	183,0	193,0
0.5	0,5	20,8	39,6	84,0	112,0	133,0	162,0	179,0	193,0
	1,0	35,0	65,5	139,0	183,0	215,0	259,0	282,0	306,0
	2,0	49,0	92,0	191,0	250,0	292,0	348,0	378,0	402,0
	5,0	60,0	111,0	227,0	287,0	335,0	391,0	421,0	447,0
	10,0	63,0	116,0	232,0	292,0	340,0	396,0	426,0	452,0
	20,0	64,6	118,0	234,0	294,0	342,0	398,0	428,0	454,0
1.0	1,0	60,6	114,0	239,0	308,0	368,0	440,0	480,0	510,0
	2,0	89,0	164,0	334,0	431,0	501,0	585,0	627,0	668,0
	5,0	110,0	206,0	368,0	467,0	547,0	642,0	690,0	726,0
	10,0	116,0	212,0	374,0	473,0	553,0	648,0	696,0	732,0
	20,0	118,0	214,0	376,0	475,0	555,0	650,0	698,0	734,0
2.0	2,0	131,0	242,0	488,0	625,0	719,0	827,0	881,0	928,0
	5,0	170,0	300,0	588,0	725,0	828,0	948,0	1008	1059
	10,0	178,0	318,0	606,0	743,0	846,0	966,0	1026	1077
	20,0	184,0	325,0	613,0	750,0	853,0	973,0	1033	1084
5.0	5,0	242,0	430,0	790,0	965,0	1170	1190	1245	1295
	10,0	270,0	472,0	839,0	1011	1121	1248	1310	1362
	20,0	280,0	482,0	849,0	1021	1131	1258	1320	1372
10.0	10,0	310,0	526,0	911,0	1083	1193	1320	1382	1434
20.0	20,0	340,0	558,0	948,0	1121	1231	1358	1420	1472
	20,0	360,0	580,0	970,0	1143	1253	1380	1442	1494

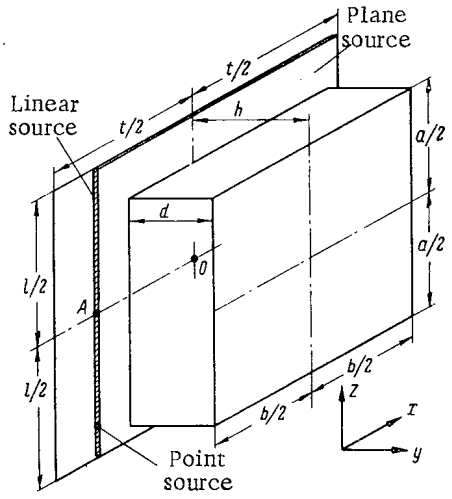

Fig. 1. Scheme of calculation.

TABLE 2. Values of K_1 and K_2

$\frac{l}{a}=\frac{t}{b}$	$\frac{a}{h}=\frac{b}{h}$ 0,5	1,0	2,0	5,0	10,0	20,0
0,5	0,990	0,990	0,990	0,990	0,990	0,990
1,0	0,945	0,919	0,902	0,892	0,887	0,885
1,2	0,920	0,882	0,850	0,824	0,812	0,806
1,5	0,880	0,818	0,775	0,734	0,715	0,700
2,0	0,780	0,690	0,610	0,540	0,505	0,490

Here W_{aA} = integral absorbed dose rate due to point radiation source, located at center of the linear source (point A) and possessing the same activity as the linear source. In the case of a plane radiation source, located (as shown in Fig. 1) symmetrically with respect to the irradiated object, and with uniform activity distribution over the irradiator plane,

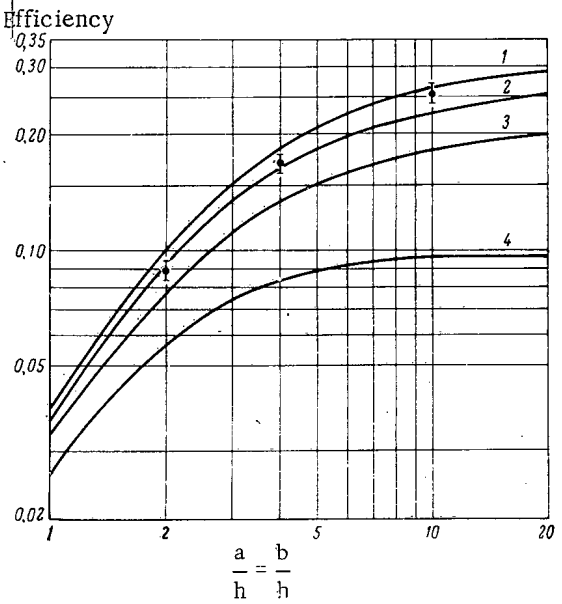

Fig. 2. Efficiency of irradiation apparatus with plane irradiator (for γd = 1), plotted versus a/h = b/h, l /a = t/b, equal to 1.0 (1), 1.2 (2), 1.5 (3), 2.0 (4). Points represent l − a = 20 cm.

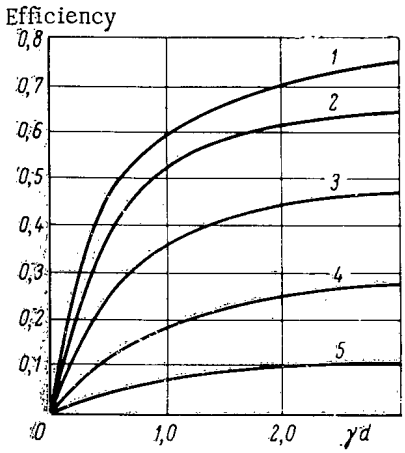

Fig. 3. Efficiency of irradiation apparatus, plotted versus thickness of irradiated object, for various values of a/h = b/h ((1) 40, (2) 10, (3) 4, (4) 2, (5) 1). Irradiated object located on both sides of irradiator (l/a = t/b = 1.0).

$$W_{apl} = W_{a0} K_1\left(\frac{a}{2h}, \frac{l}{a}\right) K_2\left(\frac{b}{2h}, \frac{t}{b}\right) = 189 q i E_0 \Phi\left(\frac{a}{2h}, \frac{b}{2h}, \gamma d\right) K_1 K_2; \quad (4)$$

$$(\text{Efficiency})_{pl} = \frac{\Phi\left(\frac{a}{2h}, \frac{b}{2h}, \gamma d\right) K_1\left(\frac{a}{2h}, \frac{l}{a}\right) K_2\left(\frac{b}{2h}, \frac{t}{b}\right)}{\pi}. \quad (5)$$

Here W_{a0} = integral absorbed dose rate in object, due to point source at center of plane (point 0) and having the same activity as the plane source. The values of K_1 and K_2 are given in Table 2.

In the irradiation of three-dimensional objects, the absorbed dose field must obey strict uniformity requirements [4-6]. It is thus necessary to use not the whole of the irradiator, but only that part in which the absorbed dose field has the required degree of uniformity [4, 6]. We then have l > a and t > b. From Fig. 2, which plots the efficiency versus a/h = b/h for various l/a = t/b, we can estimate the radiation losses for various relative dimensions of the irradiator and object. As an example, this figure plots the efficiency versus a/h = b/h for l − a = 20 cm (in which case l/a = t/b = var). It is seen that, other conditions being constant, there is a significant gain in efficiency by the use of large plane irradiators, i.e., by "smearing" out the activity q over a large surface (l/a = const., q = const.). This increases the size of the irradiated object and correspondingly decreases the mean absorbed dose rate. However, it is reasonable to increase the size of the irradiating plane only as long as the efficiency gain justifies the increased complexity of the equipment. There is also distinct decrease in efficiency with increase of l/a and t/b, i.e., with increased overlapping. From Fig. 3, which plots the efficiency versus the thickness of the irradiated object, it is seen that the efficiency increases with the object thickness more rapidly with large than with small irradiators.

It is interesting to consider the maximum attainable efficiency of an irradiation apparatus with plane irradiator. From Fig. 3 it is seen that, with b/h = a/h = 40 and d = 34 cm (l = a, t = b) the efficiency of such an irradiator is 62%, provided that the irradiated object is disposed on both sides of the source. The practical efficiency will be even lower, owing to self-absorption in the source. In practical conditions this value is difficult to reach. For example, to get the stated efficiency for an object of thickness 34 cm, we must have a = b = 16 m. Usually l > a and t > b, which leads to even lower efficiencies, other things being equal. However, we must note that the presence of a series of radiation conveyers moving round the plane can increase the efficiency of an irradiation apparatus.

LITERATURE CITED

1. A. Kh. Breger, et. al., Dokl. AN SSSR, 150, 866 (1963).
2. B. I. Vainshtein, Dokl. AN SSSR, 154, 411 (1964).
3. B. Manowitz, et. al., Large Radiation Sources in Industry, Vol. 1, IAEA, Vienna (1960), p. 120.
4. A. V. Bibergal', V. I. Sinitsyn, and N. I. Leshchinskii, Isotope Gamma Equipment [in Russian], Atomizdat, Moscow (1960).
5. I. Hubbel, Nucleonics, 21, No. 3, 144 (1963).
6. A. V. Bibergal', M. M. Korotkov, and T. G. Ratner, Atomnaya Énergiya, 7, 244 (1959).
7. F. A. Makhlis, Atomnaya Énergiya, 15, 508 (1963).
8. F. A. Makhlis, Atomnaya Énergiya, 17, 147 (1964).
9. N. G. Gusev, E. E. Kovalev, and V. I. Popov, In: "Proceedings of Second International Conference on the Peaceful Uses of Atomic Energy," Reports of Soviet Scientists, T. 6. M., Atomizdat (1959), p. 211.
10. N. P. Syrkus, Dissertation, FKhI im. L. Ya. Karpov, Moscow (1964).
11. A. Kh. Breger, Dissertation, Institut Élektrokhimii AN SSSR, Moscow (1961).

All abbreviations of periodicals in the above bibliography are letter-by-letter transliterations of the abbreviations as given in the original Russian journal. ***Some or all of this periodical literature may well be available in English translation.*** **A complete list of the cover-to-cover English translations appears at the back of this issue.**

ABSORPTION OF GAMMA RADIATION FROM A POINT SOURCE BY A MACROSYSTEM

(UDC 539.106)

B. M. Terent'ev, V. A. Él'tekov, and A. Kh. Breger

Translated from Atomnaya Énergiya, Vol. 19, No. 2,
pp. 196-199, August, 1965
Original article submitted August 20, 1964; revised February 1, 1965

An important characteristic of the RKhA radiation-chemical apparatus [1, 2] is its gamma-radiation efficiency, i.e., the ratio η of the gamma dose rate absorbed in the reaction space of the apparatus to the gamma dose rate emitted by the radiation source.

The value of η was calculated for two models of the RKhA by means of the volume-integration method and the Monte-Carlo method. The first model is a system comprising a sphere of radius R, filled with the irradiated (water-equivalent) substance; at the center of the sphere is a point source (Co^{60} or Cs^{137}).

Fig. 1a gives the values of η calculated for the first model by various methods [3], including those mentioned above. In particular, it shows the efficiencies, calculated from data in [4], for spheres of various radii in a vacuum. There is less than 1-2% discrepancy between these results and those which we calculated by the Monte Carlo method for a sphere surrounded by a medium: this shows that the contribution made by the medium surrounding the sphere is negligible in this case.

In general, the results for η_R obtained by various methods (cf. Fig. 1a) display satisfactory agreement; but volume integration for the sphere is quite reliable and economic of effort. These data (curves 1, 2, 3, Fig. 1a) will

Efficiencies of Macrosystem Comprising Cylinder and Point Source, Calculated by Various Methods (E_0 = Mean Energy of Primary Gamma Quanta)

Cylinder dimensions, cm		E_0 = 1,25 MeV					Cylinder dimensions, cm		E_0 = 0,62 MeV				
R	h	η_1	η_2	η_3	η_2^*	η_1^*	R	h	η_1	η_2	η_3	η_2^*	η_1^*
5	5	0,30	0,16	0,15	0,16±0,01	0,29±0,02	5	2,5	0,30	0,14	0,13	0,06±0,01	0,15±0,01
	25	0,37	0,21	0,19	0,20±0,01	0,36±0,02							
10	5	0,41	0,25	0,22	0,25±0,02	0,42±0,02	10	5	0,48	0,29	0,24	0,23±0,02	0,53±0,02
	20	0,56	0,37	0,32	0,37±0,02	0,56±0,02							
15	7,5	0,55	0,35	0,32	0,36±0,02	0,60±0,02	20	20	0,85	0,65	0,51	0,62±0,02	0,85±0,01
20	20	0,76	0,55	0,48	0,54±0,02	0,78±0,01	60	100	1	0,98	0,85	0,99±0,005	1±0,005
	30	0,79	0,58	0,48	0,54±0,02	0,79±0,01							
30	75	0,90	0,77	0,68	0,74±0,01	0,90±0,01	20*	20	0,88	0,70	0,55	0,44±0,02	0,88±0,01
40	60	0,95	0,85	0,76	0,83±0,01	0,96±0,01							
50	50	0,97	0,89	0,84	0,85±0,001	0,98±0,005	60*	100	1	0,98	0,85	0,81±0,01	1±0,005
60	100	0,99	0,95	0,89	0,90±0,01	1±0,005							

*Data for these dimensions correspond to a point located at center of lower face.

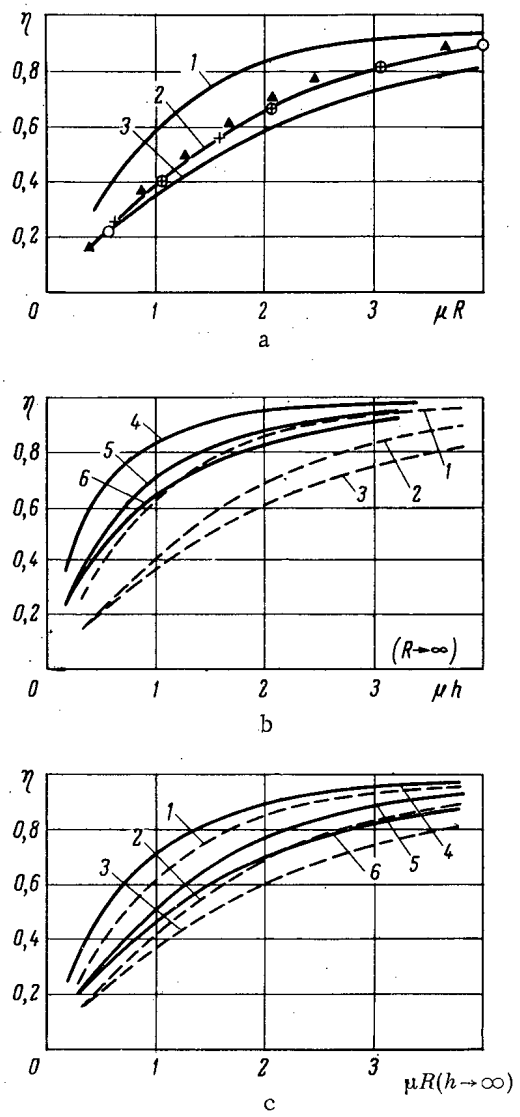

Fig. 1. η for water-equivalent macrosystems of spherical and cylindrical geometries, plotted versus their dimensions (in relaxation lengths). a) Point Co^{60} source at center of sphere: 1, 2, 3) results of calculation ignoring scattering, allowing for scattering by means of the accumulation factor, and based on the gamma method, respectively [3, 5] (+ indicates values calculated by the present authors by the Monte Carlo method for a water-equivalent sphere surrounded by the same substance; ▲ indicates data calculated from results of [6]; o indicates values based on data from [4] for sphere in vacuum). b) Point source at center of cylinder's axis: 1, 2, 3) same as for Fig. 1a; 4, 5, 6) results of calculations ignoring scattering, allowing for scattering by the gamma method, and allowing for scattering by means of (3), respectively. c) The same as in Fig. ib, but curves 4, 5, 6 calculated from (2).

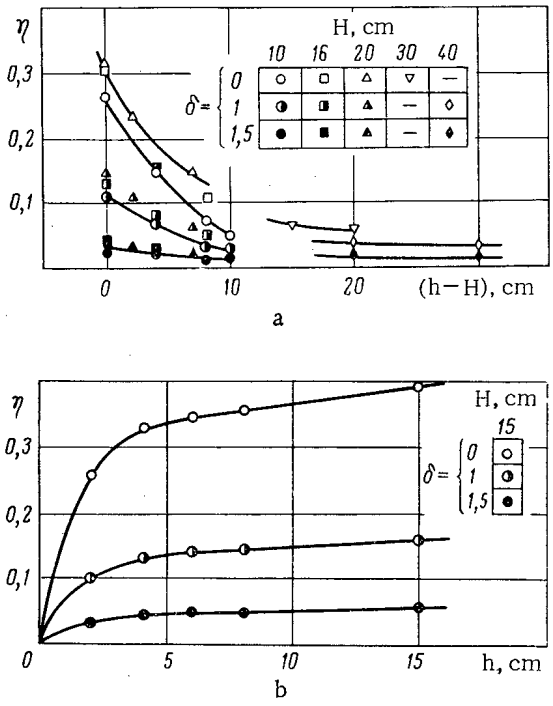

Fig. 2. η', plotted versus dimensions of water-equivalent cylinder and positions of Co^{60} source inside and outside the cylinder: a) R = 10 cm; b) R = 15 cm.

be used below as auxiliary material, to simplify the numerical analysis of the efficiency of an RKhA model with different geometry.

As the second model of the RKhA, consider a macrosystem of cylindrical configuration with a point gamma-ray source. Using the Monte Carlo method, we calculated the gamma-radiation efficiency of a finite water-equivalent circular cylinder (5-60 cm in radius and 5-200 cm long) for various positions of the source. It was assumed that the point source emitted quanta uniformly in all directions making angles of less than 90° with the axis of the cylinder (oriented from the lower to the upper face). Let us denote the η of such a source by η'. Fig. 2 gives some of the results which we obtained,* in the form of graphs of η' versus h, h − H and δ, where H = length of cylinder, h = distance between source and upper face, and δ = ratio of distance between source and cylinder axis to radius R of cylinder. In calculating each of the variants, we used the same set of 450 random gamma-quantum trajectories.

By means of the following scheme, we can calculate the efficiency of the second RKhA model from the results for the first. Assume for simplicity that the point source is at the middle of the axis of the circular cylinder, i.e., h = H/2 (putting the source at other positions on the axis introduces no new principle). This case is one of the particular source positions studied

* The remaining results, for various cylinder sizes with Co^{60} or Cs^{137} sources, are similar to those given in Fig. 2.

by the Monte-Carlo method (cf. Fig. 2). If we put x = cos θ (where θ is the angle between the cylinder axis and the distance r to the element of integration), then on integrating w.r.t. r, we get the following final expression for the efficiency of the system:

$$\eta_{cyl} = \int_0^1 dx \eta_R [\mu y(x)], \tag{1}$$

where $\eta_R[\mu y(x)]$ is formally identical with the expression found in [3] for this function for the case of the spherical RKhA model, differing only in the argument y(x), which here takes the form

$$y(x) = \begin{cases} h/x, & 0 \leqslant \arccos x \leqslant \operatorname{arctg} R/h; \\ R/\sqrt{1-x^2}, & \operatorname{arctg} \frac{R}{h} < \arccos \leqslant \pi/2. \end{cases}$$

By this means we can calculate the integral in (1) quite simply and accurately, using numerical methods such as Simpson's Rule, together with the graph of η_R versus μR already constructed for the sphere (see curve 2, Fig. 1a), and remembering that μR is replaced by $\mu y(x)$.

In addition, we can get from (1) asymptotic formulae of the forms

$$\eta_{cyl} = \int_0^1 \eta_R(\mu_R/\sqrt{1-x^2})\, dx \text{ for } h \to \infty, \tag{2}$$
$$0 \leqslant \arccos \leqslant \pi/2;$$

$$\eta_{cyl} = \int_0^1 dx \eta_R(\mu h/x) \quad \text{for} \quad R \to \infty, \tag{3}$$
$$0 \leqslant \arccos x \leqslant \pi/2,$$

where the values of η_R in (2) and (3) are taken, for given values of the arguments, from curve 2, Fig. 1a.

If, in calculations by (1), (2) and (3), we calculate the integrand from curves 1 and 3 of Fig. 1a, we can then use numerical integration to find η_{cyl} both for the primary radiation and by the gamma method [5] (see table and corresponding curves in Fig. 1b, Fig. 1c).

In the table, η_1 and η_2 are the gamma-radiation efficiencies of a water-equivalent cylinder, calculated from (1) without and with allowance for multiple scattering, respectively; η_3 is the efficiency calculated by the gamma method; η_1^*, η_2^* are the efficiencies calculated by the authors by the Monte Carlo method with a "Strela 3" computer for a cylinder in vacuum, without and with allowance for multiple scattering, respectively. In all these calculations, it was assumed that the point source lies on the axis in the central plane of the cylinder.

On comparing the results for η_{cyl} calculated from (2) and (3) with the data on η_R for the sphere, we find as expected that the values of η_{cyl} are higher than those of η_R (see Fig. 1b, Fig. 1c). In addition, on comparing the various curves for η_{cyl} is Fig. 1b, Fig. 1c, we see that the asymptotic values of the efficiency for cylinders with $R \to \infty$ are higher than the asymptotic values with $h \to \infty$. This is natural, because the first asymptotic is analogous to an absorbing layer.

The table also gives efficiencies for finite cyliners, calculated either by (1) or by the Monte Carlo method. Comparison shows that these data agree satisfactorily for all the given system dimensions when the primary gamma quantum energy is E_0 = 1.25 MeV. A further comparison between the tabulated values of η_2^* and η_1^* and the corresponding values of η_{cyl} (obtained from curves 5 and 4 of Fig. 1c) shows that the dimensions chosen for some of the cylinders are close to the limiting values, because their efficiencies, as calculated by either method, are close to the asymptotic values. This applies, in particular, to cylinders with the following values of R and h: 5 and 25; 20 and 30; 30 and 75 cm; and so forth. Similar results can be obtained for the series of cylinders with $R \to \infty$, if we carry out the calculations for a series of finite cylinders with h = const and R variable.

The table also gives values of η for finite cylinders with E_0 = 0.62 MeV, calculated by the above methods. For the cylinder with R = 5, h = 2.5, there was a certain discrepancy between η_2^* and η_2 and between η_1^* and η_1.

the results of volume integration being somewhat high. It is also seen that the results of the different methods diverge somewhat for the case when a point source with E_0 = 0.62 MeV is placed at the center of the lower face; this is apparently due to the boundary effect, which is greater for this energy than for E_0 = 1.25 MeV.

We have thus derived for the first time, for a macrosystem with cylindrical geometry (RKhA model), a formula (1) and asymptotic formulae (2) and (3) which can be used in practical calculations.

In conclusion, we note that the validity of these formulae has been demonstrated by our calculations of the efficiencies of a series of cylinders with fixed R and h in very diverse combinations: the calculations were made by the Monte Carlo method with a Strela-3 computer.

LITERATURE CITED

1. A. Kh. Breger, et. al., Dokl. AN SSSR, 131, 1308 (1960).
2. A. Kh. Breger, et. al., Ibid., 150, 866 (1963); B. M. Terent'ev, V. A. Él'tekov, and D. I. Golenko, Atomnaya Énergiya, 382 (1963).
3. B. M. Terent'ev, Dissertation, Moscow (1965).
4. M. Berger and L. Spencer, Rad. Research, 10, 552 (1959).
5. N. G. Gusev, et. al., In: "Proceedings of Second International Conference on the Peaceful Uses of Atomic Energy," Reports of Soviet Scientists, T. 6. M., Atomizdat (1959), p. 211.
6. B. L. Vainshtein, Dokl. AN SSSR, 154, 411 (1964).

GAMMA EMISSION SPECTRUM OF AN ARTIFICIAL MODEL OF RADIOACTIVE FALLOUT

(UDC 551.577.7)

Yu. A. Izraél', A. F. Nekozyrev, P. V. Nikolaev, and E. D. Stukin

Translated from Atomnaya Énergiya, Vol. 19, No. 2, pp. 199-200, August, 1965
Original article submitted October 20, 1964

To improve the accuracy of calculations on the gamma-ray spectrum of a plane source on the Earth's surface [1] and to facilitate the interpretation of aerial gamma-spectrum measurements, we have studied an artificial model of radioactive ground contamination. Below we describe the results of the first stage of this work—the measurement of gamma-ray spectra above a surface contaminated with Co^{60}. No account was taken of the non-uniformity of the ground.

To stimulate the gamma-ray field of radioactive fallout, we used 100 Co^{60} sources, each of activity 96 mg-equiv Ra. To minimize the effects of microrelief, each source was placed 10-15 cm above the ground on a wooden stand, at the center of a 40 × 40 m square. As a whole, the sources occupied a circular area of diameter 500 m. The surface density was thus about $3.8 \cdot 10^{-2}$ mcurie/m^2 [$3.5 \cdot 10^2$ MeV/(cm^2·sec)]. At 1 m above the ground, the gamma-radiation dose rate was of order 1.75 milliroentgen/h; at 200 m above the ground it was about 0.12 mr/h [2]. Above 100 m the finite size of the model began to have effect. The field ion-uniformity was 15-20% at a height of 20 m and less than 5% at a height of 40 m (in a central circle of radius 70-80 m).

The gamma-ray spectrum was measured by a helicopter flying at 50-60 km/h at a height of 20-200 m above the central circle. The measurement time was 30 sec for three flights; this ensured adequate statistical accuracy (better than 5%).

The transducer of the gamma spectrometer (which was based on an AI-100 analyser) was an NaI(Tl) crystal of size 100 × 100 mm, plus an FÉU-49 photomultiplier. The resolution of the spectrometer at its photopeak for the registration of gamma quanta from Cs^{137} (0.66 MeV) was 12.5%.

The instrumental spectra measured at various heights (Fig. 1) clearly show the two Co^{60} lines (1.17 and 1.33 MeV) and a marked contribution from scattered radiation. The scattered-radiation peak varies slightly with height, and occurs at about 70 keV. These results agree with similar measurements in [3]. In [3], which also simulated contamination with Co^{60} sources, the gamma-ray intensity at corresponding heights was about ten times less, while the crystal size was the same as ours. The statistical accuracy of the Nevada measurements was therefore rather lower.

To process the instrumental spectra, we used the matrix from [4] (up to E = 1.44 MeV), derived for an NaI(Tl) crystal of practically the same size as ours. In this matrix the coordinates used were $E^{1/2}$. If there was a discrepancy in the crystals' properties, this processing means that the efficiencies of both detectors would vary by the same factors throughout the energy range investigated.

In Fig. 2, the continuous lines are gamma-ray spectra taken at altitudes of 50 (curve 1) and 200 (curve 2) meters, derived by multiplying the instrumental spectra of Fig. 1 by the reciprocal matrix [4]. The dashed lines represent the gamma-ray spectra for a plane isotropic Co^{60} source, obtained by interpolating the sum of the spectra calculated in [5]. The experimental and theoretical curves are arbitrarily normalized to gamma-quantum energies in the range 1.0-1.21 MeV.* The shapes of the experimental and theoretical curves are seen to be in good agreement. There is some discrepancy at low energies, the experimental curves being lower: this can be explained by partial absorption of the soft radiation in the helicopter fuselage and instrument.

* The numbers on the vertical axis refer to the theoretical spectra.

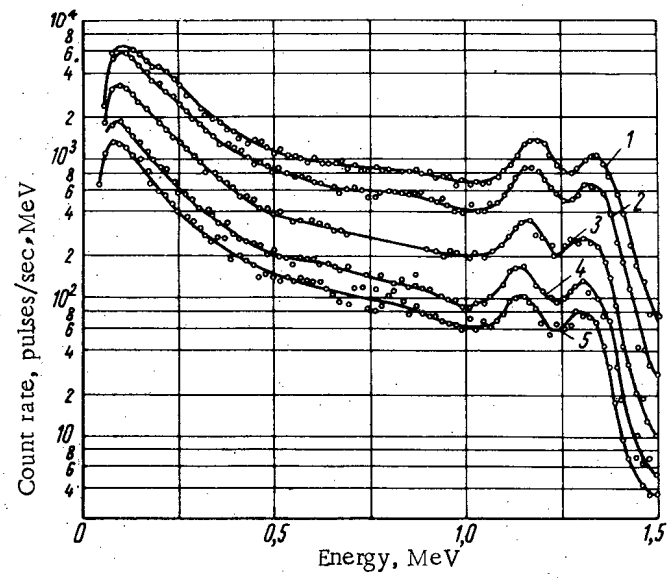

Fig. 1. Instrumental gamma-ray spectra above area simulating ground contamination by Co^{60}, at various heights in meters: 1) 20; 2) 50; 3) 110; 4) 150; 5) 200.

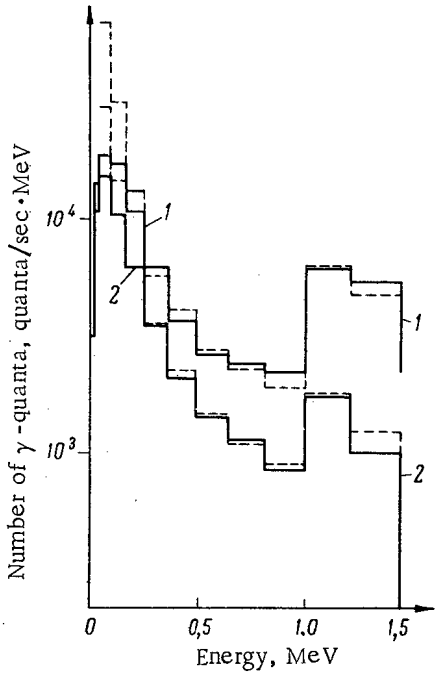

Fig. 2. Experimental (continuous) and theoretical (dashed) gamma-ray spectra above plane of isotropic sources, 50 m (1) or 200 m (2) above the Earth's surface.

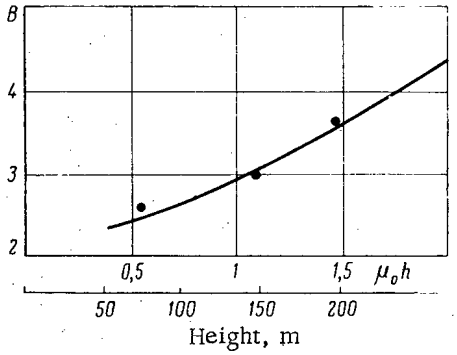

Fig. 3. Comparison of experimental and theoretical values of the dose accumulation factor for gamma radiation in air.

The solid curve in Fig. 3 represents the dose accumulation factor $B(\mu_0 h)$, allowing for multiple scattering above the plane of isotropic sources. This curve was obtained by interpolating the values of $B_g(h)$, for E_γ = 1.25 MeV, given in [1]. The dots on this graph represent values of $B(\mu_0 h)$ calculated from the experimental spectra by means of the formula [6]:

$$B(\mu_0 h) = \frac{\int_0^{E_{max}} \sigma_a(E)\, f(E, \mu_0 h)\, dE}{\int_0^{E_{max}} \sigma_a(E)\, f_0(E, \mu_0 h)\, dE}.$$

Here $\sigma_a(E)$ is the linear absorption coefficient for gamma radiation in air; $f(E, \mu_0 h)$ is the total energy flux with gamma-quantum energy E; and $f_0(E, \mu_0 h)$ is the non-scattered part of this flux at the observation point. The figure shows good agreement between the experimental and theoretical results.

LITERATURE CITED

1. O. I. Leipunskii, et. al., Propagation of Gamma Quanta in Matter [in Russian], Fizmatgiz, Moscow (1960).
2. Yu. A. Izraél', Izv. AN SSSR, Ser. Geofiz., No. 7, 1103 (1964).
3. F. J. Davis and P. Reinhardt, Health Phys., 8, 233 (1962).
4. J. Hubbell, Rev. Scient. Instrum., 29, 65 (1958).
5. R. M. Kogan and Sh. D. Fridman, Izv. AN SSSR. Ser. Geofiz., No. 4, 530 (1960).
6. Shielding of Nuclear Reactors, edited by T. Rockwell [Russian Translation], Izd-vo Inostr. Lit., Moscow (1958).

MATHEMATICAL ANALYSIS OF AIR RENEWAL IN PREMISES CONTAINING POWERFUL GAMMA-RAY EQUIPMENT

(UDC 697.92 : 539.122)

N. V. Sobol', A. A. Petushkov, and A. Kh. Breger

Translated from Atomnaya Énergiya, Vol. 19, No. 2,
p. 201, August, 1965
Original article submitted November 24, 1964; revised December 18, 1964

From experimental data on radiochemical yields and current values of the maximum permissible concentration (MPC) of toxic oxides of nitrogen and of ozone, the authors of [1] derived expressions for L, the air flow rate, and K, the number of air renewals, required in premises containing powerful gamma-ray sources, for any given values of the source activity A and the volume V of the room. However, these expressions sometimes give excessively large values for L and K, thus leading to unnecessarily high air flow rates and waste of power.

In these cases it is necessary to make use of a "forbidden time" t, measured from the moment when the source is returned to the store. During this period, access to the room is prevented, and K_a, the actual number of air renewals in the room, is less than K.

From the toxicities of the oxides of nitrogen and of ozone, t can be determined (in h) from the relation

$$t=\frac{\ln\frac{K}{K_a}}{K_a}. \tag{1}$$

If harmful substances are released from the irradiated objects in the room, and, just before the source is returned to the store, their concentration q_i is greater than the MPC, q_{0i}, we finally get

$$t=\frac{\ln\left(\frac{K}{K_a}+\sum_{i=1}^{n}4\frac{q_i}{q_{0i}}\right)}{K_a}. \tag{2}$$

This expression is valid provided that the concentration of oxides of nitrogen in the air depends linearly on the absorbed dose. From the results of [2] it follows that this condition is fulfilled for the activities of all existing and presently practicable gamma-ray sources.

When mixed or water shielding is used, hydrogen is evolved from the water into the atmosphere, and it is possible that explosive mixtures may be formed. The radiochemical yield G_{H_2} of hydrogen from water is independent of the pH and is equal to 0.42-0.45 molecules per 100 eV [3, 4]. As in the cases of other explosive substances, the maximum permissible concentration of hydrogen is one half of the lower limit for explosion hazard, i.e., $q_{OH_2} = 1.7\cdot10^3$ mg/m^3 [5, 6]. If we assume that all the gamma-ray energy from the source is absorbed in the water, and that all the hydrogen formed escapes into the air of the room, then, for $G_{H_2} = 0.45$, the rate of hydrogen formation in the air is

$$q_{H_2}=3.54\cdot10^{-3}\ \text{mg/m}^3\cdot\text{h}. \tag{3}$$

For practical values of A and V, the number of air renewals required for safety can be achieved merely by infiltration [5, 7]. As premises containing powerful gamma sources are usually ventilated, it is quite impossible for explosive mixtures to be formed, and this factor can be ignored as far as safety is concerned.

LITERATURE CITED

1. N. V. Sobol', A. A. Petushkov, and A. Kh. Breger, Atomnaya Énergiya, 16, 262 (1964).

2. M. T. Dmitriev and S. Ya. Pshezhetskii, In Symposium: "The Action of Ionizing Radiation on Inorganic and Organic Systems," [in Russian], edited by S. Ya. Pshezhetskii, Izd-vo AN SSSR, Moscow (1958), p. 171.
3. A. O. Allen, Radiation Chemistry of Water and Aqueous Solutions [Russian Translation], Atomizdat, Moscow (1963), pp. 38, 39, 49.
4. I. V. Vereshchinskii and A. K. Pikaev, Introduction to Radiation Chemistry [in Russian], Izd-vo AN SSSR, Moscow (1963), pp. 81, 99, 117.
5. G. A. Maksimov, Heating and Ventilation [in Russian], Part II, Stroiizdat, Moscow (1955), pp. 36, 40, 199, 276, 339.
6. Constructional Standards SN and P II–M. 2-62, Stroiizdat, Moscow (1964), p. 11.
7. Handbook on Heating, Ventilation, and Air Conditioning [in Russian], edited by I. G. Staroverov, Stroiizdat, Moscow (1963), p. 50.

All abbreviations of periodicals in the above bibliography are letter-by-letter transliterations of the abbreviations as given in the original Russian journal. ***Some or all of this periodical literature may well be available in English translation.*** **A complete list of the cover-to-cover English translations appears at the back of this issue.**

USE OF POLYETHYLENE TUBE AS SAMPLING LINE FOR DOSIMETRIC AIR MONITORING

(UDC 539.16.07)

E. A. Konovalov, L. M. Ploshchanskii, and V. A. Solov'ev

Translated from Atomnaya Énergiya, Vol. 19, No. 2,
pp. 201-203, August, 1965
Original article submitted September 5, 1964; revised November 14, 1964

In centralized dosimetric air monitoring, the sampling lines are usually stainless steel or aluminum tubes. These are very expensive and difficult to assemble and have a large number of sleeve joints. Furthermore, even aluminum tubes have inadequate corrosion resistance and in some premises are generally unsuitable. Lines made of welded steel tubes, as well as being difficult to assemble, have already, after a few years' use, become almost completely unserviceable, owing to accumulation of corrosion products at the bends and welds.

Rolled polyethylene tubes are free from all these deficiencies. To test the possibility of using them, instead of metal tubes, as sampling lines for dosimetric air monitoring in reactor buildings, laboratories, etc., we made thermo-mechanical tests of 20-mm diameter polyethylene tubes with 4 mm walls, manufactured by extrusion. The tests were performed with the tubes strained by being bent to 100 mm radius. The tubes were heated externally by water. As the thermal conductivity of polyethylene is relatively low (0.001 cal/sec·cm·°C), the tubes were held at each temperature for 30 min without removing the mechanical load (vacuum or pressure). The tests were made at 20-95°C and under pressures from 5 kg/cm^2 down to atmospheric and vacuums down to 700 mm Hg.

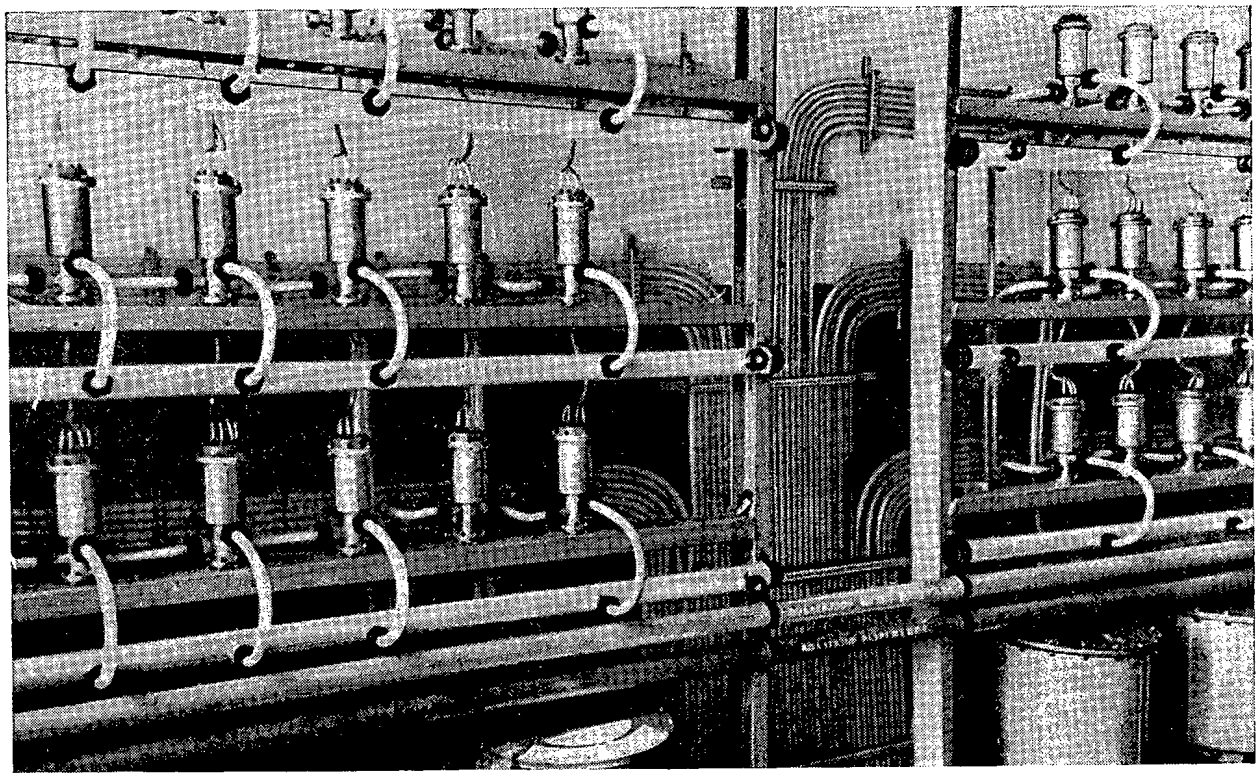

General view of polyethylene tubes mounted in valve rack for dosimetric monitoring of air.

We tested deformation of the tubes' cross sections by measuring the diameters along their entire lengths in two mutually perpendicular planes: this was taken as a criterion of thermomechanical strength.

Up to 60°C, the tube does not deform at pressures up to 5 kg/cm^2. At 80°C and 3 kg/cm^2, the onset of deformation was observed. When the tubes were kept in these conditions for 30 min, the diameter altered by 0.2-0.3 mm. At 60°C, the tube does not deform under vacuum down to 700 mm Hg. The onset of deformation was observed at 80°C and 700 mm Hg: after 30 min in these conditions, the change of diameter was 0.5-0.4 mm.

In addition to these brief tests, more prolonged tests were carried out (for 8 h) at 60°C and 600 mm Hg or 3 kg/cm^2. The tubes were stressed in this case also.

The tests showed that a polyethylene tube can be used at temperatures up to 60°C, vacuums down to 600 mm Hg, and pressures up to 3 kg/cm^2.

The method of installation and working time required for fixing polyethylene tubes are practically the same as for electrical cables. Packages of tubes can be laid in cable ducts or along the walls of a building. The annexed photograph shows a general view of polyethylene tubes mounted in a valve rack of a dosimetric air monitoring system.

The flanges on the tubes for joining them to the equipment (valves, collectors, filter holders, etc.) were made by shaping a previously heated end of the tube in a simple device.

At the beginning of 1962, the sampling tubes of the stationary dosimetric control system of the VVR-M reactor at the Ioffe Physicotechnical Institute of the USSR Academy of Sciences were completely replaced. The polyethylene tubes described above were used for the new sampling lines. In all, about 3,000 m was laid.

Routine preventive inspection and air-tightness testing is carried out every month. After two years' use, there has not been discovered a single appreciable defect due to the polyethylene tubes.

LINEAR ATTENUATION FACTORS OF ALLOYS FOR GAMMA RAYS FROM Co^{60} AND Cs^{137}

(UDC 539.121.73 : 539.166)

V. I. Kutovoi and V. I. Stetsenko

Translated from Atomnaya Énergiya, Vol. 19, No. 2,
p. 203, August, 1965
Original article submitted September 22, 1964

In the construction of radio-isotope transducers for devices using gamma radiation from Co^{60} and Cs^{137}, and in processing the experimental data, use is made of the linear attenuation factor μ or the mass attenuation factor μ_m, measured [1] or calculated [2] for the absorption of narrow beams of gamma radiation by pure metals.

In practical applications of gamma sources in radio-isotope devices, and also in research, the absorbers most commonly used are metallic alloys, which cannot be regarded as simple mixtures of the pure metals.

The linear gamma-radiation attenuation factor of an alloy depends on its constituent elements and its composition, crystal structure, temperature, etc.

The diagram shows graphs of experimentally measured values for the relative changes in linear attenuation factors for gamma rays from Co^{60} and Cs^{137}, plotted versus the percentage lead content, in the alloys Pb–Bi and Pb–Sn. The slopes of these graphs become steeper with increasing density difference between the alloy components. However, this fact does not entirely explain the shapes of the graphs: the density difference of lead and tin is 35.5%, but, in going from 0 to 100% lead in Pb–Sn, this difference causes a 44.8% change in the linear attenuation factor

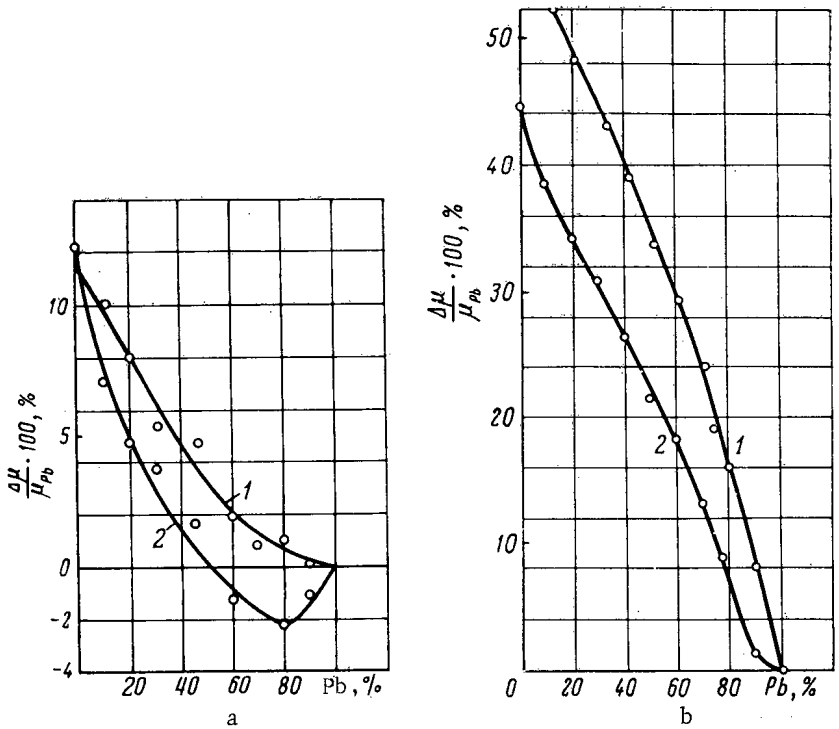

Relative change of linear attenuation factors for γ rays from Co^{60} and Cs^{137}, plotted versus percentage lead content in Pb–Bi (a) and Pb–Sn (b) alloys. 1) Gamma rays from Cs^{137}; 2) gamma rays from Co^{60}.

for gamma rays from Co^{60}, while for gamma rays from Cs^{137} the change is 52.0%. This discrepancy can be explained only by a change in the alloy's crystal structures as the lead content varies.

As the lead content of Pb–Bi decreases, the attenuation factor for gamma rays from Co^{60} at first increases, reached a maximum at 80% lead content, and then decreases to 12.3%.

The graphs can be used to determine the change in linear attenuation factors of Pb–Sn and Pb–Bi alloys for gamma rays from Co^{60} and Cs^{137}.

LITERATURE CITED

1. S. Simizu, T. Hanai, and S. Okomoto, Phys. Rev., 85, No. 2 (1952).
2. N. G. Gusev, Handbook on Radioactive Radiation and Shielding [in Russian], Medgiz, Moscow (1956).

USE OF RADIOACTIVE ISOTOPES TO CONTROL THE LINING CONDITION OF A ROTARY CEMENT KILN

(UDC 539.163:666.94.041)

E. M. Lobanov, A. O. Solodovnikov, B. E. Krylov, B. I. Nudel'man, and M. N. Rozov

Translated from Atomnaya Énergiya, Vol. 19, No. 2, pp. 204-205, August, 1965
Original article submitted September 5, 1964

One of the weak links in cement production is the state of the refractory linings of rotary cement kilns: their stability determines the furnace productivity and the cement quality.

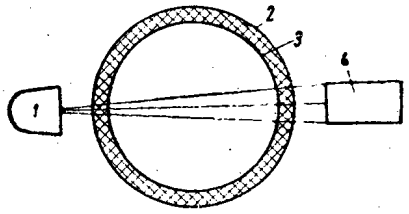

Fig. 1. System for radioscopy of kiln. 1) Container with radioactive isotope; 2) kiln body; 3) lining; 4) detector.

The Activation Analysis Laboratory of the Nuclear Physics Institute of the Uzbek Academy of Sciences, working with members of the industry, have suggested a method for controlling the lining states of cement furnaces, using Co^{60} gamma-ray sources.

A Co^{60} source and a scintillation gamma detector are fixed at diametrically opposed sides of the kiln, on a travelling carriage (Fig. 1) moving along the heating zone of the kiln at 180 mm/min. The intensity of the gamma radiation passing through the kiln depends on the lining condition.

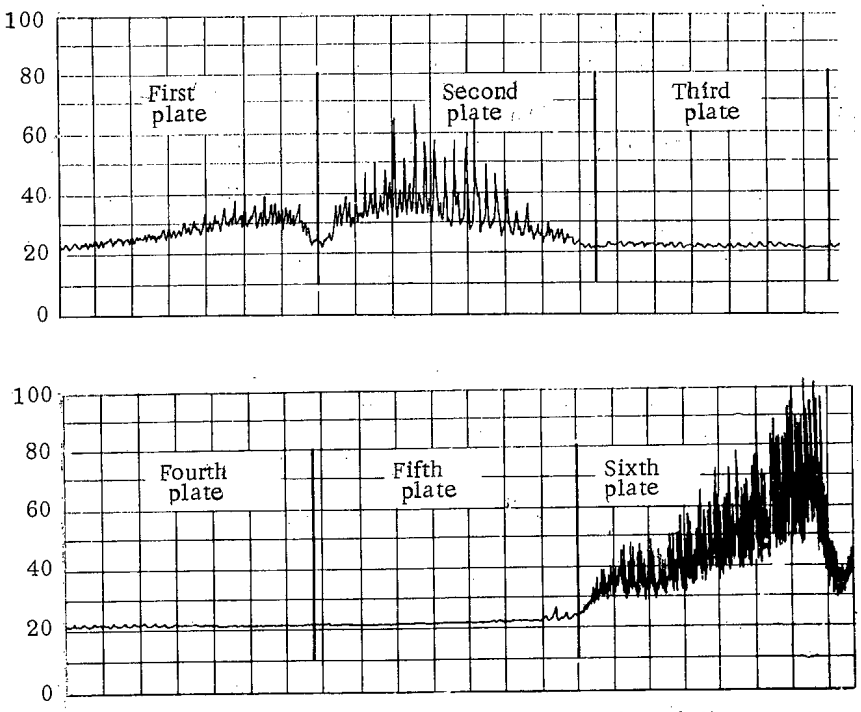

Fig. 2. Diagram recorded before shutting down kiln.

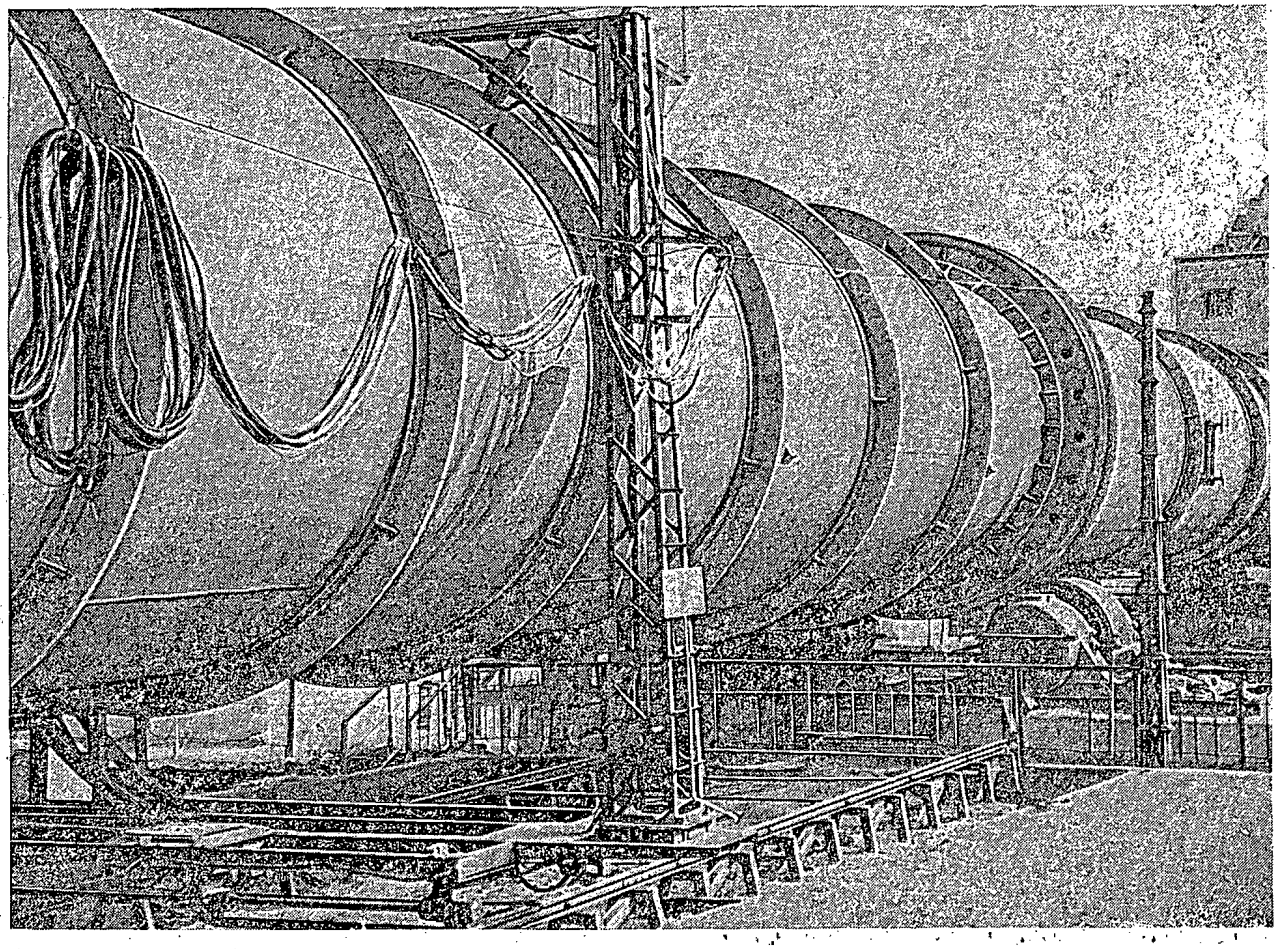

Fig. 3. Radio-isotope device on cement kiln of Begovatskii Cement Combine.

The recording device was a self-recording electronic potentiometer of type PSR1-01 with 100 mV scale, which continuously recorded the measurement readings on a paper tape.

All the gauges and carriage controls were located on a control panel under the eye of the kiln operator. To protect the detector from high temperatures, it was supplied with forced-water cooling.

Before shutting down the kiln, we carried out an experiment which yielded a diagram indicating the presence of defects in the lining at three places in the sintering zone. The results showed that there was much greater burn-out at one part of the zone than at the other two (Fig. 2). During repairs, we measured the effective thickness of the lining and the coating along the sintering zone. The measurements were in good agreement with the data from the radiometric equipment.

When fettling and calibration of the device were complete, the latter was put into experimental service. With its help, we were able to keep a continuous record of the deposition of a new coating (Fig. 3).

The test run showed that the device can be used for systematic monitoring of the condition of the refractory lining of a cement kiln during the basic technological cycle, giving advance warning of the occurrence of local burning and thus ensuring longer inter-repair working: this is of importance in cement production.

III INTERNATIONAL SYMPOSIUM ON INELASTIC SCATTERING OF NEUTRONS ON SOLIDS AND LIQUIDS

Translated from Atomnaya Énergiya, Vol. 19, No. 2,
pp. 206-207, August, 1965

The third symposium on "Inelastic neutron scattering by solids and liquids" was held in Bombay in December 1964. The symposium was under the joint sponsorship of the IAEA and the Atomic Energy Authority of India. Some 90-odd scientists took part in the symposium, and 68 papers were presented. The three-man Soviet delegation presented 9 papers.

Most of the papers presented dealt with the dynamics of metals. One by A. Woods (Canada) reported the latest research findings on the transitional metals of group V (Nb, Ta) and VI (Mo, W); these studies were carried out to find some correlation between the electronic properties and dynamics of metals. Dispersion curves for representatives of either group had much in common, but important differences between the groups emerged. For example, the Fourier expansion coefficients $\nu(\bar{q})$ related to the force constants are similar for Nb and Ta, for Mo and W, but differ in both magnitude and sign for the two groups. Screening of ions by s-electrons as well as by d-electrons must be invoked to account for certain anomalies in the dispersion curves of Nb and Mo. The need to take screening by s-electrons into account was also pointed to in a theoretical paper by T. Toya (Japan).

Several papers were presented on the lattice dynamics of the complex metals tin, magnesium, zinc. A very smooth variation of the acoustic branch and a low-lying optical branch whose existence had been predicted by Musgrave and attributed by that author to a phase transformation at high pressures was detected on the tin dispersion curves for the <100> and <001> directions. A paper by E. G. Brovman and Yu. M. Kagan (USSR) offered the first explanation for the sign of the anisotropy of the Mössbauer coefficient in white tin [β-tin]. But computed limiting values of the frequencies deviate slightly the experimentally derived values. This discrepancy appears to be due to the "loose" structure of the white tin lattice which calls for taking the neighbors of more remote coordination spheres, and not just the fifth, into account.

The effect of several types of imperfections on the dynamics of metals was discussed in several theoretical papers. Results of experimental measurements were presented in a paper by D. Dolling (Canada) discussing the change brought about in the dynamics of Ge and Si by slight (≈0.1%) impurities (arsenic and gallium for Ge, phosphorus for Si). The dispersion curves of Ge and Si, with and without impurities added, do not differ within the limits of error, which contradicts the data on the eleastic constants (C_{44} is 5% less for n-type Ge than for pure Ge).

Several papers discussed the effect of anharmonicity processes on the dynamics of metals. For example, R. Cowley (Canada) used Green's functions as a tool in computing thermal expansion, pressure dependence of the Curie point, nonlinear dielectric constants, reflections of u−k-rays, and the lifetime of transverse optical phonons in the case of lead titanate, and obtained satisfactory agreement with experimental evidence. A. Akasu and R. Osborn (USA) took anharmonicity effects into account with the aid of damping theory. Damping theory yields a square-law temperature dependence, at high temperatures, of the variation in width of one-phonon groups of scattered neutrons, whereas all earlier theories yielded a linear dependence. These results provided a more satisfactory explanation of high-temperature measurements for lead. V. A. Zhernov and Yu. M. Kaga (USSR) demonstrated that the degeneration of branches in the anharmonicity case may lead not only to substantial deformation of one-phonon groups, but also to the appearance of some additional groups. Experimental research on the dynamics of alloys is of special interest, since correct theoretical treatment of these systems is hampered by the high concentration of the original components. Measurements of the dispersion curves of β-brass (D. Dolling, Canada) showed them to be virtually unaffected in an order-disorder transition, i.e., short-range order (≈100A) is retained above the phase transition point. These results are at variance with the elastic-constant data (C_{44} shows anomalous behavior in the transition through T_k). Values of the limiting frequencies obtained were almost twice the values arrived at from measurements of diffuse scattering of x-rays.

Even though the dynamics of magnetic materials form that field of solid state physics where neutron-physics techniques perform a unique service, to date these investigations have undergone very sluggish development. 5 papers (three theoretical and two experimental) were presented on the dynamics of magnetic materials. V. Marshall (Britain) considered the dynamics of spin waves in his review paper, on research carried out by the Mössbauer effect, nuclear magnetic resonance, and neutron scattering techniques. G. Lowe (Britain) made a detailed study of the information obtainable from studies of diffuse elastic neutron scattering in the investigation of magnetic and nonmagnetic defects and in form factor determinations. In a second paper, G. Lowe made a comparison between experimentally derived dispersion curves for MnF_2 which have been reported in the literature and calculations based on simple spin theory. Satisfactory agreement between experiment and calculations was obtained for the <001> direction.

One paper on dispersion curves merits particularly close attention by scientists. Hematite is a weak antiferromagnetic material in the vicinity of $-20°C$. As I. E. Dzyaloshinskii demonstrated, the dispersion should show a deviation from linearity leading to the formation of an energy gap at zero in the case of weak antiferromagnetic materials, in response to small magnon pulses. No such departure from linearity was established for the <111> direction, within the limits of error. Hence the energy gap <1 MeV for the acoustic magnon branch, and the corresponding anisotropy is less than 10^{-3}.

26 papers were devoted to the dynamics of complex molecular systems in the solid and liquid states. The experimental investigations centered on ferroelectric crystals, crystals containing the molecular groups NH_4, H_3O, H_2O and others, some hydrogen halides, hydrides of metals. These do not lend themselves to such a straightforward interpretation of the experimental data as in the case of metals. A generous volume of research on the dynamics of the molecular groups NH_4 and H_2O was presented by the Joint Institute for Nuclear Research (Dubna). Torsional vibrations of NH_4 and other functional groups in crystals are matched by narrow peaks in the frequency spectrum, peak width $\lesssim 1$ MeV. The presence of these narrow lines aids the study of anharmonicity, phase transitions, and other processes affecting the dynamics of molecular systems. A complex approach (neutron scattering and absorption of u-k-rays) was demonstrated by I. Pelach, et. al. (Israel) in research on the ferroelectric salt KH_2PO_4. This study revealed an asymmetric barrier at the center of the potential well in the case of the hydrogen atom. V. Whitmore (USA) was successful in resolving peaks of one-quantum and two-quantum transitions in the spectrum of neutrons scattered on zirconium hydride, and in his approach to estimating the natural level width.

A paper on lithium hydride (M. G. Zemlyanov, et. al., USSR) attracted serious attention by the high level achieved in theoretical interpretation of the results; this report is unique, standing out in the many papers dealing with many-atom lattices, in which the effect of the polarization vectors of atom vibrations on the spectrum of scattered neutrons is treated. Two papers by the K. Larsson team (Sweden) studied inelastic coherent scattering of neutrons by argon and by aluminum in solid and liquid states. The transition from solid to liquid state is not accompanied by any abrupt change in the scattered neutron spectrum. We take special note of a paper by A. Woods (Canada) on measurements of dispersion curves for helium at large momentum transfers (1.7 to 3.8 A^{-1}). The dispersion curve was shown to leave the plateau at an energy close to double the energy at the roton minimum, and to terminate at a momentum close to double the momentum of the roton minimum. These results confirmed the hypothesis developed by L. P. Pitaevskii in 1959.

In contrast to the two last symposia, this symposium came up with no original papers on experimental research techniques in inelastic neutron scattering. This is a major drawback to be noted.

Several review papers were presented. A report by F. L. Shapiro (Joint Institute for Nuclear Research, Dubna) on the IBR pulsed reactor, and research being planned and now in progress using that reactor, met with interest, since a reactor of this type offers important advantages over a stationary-type reactor in many research applications. In a review paper, H. Palevsky (USA) reported on experimental devices in the Brookhaven National Laboratory HFBR reactor. Other review papers were presented by nuclear research centers in India, Italy, and Sweden. Typical features of the work at these centers are: 1) research on the dynamics of matter by inelastic neutron scattering, using both crystal spectrometers and time-of-flight spectrometers; 2) scintillation counters and pressurized He^3 counters are being used extensively to detect scattered neutrons.

Delegates went on record at the organization session in favor of scheduling a symposium on inelastic scattering of neutrons on solids and liquids in Poland in two years, to which the Polish delegation lent its assent.

The proceedings of the symposium will be published by IAEA in 1965.

M. G. Zemlyanov

SYMPOSIUM ON THE PHYSICS AND CHEMISTRY OF FISSION

Translated from Atomnaya Énergiya, Vol. 19, No. 2,
pp. 207-208, August, 1965

A symposium on the physics and chemistry of nuclear fission was held at Salzburg (Austria) in March 1965 under IAEA auspices. 200 or so scientists from 26 nations and 5 international research centers were in attendance. 80 papers were heard on various aspects of the process of nuclear fission.

The symposium devoted much attention to discussion of research on the properties of transitional states of nuclei near the fission barrier. W. Swiatecki (USA) stressed the point that research on various modes of nuclear motion near the saddle point could serve precisely as the first stage on the path of ascertaining the dynamics of the nuclear fission process. Papers submitted by J. Griffin (USA) and by V. M. Strutinskii, V. A. Pavlinchuk (USSR) attempted to account for experimental facts by the concept of pairing of nucleons in a cold nucleus and the "energy gap" concept. To clarify the properties of the transitional states of the nucleus at the saddle point in detail, the experimenters studied the fission process as initiated by various particles. A paper by N. S. Rabotnov, et. al. (USSR) presented results of a study of the angular distributions of fission fragments in photofission of even-even nuclides by photons of different energies. These studies enabled the authors to study fission of nuclei in the dipole and quadrupole capture of γ-photons, and to determine the fission thresholds in terms of the states 2^+, $K = 0$; 1^-, $K = 0$; and 1^-, $K \neq 0$. R. Lamphere (USA) presented results on angular anisotropy of fragments in the fission of many even-even nuclides by neutrons. Information made available in this paper shed light on transitional states at the saddle point in the case of even-odd compound nuclei. Papers by D. Eccleshall, et. al. (Britain) and J. Huizenga (USA) studied (d, pf), (t, pf), (α, $\alpha' f$) reactions near the fission threshold. The inadequate statistical precision and inadequate energy resolution made it impossible to distinguish rotational states belonging to the same rotational band but further efforts should yield highly interesting results. In this context, we draw attention to some highly complex work carried out by J. Dabbs, et. al. (USA) on the angular anisotropy of fission fragments in the fission of oriented nuclei by resonance neutrons.

The distribution of fission energy between the kinetic energy of fission fragments and their excitation energy was the subject of lively discussion. The energy balance is not in doubt in the case of high-yield fragments in the fission of nuclei by thermal neutrons. But data on the very improbable modes of fission producing fragments of approximately equal masses were contradictory. Papers by V. F. Apalin et. al. (USSR), P. P. D'yachenko, et. al. (USSR), W. Gibson, et. al. (USA) reported the kinetic energy of fragments produced in fission of U^{235} induced by thermal neutrons into symmetric fragments as close to 150 MeV. J. Fraser (Canada) assigned a value roughly 20 MeV lower. Experimental data on neutron yields from inidividual fragments, reported in the paper by A. F. Apalin, et. al. mentioned earlier, stimulated close interest.

H. Schmidt, et. al. (USA) reported results of a study of Ra^{226} fission induced by 12 MeV protons. The authors analyzed the data from the vantage point of the hypothesis of two modes of fission. The paper indicated a slight discrepancy between angular distributions for the symmetric and asymmetric modes of fission, but the authors are inclined to account for it in terms of an admixture of the (p, nf) process.

A paper by R. Vandenbosch, et. al. (USA) reported on an extended research program. These authors studied the (d, pf) reaction on U^{234}. Fission-fragment masses, kinetic energies, proton energy, and angular anisotropy of fragments were measured. The (d, pf) reaction was shown to have additional fission channels not found in the (n, f) reaction, angular anisotropy was shown to be independent of fragment masses, and a variation in K. E. from channel to channel was observed. The inferred independence of angular anisotropy of fission fragments from their mass is in agreement with a conclusion drawn in a paper by A. I. Sergachev, et. al. (USSR), who studied similar phenomena in neutron-induced fission of Th^{232}.

Interesting results were reported by J. Milton and J. Fraser (Canada), implying that about 10% of the prompt-fission neutrons are emitted at the instant of scission, but from moving fragments.

An original paper was presented by G. Bowman, et. al. (USA). Involved investigations of gamma rays emitted in nuclear fission were performed. The spectra and multiplicity of gamma photons were measured for different fission-fragment masses and kinetic energies. The Doppler shift in the gamma-ray lines was used to identify the fragment to which the line belonged, and in this way gamma-ray spectra were obtained not only for each fragment mass ratio but also for each fragment mass. By studying x-ray spectra we can also determine the charges on fragments. Results on this point were also presented in papers by H. Mayer-Leibnitz et al. (West Germany) and T. Thomas et al. (USA).

I. Halpern (CERN) discussed the time of emission and the energy of α-particles sometimes observed in the fission of nuclei. Calculations yielding information on the velocities of the fragments at the time of emission and on the kinetic energy spread of α-particles were cited in the paper. M. Muga (USA) studied tripartition of nuclei into fragments of comparable mass. This process has an extremely low probability (approximately one case in 10^6 events of ordinary bipartition of nuclei).

Many interesting data were offered in papers on the effective fission cross section of nuclides. A paper by Wang Shih-ti, et. al. (Joint Institute for Nuclear Research) reported fission cross sections studied in the range from 2 eV to 30 keV. Parameters of 78 levels were obtained over the energy range to 50 eV, and average characteristics of cross sections were obtained in the 0.3 to 30 keV range. P. White (Britain) reported on measurements of the fission cross sections of U^{233}, U^{234}, U^{236}, Np^{237}, Pu^{239}, Pu^{241} in the energy range from 40 to 500 keV. The results of measurements of the fission cross section of Pu^{240} well below threshold and above the threshold (from 30 keV to 2 MeV) are reported in a paper presented by M. De Vroey, et. al. (Britain).

Some interesting results on the relationship between the relative yield of delayed neutrons and the excitation nuclei of the fissioning nucleus were reported by B. P. Maksyutenko (USSR).

Finally, we may note some papers which mentioned new techniques. G. Andritsopoulos, et. al. (Britain) and W. Stein (USA) described a method for simultaneously measuring time of flight and fission-fragment energy. Further development of this method will make it possible to determine fragment mass, number of neutrons emitted by each fragment, and the kinetic energy of each fragment. These measurements were carried out with a four-dimensional analyzer. The amplitude defect for semiconductor detectors was investigated by H. V. Schmidt, et. al. (USA). Heavy ions accelerated by a tandem electrostatic accelerator were used to simulate fission fragments. H. Ewald (West Germany) studied the mechanism by which fission fragments become enveloped in an electron cloud, at different fragment masses and fragment energies.

Multiparameter correlation studies involving a wide use of semiconductor detectors and recording of experimental data on punched tape or magnetic tape for subsequent sorting and processing on an electronic computer were typical of the papers presented at the symposium.

B. D. Kuz'minov

IAEA-WHO VIENNA MARCH 1965 SYMPOSIUM ON PERSONNEL DOSIMETRY FOR ACCIDENTAL INTERNAL AND EXTERNAL OVEREXPOSURES

Translated from Atomnaya Énergiya, Vol. 19, No. 2,
pp. 209-211, August, 1965

In March 1965, the IAEA [International Atomic Energy Agency] and the WHO [World Health Organization] jointly sponsored a symposium in Vienna on personnel dosimetry in accidental internal and external overexposures. Representatives from 28 countries and organizations took part in the deliberations, and about 50 papers were submitted and heard.

The papers dealt with general problems in the dosimetry of accidental overexposure, with dose measurement techniques in external exposures, with determinations of internal contamination by radioactive pollutants, with estimates of dosage in-take in external and internal exposures, and with experience and practice at the various centers.

Papers by G. Andrew (USA), C. Duncan (Britain), and E. Vallario (USA) discussed general dosimetry problems in accidental overexposures. The speed and precision of dose measurements in accidental overexposures must satisfy both medical and administrative-juridical requirements. Medical requirements depend on the stage of investigation of accidental overexposure of personnel. In the first stage (getting the overexposed victims proper medical attention and observation, sorting them out from those less seriously exposed), information on exposure dose and on the activity of internal contaminants must be obtained as rapidly as possible to within an order of magnitude. In the second stage, the precision of measurements of large doses must be higher, within a factor of 2-3. In Duncan's view, the accuracy of dose determination must be within a factor of 1.5 to 2 over the 200 to 1000 rad range, while Vallario sets it as not less than 20%. Increased precision in this dose range is needed to resolve the problem of injection of brain matter into the organism of the victim. Administrative-juridical requirements reduce to the specification that the exposure not exceed a preset level. More precise information on the biological sequelae of accidental overexposure calls for tightening the precision to within ± 10% (for the whole body and for critical organs).

The dosimetry system for handling accidental overexposures must include: 1) arrays of stationary dosimeters placed around the facility or other proposed radiation source for the purpose of recording gamma dosage and the energy spectrum of neutrons emitted. Chemical and thermoluminescent gamma-ray dosimeters are acceptable, neutron detectors may be activation detectors (indium, gold, copper, sulfur, etc.); 2) personnel film-badge detectors and activation detectors; 3) instruments for measuring the activity of blood circulating in the human organism (whole-body counters), equipment for sampling blood serum, hair, and excretions. The data accumulated by this system may yield sufficiently precise information on the dose absorbed by the whole body and by critical human organs.

Most of the papers submitted dealt with techniques for measuring external overdosage (23 papers). Dz. Trouzil (Czechoslovakia) suggested three ways to raise the maximum dosage recorded photographically; partial breakdown of the latent image in an emulsion; depressing the chemical activity of the developing agent by introducing inhibitors; and by broadening the operating range of densitometers to a photographic density of six. These photodosimetric techniques can be used to measure doses from 10 mr to 1000 r. F. Wachsmann (West Germany) suggested processing photographic film with a mixture of developer and fixing agent simultaneously, to speed up the acquisition of information in determinations of heavy exposure dosage. Visual dose measurements by comparing the optical density of the developed film to that of standard films irradiated by known doses have been done. The design of a special developing box (the size of a cigar holder, weighing 150 g) renders daylight development possible. The range of doses measured runs from 10 to 2000 r. One worker can process 40 film badges in an hour by this method. G. Handloser (USA), H.G. Hardt (West Germany), Z. Spurny (Czechoslovakia), J. Webb (Britain), K. Becker (OESR, EAYaE) presented results of investigations made on the thermoluminescent dosimeters and phosphate-glass dosimeters. A broad range of doses recorded (10 mrad to 1 mrad), the linearity over that range, the swiftness of dose determination after exposure, low price and simple design all combine to make these dosimeters strong competitors of photographic emulsions, particularly in the range of high radiation doses.

Papers by R. Barrol (USA), W. Reining (USA), G. Smith (Britain), M. Brichka (France) discussed activation analysis techniques in neutron measurement. The review paper by Barrol was based on an analysis of published data, and suggested values of resonance integrals for the most widely used isotopes: Na^{23}, Mn^{55}, Co^{59}, Cu^{63}, In^{115}, Au^{197}, Th^{232}, and U^{238}. Brichka made a proposal to measure dose and neutron flux over the energy range from thermal energies to 7 MeV, using spherical moderators of different diameters: 5 cm, 6.4 cm, 25.3 cm, 30.5 cm. A LiI crystal (to measure dose rate and neutron flux density) or a gold indicator (to measure dose and neutron flux) is placed at the center of the sphere. L. Sklavenitis (France) reported on a possible application of activation detectors to estimate large doses due to high-energy particles. His paper proposed formulas for calculating high-energy proton and neutron flux, and presented findings on the spectral composition of particles in the 24 BeV proton synchrotron. D. Petersen (USA) described a method for determining fast-neutron dosage from P^{32} activity in human hair. R. Lehman (USA) offered findings on neutron spectra at various depths in a human mannikin. The work was conducted with nuclear plates at various distances (from 25 to 200 meters) from a bare-pulsed reactor. The results of these studies showed that the spectrum of neutrons of higher than 0.5 MeV energy did not change in the interior of the mannikin and was independent of the distance to the reactor.

R. Hoseman (West Germany) described one specimen of a film badge with radiation component (vacuum diode in which the emission energy is converted to potential electrical energy) having an interelectrode voltage proportional to radiation dose. The outer electrode was made of a substance with a high activation cross section as required to measure neutron dose effectively. This dosimeter offers important advantages not found in conventional ionization pocket dosimeters: it is self-charging, has low leakage, and makes it possible to measure large doses thanks to the absence of recombination.

J. Chanterre (France) proposed a novel technique for determining the dosage of fast and thermal neutrons from phosphorus activation in bone tissue. The thermal-neutron dose was determined by the $P^{31}(n, \gamma)P^{32}$ reaction, the fast-neutron dose (energies above 1.8 MeV) by the $P^{31}(n, p)Si^{31}$ reaction. This approach makes it possible to determine the neutron dose distribution over the human organism when bone samples are taken from several sites.

Eight papers dealt with determinations of internal contamination by radioactive materials. Sedlet (USA) noted that NaI (Tl) crystal counters 20 by 10 cm in size and shielded with lead or iron are capable of measuring radioactivity in the body below tolerance, even when they are placed in an ordinary unshielded room. The paper discussed the difficulties in determining internal contamination in the immediate wake of an accident, and ways of getting around the difficulties. H. Kieffer (West Germany) proposed some techniques and devices for measuring activity in lesions and discussed specific requirements applying to such devices: small size, attention to absorption of α- and β-emissions in the wound, sterility, insensitivity to moisture. A method for determining beta-emitters with β-particle energy surpassing 1 MeV in secretions, by using a Cherenkov counter, was described by J. Narrog (West Germany). The time it takes to measure strontium activity is 60 min or 90 min depending on the method used to isolate strontium. R. May (Britain) described two portable devices for determining the gamma-ray spectrum and gamma-emission intensity of Na^{24} (in the human body after accidental neutron overexposure, and to estimate iodine activity in the thyroid and in milk).

7 reports concerned dose estimates in external and internal exposures. D. Mechadi (France) presented an interesting paper on how to calculate the average absorbed neutron dose in brain tissue over the energy range from thermal energies up to 10 MeV. Doses were computed on the basis of the Snyder-Neufeld theoretical papers and the Booth-Smith experiments for three cases of exposure: in front, in back, and on both sides by identical fluxes. The report implies that the average absorbed dose in brain tissue is 1.5 to 5 times below the surface dose, depending on the spectrum and direction of the incident neutrons. The report cited data on average absorbed doses in the brain tissue of victims suffering overexposure in the accidents at the Y-12 plant and in Vichy.

M. M. Komochkov (USSR) presented a report on an experimental estimate of absorbed dose in exposure to high-energy protons and neutrons. The method is based on rapid measurement of the activity of C^{11}, N^{13}, and (formed by irradiation of tissue by particles whose energies surpass 20 MeV. When a Tiss beta-sensor was sensitivity of the method was ≈100 mrad. The results were checked by exposing dogs to irradiation. G. (France) chose to record Be^{7} formed in tissue by disintegrations of the nuclei of carbon, nitrogen, and carbon atoms in a similar determination of high-energy proton dosage. The sensitivity of the method was 250 rad.

F. Breuer and E. Casnati (Italy) proposed formulas based on a critical review of published techniques, for calculating absorbed doses due to α-, β-, and γ-contamination of the skin tissue.

M. Ladu (Italy) presented results of absorbed dose measurements at various depths in a plexiglas mannikin exposed to a beam of photons from a synchrotron. The electrons were accelerated to 1 BeV.

G. M. Obaturov (USSR) presented some suitable methods and formulas for estimating absorbed doses in critical organs suffering from accidental and chronic (internal and external) exposure.

The papers were submitted on experience in dosimetric monitoring at various centers. E. Putsche (USA) made a detailed presentation of the results of plutonium activity measurements on the surface and inside the body of a human after an accident in glove-box work handling plutonium (on June 12, 1964). When 1.5 kg hot plutonium gained access to a carbon tetrachloride bath an explosion resulted. Fragments of the smashed glove-box window and plutonium spills were splattered all over the room. The operator's left hand was injured, with the thumb and index finger requiring amputation; contamination of other parts of the body exceeded 1.5 $m\mu Ci/cm^2$. The use of detergents and EDTA compounds proved quite effective. Activity was carefully monitored both on the surface and inside the organism, and excretions were given a regular radiometric analysis. But the report did not evaluate the plutonium internal exposure dose, nor did it discuss possible biological after effects. A paper by H. Parker (USA) described dosimetry techniques at the Hanford accident (on April 7, 1962). As a result of plutonium wastes getting into a supercritical volume, three men suffered appreciable exposure doses. These doses were 63, 23, and 13 r (gamma exposure) and 23-30, 9-12, and ≈3 rad (neutron exposures). Joffe (France) presented dosimetric and clinical findings on an exposure accident at a 7 MeV electron linear accelerator as a result of abnormal operating conditions. Fingers of staff members suffered most of the exposure.

J. Mirić (Yugoslavia), P. Canda (France), and F. Sipperley (USA) reported on dosimetry techniques in use at the B. Kidric institute at Vinc, on objects of the French Commissariat de l'Energie Atomique, and at the USA national reactor testing station, in both chronic and accidental γ - and n-exposures.

Sipperley's paper reported that individual doses are measured with devices which automatically display results in a form suited to processing on an electronic computer, which processes all the information obtained from personnel dosimeters or from measurements taken of blood and secretion activity, and displays definitive values of external and internal exposure doses.

A paper by L. Anderson (USA) presented techniques for determining doses of neutron and gamma radiation and neutron spectra on critical facilities at the Argonne National Laboratory. Two dosimetric systems devised at the Oak Ridge National Laboratory and at the Savannah River plant are in use, the first being the basic system, and the second an auxiliary one. K. A. Edvardsson (Sweden) reported a special accident organization set up in Sweden to begin action as soon as a signal is received on radiation hazard in any locality. Preliminary data on the degree of radiation hazard will reach this organization within 10 to 15 min after the accident occurs. G. Cowper (Canada) discussed techniques of dosimetry in reactor accidents and in measures taken to cope with the effects of reactor accidents. Some instruments described in the report designed to annunciate an alarm in the event a preset dose level is exceeded, radiometers for tritium measurements, a beta-ray dosimeter using a thin organic scintillator, are interesting items.

The symposium demonstrated the high level of interest shown by scientists of different countries in dosimetry, radiation safety, and medical treatment of personnel falling victim to accidents or dangerous overexposure. The Proceedings of the symposium will be published by IAEA in 1965.

G. M. Obaturov

NUCLEONIC INSTRUMENTATION

Translated from Atomnaya Énergiya, Vol. 19, No. 2,
p. 211, August, 1965

The ninth session of work team No. 1 of the Permanent Commission of the Council for Mutual Economic Aid [COMECON] on the uses of atomic energy for peaceful purposes was held in Prague in April 1965. Specialists on nucleonic instrumentation from Bulgaria, Hungary, East Germany, Rumania, the USSR, and Czechoslovakia were in attendance. Technical aspects of specialized production of nucleonic instruments were the main topic of discussion. Agreement was reached on basic parameters and general engineering specifications for dosimetric and radiometric devices, spectrometers, electronic equipment and assemblies for nuclear engineering applications, and medical instruments utilizing ionizing radiations. Detailed standardization lists were compiled of the instruments and equipment in large-scale production in the socialist countries. A sequence to govern future production of technical materials to aid in specializing the production of nucleonic instruments was elaborated and adopted.

Plans were also prepared for coordination of scientific and engineering research in nuclear instrument design and for the standardization of nucleonic instrumentation over the 1966-1970 period. These plans will prove a basis for annual plans of scientific and industrial collaboration between member-nations of COMECON. The proposed plan for coordinating scientific and industrial research encompasses the most pressing areas. Countries, institutes, institutions best suited to the production of specific types of instruments have been specified. The coordination of scientific and engineering research in countries of the socialist camp will aid in speeding up the development of sophisticated instrumentation and nucleonic facilities to meet the needs of scientific institutions and the needs of the several national economies.

Results of the conference of COMECON specialists on radioisotope relay-type devices, held in Warsaw in October 1964, were also discussed at this session. Appropriate proposals were formulated to speed up specialization and allocation of the production of these instruments; these proposals are to be reviewed by the Permanent Commission of COMECON on the uses of atomic energy for peaceful purposes.

This discussion took place in an atmosphere of creative activity and was affected by the striving of all the participants at this session to achieve the most effective collaboration in the field of nucleonic instrument design, standardization, and specialization within the COMECON framework.

N. A. Shekhovtsov

SOVIET PHYSICISTS VISIT BRITAIN

Translated from Atomnaya Énergiya, Vol. 19, No. 2,
pp. 211-212, August, 1965

In January 1965, Soviet scientists paid a visit to the Culham laboratory at which British scientists in fusion research are currently concentrating their basic efforts in the physics of high-temperature plasma and on the problem of controlled thermonuclear fusion. The laboratory is staffed by 1000, about 100 of whom are qualified research physicists. The laboratory consists of two experimental and one theoretical sections.

The laboratory's work is governed by the search for some way to achieve a controlled thermonuclear reaction, and this means some way to produce a stable high-temperature plasma. Since the pathways open to the solution of the problem are by no means clear at present, research in the experimental sections is pursued over a wide range of directions (adiabatic traps, cusped-geometry traps, toroidal traps, straight pinches and azimuthal pinches, and others). The theoretical section is concerned with how to confine plasmas generated in these machines.

Attention centers at present on investigations of the behavior of plasma in adiabatic traps with outwardly increasing magnetic fields (minimum-B configurations). This work is being conducted by two teams, one under Francis (the MTSE experiment), the other under Sweetman (the Pheonix-II experiment).

In the MTSE group, the adiabatic trap is filled by a plasma gun. The plasma is trapped by rapidly switching on a mirror magnetic field (field at center of trap is 4 kG, mirror ratio is 1.8, distance between mirrors is 75 cm). A stabilizing field is established by six lengthwise current-carrying conductors. When the stabilizing field is switched on, the confinement time of a low-density plasma ($n_i \approx 4 \cdot 10^{10}$ cm^{-3}, ion energy $\varepsilon_c \approx 1$ keV) is stretched from 50-80 to 250-400 μsec. No increase in confinement time in response to stabilizing field was observed in the case of denser hot plasmas ($n_i \approx 10^{14}$ cm^{-3}; ≈4-5 keV), however. In Francis' view, the reason is that when a large-diameter plasmoid is injected some of the plasma escapes to the side walls along the force tubes intersecting the chamber walls. As a result of interaction between the dense plasma and the chamber wall, a large number of neutral atoms forms and this vitiates the vacuum conditions. A large-diameter trap has been proposed to eliminate this effect.

The Sweetman group is not finishing construction work on the Phoenix-II machine, in which the minimum-B field will be established by four stabilizing conductors. The magnetic field of the trap may reach 60 kG, the longitudinal mirror ratio will be 1.8, the distance between mirrors ≈30 cm. The plasma in the trap will be generated by Lorentz ionization of fast neutral hydrogen atoms. It is expected that the saddle-point current value will be attained in the Phoenix-II mirror configuration.

Another trend in experimental work is the theta-pinch. The basic aim in theta-pinch work is to study heating and containment of a cylindrical plasma by a rapidly growing axial magnetic field. In current theta-pinch experiments using mirrorless geometry, plasma of 10^{17} cm^{-3} density has been obtained, with electron temperature estimated at 300 eV, ion temperature estimated at 500 eV.

The laboratory is also conducting experiments with cusped-geometry mirrors, studying turbulence on the ZETA machine, investigating the causes behind the anomalously rapid diffusion of the magnetic field into a plasma (on the TIBER machine) and plasma instabilities in an internal-conductor pinch (the Faust-1 machine). Some experiments are designed to investigate certain aspects of plasma physics: wave propagation in a plasma, collisions of plasmoids, shock heating of plasmas (the TARANTULA machine).

Theoretical research is centered on studying plasma instabilities in minimum-B field systems, focusing primarily on magnetohydrodynamical instabilities in those systems. Dissipative and drift instabilities of a nonuniform plasma, cyclotron instability, wave propagation, nonlinear wave coupling, and other topics are also being pursued. These studies are being conducted both analytically and with computer numerical techniques.

A. B. Mikhailovskii and K. N. Stepanov

PROCESS IRRADIATORS AT THE ALL-UNION SCIENTIFIC RESEARCH INSTITUTE FOR THE ELECTRIFICATION OF AGRICULTURE

Translated from Atomnaya Énergiya, Vol. 19, No. 2,
pp. 212-216, August, 1965

A radioisotopes laboratory has been organized at the All-Union Scientific Research Institute for the Electrification of Agriculture (VIÉSKh) for the purpose of developing practical applications for radiation sources in agriculture.

The laboratory has specially equipped rooms (Fig. 1) for working with high-level sources and for conducting radiotracer experiments. The presence of high-level sources makes it possible to expand the program of experiments on raising crop yield in the production of corn, potatoes, and miscellaneous crops as a result of pre-sowing irradiation of seeds, experiments on new and economically beneficial properties in plants, microorganisms, and livestock by radiation genetics techniques; deactivation of agricultural products and raw materials; sterilization of veterinary preparations, and other experiments.

Objects taking up as much as 122 liters in volume are irradiated in a gamma facility under a pool of water, in containers placed on the bottom of special process chutes (Fig. 2). Larger objects which cannot fit into the gamma facility containers (bags of grain, bales of raw materials, large plants, medium-sized and large animals, etc.) are irradiated in a special chamber.

Three pools lined with 1Kh18N9T stainless steel have been built to accomodate the radiation sources, irradiator assemblies, and irradiation accessories. Two of them, the receiving pool 18 and the gamma irradiator pool 6, are placed side by side and separated by a concrete wall 300 mm thick. A third pool 23 is placed in a special chamber, and communicates with the receiving tank by a tube for hydraulic transport of sources (20); the tube is 5630 mm long. Radiation shielding is provided by filling the pool with water to a height of 3200 mm. A monorail with overhead support outside the rooms (see Fig. 1) is assembled above the first two pools. A pulley hoist suspended on the monorail, with a load lifting capacity of 2 tons, moves containers from a truck to the receiving pool. The receiving pool doubles as receptacle for irradiators designed for use outside the radioisotopes laboratory, and for transfer of sources from one container to another. The receiving pool has a device for measuring source activity underwater (1).

The basic mechanical parts of the gamma irradiator are a mechanism for loading objects to be irradiated, a turntable, the irradiator-positioning carriage, and the carriage drive. The turntable is placed opposite the receiving pool and consists of three process chutes 7 proceeding up to just short of the pool. Containers are loaded in place underneath the irradiator via the process chutes, they are mounted on a standpipe 9 which serves as a rotation axis. The standpipe rests on its base 8 welded to the bottom of the tank and packed with concrete into the foundation. The support and two tapered ball bearings in it, as well as other parts of the gamma irradiator assembly operating in water, are made of 1Kh18N9T stainless steel. The upper part of the standpipe protruding above the water rotates in a radial bearing mounted in the cast iron plate 13 which covers the expanded portion of the pool. The standpipe and process chutes are rotated by a hand-operated drive 11 on the turntable resting on the cast iron plate.

The carriage is located on the opposite side of the turntable at the receiving pool. The carriage table 15 consists of longitudinal and transverse side members strapped together and two tie beams each of which supports four rods (5) each. The tie beams can be moved crosswise (moved closer or away) with the aid of right- and left-handed screws turned from a single flywheel.

The gamma process irradiator forms two parallel planes consisting of eight rods 5 each carrying three ampule holders 4. Each ampule holder is capable of taking two sources each of 200 gram-equiv. Ra activity. The total activity of the irradiator as a whole is 9600 gram-equiv. Ra. The rods are brass tubes within which the double screw is threaded. As the screw is turned the two end ampule holders are moved vertically, the middle one remaining fixed.

A chain drive actuated by an electric motor moves the carriage along the pool on two parallel guide bars.

The object to be irradiated in placed in a container which is then lowered through the loading hole to the bottom of the turntable chute. Another pulley hoist of one-ton-load lifting capacity serves to bring the container to

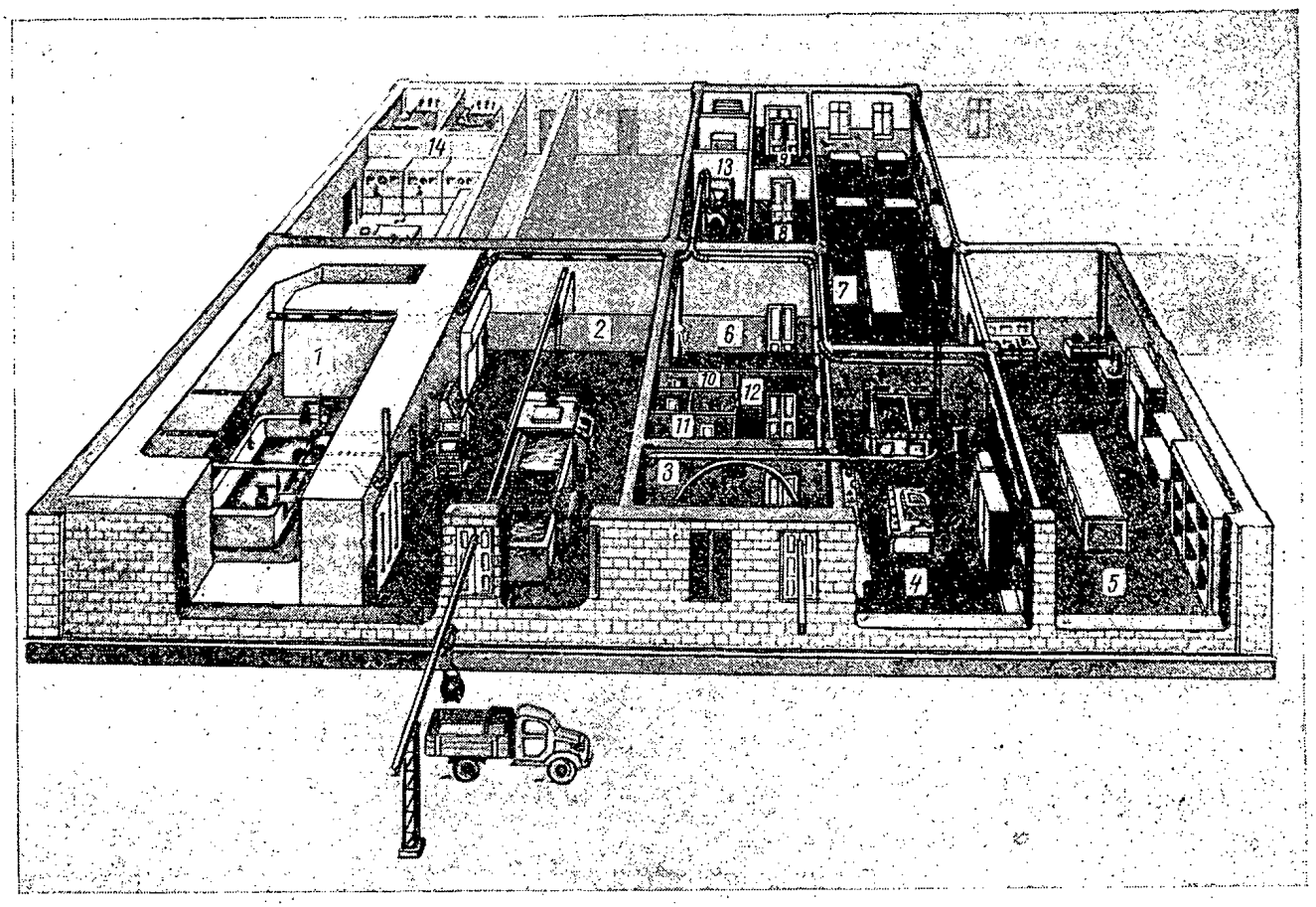

Fig. 1. VIÉSKh radioisotopes laboratory: 1) Shielded chamber; 2) high-level gamma irradiator room; 3) storage room; 4) isotopes room; 5) radiometry room; 6, 8) corridors; 7) preparation room; 9) vestibule; 10) health physics room; 11) shower room; 12) dosimetry and monitoring room; 13) fan room; 14) transformer substation.

the hole, lift and lower it. A special grappling device is attached to the pulley cable and the container which it holds is lowered down the guide tube of the chute and positioned at the bottom. The grip is then released and raised back up, and the turntable is rotated one half-turn by manual drive. The chute with container is brought into operating position beneath the cast iron plate. Before the carriage is moved from storage position to operating position for the irradiation, an irradiator corresponding the volume of the container installed must first be assembled. It takes 1.1 min to move the carriage. The carriage is automatically stopped at its extreme positions by limit switches. In overhaul and adjustment operations, the carriage can be moved manually. It takes the carriage 2 min to travel from one extreme position to the other. Ampule holders are located 10 mm from the chute walls during the irradiation.

After the exposure, a timing relay switches on the electric drive to bring the carriage with radiation sources from the operating position back to storage. When the carriage has been returned to storage position, a signal is flashed to turn the turntable and position the chute with container under the loading hole. The container is then unloaded.

Carriage travel is controlled from a control panel 10. When the irradiator size does not match the process chute the carriage cannot be moved into position. There are also interlocks to immobilize the carriage in operating position or in storage position as required. Timing relays are installed in the control panel for automatic control of exposure time, from 20 sec to 10 min and from 8 min to 8 h. The control panel has light signal panels to display irradiator position, process chute positions, amplitude holder positions, drop in water level of the pools below a predetermined level. Processes can be monitored during the irradiation and various physical, chemical and miscellaneous process variables can be sensed and measured by installing various sensors in the containers being exposed and connecting them up properly to process control instrumentation.

Transfer tubes 3 serve to transfer sources from the receiving pool to the gamma facility pool and vice versa.

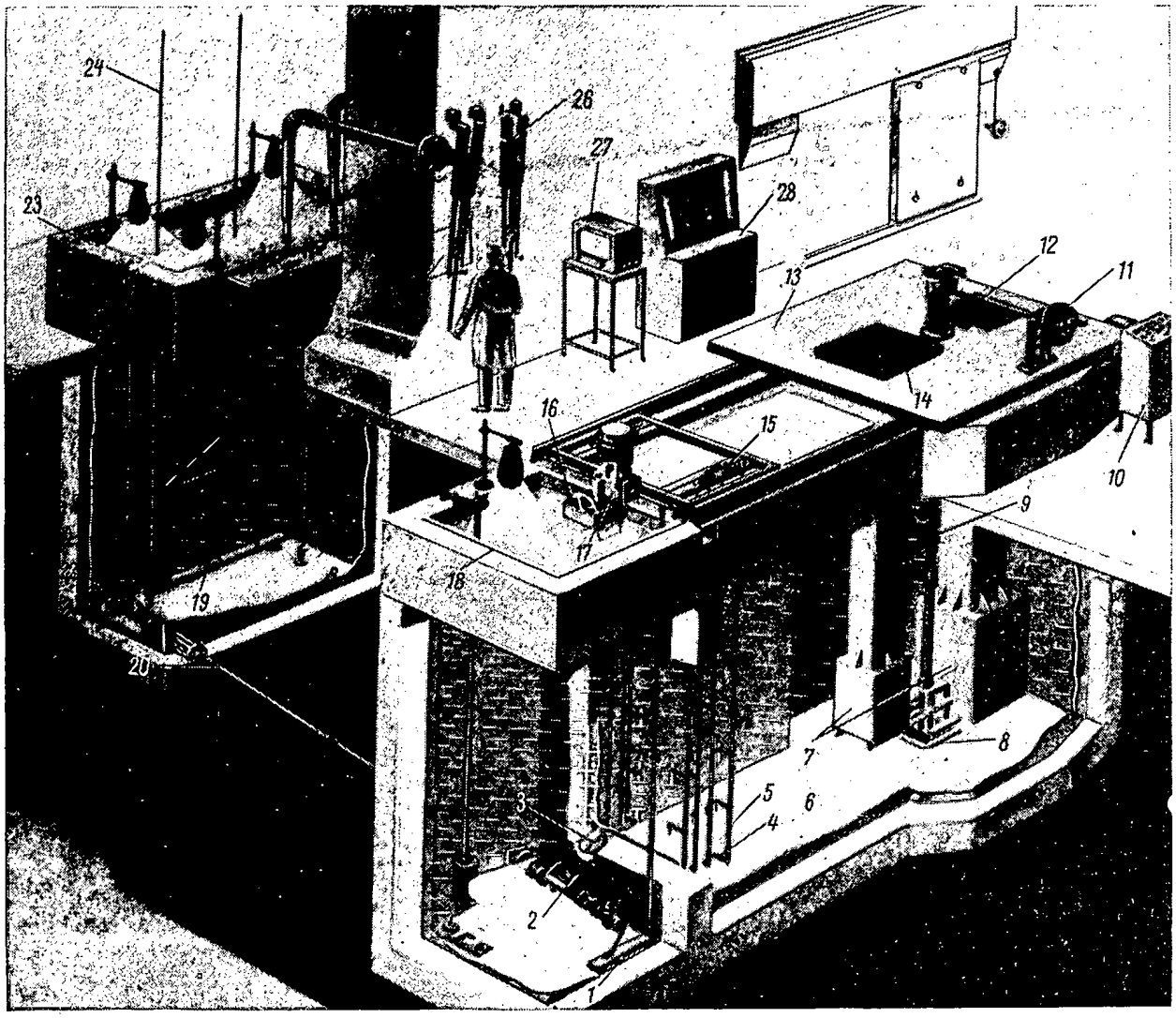

Fig. 2. Radiation facilities: 1) Activity measuring device; 2) rotary funnel; 3) transfer tube; 4) ampule holder; 5) rod; 6) gamma facility pool; 7) process chutes; 8) support; 9) standpipe; 10) gamma facility control panel; 11) manual drive for turntable; 12) loading hole; 13) cast iron plate; 14) lead plate; 15) carriage frame; 16) power drive flywheel; 17) carriage drive; 18) receiving pool; 19) movable rack; 20) hydraulic conveyer tube; 21) tee joint; 22) water seal; 23) shielded chamber pool; 24) guide rod; 25) viewing window; 26) through-wall manipulator; 27) PTU-4 closed-circuit TV; 28) shielded chamber control panel.

The range of variation in the dimensions of the volume bounded by the radiating planes and the dose rate are tabulated. The variation factor of the dose field established by the process irradiator in the volume occupied by the largest container is no larger than ± 10%.

The thickness of the shielding layer of water, of the concrete walls, floor, cast iron plate and lead plate, make it possible to reduce the radiation dose rate at worksites well below tolerance limits.

Devices installed in the chamber for irradiating objects larger than 120 liters in volume make it possible to assemble the irradiator in the pool and to extract it; the chamber also contains a facility for measuring gamma-ray fields (Fig. 3).

The basic parts of the mechanism for assmebling and extracting the process irradiator are the movable rack 19, the guide rods, 24, the pulley hoist system, and the electric power winch (see Fig. 2) which is located outside the chamber. Mounted on the rack is an irradiator casing of whatever appropriate shape (rodlike, slab, barrel, latticework). The irradiator is loaded by remote control under a layer of water, with rack and casing on the bottom of the pool. The manipulator 26 is available for loading the irradiator if required.

Variation in Dimensions of Volume Bounded by Radiating Planes, and Dose Rates

Dimensions of bounded volume, mm			Volume bounded by radiating planes	Container dimensions, mm			Container volume, liters	Dose rate in air at center of irradiator, r/sec
width	length	height		width	length	height		
1000	700	700	490	700	504	357	122.6	10.8
540	400	400	86.4	380	284	207	22.1	33.2
180	180	160	5.2	125	122	77	1.18	210.0

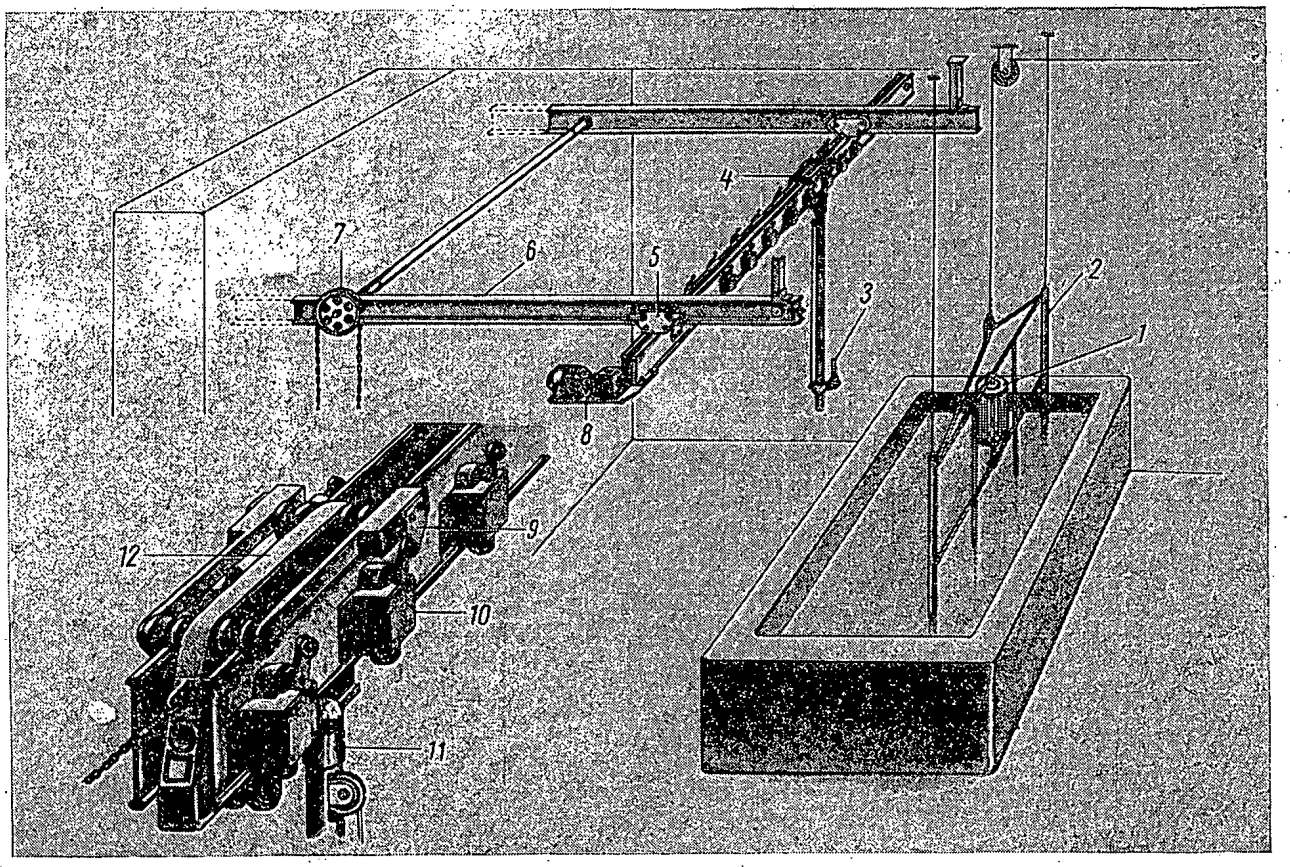

Fig. 3. Gamma field measuring arrangement: 1) Irradiator under study; 2) irradiator extraction gear; 3) sensor; 4) bottom carriage; 5) top carriage; 6) frame; 7) manual drive; 8) electric power drive; 9) runner; 10) limit switch; 11) support rod; 12) roller carriage.

The chamber shielding allows an irradiator loaded with sources of total activity ranging to 8000 gm-equiv. Ra to be withdrawn and placed above the pool water level. The maze arrangement, the designed thickness of the concrete walls, and the chamber coatings are features of the shielding (Fig. 1). The entrance to the chamber is closed off by a steel door 100 mm thick to absorb radiation scatter from a raised source.

The gamma field measuring arrangement consists of three main assemblies: the frame and manual drive, the electrically powered top carriage, the lower carriage with radiation sensor. The radiation dose in the chamber is measured at extreme points of the space bounded by the end positions of the top and bottom carriages, and the position of the r-meter sensor.

A hydraulic conveyer tube 20 (Fig. 2) serves to transfer sources from the receiving pool to the pool in the shielded chamber, and back again. The tube has an I. D. of 37 mm, and is laid horizontally at a height of 200 mm from the pool bottom. In both pools the tube terminates in a funnel 2, tee joint 21, and water seal 22. The tee joints also receives piping from the centrifugal pump.

The control panel in the shielded room 28 controls displacement of mechanisms in the chamber (frame for

assembling and withdrawing irradiators, bottom carriage of gamma field measuring arrangement) and controls the shielding steel door.

Interlocks are provided to prevent the frame from being raised when the shielded door is open and to keep it closed during exposures or when the frame is raised up from the pool, and also to prevent the frame from being raised or the door from being closed if an operator is present in the room.

The control panel has light signals for flashing the positions of the shielded door (open or closed), of the frame 19 over the pool in steps of 10 cm, of displacements of the bottom carriage (see Fig. 3) in steps of 10 cm, and for signaling changes in the pool water level should the latter drop below the present level.

An operator standing in the gamma facility room can carry out various operations in the shielded chamber with the source raised up by means of the through-wall manipulator: the position of the object to be irradiated or the position of the sensor can be adjusted with respect to the irradiator; irradiators can be loaded with sources or sources withdrawn; the configuration of the irradiator can be modified, etc.

Activities and events in the chamber can be monitored via the PTU-4 closed TV circuit (27) or the OSP-400 M viewing window (see Fig. 2).

The shielded chamber can handle not only irradiation of bulky objects (over 120 liters) but also experimental research projects where various irradiator shapes are to be simulated.

L. S. Lur'e, V. G. Khrushchev,
V. S. Eliseev, and S. V. Kuznetsov

UPDATING THE GUT-Co-400 GAMMA-THERAPY MACHINE

Translated from Atomnaya Énergiya, Vol. 19, No. 2,
pp. 216-217, August, 1965

168 gamma-therapy facilities of the GUT-Co-400 type with 250-Ci Co^{60} sources, designed for radiation treatment of malignancy patients, have been installed in public health clinics and institutions throughout the USSR over the period from 1953 through 1961; some of them have been exported. These machines have played a prominent role in the development of today's outlook on radiotherapy of oncological diseases, have met the basic demand in this form of treatment, and have provided a foundation for the design of new and more powerful gamma-therapeutic facilities.

Even though Soviet industry is now manufacturing the Luch and Rokus gamma-therapy machines on a regular basis, a decision was adopted to modernize GUT-Co-400 machines, so that the network of oncological dispensaries could be re-equipped in a short time without exorbitant capital expenditures, with expanded capacity and improved techniques of radiotherapy.

The requisite updating work on the machine was carried out in 1964 at the All-Union Radiation Technical Research Institute, under the supervision of A. G. Sul'kin. This modernization effort increased the source activity to 1000 Ci in the head of the machine, and improvements in the shielding of both patient and attendants were achieved. A diaphragm replaces the tubes in the modernized head, so that a wide range of radiation fields can be selected from and the relative dose level at the skin surface can be reduced considerably. The use of a 9 mm diameter Co^{60} source has made it possible to drastically reduce the penumbra.

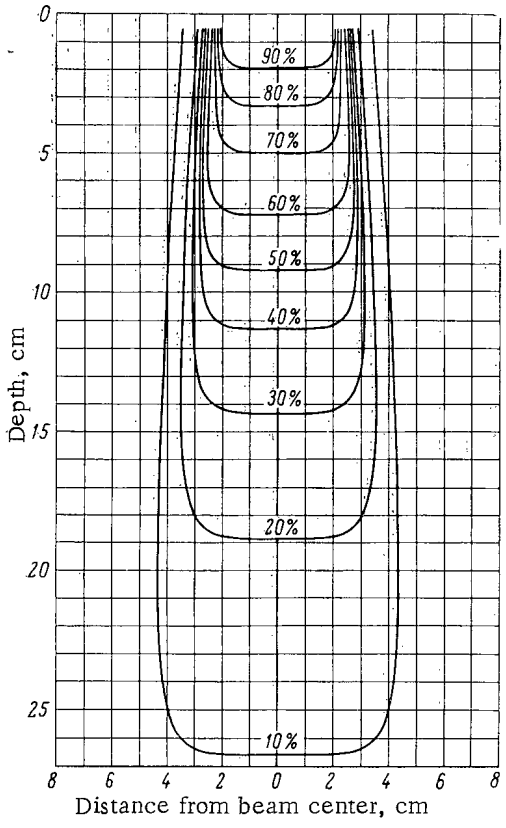

Fig. 1. Isodose distribution for irradiation field 5 by 5 cm at a separation of 50 cm between source and surface of mannikin.

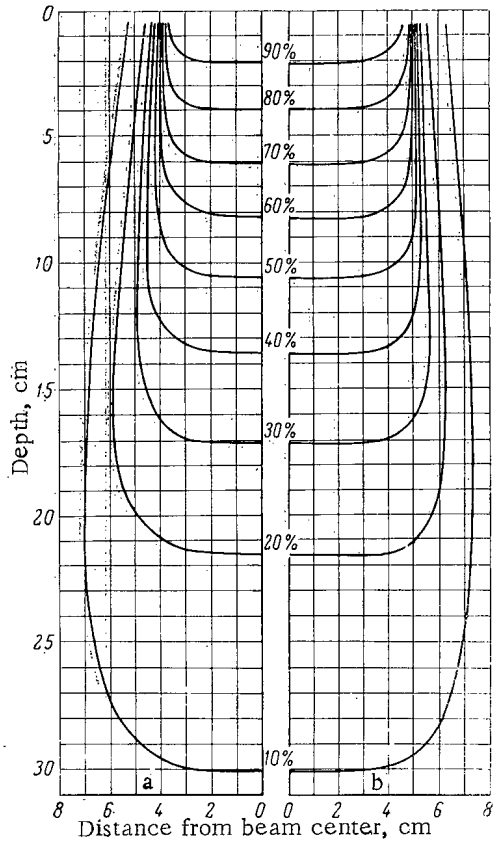

Fig. 2. Isodose distribution for irradiation field 8 by 10 cm at a separation of 60 cm between source and skin of pateint: a) On 8 cm side; b) on 10 cm side.

After an experimental specimen of the modernized radiation head had been assembled, an interdepartmental commission set up by the Ministry of Public Health of the USSR in February-March 1965 performed extensive engineering and dosimetric tests on the equipment and approved the design solution as a successful modernization of the radiation head meeting the requirements set. Close attention was given to the operating conditions to be faced by medical personnel, and the superiority of the modernized equipment over the old model was acknowledged. In the new model it is much easier to establish the required irradiation fields by adjusting the movable diaphragm; the source–skin separation can be set for skin-focus separations of 50, 60, and 75 cm by means of an optical range finder to within ± 2 mm accuracy, the dose rate at a distance of one meter from the surface of the radiation head never rises above 1 mr/h, allowing doctors and nurses to work with complete safety. Several thousand operating cycles with the Co^{60} source in motion caused no perceptible changes in the source parts, and the reliability of the source is acceptable.

A DIM-60 dosimeter was employed in dosimetric studies of the irradiation fields; photometric measurements were taken. Figs. 1 and 2 show isodose distributions for the fields of 5 by 5 cm and 8 by 10 cm at a spacing of 50 and 60 cm, respectively, between source and mannikin surface. The isodose distribution was shown to be similar to the isodose distributions of the Luch gamma-therapy machines for those dose fields.

V. N.

A NEW POLISH RADIATION CHAMBER*

Translated from Atomnaya Énergiya, Vol. 19, No. 2,
pp. 217-219, August, 1965

A chamber for work with radiation sources of very high activity (up to 20 kilocuries) is being built at the Radiation Chemistry Department of Lodz Polytechnic Institute. A novel and intriguing feature is the pneumatic system in use for conveying radioactive preparations.

The following requirements were imposed on the plans for the chamber: ease and simplicity in maintenance and operation, complete radiation safety, guaranteed reliability of all operations, control over the radiation dose in the experimental space, safe and simply delivery of sources to the chamber, use of locally available materials, minimized construction costs. These conditions were determining factors in the design of the chamber, in the choice of operating conditions, and in the choice of a pneumatic control system.

The radiation laboratory (Fig. 1) consists of an exposure chamber, the labyrinth leading to the chamber, a control panel, a preparation laboratory, and a loading container. Ordinary concrete shields the chamber, giving the uniformity required of the massive walls; a recess above the service chamber is filled with cast iron shot (granules to 5 mm size).

A cylindrical well built to accommodate the main container is located in the floor of the service (exposure) chamber. The walls of this well are made of special water-resistant concrete to keep out ground water. A well for the loading container is made in the floor of the service chamber. A 25 mm diameter hole on the axis of this well and running the entire length is used for loading and discharging radiation sources. This loading well is covered by a steel plate, and the hole is blinded by a steel slide.

Mechanical System. The principal container rests in the well built in the exposure chamber, and each of its 20 channels contains a 1500 gm-equiv. Ra source in an acid-resistant holder.

* A. Stanek and L. Szymendera, Postepy Techniki Jadrowej, 8, No. 12, 1111 (1964).

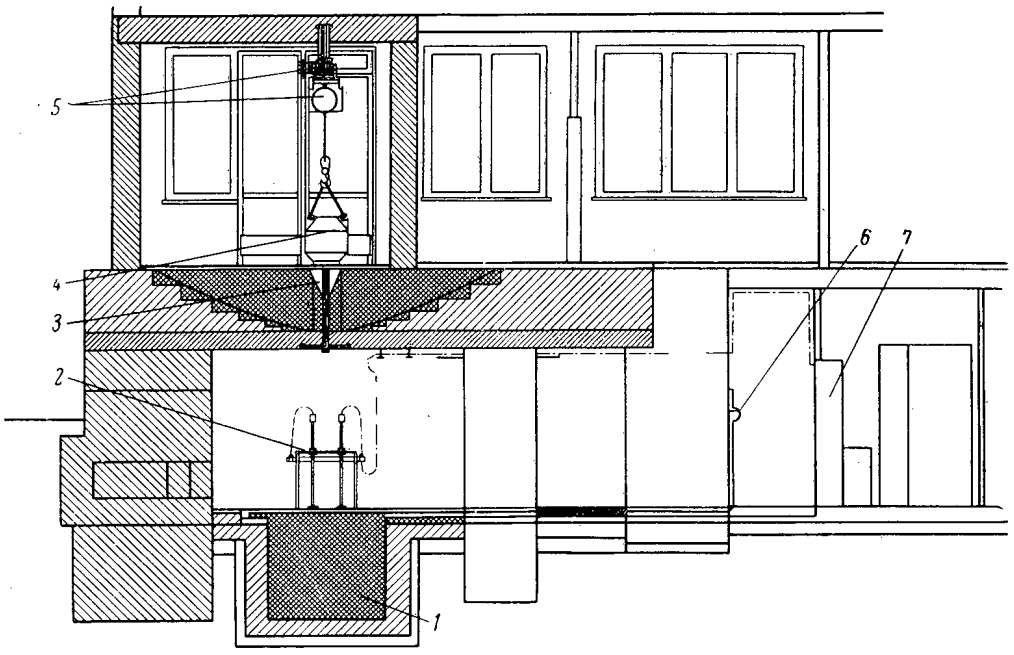

Fig. 1. Complex of rooms serving radiation chamber (seen in section): 1) principal container; 2) exposure table; 3) loading well; 4) loading container; 5) hoist; 6) compressed-air distributor; 7) control panel.

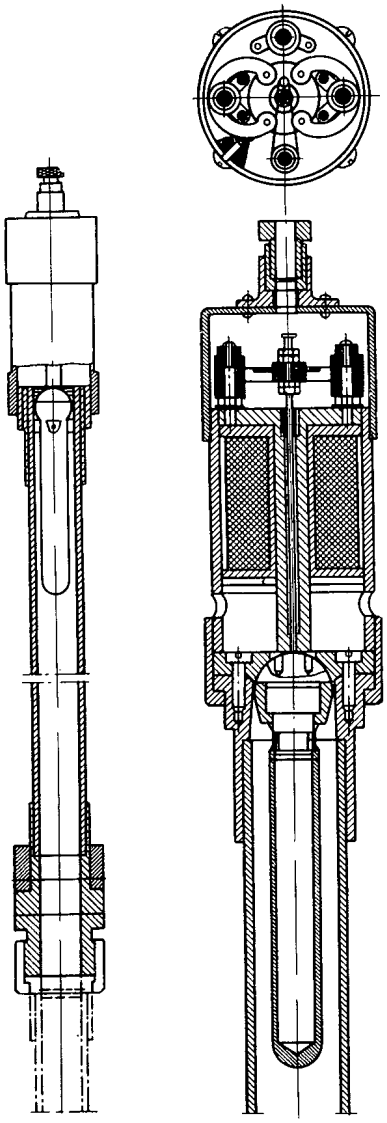

Fig. 2. Exposure head.

The low point on the channel is the off position of the source. A layer of cast iron shot filling up the container keeps the dose rate at the surface within tolerances.

An irradiation table is mounted on the principal source container. The exposure head, which connects to the channels of the principal container, is coupled by flexible hose to the irradiation table plate. The head is fixed in different positions on that plate depnding on the dose rate required for particular experiments. The exposure head terminates in a set of electromagnetic latches.

Sources and their holders are supported in the head by a pressure differential (the electromagnet is not required for this purpose). To set up the pressure difference needed to release or to hold the sources, compressed air is fed to each channel through a tube 12 mm in diameter. A model of the service table equipped with light flashing indicators giving the positions of sources is mounted on the control panel. When the control button for any one of the channels is pushed, an electromagnetic valve is actuated to open the flow of compressed air to the channel. The air carries the source holder down the channel, and then through the flexible coupling into the head resting on the table. The channel terminates in the exposure head in the form of a tapered seat.

The lid of the source holder is spherically shaped. At the end of its travel the source holder lands in the tapered seat and cuts off access of air. During the irradiation, no matter what system is used to hold the sources in place, the source holder plug works against a plunger which sends an electric pulse to the alarm annunciation system on the control panel, thus actuating safety equipment.

When the experiment is over, source holders with sources may be released by de-energizing the electromagnetic latch or by closing the electromagnetic valve; the holders may be released in succession or in batches, and fall by their own weight back to the bottom of the channels in the principal container.

Dosimetric equipment indicating the activity of the emitter in the operating container is installed in the container.

To assure safe operation, the header admitting air to the 20 tubes connected to the channels has a stop valve at the entrance; this valve is controlled by the safety alarm system. Safety, alarm, and braking actions reduce to two conditions: 1) an interlock against source travel to the operating position if people are near the exposure container; 2) prevention of access to the chamber during exposures. The first condition is brought about by direct monitoring, the second by special equipment built into the doors between the control room and the labyrinth passage. When the dorrs are opened (e. g. during preparations for the experiment) the circuit of the set of electromagnetic latches located in the door handle is opened, thereby cutting off the flow of compressed air to the valve, and the source holders drop back instantaneously to storage position.

Principal Container. This can is made of acid-resistant steel and is a welded vessel tested for pressure tightness. 20 channels of acid-resistant tubes, 25 mm I. D., are built into the container, which is 1450 mm in diameter and 1400 mm high. A holder accommodating the radioactive source is located at the bottom of the channel. The channels screw into the container lid symmetrically in 18° steps over the 400 mm diameter. The other end of the channel leads out to the annulus winding around the container lid.

There are several choices in mounting the exposure heads on the plate of the exposure table: a) 5 sources on a circle 100 mm in diameter spaced every 72°; b) 10 sources on a circle 200 mm in diameter spaced every 36°; c) 20 sources on a circle 400 mm in diameter spaced every 18°; d) 20 sources on a circle 700 mm in diameter spaced every 18°. The dose rate at the center of the exposure table will be, respectively: a)25000 r/h; b) 12500 r/h; c) 6250 r/h; d) 2000 r/h. The exposure heads are connected to the channel outlets of the principal container by flexible

tubular leaktight joints. The flexible joints allow the head mounting on the plate a certain degree of freedom depending on the operating conditions and the required isodose distribution.

Exposure Heads (Fig. 2). These heads are the terminations of the channels where the radiation sources are found during the exposure. The support for the exposure head is a coupling member running in a groove in the table plate. A tube 25 mm in diameter ending in a screw which has an annulus with a tapered opening connects up to its respective coupling member. The compressed air used to raise the source holder passes through the central hole in the screw annulus into the volume under the electromagnetic winding, and from there through six holes to the surface. The tapered seat in the annulus and the spherical plug seals off the air, so that very little compressed air is needed to support the source holder. The annulus simultaneously forms part of the electromagnetic circuit, and the source-holder plug bears against it as part of the system in which the electromagnet holds the sources in place.

The Source Holder is made of 1Kh18N9T acid-resistant stainless steel, the plug is made of Armco iron clad with cadmium 15 m* thick. The cadmium layer protects the plug against corrosive attack and simultaneously provides the required residual magnetization. The external source-holder geometry is decided by the interaction of the systems: source-holder–channel; holder–flexible hose; source-holder–exposure head; and satisfies the conditions: a) correct displacement of the source holder; b) minimizing the effort required to support the source holder (air compression); c) correct interaction of system for admitting and shutting off air (ball and cone); d) reliability of magnetic path. The correct choice of external source-holder size was confirmed by analog tests.

Pneumatic conveying of the sources makes it possible to keep the exposure head from being blocked by mechanical parts and keeps ready access open to the experiment space.

D. K.

* As in Russian original–Publisher's note.

1964 PICTURE OF THE URANIUM INDUSTRY IN THE CAPITALIST COUNTRIES

Translated from Atomnaya Énergiya, Vol. 19, No. 2,
pp. 219-224, August, 1965

Following the trend of the preceding four years, the position of the uranium industry in capitalist countries is still characterized by a supply still far out in front of the demand, curtailment of uranium ore mining operations and of concentrate production, closing down of mines and uranium concentrate processing plants, those plants still open operating well below capacity, a sluggish business picture, and a low price level on the free market. Military needs are now completely covered by deliveries under contracts already in force, and the excess is shunted off to strategic reserves. Industrial nuclear power, potentially the greatest consumer of uranium, has developed at a far slower pace to date than was anticipated in the mid-fifties. A comparison of published estimates indicates that the semiannual demand for uranium concentrates over the past 6 years (1959-1964) was 27-28 thousand tons U_3O_8, while the production of U_3O_8 ran over 33 thousand tons according to official figures. Government stockpiles will total 80 to 100 thousand tons U_3O_8 by 1970, at a total value of 1 billion dollars (USA: 50 to 60, Britain: 15-20, France: 5-7, Canada: 2-3, Australia: 2.5 thousand tons).

Uranium is currently one of the most abundant elements known. Uranium deposits are proved in over 50 countries. Reliable and probable U_3O_8 reserves in ores containing not less than 0.01% uranium constitute about 4 million tons, which is more than double the total demand extrapolated to the year 2000. Of course, industrial pay-ore reserves (this category present includes ores profitable for mining and processing when the market price of concentrate runs 11 to 20 dollars per kg U_3O_8 in the ore) do not surmount the figure of 600 thousand tons U_3O_8 in this reckoning (see Table 1).

Improvement of the industrial outlook for nuclear power development over the past two years, and a reconsideration, in 1964, of estimates of the tempos of growth in uranium demand for nuclear power stations (higher demands are expected) had lent added reality to the suggestion voiced back in 1963 that uranium demand would overtake and surpass the supply during the second half of the seventies. Data reported at the Third Geneva conference in 1964 put added emphasis on the danger of a possible shortage of cheap uranium and a price rise in the following decade if intensive prospecting and geological exploration work is not resumed in the immediate future. This viewpoint has been most clearly reflected in papers presented by French specialists (and somewhat earlier by Euratom as a whole), as well as British and American specialists, i.e., by representatives of those countries which will be the prime consumers of atomic raw material in the next two decades, but which as a rule do not have at their disposal sufficient reserves of high-grade uranium ores on their own soil.

The challenges to expand prospecting for high-grade uranium ore deposits is accounted for not alone by the accelerated rates of nuclear power development and by the dwindling of proved reserves of uranium ores to almost one half in the 1959-1964 period. The present situation sees various types of power reactors (water-cooled, water-moderated reactors and gas-cooled graphite-moderated reactors) which have achieved competitive operation with up-to-date fossile-fuel power stations, at least in regions where fossil fuels are expensive. The need is now felt to develop basic trends in technical progress in reactor design with a long-term perspective, i.e., to decide on which reactor types should be the focus of concentrated research and development efforts. There are two avenues open: either that of building improved converter reactors capable of more fully utilizing atomic raw materials reserves, and thus superior in that respect to current reactor types, or immediately working on the development of fast breeders. The latest water-cooled water-moderated reactors and gas-graphite reactors do not utilize atomic raw materials in the most efficient way. They are profitable only when reasonably cheap uranium concentrate is used, such as can be obtained by working deposits of high-grade ore. Should it turn out that the reserves of high-grade ore are much larger than now known, and are sufficient to cover the needs of nuclear power industry for the next several decades, then the development of fast breeders to open the way for profitable exploitation of very-low-grade uranium ores need not be pushed, in the view of some specialists.

TABLE 1. Industrial Uranium Reserves in the Capitalist Countries [1-17]

Country	Ore reserves, 10^6 tons	U_3O_8 content in ore		Data at beginning of year
		%	10^3 tons	
Total			570-600	1965
Canada	204.1	0.12	187.8	1964
USA	57.2	0.24	137.9*	1965
South Africa	680.0	0.02-0.03	135.7†	1964
France	23.6	0.16	33.0	1964
India	20.0	0.08-0.1	15.0	1964
Australia	10-14	0.1-0.15	14.2	1964
Spain	8.1	0.13	10.5	1965
Brazil			10.0	1962
Congo (Leopoldville)	2.7	0.35	9.4	1959
Southwest Africa	3-5	0.22	7-10	1962
Portugal	3.9	0.14	5.8	1964
Sweden		0.01-0.1	5.4	1962
Gabon	20.0	0.5	4.8‡	1964
Argentina	2-4	0.1-0.2	4.0	1964
Others			13-16	1965

* We may also count in stockpiles at concentrate mills: 771,000 tons of ore averaging 0.4% U_3O_8, i.e., 3000 tons U_3O_8.
† Uranium only, obtainable as a by-product in gold mining.
‡ Only in ores containing 0.5% U_3O_8.

Since prospecting for new uranium deposits had been sharply curtailed ten years back in the major countries, it is impossible at this juncture to get a complete picture of the reserves of high-grade ore in the capitalist countries so as to provide a reasonable basis for deciding policy in reactor design. From the reports submitted to the 1964 Geneva conference, we would gather that the geological prerequisites for at least doubling the proved reserves of high-grade ores are definitely within reach. But this could be confirmed only be a detailed geological exploration project.

Government subsidies for uranium prospecting have been cut back in most countries, and have been discontinued entirely in Canada, the USA, the Union of South Africa, and Australia. Private firms are not receiving any economic stimuli to undertake detailed prospecting and exploration activities even in districts of real promise, since the major consumers (the American and British governments) have completely suspended purchases. Prices on the free market have plummeted downward in the same time, since firms in Canada, the USA, and in South Africa to some extent, had paid off their original capital investments during the period when uranium concentrates were being stockpiled for military purposes, and are now in a position to sell concentrate at very low prices only slightly above operating costs. All the needs of nuclear power for at least the next 10 years can be covered by the supply available from the most profitable uranium enterprises.

Canada retains the leading place in pay-ore reserves. According to an estimate by the mining authority of Canada, preliminary exploration of no more than the best known uranium deposits shows the country's uranium ore reserves profitable for operations with U_3O_8 priced at 11 to 22 dollars per kg to total 453,600 tons U_3O_8, which is 2.4 times greater than current positive and probable pay reserves. If we do not consider ores which could be profitably mined and processed with U_3O_8 priced as high as 44 dollars per kg (for Canadian mining and market conditions, this would mean a minimum of 0.01% U_3O_8 in the ores), then the total reserves of these ores could be estimated at one million tons U_3O_8 (and 635,000 tons ThO_2) when potential reserves are thrown in [1].

Note that while positive and probable reserves remained at the level of previous years at some of the leading mines still in operation in Canada [18], proved ore reserves in the region of the "Nordic" mine operation increased by 46% in 1964. According to a press release by the Rio Algom firm over 50% of the territory it owns in the Elliott Lake district remains to be explored [19].

The Canadian Mokta Mining Corp., financed by French capital, intends to spend 250,000 dollars in the next 4 years in uranium prospecting in Canada. In 1964, the firm discovered a uranium deposit in Labrador and has applied

TABLE 2. Uranium Ore Mined in the Six Major Capitalist Countries, in Millions of Tons [1, 3, 4, 30]

Country	Average U_3O_8 content	1957	1959	1961	1963	1964*
USA†	0.26	3.0	6.2	7.3	5.4	4.8
Canada	0.12	6.0	12.7	7.2	5.6	5.2
U. South Africa‡	0.03-0.033	20.0	22.3	13.6	12.6	12.0
Australia* *	0.15-0.2	0.2	0.7	0.9	0.6	0.1
France	0.16-0.2		0.6	0.8	0.8	0.7

* Tentative data.
† Amount shipped from mines.
‡ Amount processed in mills.
* * Estimated.

for licenses to prospect uranium over 100 tracts in northern Saskatchewan [20].

The president of the state-owned Eldorado Mining and Refining Ltd. came out publicly for the immediate resumption of uranium exploration activities in Canada and for the preparation of new high-grade ore deposits for mining operations [1].

The 1962-1964 increase in proved pay-ore reserves in the USA totaled 20,600 tons U_3O_8, with an average of 6,900 tons U_3O_8 annually, as against 18,200 tons U_3O_8 a year in the 1958-1960 period [3, 14]. The 1964 increase in reserves (5,100 tons U_3O_8) reflects more than anything else the usual more-exact picture of reserves as deposits are worked. No resumption of prospecting for new deposits has been announced, but preparations are apparently underway [21].

There has been a report that the Union of South Africa atomic energy authority is beginning the "biggest exploration project in history" in South Africa. Proved uranium reserves profitable for working when the price of U_3O_8 is anywhere in the range up to 17.6 dollars per kg at present hardly surpass 130,000 tons in that country, as against a figure of 324,000 tons U_3O_8 back in 1958-1959.

France is presently conducting the most energetic program of geological prospecting and exploration, in the Malagasy Republic, in Gabon, the Central African Republic, and Niger. French specialists have undertaken a study of promising uranium ore districts in Brazil, Argentina, Mexico. French companies are promoting projects in preparation to exploit these uranium deposits, to built mines and processing mills in those countries, drawing in French investment capital. France is the only one of the major uranium producer countries in which proved reserves of payable uranium ores have substantially increased over the past few years. Prospecting for new deposits is continuing in metropolitan France. A maximum program is now under consideration: how to raise the level of proved uranium payable reserves in the country to 50,000 tons U_3O_8 [6].

Uranium prospecting continues in high gear in India. New deposits were discovered in 1964 in several regions of the country, and ores in some instances were equal in quality to the Jaduguda ores now being prepared for industrial exploitation [22]. Proved uranium reserves are sufficient to supply the needs of nuclear power generating stations with total output of 9 to 10 million kW [23].

Proved uranium ore reserves in Spain have risen again, but not as high as in 1963. Prospecting for deposits is being continued in the provinces of Catalonia, Aragon, and Valencia [24].

Data on uranium reserves at the Feldberg deposit near Menzenschwant (West Germany) have been published. This deposit was discovered in 1947, but publicity on it was circulated only in 1962. Uranium reserves are estimated as follows (in thousands of tons): positive: 0.2 to 0.3; probable: 1.0; possible: 2.0 to 3.0. The ore is high-grade with uranium content to 3-4%. The deposit is located in a district where mining is forbidden. Possibilities of mining operations are being studied, nevertheless [25].

In February 1964, the government of Cameroun reported finding a uranium deposit ("large quantities of high-grade ore") near Poli in the department of Benoue. Projects for detailed exploration are under consideration [26].

During the past year uranium deposits have been discovered in Saudi Arabia (northeast of the port Yanbo on the shores of the Red Sea, 380 km to the north of Jidda), in Iran (in the Yazdan district in the Shirkush mountains), in Japan (not far from Ningyo Pass in the east: 3 million tons of ore).

Additional geological research efforts by the Danish atomic commission in Greenland in the summer of 1964 confirmed extensive uranium (and thorium) ores in the Kvarnefeldt region near Narsak in the south. Encouraging results in the development of practical ore extraction methods at the Kvarnefeldt mine are reported [27].

Four deposits of "high-grade" ore have been discovered in the UAR: in the east (near Quseir on the Red Sea and at Wadi-el-Gemal), in the west (north of the Birket-Karun lake), and between Port Said and Damietta. Preliminary data indicate 2,000 tons of uranium and 25,000 tons of thorium reserves in the last district [28].

TABLE 3. Production of Uranium Concentrates in the Capitalist Countries,* in Tons U_3O_8 [1, 3, 4, 30-32]

Country	1957	1959	1961	1963	1964†
Total†	21,700	39,500	33,000	27,600	23,000
USA‡	7,840	14,870	15,785	12,900	10,748
Canada	5,950	14,420	8,746	7,592	6,286
U. South Africa	5,170	5,850	4,971	4,116	4,043
France**	296	731	1,187	1,022	1,000
Gabon			321	520	475
Australia	360†	1,000†	1,350	1,089	250
Malagasy	63	89	72	95	80
Republic**			55	75	75
			1,492††		
Spain†					
Portugal					
West Germany†		3	11	10	10
Argentina†	18	12	5	4	5
Italy	1	2			
Congo (Leopoldville)	1,500	2,110			
Zambia	25	38			

* Aside from the nations listed above, uranium raw materials are mined in small quantities in India, Japan, Brazil, Mexico, and the UAR. In different years small quantities of uranium ore have been found in Finland, Sweden, Mozambique, Morocco, Colombia, Peru, and other countries.

† Estimate

‡ USAEC purchases

** Uranium metal content in the concentrates.

†† USA imports. Weight of uranium concentration containing approximately 10% U_3O_8 indicated.

The minister of fuel and power in Turkey announced that the country possesses "rich uranium reserves" (1.5 million ton of ore) at Aydin, Demirkapi, and Gördes [29].

The Israeli geological service has begun prospecting for phosphates containing uranium in the southern part of the country [25].

The cutback in uranium ore mining operations continues (Table 2). About 23 million tons of ore were mined in 1964, although the productivity of uranium mines in the capitalist countries stood around 50 million tons of ore annually back in 1959. The number of mines in operation in the USA shrank from 1000 to 700, in Canada from 25 down to 4, in South Africa from 27 to 10. All six mines in Australia have been shut down.

Tentative data indicate that the production of uranium concentrates dropped by 4,600 tons U_3O_8 in 1964 as compared to 1963, or by 16,500 tons when compared to 1959, the year of peak level (Table 3). This is due chiefly to curtailment in U_3O_8 imports in the USA from the 1959 figure of 16,900 tons to 5,000 tons in 1964. Imports of uranium concentrates in the USA under government contracts will be completely dried up by 1967. A law actually prohibiting the use of imported uranium concentrations at American nuclear power stations was passed in 1964.

The USA government decision to stop purchasing dealt its worst blow to Canadian producers. Only 3 of a total of 19 uranium concentrate mills in Canada are still on stream. Most of the first-rate plants with large capital investments have closed down after 1 to 2 years in operation. The Canadian government made an attempt in 1963 to ease the position of its national uranium industry. A program for adding to the government stockpile was initiated so as to aid the most profitable enterprises which, by remaining afloat in the production sphere, would retain their ability to compete later on the world uranium market. But the government gave up this program as too costly after 25 million Canadian dollars had been poured into it. This means that in 1968 possibly only one plant will still be producing uranium concentrates.

Nine uranium concentrate mills closed down in 1964 (Table 4). The productive capacity of the companies now active in this field is 45% below the total capacity of all plants and facilities built in the capitalist countries in the pre-war period. Only two new plants were built in 1964: one at Ranstad in Sweden, with a capacity of 125 tons of U_3O_8 annually, scheduled to go into operation in the latter half of 1965 (Swedish shales contain about a million tons of U_3O_8) [24], another in the Jaduguda region in India, with an annual capacity of 200 tons U_3O_8, to go into operation sometime in 1967.

Spain's needs for uranium to supply three nuclear power stations are estimated at 280 to 300 tons, which is equivalent to 330-350 tons U_3O_8. This explains why the construction of a second uranium concentrate mill is being planned, with a projected capacity of 1000 tons of ore daily, containing an average of 0.12% U_3O_8 to account for an annual output of 200 tons U_3O_8. The total yield of Spanish companies is 400 tons U_3O_8 per year [4, 24].

Some new data have appeared on uranium ore mining costs and concentrate production costs. Production costs published by Canadian firms for concentrates usually include the cost of operations prior to processing such as mining, beneficiation, and mine operating costs, but most frequently fail to include the cost of geological prospecting and exploration, depreciation writeoffs, overhead, interest on capital, taxes, or rent on property. In some cases this results

TABLE 4. Number and Capacities of Uranium Ore Processing Plants [1, 3, 4, 9, 30, 31]

Country	Operating				Under construction or planned			Total number of plants at beginning of 1965*
	1960	1964	1965	1968 (estimated)	1960	1964	1965	
Total at beginning of year	83	61	52	39-40	10	8	8	93
USA	24	21	20	13-14	2	–	–	28 (18.0)
South Africa	17	13	10	5	–	–	–	17 (6.5)
Canada	17	7	3	2	–	–	–	19 (16.0)
France	5	5	5	4	–	–	–	5 (1.6)
Australia	5	2	1	1	–	–	–	5 (1.5)
Gabon†	–	1	1	1	1	–	–	1 (0.6)
Malagasy‡	1	1	1	1	–	–	–	1 (0.12)
India	1**	1**	1**	1	1	1	1	2 (0.3)
Sweden	1**	–	–	1	1	1	1	2 (0.14)
Spain	1	1	1	1	–	1	1	1 (0.2)
Portugal	1	1	1	1	1	–	–	1 (0.1)
Argentina††	2	2	2	2	–	1	1	1 (0.10)
West Germany**	1	1	1	1	–	–	–	1 (0.02)
Italy††	1	1	1	1	–	–	–	1 (0.01)
Japan††	1	1	1	1	1	1	1	1 (0.01)
UAR††	–	1	1	1	–	–	–	1 (0.01)
Mexico††	1	1	1	1	2	2	2	1 (0.02)
Brazil††	1	1	1	1	1	1	1	1 (0.02)
Congo (Leopoldville)	1	–	–	–	–	–	–	1 (2.5)
Finland**	1	–	–	–	–	–	–	1 (0.05)
Zambia**	1	–	–	–	–	–	–	1 (0.05)
Total capacity, 10^3 tons U_3O_8 annually	44	31	25	17-18				47.85

*Including number closed down or being built (total capacity in 10^3 tons U_3O_8 annually in parentheses)
†Low-grade concentrates (≈30% U_3O_8) in production; to be processed further in France.
‡Uranium-thorianite concentrates production; processed further in France.
**Pilot plant operation
††Experimental plant.

TABLE 5. USAEC Purchase Prices for Uranium Concentrates, Dollars per kg U_3O_8 [8, 14, 36]

Producers	1956/57	1959/60	1961/62	1963/64
American	23.75	19.78	18.04	17.67
Canadian	23.72	24.29	21.89	19.23
Miscellaneous*	25.92	26.42	25.26	24.9
Average	24.27	22.42	20.13	19.34

*UAR, Australia, Portugal (until 1963), Congo (till 1961).

in figures far too below the actual costs, particularly in view of the short depreciation period prevalent in that field of the country's industry. Production costs for uranium concentrations in the Elliott Lake region fluctuate between 7 and 11 dollars a ton, or 7.7 and 12.1 dollars per kg U_3O_8, mining costs run around 4.5 dollars per ton, and ore beneficiation processes cost slightly less. Average production costs in the Bancroft and Beaver Lodge region run slightly higher. Canadian specialists therefore feel that only a few companied are capable of offering concentrate at a price of 7-8 dollars per kg U_3O_8, as was indeed the case on the "free" market in 1963-1964 [33, 34].

The uranium oxide content in ores of deposits worked in France fluctuates between 0.11% and 0.19%. The cut-off grade of the ore is 0.06-0.08% U_3O_8. Deposits are worked down to a depth of 360 meters (from 36 meters at the shallowest). Open-pit mining accounts for 15% of the ore. Mining costs and costs for hauling mined ore to uranium concentrate mills run 5.5 to 8.8 dollars per kg U_3O_8, and beneficiation costs excluding capital and tax costs run 3.52 to 4.4 dollars per kg U_3O_8, averaging 11 dollars per kg U_3O_8 in standard concentrate. Concentrate purchasing prices in France dropped 20% in 1964, ending up at the level of American internal prices (17.6 dollars per kg U_3O_8) [4].

Prospecting, careful exploration, and mining preparations for 4.6 million tons of ore of 0.13% average U_3O_8 content, i.e., for 6,000 tons U_3O_8, cost 5.88 million dollars in Spain, viz. 0.99 dollars per kg U_3O_8 in the ore. Mining costs for these ores were estimated at 1.254 dollar per kg U_3O_8, and beneficiation costs at 7.7 dollars per kg U_3O_8, i.e., on the whole 9.944 dollars per kg U_3O_8 in concentrate form. Spain is therefore considering its chances of competing on the "free" market for atomic raw materials [4].

The USAEC proposes that the average purchase price for uranium concentrate on the internal market be 12.1 to 13.2 dollars per kg U_3O_8 in the 1969-1970 period [3]. Since the price is arrived at by calculating 85% of the 1963-1968 production costs plus 3.52 dollars per kg U_3O_8, average production costs for uranium concentrates in the USA will run 10 to 11 dollars per kg U_3O_8 by the end of the decade.

In the last two years, uranium ore processing techniques in the capitalist countries underwent no substantial changes. Several production improvements were developed which will find successful application in the future. At operating plants, the Canadian ones for instance, no basic changes in process flowsheets will be made since the added capital investment required could hardly be offset given the slump on the current market, or within the time left under existing contracts.

The most significant technological innovations seen in industrial practice in 1964 may be found in an experimental uranium oxide plant put into operation in South Africa to produce nuclear grade (99.99% pure) uranium oxide directly at the Buffelfontein standard concentrates mill [35]. South Africa expects to export 99.99% U_3O_8 concentrate at the same prices as the 75-90% U_3O_8 concentrate.

The Canadian Stanrock Uranium Mines Ltd. has introduced a new technology for leaching uranium from ore, known as bacterial leaching, an outcome of the natural action of bacteria on sulfide ores. This method allows for low-cost extraction of uranium from ores, mainly from fine wastes left underground [1].

Prices of uranium concentrates continued to decline (Table 5) as a result of the increase in supply over demand and the trend to survival of only the most profitable mines and mills.

The Canadian Denison Mines Ltd. is conducting talks with the French Commissariat de l'Energie Atomique aiming at an agreement under which France will receive 45,400 tons U_3O_8 over the next 25 years. French reports place the price at 11.77 dollars per kg U_3O_8, Canadian figures are 13.97 to 15.07 dollars per kg U_3O_8. In 1960 Canada sold Britain 10,900 tons U_3O_8 at an average price of 11.07 dollars per kg U_3O_8.

V. D. Andreev

LITERATURE CITED

1. J. Griffith, Canadian Mining J., 86, 113 (1965).
2. Mining J., 263, 221 (1964).
3. USAEC. Annual Report to Congress for 1964, Washington (1965), p. 42.
4. J. Sherman, Engng. and Mining J., 166, 125 (1965).
5. Geneva 1964 Conference on the Peaceful Uses of Atomic Energy, Report No. 24 (Canada).
6. Geneva 1964 Conference on the Peaceful Uses of Atomic Energy, Report No. 72 (France).
7. Geneva 1964 Conference on the Peaceful Uses of Atomic Energy, Report No. 164 (Britain).
8. Geneva 1964 Conference on the Peaceful Uses of Atomic Energy, Report No. 256 (USA).
9. Geneva 1964 Conference on the Peaceful Uses of Atomic Energy, Report No. 504 (Portugal).
10. Geneva 1964 Conference on the Peaceful Uses of Atomic Energy, Report No. 715 (Argentina).
11. Geneva 1964 Conference on the Peaceful Uses of Atomic Energy, Report No. 752 (India).
12. J. Mabile, Annales des Mines, Janvier, 73 (1965).
13. Z. Éklund, IAEA Bulletin, 6, p. 16 [in Russian edition] (1964).
14. V. D. Andreev, Atomnaya Énergia, 15, 89 (1963).
15. Mining J., 264, 231 (1965).
16. Mining J., 262, 491 (1964).
17. Mineral Trade Notes, 58, 35 (1964).
18. Northern Miner, February 4, 13 (1965).
19. Northern Miner, March 25, 5 (1965).
20. Euronuclear, No. 2, 119 (1965).
21. American Metal Market, February 19, 16 (1965).

22. Mining J., 262, 122 (1964).
23. Mineral Trade Notes, 60, 50 (1965).
24. Euronuclear, No. 2, 117 (1965); Mineral Trade Notes, 60, 28 (1965).
25. Mineral Trade Notes, 58, 35 (1964).
26. Mineral Trade Notes, 58, 45 (1964).
27. TASS Release, November 9, 1964.
28. Mining J., 264, 231 (1965).
29. Euronuclear, No. 2, 116 (1965).
30. V. D. Andreev, Atomnaya Énergiya, 17, 76 (1964).
31. Minerals Yearbook, 1963, Washington (1964), p. 1169.
32. Mines et Metallurgie, No. 3591, 29 (1965).
33. Northern Miner, November 26, 73 (1964).
34. Economist, February 6, 578 (1965).
35. Mining J., 263, 335 (1964).
36. R. Faulkner, USAEC Release, September 16, Washington (1964).

All abbreviations of periodicals in the above bibliography are letter-by-letter transliterations of the abbreviations as given in the original Russian journal. *Some or all of this periodical literature may well be available in English translation.* A complete list of the cover-to-cover English translations appears at the back of this issue.

THE MILLER CONFERENCE [ON RADIATION CHEMISTRY]

Translated from Atomnaya Énergiya, Vol. 19, No. 2,
p. 224, August, 1965

The IV Miller radiation chemistry conference took place in late-April 1965 at Port Marion (North Wales). 100 research scientists from eleven countries: Austria, Britain, Hungary, Canada, Netherlands, Poland, the USSR, the USA, France, West Germany, and Czechoslovakia participated.

Both experimental and theoretical problems in the area of radiation effects on chemical compounds and systems were discussed. The conference agenda specified eight sessions for discussion of: radiation chemistry of aqueous solutions, radiation synthesis and radiation-chemical transformations, pulsed radiolysis, the role of ions and electrons, radiolysis of gaseous systems, etc.

This conference was arranged to be different from other conferences in that no printed papers would be presented. All the reports were given orally. Most of the reports were on the role of elementary particles (electrons, ions, ion radicals, etc.) in radiation-chemical processes. These studies are in progress in many countries (Britain, USSR, USA, France, West Germany, others). But presently available data are inadequate to provide a complete picture of the mechanism involved in radiation-chemical transformations induced by ionizing radiations.

Radiolysis of aqueous solutions received close attention at the conference. Research is being carried on extensively in many countries. Radiolysis of vapor systems is also the subject of many research projects in Britain, USSR, USA, France, West Germany, and elsewhere.

Radiation synthesis was reflected only cursorily at the conference. There were no original reports on the topic. This sector of radiation chemistry is developing at a very slow pace. Several interesting reports were given at the conference on reactions on the surface of solids.

The practical use of radiations in chemistry was not discussed. The conference was clearly of a theoretical nature. The proceedings of the IV Miller conference will make a valuable contribution to the development of radiation chemistry theory.

E. Volkova

BIBLIOGRAPHY

NEW BOOKS

Translated from Atomnaya Énergiya, Vol. 19, No. 2,
pp. 225-228, August, 1965

State Atom Press [Atomizdat] Releases

V. A. Kravtsov. Massy atomov i energii svyazi yader [Atomic masses and nuclear binding energies]. 1965, 376 pages. 1 ruble, 40 kopeks.

It is not so long ago that only a few sections could be found in texts on nuclear energy dealing with atomic masses and the binding energies of nuclei. At present the rapid development of the subject allows the expansion of this topic into a whole book.

One of the most important experimental characteristics of atomic nuclei eare the atomic masses and the nuclear binding energies computed from them. Once these are known, the energies of nuclear reactions, the stability of nuclei, and other characteristics of practical importance can then be found with ease, and in addition it becomes possible to verify the validity of given models of nuclear structure and even to predict the properties of nuclides not yet discovered.

This book contains numerical tables of the masses of atoms and binding energies of nuclei, plus complete tables of original experimental data from which the masses and binding energies were computed.

A. D. Vlasov. Teoriya lineinykh uskoritelei [Linear accelerator theory]. 1965, 307 pages. 1 ruble.

The development of modern physics would be inconceivable without the use of accelerators of charged particles—devices designed to accelerate electrons, protons, and heavier particles to energies on the order of millions and billions of electron-volts. While these are machines for physics research, accelerators have also met with important applications in medicine (x-ray therapy), industry (in nondestructive flaw detection), chemistry, and geology.

The theory of linear accelerators considers acceleration and focusing of particles, as well as some aspects of the shaping of particle beams before they are injected into the accelerator and after their extraction (prebunching, monochromatization of particle energies). The motion of accelerated particles is in essence inseparable from calculations of the concrete parameters of the accelerating and focusing systems.

The book offers a systematized presentation of the theory of modern linear accelerators. Proton and electron accelerators are discussed along with heavy-ion and multiply-charged-ion accelerators. Focusing techniques described include the highly effective quadrupole focusing in proton accelerators, and methods using longitudinal magnetic fields, grids, or foils. Particular attention is given to high-current high-energy accelerators, to the use of the accelerating field for focusing particles, and to the effect of phase oscillations on radial motion. The discussion of theory is backed up by a treatment of methods used in the design of accelerating and focusing systems, in selecting tolerances, and in optimizing performance variables.

Korroziya konstruktsionnykh materialov vodookhlazhdaemykh reaktorov [Corrosion of structural materials in water-cooled reactors]. A Collection of articles in condensed translations from the English, edited by Candidate Chem. Sci. V. P. Pogodin. 1965, 384 pages. 1 ruble.

Corrosion behavior is a prime factor in the choice of structural materials for nuclear reactors, for not only the operational reliability of reactor facilities but also radiation safety in operation and in maintenance depend on corrosion control. The study of the mechanism of corrosive attack on structural materials is clearly of great importance in programs to cope with undesirable corrosion phenomena such as can be encountered in reactor installations. A knowledge of the corrosion mechanism is also vital in research and development work on new corrosion-resistant materials which might provide a solution to the urgent problem of lengthening the service lives of details and assemblies in reactor installations.

This collection of articles covers corrosion of aluminum alloys, carbon steels, stainless steels, and some other materials used in reactor design and reactor plant design. New data on the development of corrosion-resistant aluminum alloys and on their corrosion mechanisms are presented.

Factors affecting corrosion and corrosion cracking of stainless steels in water and steam at high temperatures are discussed. Studies of the corrosion cracking mechanism relevant to these materials are included.

Specific aspects of corrosion in reactors are also discussed (effect of irradiation, behavior of corrosion products, corrosion accompanying deactivation).

L. S. Gorn and B. I. Khazanov. Registratory intensivnosti izluchenii [Radiation-intensity recording instruments]. 1965, 304 pages. 1 ruble, 13 kopeks.

Radiometric equipment has a prominent place in various fields of science and industry concerned with the study or use of nuclear radiations.

The equipment utilized to measure penetrating radiations consists of three basic parts: detectors, devices for discriminating signals, and recorders. Recorders are practically mandatory for any device, instrument, or facility, and frequently contain a large array of electronic equipment.

This book constitutes an attempt to generalize the material in the literature, accumulated over recent years of experience in the design of recording instrumentation. It reviews the general design principles, the basic elements and building blocks, and the structure of the circuits most widely used in radiation intensity recorders. Some concrete practical circuits are cited in the text.

Close attention is given to the use of transistors in the equipment, and also to special systems, magnetic components, tunnel diodes, and the like.

An extensive bibliography is appended.

B. R. Bergel'son and G. A. Zorikoev. Spravochnik po zashchite ot izlucheniya protyazhennykh istochnikov [Handbook on shielding for extended sources of radiation]. 1965, 175 pages. 1 ruble, 42 kopeks.

Nuclear processes which fulfill the function of sources of radioactive radiations are in widespread use at the present time owing to the vigorous development of nuclear industry. It is difficult to find a field in which radioactive sources are not being used for some scientific, technical, or medical purpose.

Special shielding must be provided, as we know, to protect personnel from the hazards of penetrating radiations whenever and wherever such sources are being handled. The problem of deciding the required size and composition of biological shielding is thus of utmost importance for specialists in many lines of work.

This handbook systematizes and in large measure supplements the equations describing attenuation of unscattered radiation from sources of different geometric configuration in shielding, the results of integrating those equations, and original data required to calculate shielding and basic parameters of gamma-radiation sources. Attenuation functions of unscattered radiation from line, circular, slab, cylindrical, and spherical sources in shielding are assembled. Numerical values of the attenuation functions are graphed for a wide range of variables, so that the field of unscattered radiation can be determined fairly rapidly and exactly in the shielding and beyond the shielding.

The handbook is based on a wealth of data published in the Soviet press and elsewhere.

Foreign Releases

E. Gebhardt and H. D. Seghezzi. Reactorwerkstoffe, Teil 1—Metallische Werkstoffe [German: Reactor materials, part 1. Metals]. B. G. Teubner Verlagsgesellschaft, Stuttgart, 1964, 304 pages.

This book is a very exhaustive and painstakingly compiled handbook, with 11 chapters and a subject index. Eight chapters, each containing data on a particular metal (uranium, plutonium, thorium, zirconium, beryllium, niobium, aluminum, magnesium), all follow a common plan. In each, highly compressed information follows in sequence on the methods used to produce the pure metal and work it, on alloying additives, on structure and crystallization, on the physical, mechanical, and chemical properties, and on radiation stability. The other three chapters offer the reader less complete but just as highly concentrated information on stainless steels (chapter 9), neutron absorbers such as hafnium, cadmium, boron (chapter 10), and liquid-metal coolants (chapter 11).

Each chapter is replete with tables, graphs, and references to the source literature.

H. W. Drawin, P. Felanbok. Data for Plasmas in Local Thermodynamic Equilibrium. Gauthier-Villars. 1965, 503 pages.

The behavior of a plasma in local thermodynamic equilibrium is described by familiar equations: Saha's formula, the Maxwell Distribution, and so forth. But practical utilization of these formulas entails formidable computational difficulties. This reference of tabulated data on plasma in thermodynamic equilibrium was computer-compiled and should go a long way in easing the work load in this area.

The bulk of the book consists of tables enabling users to compute the ionization equilibrium between n-and (n+1)- times ionized atoms of 39 elements ($n_{max} = 4$) at various plasma temperatures T (from 6500° to 139,948°K at a pitch $\Delta T = 5 \cdot 10^{-2}$ T), with the plasma density dependence of the ionization potential taken into account.

The book also contains the following tables.

1. Spectral-energy density of blackbody emission for wavelengths from 50,000 to 1000 A and temperatures from 2520° to 25,200°K.

2. Decrease in plasma ionization potential depending on the effective charge Z on plasma ions and on the density n_e (Z = 1 to 6; $n_e = 1 \cdot 10^{12}$ to $1 \cdot 10^{19}$).

3. Debye radius as a function of temperature T and effective charge Z at various plasma densities (Z = 1 to 10; $n_e = 1 \cdot 10^{11}$ to $3 \cdot 10^{19}$; T = $1 \cdot 10^3$ to $1 \cdot 10^8$ °K).

4. Spectral characteristics of emission of positive crater of a d-c arc struck between two pure carbon electrodes at a normal pressure. This arc is frequently employed as an absolute and relative standard of emission intensity.

5. Statistical weights and ionization potentials of the first six levels of all elements, and miscellaneous tables.

All of the tables are preceded by concise theoretical introductions and appropriate bibliography. The book will prove useful for research in astrophysics and magnetohydrodynamics.

Each chapter is replete with tables, graphs, and references to the source literature.

SOVIET JOURNALS AVAILABLE IN COVER-TO-COVER TRANSLATION

This list includes all Russian journals which—to the publisher's knowledge—were available in cover-to-cover translation on June 30, 1965, or for which definite and immediate plans for cover-to-cover translation had been announced by that date. The list reflects only *current* publication arrangements, but the date and issue listed for first publication refer to translations available from any source. Thus, earlier volumes of a translation journal may have been published by an organization other than that listed as the current publisher, and possibly under a different title (and, for *Doklady Akademii Nauk SSSR*, in a different arrangement of sections).

Five bits of information are furnished, separated by bullets:

1. The abbreviation(s) by which the journals are most frequently referred to in Russian bibliographies (if the name of the journal is customarily spelled out, no abbreviation is given).
2. The transliterated full name of the journal.
3. The full name of the translation journal (in bold type).
4. The year, volume (in parentheses), and issue of first publication of the translation (parentheses are empty if the Russian journal does not use volume numbers).
5. The current publisher of the translation [AGI—American Geological Institute, AGU—American Geophysical Union, AIP—American Institute of Physics, CB—Consultants Bureau, CH—Clearing House for Federal Scientific and Technical Information, CS—The Chemical Society (London), FP—Faraday Press, IEEE— Institute of Electrical and Electronic Engineers, ISA—Instrument Society of America, PP—Pergamon Press].

For convenience in locating bibliographic references the journals are listed in alphabetical order of the *abbreviated* titles.

AÉ • Atomnaya énergiya • **Soviet Journal of Atomic Energy** • 1956(1)1 • CB

Akust. zh. • Akusticheskii zhurnal • **Soviet Physics—Acoustics** • 1955(1)1 • AIP

Astrofiz. • Astrofizika • **Astrophysics** • 1965(1)1 • FP

Astr(on). zh(urn). • Astronomicheskii zhurnal • **Soviet Astronomy—AJ** • 1957(34)1 • AIP

Avtomat. i telemekh. • Avtomatika i telemekhanika • **Automation and Remote Control** • 1956(27)1 • ISA

Avto(mat). svarka • Avtomaticheskaya svarka • **Automatic Welding** • 1959(12)1 • British Welding Research Association

Avtometriya • **Autometry** • 1965(1)1 • CB

Biokhim. • Biokhimiya • **Biochemistry** • 1956(21)1 • CB

Byul. éksp(erim). biol. (i med.) • Byulleten' éksperimental'noi biologii i meditsiny • **Bulletin of Experimental Biology and Medicine** • 1959(41)1 • CB

DAN (SSSR) • *see* Doklady AN SSSR

Defektoskopiya • **Soviet Defectoscopy** • 1965(1)1 • CB

Diff. urav. • Differentsial'nye uravneniya • **Differential Equations** • 1965(1)1 • FP

Dokl(ady) AN SSSR; DAN (SSSR) • Doklady Akademii Nauk SSSR • The translation of Doklady is published in various journals, according to subject matter. The sections of Doklady contained in each of the translation journals are listed in parentheses.

Doklady Biochemistry (biochemistry) • 1957(112)1 • CB

Doklady Biological Sciences Sections (anatomy, cytology, ecology, embryology, endocrinology, evolutionary morphology, parasitology, physiology, zoology) • 1957(112)1 • CB

Doklady Biophysics (biophysics) • 1957(112)1 • CB

Doklady Botany (botany, phytopathology, plant anatomy, plant ecology, plant embryology, plant physiology, plant morphology) • 1957(112)1 • CB

Doklady Chemical Technology (chemical technology) • 1956(106)1 • CB

Doklady Chemistry (chemistry) • 1956(106)1 • CB

Doklady Earth Sciences Sections (geochemistry, geology, geophysics, hydrogeology, lithology, mineralogy, paleontology, permafrost, petrography) • 1959(124)1 • AGI

Doklady Physical Chemistry (physical chemistry) • 1957(112)1 • CB

Doklady Soil Science (soil science) • 1964(154)1 • Soil Science Society of America

Soviet Mathematics—Doklady (mathematics) • 1960(130)1 • American Mathematical Society

Soviet Oceanography (oceanology) • 1959(124)1 • AGU

Soviet Physics—Doklady (aerodynamics, astronomy, crystallography, cybernetics and control theory, electrical engineering, energetics, fluid mechanics, heat engineering, hydraulics, mathematical physics, mechanics, physics, technical physics, theory of elasticity • 1956(106)1 • AIP

Élektrokhimiya • **Soviet Electrochemistry** • 1965(1)1 • CB

Élektrosvyaz' • combined with Radiotekhnika in **Telecommunications and Radio Engineering** • 1957(16)1 • IEEE

Élektrotekh. • Élektrotekhnika • **Soviet Electrical Engineering** • 1965(36)1 • FP

Éntom(ol). oboz(r). • Éntomologicheskoe obozrenie • **Entomological Review** • 1958(37)1 • Entomological Society of America

Fiz. goreniya i vzryva • Fizika goreniya i vzryva • **Combustion, Explosion, and Shock Waves** • 1965(1) • FP

Fiziol(ogiya) rast. • Fiziologiya rastenii • **Soviet Plant Physiology** • 1957(4)1 • CB

Fiz.-khim. mekh(anika) mater(ialov); FKhMM • Fizikokhimicheskaya mekhanika materialov • **Soviet Materials Science** • 1965(1)1 • FP

Fiz. met. i metallov.; FMM • Fizika metallov i metallovedenie • **Physics of Metals and Metallography** • 1957(5)1 • Acta Metallurgica

Fiz.-tekhn. probl. razr. polezn. iskopaem. • Fizikotekhnicheskie problemy razrabotki poleznykh iskopaemykh • **Soviet Mining Science** • 1965(1)1 • CB

Fiz. tv(erd). tela; FTT • Fizika tverdogo tela • **Soviet Physics—Solid State** • 1959(1)1 • AIP

FKhMM • *see* Fiz.-khim. mekhanika materialov

FMM • *see* Fiz. met. i metallov.

FTT • *see* Fiz. tverd. tela

Geliotekh. • Geliotekhnika • **Applied Solar Energy** • 1965(1)1 • FP

Geol. nefti i gaza • Geologiya nefti i gaza • **Petroleum Geology** • 1958(2)1 • Petroleum Geology, Box 171, McLean, Va.

Geomagnet. i aéronom. • Geomagnetizm i aéronomiya • **Geomagnetism and Aeronomy** • 1961(1)1 • AGU

Inzh.-fiz. zh. • Inzhenerno-fizicheskii zhurnal • **Journal of Engineering Physics** • 1965(8)1 • FP

Inzh. zh. • Inzhenernyi zhurnal • **Soviet Engineering Journal** • 1965(5)1 • FP

Iskusstv. sputniki Zemli • Iskusstvennye sputniki Zemli • **Artificial Earth Satellites** • 1958(1)1 • CB [superseded by Kosmich. issled.]

Izmerit. tekhn(ika) • Izmeritel'naya tekhnika • **Measurement Techniques** • 1958(7)1 • ISA

Izv. AN SSSR, o(td.) kh(im.) n(auk) (*or* ser. khim.) • Izvestiya Akademii Nauk SSSR: Otdelenie khimicheskikh nauk (*or* Seriya khimicheskaya) • **Bulletin of the Academy of Sciences of the USSR: Division of Chemical Science** • 1952(16)1 • CB

Izv. AN SSSR, ser. fiz(ich). • Izvestiya Akademii Nauk SSSR: Seriya fizicheskaya • **Bulletin of the Academy of Sciences of the USSR: Physical Series** • 1954(18)3 • Columbia Technical Translations

Izv. AN SSSR, ser. fiz. atm. i okeana • Izvestiya Akademii Nauk SSSR: Seriya fiziki atmosfery i okeana • **Izvestiya, Atmospheric and Oceanic Physics** • 1965( )1 • AGU

Izv. AN SSSR, ser. fiz. zemli • Izvestiya Akademii Nauk SSSR: Seriya fiziki zemli • **Izvestiya, Physics of the Solid Earth** • 1965( )1 • AGU

Izv. AN SSSR, ser. geofiz. • Izvestiya Akademii Nauk SSSR: Seriya geofizicheskaya • **Bulletin of the Academy of Sciences of the USSR: Geophysics Series** • 1957(7)1 • AGU [superseded by Izv. AN SSSR, ser. fiz. atm. i okeana and Izv. AN SSSR, ser. fiz. zemli]

Izv. AN SSSR, ser. geol. • Izvestiya Akademii Nauk SSSR: Seriya geologicheskaya • **Bulletin of the Academy of Sciences of the USSR: Geologic Series** • 1958(23)1 • AGI

Izv. AN SSSR, ser. neorgan. mat(er). • Izvestiya Akademii Nauk SSSR: Seriya neorganicheskie materialy • **Inorganic Materials** • 1965(1)1 • CB

Izv. ... Tekhnicheskaya kibernetika • **Engineering Cybernetics** • 1963(1)1 • IEEE

Izv. v(yssh.) u(ch.) z(av.) aviats. tekh. • Izvestiya vysshikh uchebnykh zavedenii. Aviatsionnaya tekhnika • **Aviation Engineering** • 1963(6)1 • CH

Izv. v(yssh.) u(ch.) z(av.) fiz. • Izvestiya vysshikh uchebnykh zavedenii. Fizika • **Soviet Physics Journal** • 1965(8)1 • FP

Izv. v(yssh.) u(ch.) z(av.) geodez. i aérofot. • Izvestiya vysshikh uchebnykh zavedenii. Geodeziya i aérofotos"emka • **Geodesy and Aerophotography** • 1959(4)1 • AGU

Izv. v(yssh.) u(ch.) z(av.) priborostr. • Izvestiya vysshikh uchebnykh zavedenii. Priborostroenie • **Izvestiya VUZOV. Instrument Building** • 1962(5)1 • CH

Izv. v(yssh.) u(ch.) z(av.) radiofiz. • Izvestiya vysshikh uchebnykh zavedenii. Radiofizika • **Izvestiya VUZOV. Radiophysics** • 1958(1)1 • CH

Izv. v(yssh.) u(ch.) z(av.) radiotekhn(ika) • Izvestiya vysshikh uchebnykh zavedenii. Radiotekhnika • **Izvestiya VUZOV. Radio Engineering** • 1959(2)1 • CH

Izv. v(yssh.) u(ch). z(av.) tekh. teks. prom. • Izvestiya vysshikh uchebnykh zavedenii. Tekhnologiya tekstilnoi promyshlennosti • **Technology of the Textile Industry, USSR** • 1960(4)1 • The Textile Institute (Manchester)

Kauch. i rez. • Kauchuk i rezina • **Soviet Rubber Technology** • 1959 (18)3 • Maclaren and Sons Ltd.

Khim. getero(tsik). soed. • Khimiya geterotsiklicheskikh soedinenii • **Chemistry of Heterocyclic Compounds** • 1965(1)1 • FP

Khim. i neft. mash(inostr). • Khimicheskoe i neftyanoe mashinostroenie • **Chemical and Petroleum Engineering** • 1965( )1 • CB

Khim. i tekhnol. topliv i masel • Khimiya i tekhnologiya topliv i masel • **Chemistry and Technology of Fuels and Oils** • 1965( )1 • CB

Khim. prirod. soed. • Khimiya prirodnykh soedinenii • **Chemistry of Natural Compounds** • 1965(1)1 • FP

Kib. • Kibernetika • **Cybernetics** • 1965(1)1 • FP

Kinet. i katal. • Kinetika i kataliz • **Kinetics and Catalysis** • 1960(1)1 • CB

Koks i khim. • Koks i khimiya • **Coke and Chemistry, USSR** • 1959( )8 • Coal Tar Research Assn. (Leeds, England)

Kolloidn. zh(urn). • Kolloidnyi zhurnal • **Colloid Journal** • 1952(14)1 • CB

Kosmich. issled. • Kosmicheskie issledovaniya • **Cosmic Research** • 1963(1)1 • CB

Kristallog. • Kristallografiya • **Soviet Physics—Crystallography** • 1957 (2)1 • AIP

Liteinoe proiz(-vo). • Liteinoe proizvodstvo • **Russian Castings Production** • 1961(12)1 • British Cast Iron Research Association

Mag. gidrodin. • Magnitnaya gidrodinamika • **Magnetohydrodynamics** • 1965(1)1 • FP

Mekh. polim. • Mekhnika polimerov • **Polymer Mechanics** • 1965(1)1 • FP

Metalloved. i term. obrabotka metal.; MiTOM • Metallovedenie i termicheskaya obrabotka metallov • **Metal Science and Heat Treatment** • 1958(6)1 • CB

Metallurg • **Metallurgist** • 1957( )1 • CB

Mikrobiol. • Mikrobiologiya • **Microbiology** • 1957(26)1 • CB

MiTOM • *see* Metalloved. i term. obrabotka metal.

Ogneupory • **Refractories** • 1960(25)1 • CB

Opt. i spektr.; OS • Optika i spektroskopiya • **Optics and Spectroscopy** • 1959(6)1 • AIP

Osnovan. fund. i mekh. gruntov • Osnovaniya fundamenty i mekhanika gruntov • **Soil Mechanics and Foundation Engineering** • 1964 ( )1 • CB

Paleon. zh(urn). • Paleontologicheskii zhurnal • **Journal of Paleontology** • 1962( )1 • AGI

Plast. massy • Plasticheskie massy • **Soviet Plastics** • 1960(8)7 • Rubber and Technical Press, Ltd.

PMM • *see* Prikl. matem. i mekhan.

PMTF • *see* Zhur. prikl. mekhan. i tekhn. fiz.

Pochvovedenie • **Soviet Soil Science** • 1958(53)1 • Soil Science Society of America

Poroshk. met. • Poroshkovaya metallurgiya • **Soviet Powder Metallurgy and Metal Ceramics** • 1962(2)1 • CB

Priborostroenie • **Instrument Construction** • 1959(4)1 • Taylor and Francis, Ltd.

Pribory i tekhn. éksp(erimenta); PTÉ • Pribory i tekhnika éksperimenta • **Instruments and Experimental Techniques** • 1958(3)1 • ISA

Prikl. biokhim. i mikrobiol. • Prikladnaya biokhimiya i mikrobiologiya • **Applied Biochemistry and Microbiology** • 1965(1)1 • FP

Prikl. matem. i mekh(an).; PMM • Prikladnaya matematika i mekhanika • **Applied Mathematics and Mechanics** • 1958(22)1 • PP

Information Transmission • 1965(1)1 • FP

Probl. severa • Problemy severa • **Problems of the North** • 1958( )1 • National Research Council of Canada

PTÉ • *see* Pribory i tekhn. éksperimenta

Radiokhim. • Radiokhimiya • **Soviet Radiochemistry** • 1962(4)1 • CB

Radiotekh. • Radiotekhnika • combined with Élektrosvyaz' in **Telecommunications and Radio Engineering** • 1961(16)1 • IEEE

Radiotekhn. i élektron(ika) • Radiotekhnika i élektronika • **Radio Engineering and Electronic Physics** • 1961(6)1 • IEEE

Stal' • **Stal' in English** • 1959(19)1 • The Iron and Steel Institute

Stanki i instr. • Stanki i instrument • **Machines and Tooling** • 1959 (30)1 • Production Engineering Research Association

Stek. i keram. • Steklo i keramika • **Glass and Ceramics** • 1956(13)1 • CB

Svaroch. proiz(-vo). • Svarochnoe proizvodstvo • **Welding Production** • 1959(5)4 • British Welding Research Association (London)

Teor. i éksperim. khim. • Teoreticheskaya i éksperimental'naya khimiya • **Theoretical and Experimental Chemistry** • 1965(1)1 • FP

Teor. veroyat. i prim. • Teoriya veroyatnostei i ee primenenie • **Theory of Probability and Its Application** • 1956(1)1 • Society for Industrial and Applied Mathematics

Teploénergetika • **Thermal Engineering** • 1964(11)1 • PP

Teplofiz. vys(ok). temp. • Teplofizika vysokikh temperatur • **High Temperature** • 1963(1)1 • CB

Tsvet. metally • Tsvetnye metally • **The Soviet Journal of Nonferrous Metals** • 1960(33)1 • Primary Sources

Usp. fiz. nauk; UFN • Uspekhi fizicheskikh nauk • **Soviet Physics—Uspekhi** • 1958(66)1 • AIP

Usp. khim.; UKh. • Uspekhi khimii • **Russian Chemical Reviews** • 1960(29)1 • CS

Usp. mat. nauk; UMN • Uspekhi matematicheskaya nauk • **Russian Mathematical Surveys** • 1960(15)1 • Cleaver-Hume Press, Ltd.

Vest. Akad. med. nauk SSSR • Vestnik Akademii meditsinskikh nauk SSSR • **Vestnik of USSR Academy of Medical Sciences** • 1962(17)1 • CH

Vest. mashinostroeniya • Vestnik mashinostroeniya • **Russian Engineering Journal** • 1959(39)4 • Production Engineering Research Association

Vest. svyazi • Vestnik svyazi • **Herald of Communications** • 1954(14)1 • CH

Vysoko(molek). soed(ineniya) • Vysokomolekulyarnye soedineniya (SSSR) • **Polymer Science (USSR)** • 1959(1)1 • PP

Yadernaya fizika • **Soviet Journal of Nuclear Physics** • 1965(1)1 • AIP

Zashch(ita) met(allov) • Zashchita metallov • **Protection of Metals** • 1965(1)1 • CB

Zav(odsk). lab(oratoriya); ZL • Zavodskaya laboratoriya • **Industrial Laboratory** • 1958(24)1 • ISA

ZhÉTF pis'ma redaktsiyu • **JETP Letters** • 1965(1)1 • AIP

Zh(ur). anal(it). khim(ii); ZhAKh • Zhurnal analiticheskoi khimii • **Journal of Analytical Chemistry** • 1952(7)1 • CB

Zh(ur). éks(perim). i teor. fiz.; ZhÉTF • Zhurnal éksperimental'noi i teoreticheskoi fiziki • **Soviet Physics—JETP** • 1955(28)1 • AIP

Zh(ur). fiz. khimii; ZhFKh • Zhurnal fizicheskoi khimii • **Russian Journal of Physical Chemistry** • 1959(33)7 • CS

Zh(ur). neorg(an). khim.; ZhNKh • Zhurnal neorganicheskoi khimii • **Russian Journal of Inorganic Chemistry** • 1959(4)1 • CS

Zh(ur). obshch. khim.; ZhOKh • Zhurnal obshchei khimii • **Journal of General Chemistry of the USSR** • 1949(19)1 • CB

Zh(ur). org. khim.; ZhOrKh(im) • Zhurnal organicheskoi khimii • **Journal of Organic Chemistry of the USSR** • 1965(1)1 • CB

Zh(ur). prikl. khim.; ZhPKh • Zhurnal prikladnoi khimii • **Journal of Applied Chemistry of the USSR** • 1950(23)1 • CB

Zh(ur). prikl. mekhan. i tekhn. fiz. • Zhurnal prikladnoi mekhaniki i tekhnicheskoi fiziki • **Journal of Applied Mechanics and Technical Physics** • 1965( )1 • FP

Zh(ur). prikl. spektr. • Zhurnal prikladnoi spektroskopii • **Journal of Applied Spectroscopy** • 1965(2)1 • FP

Zh(ur). strukt(urnoi) khim.; ZhSKh • Zhurnal strukturnoi khimii • **Journal of Structural Chemistry** • 1960(1)1 • CB

Zh(ur). tekhn. fiz.; ZhTF • Zhurnal tekhnicheskoi fiziki • **Soviet Physics—Technical Physics** • 1956(26)1 • AIP

Zh(ur). vses. khim. ob-va im. Mendeleeva • Zhurnal vsesoyuznogo khimicheskogo obshchestva im. Mendeleeva • **Mendeleev Chemistry Journal** • 1965(10)1 • FP

Zh(ur). vychis. mat. i mat. fiz. • Zhurnal vychislitel'noi matematika i matematicheskoi fiziki • **USSR Computational Mathematics and Mathematical Physics** • 1962(1)1 • PP

ZL • *see* Zavodsk. laboratoriya

IMPORTANT CONSULTANTS BUREAU/PLENUM PRESS BOOKS

STABILITY AND OSCILLATIONS OF ELASTIC SYSTEMS

Paradoxes, Fallacies, and New Concepts

By Ya. G. Panovko and I. G. Gubanova

Foreword by Prof. Flügge, Stanford University

The authors have written this thought-provoking work as "a book to be read," a collection of sketches, devoted to selected topics in the theory of the stability and the theory of the oscillations of elastic and incompletely elastic systems. A Consultants Bureau book translated from Russian.

Approx. 291 pages 1965 $17.50

STABLE RADICALS

By A. L. Buchachenko

This book fulfills the need for systematization of present knowledge of all the known stable radicals and the examination of the basic aspects of their investigation and application. Particular attention is paid to the electronic structure of stable radicals and the correlation of their structure and properties. A Consultants Bureau book translated from Russian.

188 pages 1965 $15.00

OXIDATION OF METALS

By Karl Hauffe

This first English edition of the well-known German text **Oxydation von Metallen und Metallegierungen** has been thoroughly revised by the author. It includes tables of diffusion parameters (pre-exponential factors and activation energies) for self-diffusion, for several metal-alloy systems, and for inorganic compounds, along with 231 figures and graphs and many literature references. A Plenum Press book.

466 pages 1965 $19.50

INFRARED BAND HANDBOOK

Supplements 3 and 4

Herman A. Szymanski, Editor

These two supplements cover more than 400 additional organic and inorganic compounds with infrared bands in the range of 2 to 25 microns. Bound as a single volume, they tabulate 4906 bands bringing the total number of bands covered to more than 17,000. Published by the Plenum Press Data Division.

Approx. 250 pages 1965 $15.00

HANDBOOK OF THERMIONIC PROPERTIES

Electronic Work Functions and Richardson Constants of Metals and Compounds

By V. S. Fomenko. G. V. Samsonov, Editor

An up-to-date aid to to the scientist and engineer in the research and development fields of cathode materials, electron microscopy, semiconductor techniques, materials testing, and applied physics. Published by the Plenum Press Data Division.

Approx. 110 pages 1966 $12.50

TWILIGHT:

A Study in Atmospheric Optics

By G. V. Rozenberg

Foreword by J. V. Dave,
National Center for Atmospheric Research

This is the only book in the world scientific literature that is devoted to the discussion of the twilight as an optical phenomenon and as a means for investigation of the atmosphere — especially its high layers. A Plenum Press book translated from Russian.

Approx. 380 pages 1965 $20.00

MATSCIENCE SYMPOSIA ON THEORETICAL PHYSICS

Alladi Ramakrishnan, Editor

A new and continuing series emanating from the symposia held at the Institute of Mathematical Sciences, Madras, India

Volume 1: Proceedings of the First Anniversary Symposium

This symposium was arranged in tribute to Prof. R. E. Marshak, who accepted the first Niels Bohr visiting professorship at the new Institute of Mathematical Sciences. Prof. Marshak contributed the paper "Group Symmetries with R-Invariance" included in this proceedings. A Plenum Press book.

Approx. 170 pages 1965 $9.50

CONSULTANTS BUREAU / PLENUM PRESS
227 West 17th Street, New York, New York 10011